Design of process for recovery of gold and nickel ions from wastewater of metal plating process in electronics industry using hollow fiber supported liquid membrane

Mr. Wanchalerm Srirachat

จุฬาลงกรณ์มหาวิทยาลัย
CHULALONGKORN UNIVERSITY

A Dissertation Submitted in Partial Fulfillment of the Requirements
for the Degree of Doctor of Engineering in Chemical Engineering
Department of Chemical Engineering
FACULTY OF ENGINEERING
Chulalongkorn University
Academic Year 2022
Copyright of Chulalongkorn University

การออกแบบกระบวนการนำกลับไอออนทองและนิกเกิลจากน้ำทิ้งของกระบวนการชุบโลหะในอุตสาหกรรมอิเล็กทรอนิกส์ด้วยเทคนิคเยื่อแผ่นเหลวที่พยุงด้วยเส้นใยกลวง

นายวันเฉลิม ศรีระชาติ

จุฬาลงกรณ์มหาวิทยาลัย
CHULALONGKORN UNIVERSITY

วิทยานิพนธ์นี้เป็นส่วนหนึ่งของการศึกษาตามหลักสูตรปริญญาวิศวกรรมศาสตรดุษฎีบัณฑิต
สาขาวิชาวิศวกรรมเคมี ภาควิชาวิศวกรรมเคมี
คณะวิศวกรรมศาสตร์ จุฬาลงกรณ์มหาวิทยาลัย
ปีการศึกษา 2565

ลิขสิทธิ์ของจุฬาลงกรณ์มหาวิทยาลัย

Thesis Title	Design of process for recovery of gold and nickel ions from wastewater of metal plating process in electronics industry using hollow fiber supported liquid membrane
By	Mr. Wanchalerm Srirachat
Field of Study	Chemical Engineering
Thesis Advisor	Professor URA PANCHAROEN, Ph.D.
Thesis Co Advisor	Associate Professor SOORATHEP KHEAWHOM, Ph.D.

Accepted by the FACULTY OF ENGINEERING, Chulalongkorn University in Partial Fulfillment of the Requirement for the Doctor of Engineering

..... Dean of the FACULTY OF ENGINEERING
(Professor SUPOT TEACHAVORASINSKUN, D.Eng.)

DISSERTATION COMMITTEE

..... Chairman
(Associate Professor Prakorn Ramakul, D.Eng., Ph.D.)

..... Thesis Advisor
(Professor URA PANCHAROEN, Ph.D.)

..... Thesis Co-Advisor
(Associate Professor SOORATHEP KHEAWHOM, Ph.D.)

..... Examiner
(Professor SARAWUT RIMDUSIT, Ph.D.)

..... Examiner
(Associate Professor Sorada Kanokpanont, Ph.D.)

..... Examiner
(Associate Professor KREANGKRAI MANEEINTR, Ph.D.)

จุฬาลงกรณ์มหาวิทยาลัย
CHULALONGKORN UNIVERSITY

วันเฉลิม ศรีระชาติ : การออกแบบกระบวนการนำกลับไอออนทองและนิกเกิลจากน้ำทิ้งของกระบวนการชุบโลหะในอุตสาหกรรมอิเล็กทรอนิกส์ด้วยเทคนิคเยื่อแผ่นเหลวที่พยุงด้วยเส้นใยกลวง. (Design of process for recovery of gold and nickel ions from wastewater of metal plating process in electronics industry using hollow fiber supported liquid membrane) อ.ที่ปรึกษาหลัก : ศ. ดร.อุรา ปานเจริญ, อ.ที่ปรึกษาร่วม : รศ. ดร.สุรเทพ เขียวหอม

การชุบเคลือบผิวด้วยโลหะนิกเกิลและทองแบบไม่ใช้ไฟฟ้าถูกนำมาใช้แพร่หลายในวงการผลิตแผ่นวงจรอิเล็กทรอนิกส์ โดยในกระบวนการชุบนั้นบ่อน้ำล้างจะทำหน้าที่ชะล้างคราบน้ำยาชุบส่วนเกินที่ติดมากับชิ้นงาน จึงมีการสะสมของปริมาณไอออนนิกเกิลและทองซึ่งมีมูลค่าเชิงเศรษฐศาสตร์

งานวิจัยนี้ศึกษาการเลือกสกัดและนำกลับไอออนนิกเกิลและทองในขั้นตอนเดียวโดยใช้เทคนิคเยื่อแผ่นเหลวที่พยุงด้วยเส้นใยกลวง สารละลายป้อนที่ใช้คือน้ำทิ้งจากบ่อล้างชิ้นงานจริงหลังชุบนิกเกิลและทอง มีค่าความเข้มข้นของไอออนนิกเกิล (15 มิลิกรัมต่อลิตร) และไอออนทอง (25 มิลลิกรัมต่อลิตร) ในระดับที่ต่ำ ความเป็นกรด-ด่างเท่ากับ 8.6±0.05 ปัจจัยที่ศึกษาได้แก่ ชนิดและความเข้มข้นของสารสกัดและสารนำกลับ ความเป็นกรดด่างของสารนำกลับและชนิดของสารเจือจาง ผลการทดลองพบว่า ระบบเยื่อแผ่นเหลวที่พยุงด้วยเส้นใยกลวงซึ่งใช้สารสกัดประเภทฟอสฟอรัสอินทรีย์ 2 ชนิดแบบเสริมฤทธิ์ ได้แก่ D2EHPA ความเข้มข้น 0.25 โมลต่อลิตร และ TBP ความเข้มข้น 0.25 โมลต่อลิตร ละลายในสารเจือจางเคโรซีน สารนำกลับคือกรดไฮโดรคลอลิกความเข้มข้น 0.50 โมลต่อลิตร อัตราการไหลของสารป้อนและสารนำกลับเท่ากับ 200 มิลลิลิตรต่อนาที สามารถให้ประสิทธิภาพการเลือกสกัดแยกและนำกลับไอออนนิกเกิลได้เหมาะสมที่สุดด้วยร้อยละการสกัดสูงสุด 85.7 และร้อยละการนำกลับสูงสุด 83.2 โดยในระยะเวลา 28 นาที สามารถสกัดไอออนนิกเกิลได้ร้อยละ 80 ทั้งนี้สามารถแยกไอออนนิกเกิลออกจากไอออนทองได้ดีซึ่งมีร้อยละการสกัด 15.6 และร้อยละการนำกลับ 1.94

นอกจากนี้การทดลองใช้สารเจือจางทางเลือกประเภทน้ำมันจากพืช ได้แก่ น้ำมันปาล์ม น้ำมันดอกทานตะวัน น้ำมันถั่วเหลือง น้ำมันมะพร้าวและน้ำมันรำข้าว ซึ่งมีความเป็นมิตรต่อสิ่งแวดล้อมมากกว่าเคโรซีน สามารถให้ประสิทธิภาพการแยกไอออนนิกเกิลและทองได้ใกล้เคียงกับเคโรซีน รวมถึงแบบจำลองการถ่ายโอนมวลที่พัฒนาขึ้นสามารถใช้ทำนายความเข้มข้นของไอออนนิกเกิลที่ช่วงเวลาต่าง ๆ ได้อย่างดี โดยผลที่ได้จากการคำนวณมีความสอดคล้องกับผลการทดลองจริง งานวิจัยนี้ได้เสนอวิธีการนำโลหะที่มีค่ากลับมาใช้ใหม่ เพื่อเป็นการลดต้นทุนและการจัดการน้ำเสียอย่างยั่งยืน

จุฬาลงกรณ์มหาวิทยาลัย
CHULALONGKORN UNIVERSITY

สาขาวิชา	วิศวกรรมเคมี	ลายมือชื่อนิสิต .....
ปีการศึกษา	2565	ลายมือชื่อ อ.ที่ปรึกษาหลัก .....
		ลายมือชื่อ อ.ที่ปรึกษาร่วม .....

5971440321 : MAJOR CHEMICAL ENGINEERING
KEYWORD: Hollow fiber supported liquid membrane, Electroless nickel immersion gold plating, Rinse wastewater, Gold(I), Nickel(II)

Wanchalerm Srirachat : Design of process for recovery of gold and nickel ions from wastewater of metal plating process in electronics industry using hollow fiber supported liquid membrane. Advisor: Prof. URA PANCHAROEN, Ph.D. Co-advisor: Assoc. Prof. SOORATHEP KHEAWHOM, Ph.D.

In the manufacture of printed circuit boards (PCBs), electroless nickel immersion gold (ENIG) plating is widely applied. During the plating process, excess nickel and gold plating solutions, which adheres to the workpiece, is removed. As a result, economical quantities of nickel and gold ions accumulate in the rinse water baths and can then be collected.

In this work, the simultaneously selective extraction and recovery of nickel and gold ions using a single-step operation of hollow fiber supported liquid membrane (HFSLM) technique was studied. Real rinse wastewater from the plating process containing trace nickel ions (Ni(II)) of 15 mg/L and gold ions (Au(I)) of 25 mg/L at initial pH value of 8.6±0.05 was used as feed solution. The influence of operating conditions: types of extractant and strippant at different concentrations, pH of stripping solution as well as types of diluents were also examined. Results demonstrate that the HFSLM system, using the liquid membrane phase consisting of synergistic binary organophosphorus extractants viz. 0.25 mol/L D2EHPA and 0.25 mol/L TBP dissolved in kerosene diluent, 0.50 mol/L HCl as stripping solution, and 200 mL/min flow rate for both feed and stripping solutions operating via recycling mode and countercurrently flow, can achieve the optimum selective separation efficiency of Ni(II) ions with 85.7% extraction and 83.2% stripping . Extraction of Ni(II) ions can rapidly reach 80% within 28 min. In contrast, percentages of extraction and stripping of Au(I) ions attained 15.6 and 1.94%, respectively.

Furthermore, various types of vegetable oil (palm, sunflower, soybean, coconut and rice bran) were investigated as diluents in the liquid membrane phase being more eco-friendly than kerosene diluent. Thus, it was found that all vegetable oil-based diluents can provide the separation efficiency close to kerosene. In addition, the developed mathematical model regarding mass transfer for predicting the concentration of Ni(II) ions in both feed and stripping solutions, was found to be of high accuracy and in good agreement with the obtained experimental data. This research paves the way towards reusing valuable metals for cost reduction and sustainable wastewater management.

จุฬาลงกรณ์มหาวิทยาลัย
CHULALONGKORN UNIVERSITY

Field of Study:	Chemical Engineering	Student's Signature .....
Academic Year:	2022	Advisor's Signature .....
		Co-advisor's Signature .....

ACKNOWLEDGEMENTS

Foremost, my deep gratitude goes to my supervisor, Professor Ura Pancharoen, who has expertly guided me through my Ph.D. study. Under his supervision, I learned how to define a research problem, find a solution to it, and finally publish the results. I also wish to express my sincere appreciation to Associate Professor Soorathep Kheawhom, my Co-advisor, for encouraging me in my work and providing insightful suggestions throughout my studies.

Besides my advisors, I would like to express my gratitude to members of the dissertation committee: Associate Professor Prakorn Ramakul, Associate Professor Sorada Kanokpanont, Professor Sarawut Rimdusit, and Associate Professor Kreangkrai Maneeintr, for their invaluable help and advice.

My grateful thanks are also extended to the funding sources of my research. I profoundly appreciate the support from the Thailand Research Fund (TRF) and Chulalongkorn University under the Research and Researchers for Industries (RRI) Ph.D. Program (Grant No. PHD PHD60I005). Thanks are also given to Mektec Manufacturing Corporation (Thailand) Ltd.; the Mass Separation Laboratory, Department of Chemical Engineering, Faculty of Engineering, Chulalongkorn University as well as sincere thanks also go to Department of Mining and Petroleum Engineering, Chulalongkorn University. Without their valuable support and funding, this project could not have reached its goal.

I will always remember my friends and fellow lab mates too for the fun-time we spent together and for their loyal support, which sustained me throughout the entire research program.

Wanchalerm Srirachat

จุฬาลงกรณ์มหาวิทยาลัย
CHULALONGKORN UNIVERSITY

TABLE OF CONTENTS

Page

..... iii
ABSTRACT (THAI) iii
.....iv
ABSTRACT (ENGLISH).....iv
ACKNOWLEDGEMENTS.....v
TABLE OF CONTENTS.....vi
LIST OF TABLES.....xii
LIST OF FIGURES xvi
CHAPTER I.....1
INTRODUCTION 1
1.1 General introduction 1
1.1.1 Extractants 2
1.1.2 Diluents 4
1.1.3 Feed solutions.....4
1.1.4 Stripping solutions.....5
1.1.5 Transportation of metal ions across HFSLM 6
1.1.6 Mass transfer across HFSLM 8
1.1.7 Flow patterns of HFSLM 10
1.1.8 Properties of HFSLM 11
1.1.9 Aqueous feed acidity 1
1.1.10 Carrier concentration.....1
1.1.11 Flow rates of both aqueous solutions 1
1.1.12 Flow patterns of aqueous solutions 2
1.1.13 Mathematical modelling.....2
1.2 Objectives of the dissertation.....2

1.3 Scope of the dissertation 3
1.4 Expected results 3
1.5 Description of the dissertation 4
CHAPTER II 8
Selective separation of trace nickel(II) and gold(I) ions via hollow fiber supported liquid membrane enhanced by synergistic extractants D2EHPA/TBP 8
2.1 Graphical abstract 9
2.2 Abstract 9
2.3 Introduction 10
2.4 Experimental 14
2.4.1 Chemicals and reagents 14
2.4.2 Apparatus and experimental procedure 17
2.5 Results and discussion 20
2.5.1 Effect of type of extractant 20
2.5.2 Effect of mixed extractants 27
2.5.3 Effect of molar ratio of mixed D2EHPA/TBP extractant 32
2.5.4 Effect of extractant concentration 36
2.5.5 Effect of the type of strippant 41
2.5.6 Effect of stripping agent concentration 44
2.5.7 Equilibrium study of Ni^{2+} extraction via HFSLM 48
2.5.8 Mass transfer coefficient for Ni^{2+} extraction from the real rinse wastewater of the ENIG plating process via HFSLM 49
2.5.9 Determination of the reaction order and the reaction rate constant for Ni^{2+} and $[Au(CN)_2]^-$ extraction from the real rinse wastewater of the ENIG plating process via HFSLM 50
2.6 Conclusions 52
2.7 Supplementary information 52
2.8 Acknowledgements 60
2.9 References 60

จุฬาลงกรณ์มหาวิทยาลัย
Chulalongkorn University

CHAPTER III 70

Selective elimination of Ni(II) ions from rinse wastewater of ENIG plating via HFSLM, applying vegetable oils as alternative greener diluents: Experiment, kinetic and mass transfer model 70

3.1 Graphical abstract 71

3.2 Abstract 72

3.3 Introduction 72

3.4 Experimental 74

3.4.1 Chemicals and reagents 74

3.4.2 Apparatus and experimental procedure 75

3.4.3 Calculations of separation efficiency 76

3.5 Results and discussion 77

3.5.1 Effect of vegetable oil-based diluents on Ni^{2+} and $[Au(CN)_2]^-$ extractions 77

3.5.2 Effect of mixed extractants D2EHPA and TBP in the liquid membrane phase 83

3.5.3 Effect of stripping phase pH 87

3.5.4 Equilibrium distribution of Ni^{2+} and $[Au(CN)_2]^-$ separation via HFSLM system 90

3.5.5 Reaction order and reaction rate constant 96

3.5.6 Validation of the mathematical Model 100

3.6 Conclusions 104

3.7 Appendix A 105

3.7.1 Transport mechanism of Ni^{2+} across the liquid membrane phase 114

3.7.2 Development of the mathematical model 119

3.8 Acknowledgements 128

3.9 Nomenclatures 129

3.10 References 130

CHAPTER IV 132

An investigation of saturated vapor pressure regarding low-volatility organophosphorus extractants Di-(2-Ethylhexyl) Phosphoric Acid and Tributyl Phosphate: Correlation and thermodynamics study 132

4.1 Graphical abstract 133

4.2 Abstract 133

4.3 Introduction 134

4.4 Experimental 139

4.4.1 Chemicals 139

4.4.2 Saturated vapor pressure determination 141

4.5 Mathematical modeling and parameter estimation 144

4.5.1 Saturated vapor pressure correlation 144

4.5.2 Acentric factor estimation 145

4.5.3 Enthalpy or latent heat of vaporization 145

4.5.4 Entropy of vaporization 146

4.5.5 Saturated liquid heat capacity 147

4.6. Results and discussion 148

4.6.1 Saturated vapor pressure 148

4.6.2 Enthalpy and entropy of vaporization 157

4.6.3 Saturated Liquid Heat Capacity 164

4.7. Conclusions 168

4.8 Supplementary Information 168

4.8.1 References for the supplementary information 185

4.9 Acknowledgements 190

4.10 References 190

CHAPTER V 197

Isobaric Vapor-Liquid Equilibrium for Binary System Related to the Organophosphoric Extractant of D2EHPA + n-Dodecane and TBP + n-Dodecane at 0.13, 2.40 and 6.67 kPa 197

5.1 Graphical abstract 198

5.2 Abstract 198

จุฬาลงกรณ์มหาวิทยาลัย
CHULALONGKORN UNIVERSITY

5.3 Introduction.....199
5.4. Experimental.....200
5.4.1 Chemical.....200
5.4.2 Apparatus and procedure.....203
5.5. Results and discussion.....206
5.5.1 Experimental results.....206
5.5.2 Thermodynamic consistency verification.....217
5.5.3 Data correlation.....220
5.6. Conclusions.....223
5.7 Supplementary information.....223
5.7.1 Saturated vapor pressure.....223
5.7.2 Vapor liquid equilibrium.....224
5.7.3 Relative volatility.....225
5.7.4 Activity coefficient and data correlation.....225
5.7.5 Thermodynamic consistency verification.....227
5.7.6 References for the supplementary information.....233
5.8 Acknowledgements.....234
5.9 References.....234
CHAPTER VI.....238
CONCLUSION.....238
6.1 Conclusion.....238
6.2 Limitation.....241
6.3 Recommendations for future research.....241
APPENDICES.....243
APPENDIX A.....244
LIST OF PUBLICATION.....244

จุฬาลงกรณ์มหาวิทยาลัย
CHULALONGKORN UNIVERSITY

REFERENCES 246
VITA 248

จุฬาลงกรณ์มหาวิทยาลัย
CHULALONGKORN UNIVERSITY

LIST OF TABLES

Table 1.1 Summary of previous research on separation of Ni^{2+} via various membrane systems. 4

Table 1.2 Summary of previous research on separation of $[Au(CN)_2]^-$ via various membrane systems. 1

Table 1.3 The key characteristics of real rinse wastewater in this study. 5

Table 1.4 Properties of the HF module. 12

Table 2.1 Compositions in the real rinse wastewater of the ENIG plating process used as feed solution in this study. 15

Table 2.2 Chemicals used in this study. 16

Table 2.3 Effect of a single and mixed extractants for Ni^{2+} and $[Au(CN)_2]^-$ extraction via HFSLM: feed phase; 15 mg/L Ni^{2+}, 25 mg/L $[Au(CN)_2]^-$, pH 8.6±0.05 | liquid membrane phase; 0.50 mol/L extractant in kerosene | stripping phase; 0.50 mol/L HCl, pH 0.38±0.05 | $q_F = q_S$ = 200 mL/min | t = 2 h | T = 303±1 K. 21

Table 2.4 Separation time of Ni^{2+} and $[Au(CN)_2]^-$ applying different extractant systems. 25

Table 2.5 Physicochemical properties of D2EHPA and TBP extractant. 30

Table 2.6 Effect of molar ratio of mixed D2EHPA/ TBP extractants for Ni^{2+} and $[Au(CN)_2]^-$ extraction via HFSLM: feed phase; 15 mg/L Ni^{2+}, 25 mg/L $[Au(CN)_2]^-$, pH 8.6±0.05 | liquid membrane phase; 0.50 mol/L total concentration of mixed D2EHPA/TBP extractants in kerosene | stripping phase; 0.50 mol/L HCl, pH 0.38±0.05 | $q_F = q_S$ = 200 mL/min | t = 2 h | T = 303±1 K. 35

Table 2.7 Effect of extractant concentration for Ni^{2+} and $[Au(CN)_2]^-$ extraction via HFSLM: feed phase; 15 mg/L Ni^{2+}, 25 mg/L $[Au(CN)_2]^-$, pH 8.6±0.05 | liquid membrane phase; 0.01 to 1.0 mol/L extractant in kerosene | stripping phase; 0.50 mol/L HCl, pH 0.38±0.05 | $q_F = q_S$ = 200 mL/min | t = 2 h | T = 303±1 K. 37

Table 2.8 Effect of strippants on the selective stripping of Ni^{2+} and $[Au(CN)_2]^-$: feed phase; 15 mg/L Ni^{2+}, 25 mg/L $[Au(CN)_2]^-$, pH 8.6±0.05 | stripping solution; 0.50 mol/L strippant | $q_F = q_S$ = 200 mL/min | t = 2 h | T = 303±1 K. 42

Table 2.9 Effect of strippant concentration for Ni^{2+} and $[Au(CN)_2]^-$ extraction via HFSLM: feed phase; 15 mg/L Ni^{2+}, 25 mg/L $[Au(CN)_2]^-$, pH 8.6±0.05 | liquid

membrane phase; mixture of 0.25 mol/L D2EHPA and 0.25 mol/L TBP extractants in kerosene | stripping phase; HCl | $q_F = q_S$ = 200 mL/min | t = 2 h | T = 303±1 K.....47

Table 2.10 Equilibrium constant (K_{Ex}) for Ni^{2+} extraction via HFSLM.....48

Table 2.11 Mass transfer coefficient of Ni^{2+} and $[Au(CN)_2]^-$ extraction via HFSLM: feed phase; 15 mg/L Ni^{2+}, 25 mg/L $[Au(CN)_2]^-$, pH 8.6±0.05 | liquid membrane phase; total extractant concentration of 0.50 mol/L in kerosene | stripping phase; 0.50 mol/L HCl, pH 0.38±0.05 | $q_F = q_S$ = 200 mL/min | t = 2 h | T = 303±1 K. 50

Table 2.12 Analysis of reaction order and rate constants: feed phase; 15 mg/L Ni^{2+}, 25 mg/L $[Au(CN)_2]^-$, pH 8.6±0.05 | liquid membrane phase; total extractant concentration of 0.50 mol/L in kerosene | stripping phase; 0.50 mol/L HCl, pH 0.38±0.05 | $q_F = q_S$ = 200 mL/min | t = 2 h | T = 303±1 K.....51

Table 3.2 Extraction percentage (%E), distribution ratio (D), and selectivity (S) of Ni^{2+} and $[Au(CN)_2]^-$ separation via HFSLM using various types of vegetable oil-based diluents.....79

Table 3.3 Reaction rate order (m, n) and reaction rate constants of extraction and stripping of Ni^{2+} via HFSLM by mixed extractants (0.25 mol/L D2EHPA and 0.25 mol/L TBP) in various vegetable oil-based diluents with 0.50 mol/L HCl as strippant. 98

Table 3.4 Reaction order (m, n) and reaction rate constants of extraction and stripping of $[Au(CN)_2]^-$ via HFSLM by mixed extractants (0.25 mol/L D2EHPA and 0.25 mol/L TBP) in various vegetable oil-based diluents with 0.50 mol/L HCl as strippant.....99

Table A3.1 Properties of real rinse wastewater from ENIG plating process as feed solution.....105

Table A3.2 Chemicals used in this study. 106

Table A3.3 Typical characteristics of Liqui-Cel® Extra-Flow hollow fiber module. 107

Table A3.4 Reaction rate order (m, n) and reaction rate constants of extraction and stripping of Ni^{2+} via HFSLM by mixed extractants (0.25 M D2EHPA and 0.25 M TBP) in various vegetable oil-based diluents with 0.50 M HCl as strippant.....108

Table A3.5 Reaction order (m/n) and reaction rate constants of extraction and stripping of $[Au(CN)_2]^-$ via HFSLM by mixed extractants (0.25 mol/L D2EHPA and 0.25 mol/L TBP) in various vegetable oil-based diluents with 0.50 mol/L HCl as strippant.....111

จุฬาลงกรณ์มหาวิทยาลัย
CHULALONGKORN UNIVERSITY

Table 4.1 Source and purity of the chemicals used in this work.....140

Table 4.2 Verification results for distillation temperatures T of n-tetradecane and n-hexadecane at system pressure range of p = (0.13-6.7) kPa. 143

Table 4.3 Experimental saturated vapor pressures p_{sat} and calculated enthalpy $\Delta_{\mathrm{vap}}H$, entropy $\Delta_{\mathrm{vap}}S$ of vaporization and saturated liquid heat capacity C_{σ}^{l} for D2EHPA and TBP at different temperatures T .[a].....152

Table 4.4 Regression constants for the correlation of saturated vapor pressure p_{sat} 156

Table 4.5 Estimated acentric factor values ω of D2EHPA and TBP. 156

Table 4.6 Regression constants for the correlation of enthalpy of vaporization $\Delta_{\mathrm{vap}}H$ 160

Table 4.7 Regression constants for the correlation of entropy of vaporization $\Delta_{\mathrm{vap}}S$ and saturated liquid heat capacity C_{σ}^{l}. 164

Table S4.1 Previous works on thermophysical properties of pure D2EHPA and TBP. 169

Table S4.2 Calibration results of temperature T measurements. 183

Table S4.3 Calibration results of pressure p measurements. 183

Table S4.4 Repeatability (r), Reproducibility (R) and standard uncertainty $u(p)$ of vapor pressure measurement. 184

Table 5.1 Chemicals used in this study. 202

Table 5.2 Verification results for distillation temperatures T of n-dodecane and n-hexadecane at system pressure range of p = (0.13 – 6.7) kPa. 206

Table 5.3 Antoine equation parameters of pure components, namely D2EHPA, TBP and n-dodecane. 209

Table 5.4 Isobaric experimental VLE data of liquid phase (x_1) and vapor phase (y_1) mole fractions, activity coefficient (γ_1 and γ_2) of the system D2EHPA (1) + n-dodecane (2) at pressures of 0.13, 2.40 and 6.67 kPa[a].....210

Table 5.5 Isobaric experimental VLE data of liquid phase (x_1) and vapor phase (y_1) mole fractions, activity coefficient (γ_1 and γ_2) of the system TBP (1) + n-dodecane (2) at pressures of 0.13, 2.40 and 6.67 kPa[a].....211

จุฬาลงกรณ์มหาวิทยาลัย
CHULALONGKORN UNIVERSITY

Table 5.6 Experimental and calculated infinite dilution activity coefficient γ_1^{∞} and γ_2^{∞} for all systems. 213

Table 5.7 Thermodynamic consistency test of VLE data by Herington area test....217

Table 5.8 Parameters for the NRTL and Wilson models for D2EHPA (1) + n-dodecane (2) and TBP (1) + n-dodecane (2) at p = 0.13, 2.40 and 6.67 kPa.....222

Table S5.1 Critical properties namely, T_c, P_c and , Z_c of D2EHPA, TBP and n-dodecane. 227

จุฬาลงกรณ์มหาวิทยาลัย
CHULALONGKORN UNIVERSITY

LIST OF FIGURES

Figure 1.1 (a) Printed circuit boards (PCBs), and (b) Schema of layer configurations of the ENIG board finish.....1

Figure 1.2 Schematic diagram of the nickel and gold plating of the ENIG process.....2

Figure 1.3 Facilitated coupled-transport of ions through the liquid membrane.....8

Figure 2.1 Schematic diagram of the ENIG plating process on PCBs. 11

Figure 2.2 Schematic flow diagram of the separation system via HFSLM: **1** feed solution reservoir, **2** stripping solution reservoir, **3** hotplate and stirrer with Pt-100 temperature sensor, **4** peristaltic pump, **5** flow regulator valve, **6** flow meter, **7** pressure gauge, and **8** hollow fiber module. 18

Figure 2.3 Extraction percentage and concentration of Ni^{2+} and $[Au(CN)_2]^-$ in aqueous feed phase with continuous separation time (t): (a) 0.50 mol/L D2EHPA extractant and (b) 0.50 mol/L TBP extractant: feed phase; 15 mg/L Ni^{2+}, 25 mg/L $[Au(CN)_2]^-$, pH 8.6±0.05 | liquid membrane phase; 0.50 mol/L D2EHPA in kerosene | stripping phase; 0.50 mol/L HCl, pH 0.38±0.05 | $q_F = q_S$ = 200 mL/min | t = 2 h | T = 303±1 K. 26

Figure 2.4 Effect of mixed extractants on Ni^{2+} and $[Au(CN)_2]^-$ extraction from aqueous feed phase via HFSLM: feed phase; 15 mg/L Ni^{2+}, 25 mg/L $[Au(CN)_2]^-$, pH 8.6±0.05 | liquid membrane phase; 0.50 mol/L of total extractant concentration in kerosene | stripping phase; 0.50 mol/L HCl, pH 0.38±0.05 | $q_F = q_S$ = 200 mL/min | t = 2 h | T = 303±1 K.....27

Figure 2.5 Extraction percentage and concentration of Ni^{2+} and $[Au(CN)_2]^-$ in aqueous feed phase over separation time (t): feed phase; 15 mg/L Ni^{2+}, 25 mg/L $[Au(CN)_2]^-$, pH 8.6±0.05 | liquid membrane phase 0.25 mol/L D2EHPA and 0.25 mol/L TBP extractants in kerosene | stripping phase; 0.50 M HCl, pH 0.38±0.05 | $q_F = q_S$ = 200 mL/min | t = 2 h | T = 303±1 K.....28

Figure 2.6 Effect of concentration and molar ratio of the D2EHPA/ TBP synergistic extractants: feed phase; 15 mg/L Ni^{2+}, 25 mg/L $[Au(CN)_2]^-$, pH 8.6±0.05 | liquid membrane phase; mixed D2EHPA/TBP extractant in kerosene | stripping phase; 0.50 mol/L HCl, pH 0.38±0.05 | $q_F = q_S$ = 200 mL/min | t = 2 h | T = 303±1 K. 36

Figure 2.7a Effect of D2EHPA extractant concentrations: feed phase; 15 mg/L Ni^{2+}, 25 mg/L $[Au(CN)_2]^-$, pH 8.6±0.05 | liquid membrane phase; D2EHPA in kerosene |

stripping phase; 0.50 mol/L HCl, pH 0.38±0.05 | $q_F = q_S$ = 200 mL/min | t = 2 h | T = 303±1 K. 38

Figure 2.7b8Effect of TBP extractant concentrations: feed phase; 15 mg/L Ni^{2+}, 25 mg/L $[Au(CN)_2]^-$, pH 8.6±0.05 | liquid membrane phase; TBP in kerosene | stripping phase; 0.50 mol/L HCl, pH 0.38±0.05 | $q_F = q_S$ = 200 mL/min | t = 2 h | T = 303±1 K.....39

Figure 2.7c9Effect of mixed D2EHPA and TBP extractant concentrations (1:1 ratio): feed phase; 15 mg/L Ni^{2+}, 25 mg/L $[Au(CN)_2]^-$, pH 8.6±0.05 | liquid membrane phase; mixed of D2EHPA and TBP extractant in kerosene | stripping phase; 0.50 mol/L HCl, pH 0.38±0.05 | $q_F = q_S$ = 200 mL/min | t = 2 h | T = 303±1 K. 40

Figure 2.810Effect of strippant concentration: feed phase; 15 mg/L Ni^{2+}, 25 mg/L $[Au(CN)_2]^-$, pH 8.6±0.05 | liquid membrane phase; mixture of 0.25 mol/L D2EHPA and 0.25 mol/L TBP extractants in kerosene | stripping phase; HCl | $q_F = q_S$ = 200 mL/min | t = 2 h | T = 303±1 K.....45

Figure 2.911Stripping percentage of Ni^{2+} and $[Au(CN)_2]^-$ ions via HFSLM with various pH of HCl strippant: feed phase; 15 mg/L Ni^{2+}, 25 mg/L $[Au(CN)_2]^-$, pH 8.6±0.05 | liquid membrane phase; mixture of 0.25 mol/L D2EHPA and 0.25 mol/L TBP extractants in kerosene | stripping phase; HCl | $q_F = q_S$ = 200 mL/min | t = 2 h | T = 303±1 K.....46

Figure 3.1 Extraction percentage (%E): (a) Ni^{2+} and (b) $[Au(CN)_2]^-$ via HFSLM with various types of vegetable oil-based diluents. 80

Figure 3.2 pH of aqueous feed phase before (feed,i) and after (feed,f) separation via HFSLM, using various types of vegetable oil-based diluents in the liquid membrane phase. 82

Figure 3.3 Effect of mixed extractants 0.25 M D2EHPA and 0.25 M TBP on the synergistic extraction of Ni^{2+} and antagonistic extraction of $[Au(CN)_2]^-$ with various types of vegetable oil-based diluents: (a) palm oil, (b) sunflower oil (c) soybean oil (d) coconut oil, and (e) rice bran oil. 86

Figure 3.4 Stripping percentage (%S) of Ni^{2+} and $[Au(CN)_2]^-$ separation via HFSLM with various pH of stripping phase and vegetable oil-based diluents: (a) palm oil, (b) sunflower oil, (c) soybean oil, (d) coconut oil, and (e) rice bran oil. 90

Figure 3.5 Equilibrium distribution and concentration profiles of Ni^{2+} and $[Au(CN)_2]^-$ with time in the various phases (feed, liquid membrane and stripping): (a) palm oil, (b) sunflower oil, (c) soybean oil, (d) coconut oil, and (e) rice bran oil-based diluents. 95

Figure 3.6 Adaptability of the mathematical model to predict the extraction. 104

Figure A3.1 The separation system via HFSLM: **1** feed solution reservoir, **2** stripping solution reservoir, **3** hotplate and stirrer with Pt-100 temperature sensor, **4** peristaltic pump, **5** flow regulator valve, **6** flow meter, **7** pressure gauge, and **8** hollow fiber module. 114

Figure A3.2 Concentration profiles at steady-state of Ni^{2+} and other species across the supported liquid membrane using D2EHPA extractant. 115

Figure A3.3 Concentration profiles at steady-state of Ni^{2+} and other species across the supported liquid membrane using TBP extractant. 115

Figure A3.4 Concentration profiles at steady state of Ni^{2+} ions and other species across liquid membrane using mixed extractants of D2EHPA and TBP.....116

Figure A3.5 Schema of metal ions transport across tube and shell sides of the hollow fibers. 120

Figure 4.1 Structures of the organophosphorus extractants of this study. 139

Figure 4.2 Schematic diagram of the vacuum distillation apparatus (i-Fischer Engineering GmbH, AUTODEST® 851 AC) [36]. 142

Figure 4.3 Experimental saturated vapor pressures p_{sat} of D2EHPA in temperature range T = (450-550) K. ●, This work; ■, ref [1]; and ---, fitted by Eq. (4.4). 153

Figure 4.4 Experimental saturated vapor pressures p_{sat} of TBP in the temperature range T = (380-480) K. ●, This work; ■, ref [1]; ▲, ref [20]; ♦, ref [24]; ○, ref [28]; Δ, ref [29]; □, ref [30]; x, ref [31]; ◊, ref [52]; and ---, fitted by Eq. (4.4). 154

Figure 4.5 The electrostatic charge potential surface for molecule (a) D2EHPA and (b) TBP.....155

Figure 4.6 Dimers of D2EHPA.....155

Figure 4.7 Enthalpy of vaporization $\Delta_{\mathrm{vap}}H$ in the temperature range T = (380-550) K. ●, D2EHPA; ■, TBP; and ---, fitted by Eq. (4.10).....161

Figure 4.8 Plots of $\frac{\mathrm{d}\left(\Delta_{\mathrm{vap}}H\right)}{\mathrm{d}T}$ versus T for pure D2EHPA and TBP in this work. ΔT = 1.0 K; ●, D2EHPA; ■, TBP.....162

Figure 4.9 Entropy of vaporization ΔS_{vap} in the temperature range T = (380-550) K. ●, D2EHPA; ■, TBP; ▲, Trouton's rule; and ---, fitted by Eq. (4.12). 163

Figure 4.10 Saturated liquid heat capacity C_{σ}^{l} in the temperature range T = (380-550) K. ●, D2EHPA; ■, TBP; and ---, fitted by Eq. (4.18).....167

Figure 5.1 Schematic diagram of the experimental glass vapor-liquid equilibrium ebulliometer apparatus: **1** Heating bulb (inside immersion heater and outside flow heater) **2** Cottrell pump **3** Separation Chamber **4** Condenser **5** Mixing chamber **6** Vapor-phase temperature sensor (Pt-100) **7** Liquid-phase sampling point **8** Vapor-phase sampling point **9** Liquid-phase sampling vessel **10** Vapor-phase sampling vessel [13].....206

Figure 5.2 Comparison of saturated vapor pressure of pure D2EHPA. ●, this work; ▲ [21]; ■, [16].....207

Figure 5.3 Comparison of saturated vapor pressure of pure TBP. ●, this work; ▲, [21]; ■, [22]; ▲, [23]; ■, [24]; ●, [25]; ■, [19].....208

Figure 5.4 Comparison of saturated vapor pressure of pure n-dodecane. ●, this work; ▲, [26]; ■, [27]; ▲, [28].....208

Figure 5.5 Comparison of saturated vapor pressure of pure n-hexadecane. ●, this work; ▲, [29]; ■, [26]; ▲, [15].....209

Figure 5.6 VLE phase diagrams for D2EHPA (1) + n-dodecane (2). ●, ▲, ■: experimental data for $T-x$ plot at 0.13, 2.40 and 6.67 kPa, respectively; ○, Δ, □: experimental data for $T-y$ plot at 0.13, 2.40 and 6.67 kPa, respectively; ******: Raoult's law, – – –: NRTL, ——: Wilson activity coefficient model for $T-x-y$ plots.....214

Figure 5.7 VLE phase diagrams for TBP (1) + n-dodecane (2). ●, ▲, ■: experimental data for $T-x$ plot at 0.13, 2.40 and 6.67 kPa, respectively; ○, Δ, □: experimental data for $T-y$ plot at 0.13, 2.40 and 6.67 kPa, respectively; ******: Raoult's law, – – –: NRTL, ——: Wilson activity coefficient model for $T-x-y$ plots.....215

Figure 5.8 Comparison of VLE phase diagrams between D2EHPA (1) + n-dodecane (2) and TBP (1) + n-dodecane (2) at pressure of 0.13, 2.40 and 6.67 kPa. ●, ○: $T-x-y$ plots of D2EHPA (1) + n-dodecane (2); ▲, Δ: $T-x-y$ plots of TBP (1) + n-dodecane (2); ******: Raoult's law, – – –: NRTL, ——: Wilson activity coefficient model for $T-x-y$ plots.....216

Figure 5.9 Diagrams of $\ln(\gamma_1/\gamma_2)$ to x_1 for the binary system of D2EHPA (1) + n-dodecane (2).....218

Figure 5.10 Diagrams of $\ln(\gamma_1/\gamma_2)$ to x_1 for the binary system of TBP (1) + n-dodecane (2).....219

Figure S5.111FT-IR spectrum of pure D2EHPA.....230

Figure S5.212FT-IR spectrum of pure TBP.....231

Figure S5.313FT-IR spectrum of pure n-dodecane. 231

Figure S5.414 Calibration curve between mass fraction and peak area from FT-IR spectrum of D2EHPA (1) + n-Dodecane (2) binary mixtures. 232

Figure S5.515 Calibration curve between mass fraction and peak area from FT-IR spectrum of TBP (1) + n-Dodecane (2) binary mixtures. 232

จุฬาลงกรณ์มหาวิทยาลัย
CHULALONGKORN UNIVERSITY

CHAPTER I

INTRODUCTION

1.1 General introduction

The electroless nickel immersion gold (ENIG) plating process is a flat and solderable metal plating process applied in the manufacture of printed circuit boards (PCBs), especially a flexible circuit type and ceramic substrates. Recently, ENIG plating has received much attention since it meets the requirements for lead-free assembly [1, 2]. As illustrated in Fig. 1.1 all surfaces intended for the finish first have a layer of nickel applied to the copper layer in an electroless process, as a diffusion barrier. In a second step, a thin layer of gold is plated over the surface [1].

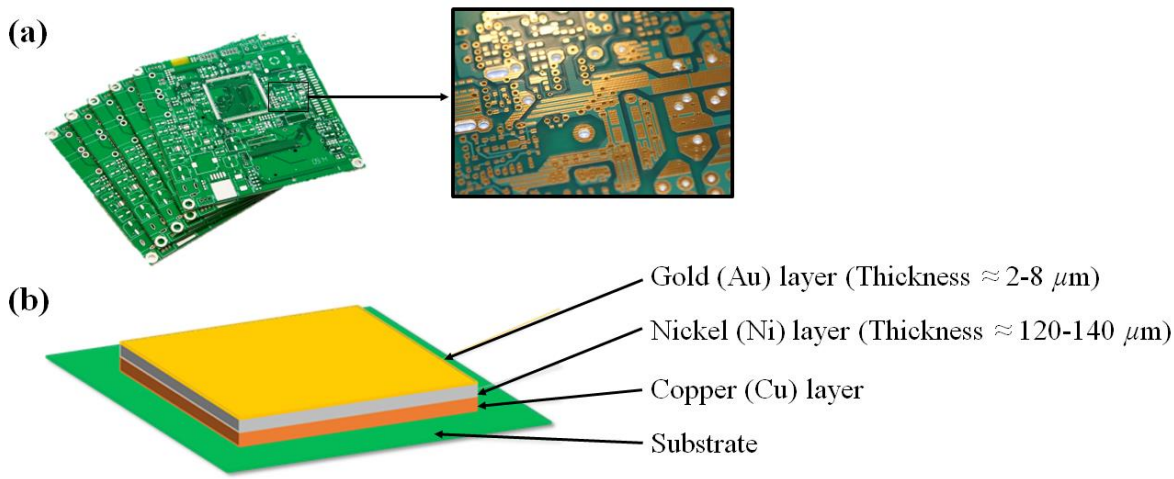

Figure 1.1 (a) Printed circuit boards (PCBs), and (b) Schema of layer configurations of the ENIG board finish.

In Fig. 1.2, it is noted that during the plating process, excess nickel and gold plating, which adheres to the workpieces, are removed. As a result, a significant amount of Ni^{2+} and $[Au(CN)_2]^-$ accumulates in the rinse water baths and can then be collected. Thus, the opportunity to reclaim these precious and valuable metals and reuse them to achieve cost reduction and sustainable wastewater treatment is paramount.

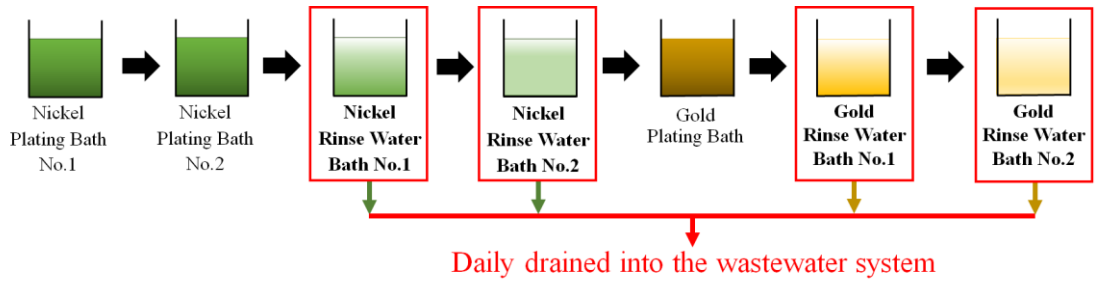

Figure 1.2 Schematic diagram of the nickel and gold plating of the ENIG process.

Several conventional methods have been highlighted in the process of wastewater treatment for the separation of target metal ions i.e. chemical precipitation, coagulation and flocculation, ion exchange, adsorption, electrochemical treatment, and photocatalysis [3-7]. However, these methods have several disadvantages such as high capital and operational costs, and generate metal sludge, which require further treatment. Solvent extraction, one of the conventional methods, has been widely used in hydrometallurgical processes owing to its high efficiency of purification and simple operation [8]. Yet, solvent extraction has its limits and is found to be ineffective in separating the target species at trace concentration level [9]. Both separation and recovery of trace concentration of Ni^{2+} and $[Au(CN)_2]^-$ are valuable, and an appropriate method needs investigating.

Recently, liquid membranes (LM) have received much attention, involving the separation and removal of target organic and inorganic species [10]. Due to its

จุฬาลงกรณ์มหาวิทยาลัย
Chulalongkorn University

simplicity, high efficiency, high selectivity, cost-effectiveness, low energy and chemical consumption, the hollow fiber supported liquid membrane (HFSLM) technique, especially, is a promising system for processing target metal ions [11, 12]. Furthermore, such a method can simultaneously perform extraction and stripping in a single-step of operation. The high mass transfer area (surface area) of the HFSLM module (approximately 10^4 m^2/m^3) attains a high separation rate [13]. HFSLM can be regarded as a green technology over conventional methods on account of its reusability of liquid membrane and zero discharge of effluent. Such are the advantages of HFSLM over conventional methods. Accordingly, the HFSLM technique has been extensively investigated including extraction and separation of metal ions [14, 15], removal of contaminants from wastewater [16, 17], and extraction of drugs and amino acids [18, 19]. In Table 1.1 and 1.2, a summary of previous studies on Ni^{2+} and $[Au(CN)_2]^-$ separation via different membrane techniques are presented.

จุฬาลงกรณ์มหาวิทยาลัย
CHULALONGKORN UNIVERSITY

Table 1.1 Summary of previous research on separation of Ni^{2+} via various membrane systems.

Other ions	Sources	Separation techniques	Initial concentration of Ni^{2+} ions in feed solution	Extractant	Diluent	Stripping solutions	Separation or recovery efficiency	Publishing Year [Ref.]
Na^+	Spent Electroless Nickel (EN) plating bath	Electrodialysis (Ion exchange membrane)	3,690 mg/L (pH = N/A)	-	-	-	30%	1999 [20]
Co^{2+}	Industrial Wastewater	Micellar-enhanced UF (Pressure = 0.5-2 bar)	29.35 mg/L (pH = 5.5)	1) D2EHPA 2) EHPNA 3) PONPE10 4) SDS	-	-	46-54%	1999 [21]
SO_4^{2-}, Cl^-	Electroplating Rinse Water	NF (Pressure = 2.8 bar)	29.35–880.75 mg/L (pH = 3-7)	-	-	-	89-96%	1999 [22]
-	Industrial Wastewater	Micellar-enhanced UF (Pressure = 1-5 bar)	10 mg/L (pH = 5.3-6.3)	1) SDS 2) MAPE	-	-	88-99.2%	2002 [23]
Co^{2+}	Industrial Wastewater	Chelation – UF (Pressure = 2-5 bar)	25 mg/L (pH = N/A)	PEI	-	-	24.1-94.2%	2002 [24]
NO_3^-	Spent rinse water from metal plating	RO (Flat sheet membranes) (Pressure = 20 bar)	3.36 mg/L (pH = 3.6-7)	-	-	-	96.8%	2002 [25]
Cu^{2+}, Zn^{2+}	Wastewater from electronic industry	Flotation – UF (Pressure = <1 bar)	3.3 mg/L (pH = 8-10)	Powdered synthetic zeolites	-	-	98.5%	2003 [26]
Na^+, Mg^{2+}, Cl^-, SO_4^{2-}	Wastewater from Ni-P electroless plating	NF (Pressure = 2-8 bar)	5.87 mg/L (pH = 4-8)	-			92-93%	2004 [27]
Zn^{2+}, Cl^-	Synthetic Wastewater	RO (Pressure = 11 bar)	44-169 mg/L (pH = 6.5-7.5)	EDTA	-	-	99.7%	2005 [28]
Cu^{2+}, Na^+, SO_4^{2-}	Synthetic Wastewater	RO (Pressure = 5 bar)	500 mg/L (pH = 4-11)	EDTA	-	-	99.5%	2007 [29]
Cu^{2+}, SO_4^{2-}	Industrial Wastewater	Complexation – UF (Pressure = 2-4 bar)	50 mg/L (pH = 3-9)	PEI	-	-	98-99%	2008 [30]
SO_4^{2-}	Synthetic wastewater	NF (Pressure = 4-20 bar)	5-250 mg/L (pH = 2-8)	-			92-98%	2008 [31]
Zn^{2+}, Cl^-, SO_4^{2-}	Industrial wastewater	Complexation – UF (Pressure = 5 bar)	58.71 mg/L (pH = 7-9)	PAA	-	-	31.5-98.2%	2009 [32]
Na^+, Mg^{2+}, Ca^{2+}, SO_4^{2-}, Cl^-	Synthetic wastewater	NF (Flat sheet membrane) (Pressure = 4-20 bar)	5-10 mg/L (pH = 2-10)	-	-	-	96.87-97.96%	2009 [33]
Cu^{2+}, Cd^{2+}, Zn^{2+}, Ca^{2+}, Mg^{2+}, Al^{3+}, Fe^{2+}, PO_4^{3-}, SO_4^{2-}, F^-, Cl^-, NO_3^-	Wastewater from fertilization process	Micellar-enhanced UF Pressure = 3 bar	0.95-1.76 mg/L (pH = 3.5-5)	SDS	-	-	73.6-85.1%	2012 [34]
-	Diluted wastewater	MFEDI	10 mg/L	-	-	-	88%	2015 [35]

Note: **MFEDI** = Membrane-free electrodeionization, **NF** = Nanofiltration, **RO** = Reverse osmosis, **UF** = Ultra filtration, **D2EHPA** = Di-(2-ethylhexyl) phosphoric acid, **EDTA** = Ethylenediaminetetraacetic acid, **EHPNA** = 2-Ethylhexyl phosphonic acid mono-2-ethylhexyl ester, **MAPE** = Monoalkylphenol polyetoxylate (non-ionic surfactant), **PAA** = Polyacrylic acid, **PEI** = Polyethylenimine, **PONPE10** = Polyoxyethylene nonylphenyl ether with 10 ethylene oxide units (non-ionic surfactant), **SDS** = Sodium dodecyl sulfate (anionic surfactant)

Table 1.2 Summary of previous research on separation of $[Au(CN)_2]^-$ via various membrane systems.

Other ions	Sources	Separation techniques	Initial concentration of $[Au(CN)_2]^-$ ions in feed solution	Extractant	Diluent	Stripping solutions	Separation or recovery efficiency, %	Publishing Year [Ref.]
Fe^{2+}, Co^{3+}, Cu^{2+} Ni^{2+}, Ag^{+}, Ca^{2+}, CN^{-}	N/A	SLM	0.1 mg/L (pH = 8)	1) Amines 2) TBP	n-Heptane	Methanol	N/A	1992 [36]
Fe^{2+}, Cu^{2+}, Ni^{2+}, $Co3^{+}$, Ag^{+}, CN^{-}	N/A	SLM	100 mg/L (pH = 7-10)	Amines	n-Heptane	NaOH, Tu + H_2SO_4	N/A	1993 [37]
Fe^{2+}, Cu^{+}, Ni^{2+}, Ag^{+}, CN^{-}	N/A	HFSLM	10 mg/L (pH = 9-12)	LIX-79 (2 – 16% v/v)	n-Heptane	NaOH	99%	2000 [38]
Ni^{2+}, Fe^{3+}, CN^{-}	N/A	FSSLM	0.025-0.254 mg/L (pH = 1-11)	1) Cyanex 921 2) Cyanex 923 (5 - 20% w/v)	Xylene	Distilled water	87.3%	2002 [39]

Note: **SLM** = Supported liquid membrane, **HFSLM** = Hollow fiber supported liquid membrane, **FSSLM** = Flat-sheet supported liquid membrane, **TBP** = Tributyl phosphate,

LIX-79 = 1,3-Bis(2-ethylhexyl) guanidine, **Cyanex 921** = Trioctylphosphine oxide, **Cyanex 923** = Mixture of Tri-n-hexylphosphine oxide and tri-n-octylphosphine oxide, **N/A** = Not available

HFSLM is a cutting-edge system that has been well applied in separation processes, is seen as a promising system for processing target species. HFSLM has high selectivity allowing simultaneous extraction and stripping processes in a single-step. However, no research has fully investigated the use of the HFSLM technique for the simultaneous and selective separation of Ni^{2+} and $[Au(CN)_2]^-$ from rinse wastewater of the ENIG process.

1.1.1 Extractants

The extractant used as a carrier for supported liquid membrane (SLM) is basically an organic solvent. Metal ion transfer through supported liquid membrane is described below. The chemistry of extraction reaction can be classified as follows [40-42]:

Extraction by compound formation

Extraction reaction via compound formation mechanism occurs when extractants exhibit chelating properties or acidic properties. The mechanism of extraction via compound extraction is shown, accordingly:

$$M^{n+}_{(aq)} + nHR_{(org)} \rightleftharpoons MR_{n(org)} + nH^{+}_{(aq)} \quad (1.1)$$

Chelating extractants: These types of extractants can react with cation species. Such extractants chemically bond to cation species at two sites in the same manner as holding an object between the ends of the thumb and the index finger. When the chelating extractants bond with the cation species, hydrogen ion (H^+) is released into the feed solution. Thus, the efficiency of extraction increases with increased pH of feed solution. As the pH of feed solution is

decreased, stripping reaction is seen to occur. Examples of chelating extractants are LIX-84I, LIX 64N and LIX 62N etc.

Acidic extractants: Acidic extractants are organic acids and their derivatives and are related to proton donors. Acidic extractants react with cation species in the feed solution the same as chelating extractants. Some commercially acidic extractants are D2EHPA, PC88A, Cyanex 272 (phosphoric acid derivatives) and so forth. These types of extractants have been widely used in hydrometallurgical processes for the extraction of various metal ions such as Cu, Ni, Fe, Mn etc.

Extraction by ion-pair formation

Basic extractants (anion-exchangers) are utilized to extract metal ions via ion-pair formation chemistry. Basic extractants contain primary, secondary, tertiary amines, and their derivatives, quaternary amine salts and other proton acceptors. Amine based extractants employ two modes of action during extraction via ion pair formation chemistry. Initially, amine based extractants (as a free base form) are able to extract acid from the aqueous solution. Then, by anion exchange reaction, metal ions are extracted. Alamine 336, Aliquat 336, and Alamine 304 are examples of basic extractants.

Extraction by solvation

The solvating extractants or neutral extractants, also known as selective extractants, are weak basic: they extract either neutral metal complexes or acids by forming a solvate. These types of extractants are organic species with electron donor or acceptor properties, or solvating carriers. Solvating extractants will coordinate with

certain neutral metal ions by replacing water molecules of hydration around neutral metal ions. Thereby, hydrophobic ions are formed. Some solvating extractants are MIBK, TBP, TOPO etc. The extraction mechanism for extraction reaction via solvation is shown in Eqs. (1.2) and (1.3) [43-45]:

$$M_nX_{(aq)} + yS_{(org)} \rightleftharpoons MX_nS_{y(org)} \tag{1.2}$$

$$HMX_{n+1(aq)} + yS_{(org)} \rightleftharpoons \left(HS_y\right)^{+}\left(MX_{n+1}\right)^{-}_{(org)} \tag{1.3}$$

1.1.2 Diluents

Diluents have been applied to diminish the viscosity of solvents, which leads to the diffusivity of the solute complex within the membrane. Generally, diluents are inert solvents, and should have high dielectric constant, low viscosity, high boiling point, and low toxicity. Diluents play a significant role on the extraction of metals regarding both physical and chemical interactions that exist between diluents and extractants. Various types of diluents are widely used in hydrometallurgical processes such as kerosene, toluene, hexane, cyclohexane etc. [46]. Solvent physical properties are seen to have an influence on the extraction of metal ions. As the dipole moment and dielectric constant of diluents decrease, extraction efficiency increases.

1.1.3 Feed solutions

Real rinse wastewater from the ENIG plating process used as the feed solution in this study was obtained from Mektec Manufacturing Co., Ltd., Thailand. The characteristics of obtained rinse wastewater are described in Table 1.3.

Table 1.3 The key characteristics of real rinse wastewater in this study.

Color	pH	Ni^{2+} (mg/L)	$[Au(CN)_2]^-$ (mg/L)
Light green to colorless	8.6±0.5	15	25

1.1.4 Stripping solutions

As regards metal recovery and the regeneration of an extractant, stripping reaction is significant. Therefore, types and concentrations of stripping solutions play an essential role in the performance of metal recovery across the HFSLM system. The selection of stripping solutions depends on both the target species of metal extracted and the types of extractants used.

In the case of target species i.e. metal cations, an acidic extractant or a chelating extractant is employed. Therefore, an acidic stripping solution is required. Thus, H^+ in acidic stripping solution substitutes metal cations in the organometallic complex; thereby, the free metal cations are captured by the stripping solutions.

Regards metal anions extraction, the basic extractant or neutral extractant is applied. Accordingly, a basic stripping solution is required. Thus, anions in the basic stripping solution substitutes metal anions in the organometallic complex; thereby, the metal anions are released into the stripping solutions.

A number of researches have been undertaken in creating and improving novel extractants. Meanwhile, few studies have investigated the enhancement of stripping efficiency. It is observed that an increase in stripping concentration can result in higher stripping efficiency.

จุฬาลงกรณ์มหาวิทยาลัย
CHULALONGKORN UNIVERSITY

1.1.5 Transportation of metal ions across HFSLM

The transport phenomena of target species that diffuse through the liquid membrane phase can be achieved either via passive transport or active transport (or facilitated) [47, 48].

Passive transport

Passive transport means simply the diffusion of solute across the liquid membrane phase due to their concentration gradient in the feed phase and the stripping phase. Such a process is limited by the equilibrium condition between the two aqueous phases, and is mainly used when one species in a liquid mixture is soluble in the organic phase.

Facilitated transport

In facilitated transport, the liquid membrane phase contains a carrier (or extractant) dissolved in an organic solvent (or diluent). The carrier acts as a catalyst because it increases the solubility of the chemical space in the membrane by promoting the transfer speed. The driving force of facilitated transport is the concentration gradient between the feed phase and the stripping phase. Facilitated transport can be divided as follows:

Co-transport: In this case, the neutral carrier is employed and the feed solutions contain a pair of cations and anions (M^{m+} mX^{-}) associated and extracted (dissociated) reversibly by carrier (*L*). The cation and anion migrate in the same direction of the source phase to the stripping phase owing to the concentration gradient. The mechanism of this type of transport is shown below:

$$M^{m+}{}_{(aq)} + mX^{-}{}_{(aq)} + L_{(org)} \rightleftharpoons \left(ML^{m+}mX^{-}\right)_{(org)} \qquad (1.4)$$

Counter-transport: In this case, the carrier can be acidic or basic. For counter cation transport, the carrier in the membrane phase is an acid, and this process is done by a cation-exchange proton. The mechanism of counter cations transport is described in Eq. (1.5).

$$M^{m+}{}_{(aq)} + mHL_{(org)} \rightleftharpoons \left(ML_m\right)_{(org)} + mH^{+}{}_{(aq)} \tag{1.5}$$

In the case of the counter-facilitated transport of anions, the carrier in the liquid membrane phase exchanges an anion (basic agent) by interaction with the substrate at the interface between feed and liquid membrane phases. Thus, a neutral entity (A^-L^+) is formed. Thereafter, A^-L^+ diffuses through the liquid membrane phase to the interface between liquid membrane and stripping phases. The anion (A^-) is released and diffuses to the stripping phase, whereas the cationic species (L^+) associates with another anion (X^-) present in the stripping phase to form LX. Subsequently, LX diffuses through the liquid membrane in the opposite direction of A^-. Anions facilitated transport is governed by the association between the substrate and carrier, the gradient of the concentration of anion X and electroneutrality of the feed and stripping phases. The mechanism of counter anions transport is described in Eq. (1.6). In Fig. 1.3, the facilitated transport of ions through liquid membrane is depicted [48].

$$A^-{}_{(aq)} + XL_{(org)} \rightleftharpoons \left(A^-L^+\right)_{(org)} + X^-{}_{(org)} \tag{1.6}$$

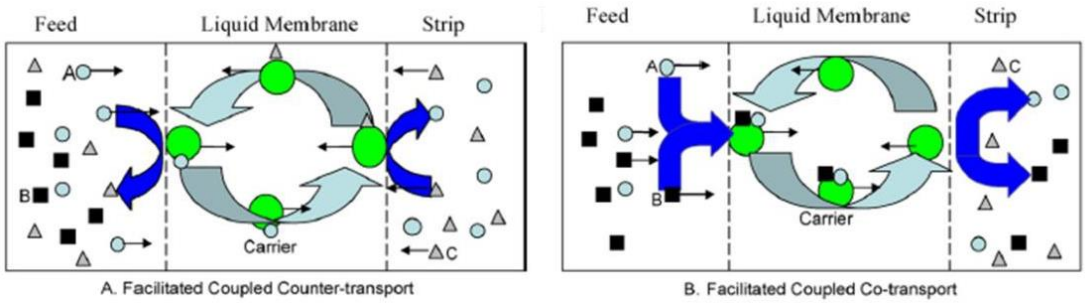

Figure 1.3 Facilitated coupled-transport of ions through the liquid membrane.

1.1.6 Mass transfer across HFSLM

The overall mass transfer resistance across HFSLM is considered based on the summation of each individual mass transfer resistances: namely, (1) the liquid phase resistance in the feed phase, (2) the interfacial resistance of the extraction reaction, (3) the membrane phase resistance, (4) the shell-side resistance, (5) the resistance of the stripping reaction, and (6) the strip-side resistance, which can be expressed as in Eq. (1.7) [49].

$$\frac{1}{K}=\frac{1}{k_a}+\frac{1}{k_e}+\frac{1}{m_f k_m}+\frac{1}{m_f k_o}+\frac{1}{m_f k_s}+\frac{1}{\left(m_f / k_s\right) k_{as}} \tag{1.7}$$

where k_a is the mass transfer coefficient in the feed phase, k_e is the mass transfer due to extraction reaction rate, k_s is the mass transfer due to stripping reaction rate, k_m is the mass transfer coefficient of the complex species in the LMs phase, k_o is the mass transfer coefficient in the shell side and k_{as} is the mass transfer coefficient in the stripping solution. The partition coefficient of target metal is the ratio between concentrations of target metal ions in the organic phase divided by the concentration of target metal ions in the feed phase.

Based on the concept of instantaneously stripping reaction was found to occur, the mass transfer resistance of the stripping side can be negligible. Thus, the total mass transfer resistances can be simplified, as shown in Eq. (1.8):

$$\frac{1}{K}=\frac{1}{k_a}+\frac{1}{k_e}+\frac{1}{m_f k_m}+\frac{1}{m_f k_o} \tag{1.8}$$

Eq. (1.9), the mass transfer coefficient in the aqueous phase is given:

$$k_a=1.62\frac{D_f}{d_i}\left(\frac{d_i^2 v_f}{D_f}\right)^{0.33} \tag{1.9}$$

where D_f is the diffusivity of metal ions in feed phase (cm^2/s), v_f is the velocity of feed solution (cm/s) and d_i is the inner diameter of the fiber (cm).

The mass transfer coefficient in the liquid membrane phase can be calculated, as shown in Eq. (1.10):

$$k_m=\frac{D_m \varepsilon d_{lm}}{\delta \tau d_o} \tag{1.10}$$

จุฬาลงกรณ์มหาวิทยาลัย
Chulalongkorn University

where D_m is the diffusivity of metal ions in the liquid membrane (cm^2/s), d_{lm} is the log-mean diameter (cm), d_o is the outer diameter of the fiber (cm), ε is the porosity of the hollow fiber, τ is the tortuosity of the hollow fiber, and δ is the membrane thickness (cm).

The mass transfer coefficient on the shell side can be evaluated by Eq. (1.11):

$$k_a=1.25\frac{D_m}{d_h^{0.07}}\left(\frac{d_h v_s}{\vartheta L}\right)^{0.93}\left(\frac{\upsilon}{D_m}\right)^{0.33} \tag{1.11}$$

where v_s is the velocity of stripping solution (cm/s), and υ is the kinematic viscosity (cm^2/s).

The diffusivity of metal ions can be calculated by using the empirical equation as proposed by Wilke and Chang [50] as shown below:

$$D_m = \frac{7.4\times10^{-8}\left(\phi_w M_w\right)^{1/2} T}{\eta_w \upsilon_m^{0.6}} \tag{1.12}$$

where ϕ_w is the association factor of water, M_w is the molecular weight of water, η_w is the viscosity of water, and υ_m is the molar volume of metal ions species at normal boiling point.

1.1.7 Flow patterns of HFSLM

The flow patterns in the HFSLM operation can be classified as follows:

Batch operation

Batch operation is suitable for the separation of target metal ions from a small volume of aqueous feed solutions and slow extraction and stripping reactions. Both aqueous feed and stripping solutions were circulated along the tube side and shell side, respectively. High efficiency regards the separation of metal ions can be achieved by this type of flow pattern.

Continuous operation

This type of flow pattern is suitable for the separation of target metal ions in a large volume of feed solutions. Continuous operation can be carried out by connecting the module in series or parallel mode. Both aqueous feed and stripping solutions are fed single-pass flow or one-through mode. In the case of a series module continuous

operation, a high residence time of both aqueous solutions is needed. This mode is favorable for slow reactions of extraction and stripping. On the other hand, parallel module continuous operation is recommended for fast reaction since a shorter residence time is required compared with the series mode.

Semi-continuous operation

Semi-continuous operation is a continuous process of a large volume of feed solution. Such an operation can be carried out by a single-pass flow of feed solution and circulated flow of stripping solution. Regards this type of flow, a concentration of metal ions in stripping solution can be achieved up until equilibrium is reached.

1.1.8 Properties of HFSLM

HFSLM used in this work is a 2.5 x 8 inch Liqui-Cel® Extra-Flow which contains microporous polypropylene hollow fibers. The microporous polypropylene fibers are woven into fabric and wrapped around a central-tube feeder to supply the shell side fluid. Properties of the HF module are shown in Table 1.4.

จุฬาลงกรณ์มหาวิทยาลัย
CHULALONGKORN UNIVERSITY

Table 1.4 Properties of the HF module.

Properties	Units	Values
Material		Polypropylene
Module diameter	m	6.3×10^{-2}
Module length	m	2.03×10^{-1}
Number of hollow fibers	fibers	35,000
Effective length of a hollow fiber	m	1.5×10^{-1}
Inside diameter of a hollow fiber	m	2.4×10^{-4}
Outside diameter of a hollow fiber	m	3×10^{-4}
Average pore size	m per fiber	3×10^{-8}
Pore size	m per fiber	5×10^{-8}
Porosity	-	3×10^{-2}
Effective surface area	m^2 per fiber	1.4
Area per unit volume	$m^2 \cdot m^{-3}$	2.93×10^{3}
Tortuosity factor	-	2.6
Maximum pressure difference	$kg\cdot m^{-2}$	4.2×10^{4}
Operating temperature	K	273-333

จุฬาลงกรณ์มหาวิทยาลัย
CHULALONGKORN UNIVERSITY

1.1.9 Aqueous feed acidity

The acid-base condition in feed solution plays an important role in metal ions separation. In order to optimize the suitable acid-base condition, transport mechanisms of metal ions are examined [51, 52].

In the case of coupled facilitated counter-transport: H^+ transport from the stripping phase to the aqueous phase, the dissociation equilibrium constant of extractant (pKa) is taken together in order to provide the driving force. The acidity values are seen to decrease in the following order i.e. $pH_{feed} > pKa > pH_{stripping}$.

In the case of coupled facilitated co-transport, it is found that the pH of the stripping phase is higher than that in the aqueous feed solution. This type of transport corresponds to the decomposition of acidic molecules in aqueous feed solution and the reaction of metal anion complexes with anions in the stripping phase.

In the case of simple facilitated transport, the pH of both aqueous solutions does not affect this type of transport mechanism due to the solvating interactions at the interfaces, which occurred.

จุฬาลงกรณ์มหาวิทยาลัย
Chulalongkorn University

1.1.10 Carrier concentration

It is evident that extraction and stripping percentages increase, when carrier concentration is increased. However, the percentages of extraction decrease due to the viscosity at higher carrier concentration [9].

1.1.11 Flow rates of both aqueous solutions

Flow rates of both aqueous solutions play an important role on the stability of liquid membrane and the contacting time of target species and liquid membrane. It has been reported that higher flow rates of both aqueous phases lead to a decrease in contacting

time and degrade the stability of liquid membrane. Equal flow rates of both aqueous solutions are recommended, therefore, in order to prevent the pressure drop in the system [53].

1.1.12 Flow patterns of aqueous solutions

Two types of flow patterns fed through the HFSLM system are (1) co-current, and (2) counter-current. It is noted that, the counter-current pattern provides a variation in concentration of metal ions and H^+ in both aqueous phases, which are a driving force in this system, thus the separation efficiency increases [54].

1.1.13 Mathematical modelling

Mathematical modelling for Ni^{2+} transportation across HFSLM system has been developed. The mass transfer coefficients were calculated in order to determine the rate controlling step through the HFSLM system. Kandwal et. al. [55] developed the mathematical model based on convection and diffusion of cesium ions.

Herein, a mathematical modelling for the transportation of Ni^{2+} via HFSLM was developed. Axial convection, axial diffusion, radial diffusion and chemical reactions were investigated via mathematical modeling.

1.2 Objectives of the dissertation

(I) To investigate the influence of operating parameters on the separation of Ni^{2+} from the rinse wastewater of the ENIG plating process via HFSLM.

(II) To develop a mathematical modelling for Ni^{2+} extraction and stripping (recovery).

1.3 Scope of the dissertation

This study highlights the exploration of an efficient method at trace level of Ni^{2+} and $[Au(CN)_2]^-$ separation from the rinse wastewater of the ENIG plating process. The scope of this study is as follows:

(I) The experiments have focused on the separation of Ni^{2+} and $[Au(CN)_2]^-$ from the rinse wastewater of the ENIG plating process.

(II) The investigated parameters are as follows:

- Type and concentration of extractants
- Synergistic extractants
- Type of diluents
- Type and concentration of stripping solutions
- Reaction time

(III) The mathematical model was employed to describe the experimental results.

(IV) The model was developed for Ni^{2+} extraction and stripping based on mass conservation concept. The model was validated by comparison with the experimental results.

จุฬาลงกรณ์มหาวิทยาลัย
CHULALONGKORN UNIVERSITY

1.4 Expected results

(I) High efficiency of Ni^{2+} extraction and stripping from the rinse wastewater of the ENIG plating process.

(II) Validation of the mathematical model based on mass conservation (axial convection, axial diffusion and radial diffusion) and chemical reaction.

1.5 Description of the dissertation

This dissertation is divided into 6 chapters. Chapter I provides a brief introduction and rationale of this work. Chapter II presents the published articles regarding the selective separation of Ni(II) from the rinse wastewater of the electroless nickel immersion gold (ENIG) plating process via HFSLM. Additionally, vegetable oil-based diluents are employed in order to find alternative greener diluents in order to curb environmental problems, as shown in Chapter III. Chapter IV reports the saturated vapor pressure data of D2EHPA and TBP, which is usefully employed for the design of a distillation column or evaporator for recycling of both extractants from organic wastewater. Furthermore, in Chapter V, the experimental isobaric vapor-liquid equilibrium (VLE) data for the binary systems of D2EHPA + n-dodecane and TBP + n-dodecane were measured at pressures of 0.13, 2.40 and 6.67 kPa. Chapter VI summarizes the conclusion of this dissertation. Chapters II-V are outlined as follows:

Chapter II

จุฬาลงกรณ์มหาวิทยาลัย
CHULALONGKORN UNIVERSITY

This chapter aims to investigate the performance of the HFSLM technique and the synergistic binary mixture of D2EHPA/TBP as an effective way to simultaneously and selectively separate the valuable metal ions, in trace amounts, of Ni^{2+} and $[Au(CN)_2]^-$ in the real rinse wastewater of the ENIG process. The effects of several process parameters have been investigated e.g. the concentrations and molar ratios of D2EHPA and TBP in the liquid membrane phase, types of strippant, and pH of stripping solutions. Herein, a novel approach for a better understanding of the structural chemistry and reaction mechanisms in the synergistic system is provided. Full details are available in

Chapter II and in the published article in the Arabian Journal of Chemistry 14 (2021) Article 103427 [56].

Chapter III

This chapter highlights the effect of various types of vegetable oils as non-toxic diluents on the elimination of a low concentration of Ni^{2+}, and sets out to recover $[Au(CN)_2]^-$ from the real rinse wastewater of the ENIG plating process via HFSLM. Parameters studied are as follows: types and concentration of extractants, types of vegetable-oil based diluents used to prepare the liquid membrane as well as pH and concentration of the stripping solutions. Performance of separation systems are investigated in terms of the efficiency of extraction and stripping of Ni^{2+}, $[Au(CN)_2]^-$, distribution ratio, selectivity and synergistic coefficient. Moreover, a mathematical model, based on conservation of mass considering axial convection, diffusion, reactions at the liquid-membrane interfaces, and mass accumulation, has been developed to predict the extraction and stripping of Ni^{2+}. Full details are available in Chapter III.

จุฬาลงกรณ์มหาวิทยาลัย
CHULALONGKORN UNIVERSITY

Chapter IV

This chapter investigates the saturated vapor pressure of D2EHPA and TBP extractants used in liquid membrane phase of the HFSLM system. Saturated vapor pressure and temperature are necessary thermophysical properties of any fluid system in distillation and evaporation processes. These properties are also necessary in the calculation of activity coefficients and vapor-liquid equilibrium of the mixture components. Due to the large difference in boiling temperature between the extractants

(DHEHPA and TBP) and organic solvents, separation as carried out by distillation or evaporation was found to be the most suitable. However, no effort has been made concerning the saturation line between vapor pressure and temperature for these pure extractants. Thus, both the saturated vapor pressure and temperature of D2EHPA and TBP were implemented at T = (383.8-546.2) K. The experimental data were fitted and correlated by employing Antoine, August, Riedel vapor pressure and Wagner equation. The enthalpy and entropy of vaporization, saturated liquid heat capacity as well as acentric factor were calculated via the experimental data by the Clausius-Clapeyron equation along with Elliott-Suresh-Donohue equation of state (ESD EOS). The calculated quantities have been discussed in terms of molecular structure, strength of intermolecular attraction and molar mass. Full details are available in Chapter IV and in the published article in Vacuum 156 (2018) 237-247 [57].

Chapter V

This chapter demonstrates the vapor liquid equilibrium (VLE) of D2EHPA (extractant) + n-dodecane (diluent) and TBP (extractant) + n-dodecane (diluent). Vapor-liquid equilibrium (VLE) data is a basic requirement of any multicomponent liquid mixtures, which will be separated via distillation processes. Accordingly, such VLE results indicate the possibility of azeotropic phenomenon as well as an ideality behavior of the mixture in both vapor and liquid phase. Kerosene is a popular diluent for D2EHPA and TBP extracants; mixtures (C9 – C16) are experimentally represented as n-dodecane (C12). Due to the large difference in boiling temperature between the extractants (D2EHPA and TBP) and organic solvent (n-dodecane), separation as carried out via distillation is found to be the most suitable. However, no effort has been made

จุฬาลงกรณ์มหาวิทยาลัย
CHULALONGKORN UNIVERSITY

concerning the VLE data of bubble and dew lines for these binary mixtures of D2EHPA + n-dodecane and TBP + n-dodecane. Thus, the VLE of these two systems have been determined at low level pressures of 0.13, 2.40 and 6.67 kPa. Both the Herington area test and Van Ness point test have been validated via the experimental data (VLE). Further, Raoult's law, NRTL and Wilson model were employed to correlate with these experimental VLE data. Such data provide an insight into the molecular interaction. Full details are available in Chapter IV and in the published article in Vacuum 160 (2019) 60-69 [58].

จุฬาลงกรณ์มหาวิทยาลัย
CHULALONGKORN UNIVERSITY

CHAPTER II

Selective separation of trace nickel(II) and gold(I) ions via hollow fiber supported liquid membrane enhanced by synergistic extractants D2EHPA/TBP

Wanchalerm Srirachat[a], Parnuwat Usapein[b], Soorathep Kheawhom[a], Ura Pancharoen[a,*]

[a] *Department of Chemical Engineering, Faculty of Engineering, Chulalongkorn University, Patumwan, Bangkok 10330, Thailand*

[b] *Rattanakosin College for Sustainable Energy and Environment, Rajamangala University of Technology Rattanakosin, Nakhon Pathom 73170, Thailand*

* Corresponding author

This article has been published in Journal: Arabian Journal of Chemistry.

Volume: 14. Issue: 12. Year: 2021. Article no. 103427.

https://doi.org/10.1016/j.arabjc.2021.103427.

2.1 Graphical abstract

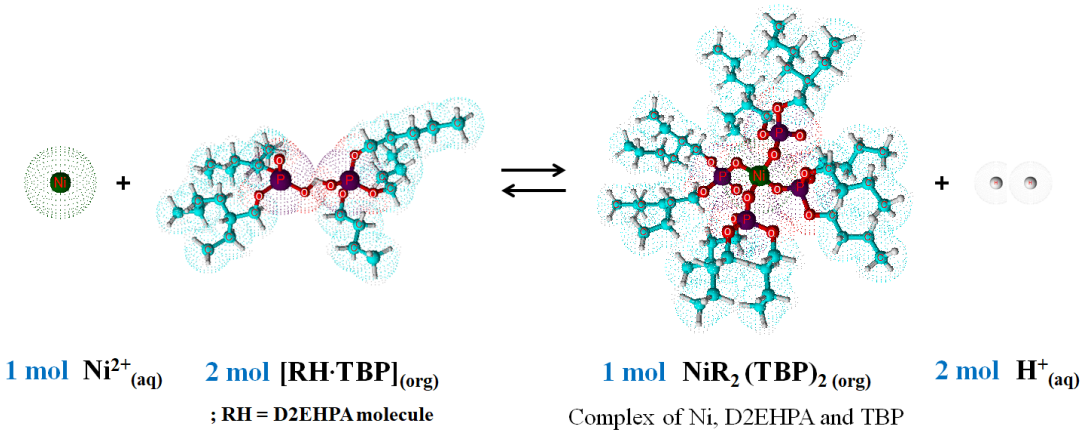

2.2 Abstract

This work presents the selective and simultaneous separation of nickel (Ni^{2+}) and gold $[Au(CN)_2]^-$) ions, in trace amounts, from alkaline solution via hollow fiber supported liquid membrane (HFSLM) technique. HFSLM is challengingly carried out in real rinse wastewater generated by the ENIG plating process. The influence of various chemical parameters, including the type of extractant and their concentrations, molar ratios of mixed extractant as well as type of strippant, are also studied. The organophosphorus extractant mixtures of D2EHPA and TBP provide a synergistic effect for target Ni^{2+} but has an antagonistic effect as regards the extraction of non-target $[Au(CN)_2]^-$. Compared to other inorganic acids, HCl is seen to be the most suitable strippant for the selective stripping. Results demonstrate that percentages of extraction and stripping of Ni^{2+} achieved 85.7 and 83.2%, respectively. In contrast, percentages of extraction and stripping of non-target $[Au(CN)_2]^-$ attained 15.6 and 1.94%.

Keywords: Hollow fiber supported liquid membrane; Electroless nickel immersion gold plating; Rinse wastewater; Gold(I); Nickel(II)

จุฬาลงกรณ์มหาวิทยาลัย
CHULALONGKORN UNIVERSITY

2.3 Introduction

Electroless nickel immersion gold (ENIG) is a flat and solderable metal plating process applied in the manufacture of printed circuit boards (PCBs), especially flexible circuit types and ceramic substrates. Recently, ENIG plating has received much attention since it meets the requirements for lead-free assembly [1, 2]. The ENIG process consists of a series of unitary and separate processes, from substrate acid cleaning and activation to the electroless Ni deposition and immersion gold plating, as illustrated in Fig. 2.1 [1]. In the case of PCBs, a nickel-phosphorus (Ni-P) metal layer is necessary to protect copper (Cu) lines from quick oxidation in order to guarantee good resistance to corrosion and mechanical properties. To prevent the oxidation of Ni surfaces and to assure better conductivity, Au layers can be deposited simply by immersing the Ni-P layers in the suitable solution. The ENIG plating process involves galvanic displacement reaction whereby Ni atoms dissolve from the substrate into the solution while Au ions are reduced on the electroless nickel substrate [3, 4].

จุฬาลงกรณ์มหาวิทยาลัย
CHULALONGKORN UNIVERSITY

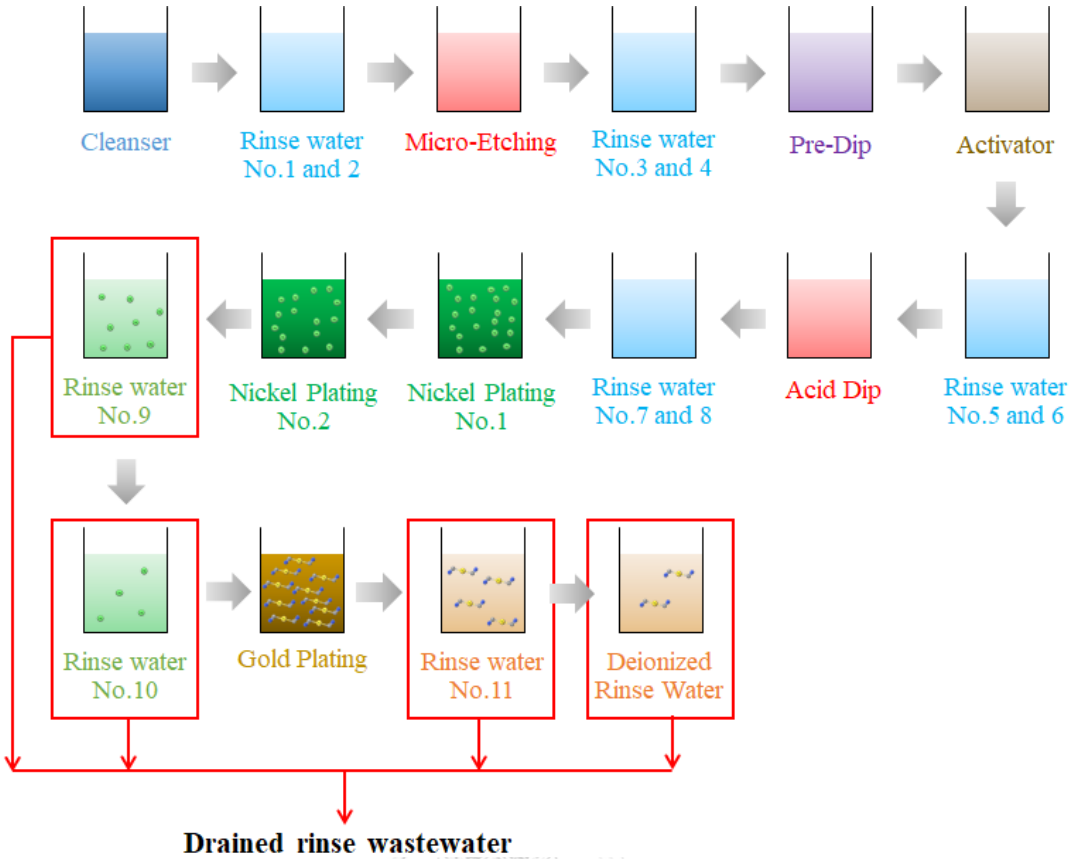

Figure 2.1 Schematic diagram of the ENIG plating process on PCBs.

In general, rinse water baths are used to remove the excess Ni and Au plating solutions, which still adhere to the electroplated parts. Excess solutions contain very small but economically significant quantities of precious metals viz. Ni^{2+} and $[Au(CN)_2]^-$ ions. Owing to its outstanding physical and chemical properties, Ni is considered a highly valued metal for its wide range of applications [5]. The attributes of Ni such as high-temperature stability, strength, ductility, toughness, recyclability, as well as catalytic and electromagnetic properties help achieve sustainability. Unfortunately, Ni is also a toxic and hazardous heavy metal. Exposure to Ni has direct and serious consequences for human beings viz. cancer in the respiratory system, headaches, nausea, skin allergies, lung fibrosis, etc [6, 7]. Thus, the necessity to remove Ni is not only due to the rise in environmental awareness but also due to stringent

จุฬาลงกรณ์มหาวิทยาลัย
CHULALONGKORN UNIVERSITY

legislation regarding the disposal of toxic substances. Likewise, Au is not only valuable as a noble metal in economic activity, but also widely used in various fields [8, 9]. Due to continued buoyant demand and a relatively high stable price, Au has been the focus of intense activity in the areas of exploration and metallurgy. Both the diminishing availability of mineral resources and the increasing necessity for Au metal emphasize the importance of its recovery from scrap material and wastewater [10, 11]. Such demand has led companies to focus on their ability to clean up the wastewater.

Conventional methods in the treatment of wastewater include chemical precipitation, coagulation and flocculation, ion exchange, adsorption, electrochemical treatment, and photocatalysis [12-16]. However, these methods have several disadvantages such as high capital and operational costs, and generate metal sludge, which requires further treatment.

At present, the use of liquid membrane techniques in wastewater treatment has become increasingly applied. The HFSLM technique is very promising having several advantages: its simplicity, and cost-effectiveness [17, 18], low energy consumption and less chemicals used compared with traditional solvent extraction and other membrane processes [19-21]. Furthermore, the HFSLM system can simultaneously perform extraction, stripping and regeneration in a single-unit operation [22-24]. Due to its high surface area and mass transfer area of the liquid membrane module (approximately 10^4 m^2/m^3), HFSLM can effectively attain a high separation rate, high selectivity, and high overall separation [25, 26]. HFSLM can be regarded as a green technology over conventional methods on account of its reusability of liquid membrane and zero discharge of effluent. Accordingly, HFSLM is a cutting-edge system that has been successfully applied in mass separation processes, including extraction and recovery of

จุฬาลงกรณ์มหาวิทยาลัย
CHULALONGKORN UNIVERSITY

target metal ions at trace concentration level [27, 28], removal of contaminants from wastewater [29, 30], and extraction of drugs and amino acids [31, 32]. However, no research has fully investigated the use of the HFSLM technique for the simultaneous and selective separation of Ni^{2+} cations and $[Au(CN)_2]^-$ anions from rinse wastewater after plating of the ENIG process. To the best of our knowledge, this work is new and authentic.

Di-(2-ethylhexyl) phosphoric acid (D2EHPA) is one of the organophosphoric extractants widely used as an extractant or carrier for the reactive extraction of several metal ions such as Ni^{2+} [33], Cu^{2+} [34], Cd^{2+} [35], Fe^{3+} [36], Mn^{2+} [37] and Zn^{2+} [38]. Besides, tributyl phosphate (TBP) is known to be one of the major neutral or solvating extractants and an effective organic phase modifier in numerous applications for extraction of several metal ions such as Ni^{2+} [27], Cd^{2+} [39], Cu^{2+} [40], Co^{2+} [41], Fe^{3+} [42] and Zn^{2+} [43]. It is noted that the addition of TBP to the organic phase containing the D2EHPA extractant improves phase separation by modifying the extraction mechanism, thereby promoting the efficient separation of heavy metals [44-52].

จุฬาลงกรณ์มหาวิทยาลัย
CHULALONGKORN UNIVERSITY

This present work aims to evaluate the performance of HFSLM and the synergistic binary mixture of D2EHPA/TBP extractants as an effective way to simultaneously and selectively separate valuable metal ions, in trace amounts, of Ni^{2+} and $[Au(CN)_2]^-$ from the real rinse wastewater produced by the electroless nickel immersion gold (ENIG) plating process. The effects of several process parameters have been investigated e.g. the concentrations and molar ratios of D2EHPA and TBP extractants in the liquid membrane phase, types of strippant, and pH of stripping solutions.

2.4 Experimental

2.4.1 Chemicals and reagents

The real rinse wastewater containing Ni^{2+} and $[Au(CN)_2]^-$ as an aqueous feed solution generated by the ENIG plating process was supplied by Mektec Manufacturing Corporation (Thailand) Ltd. In Table 2.1 below, the typical compositions analyzed by Mektec Manufacturing Corp. are given. The extractants D2EHPA and TBP were commercially obtained from Merck. The extractants were diluted in commercial grade kerosene for preparation of the organic liquid membrane phase. Kerosene was employed as a liquid membrane diluent for D2EHPA and TBP extractants due to its low viscosity, availability and non-polar characteristic. The inorganic acids viz. HCl, H_2SO_4 and HNO_3 were employed as aqueous stripping solutions. Distilled water was used for preparing all stripping solutions. As listed in Table 2.2, information of all chemicals used in this study are detailed. These chemicals were used without further purification.

จุฬาลงกรณ์มหาวิทยาลัย
CHULALONGKORN UNIVERSITY

Table 2.1 Compositions in the real rinse wastewater of the ENIG plating process used as feed solution in this study.

Component	Chemical formula	Concentration		% Relative molar concentration
		mg/L	mol/L	
Aurodicyanate ions	$[Au(CN)_2]^-$	25	0.1×10^{-3}	0.23
Nickel(II) ion	Ni^{2+}	15	0.3×10^{-3}	0.59
Lead(II) ion	Pb^{2+}	1	0.01×10^{-3}	0.02
Potassium ion	K^+	667	17.1×10^{-3}	39.35
Sodium ion	Na^+	59	2.6×10^{-3}	5.93
Cyanide ion	CN^-	18	0.7×10^{-3}	1.64
Sulfate ion	SO_4^{2-}	25	0.3×10^{-3}	0.59
Hydroxide ion	OH^-	276	16.2×10^{-3}	37.48
Hypophosphate ion	$H_2PO_3^-$	45	0.6×10^{-3}	1.27
Acetate ion	CH_3COO^-	0.4	0.01×10^{-3}	0.02
Pyrophosphate	$P_2O_7^{4-}$	88	0.5×10^{-3}	1.17
Hydrazine	N_2H_4	163	5.1×10^{-3}	11.71

จุฬาลงกรณ์มหาวิทยาลัย
CHULALONGKORN UNIVERSITY

Table 2.2 Chemicals used in this study.

Chemicals	Chemical formula	Molar mass	CAS No.	Purity, %wt.	Purification method	Source
Di-(2-ethylhexyl) phosphoric acid (D2EHPA)	$C_{16}H_{35}O_4P$	322.42	298-07-7	≥95.0 (Synthesis Grade)	None	Merck
Tributyl Phosphate (TBP)	$C_{12}H_{27}O_4P$	266.31	126-73-8	≥99.0 (Synthesis Grade)	None	Merck
Kerosene, Exxols™ D40	C_6-C_{16}	143	64742-47-8	≥98.0 (Commercial Grade)	None	ExxonMobil
Distilled water	H_2O	18.02	7732-18-5	>99.99 (Analytical Grade)	None	Merck
				Concentration, %wt.		
Hydrochloric acid	HCl	36.46	7647-01-0	37.0-38.0 (Analytical Grade)	None	Merck
Nitric acid	HNO_3	63.01	7697-37-2	≥65.0 (Analytical Grade)	None	Merck
Sulfuric acid	H_2SO_4	98.08	7664-93-9	95.0-97.0 (Analytical Grade)	None	Merck

2.4.2 Apparatus and experimental procedure

Liqui-Cel® Extra-Flow consisting of 35,000 woven fibers of hydrophobic microporous polypropylene was selected as the solid support for the liquid membrane. The membrane had an inside diameter of 240 μm, a thickness of 60 μm, an effective length of 15 cm, a porosity of 30%, an average pore size of 0.03 μm, an effective surface area of 1.4 m^2, and tortuosity factor of 2.6 [42, 53]. Woven fibers provide more uniform spacing, leading to a higher mass transfer coefficient than that obtained from a single fiber, in comparison with the flat sheet supported liquid membrane technique (FSSLM) [54, 55].

The separation process of metal ions (Ni^{2+} and $[Au(CN)_2]^-$) via a single module HFSLM system was carried out using the same method as reported previously [42]. First, 500 mL of the organic solution as liquid membrane was prepared by dissolving a certain amount of the extractants (D2EHPA and/or TBP) in kerosene to obtain the desired concentration, ranging from 0.01 to 1.00 mol/L. Then, the organic membrane solution was pumped counter-currently through both tube and shell sides of the hollow fiber module before use in order for the liquid membrane to embed in the micropores of the hollow fibers. Subsequently, the solution was recirculated at an equal flow rate of 100 mL/min for 40 min. After impregnation, 500 mL of distilled water was slowly fed through the system to remove all excess organic solution from the support membrane surface. Consequently, 1 L of the real rinse wastewater, as feed solution, and 1 L of stripping solution was pumped counter-currently at an equal flow rate of 200 mL/min into the tube and shell sides of the hollow fiber module, respectively. The feed solution of pH 8.6±0.05 consisted of 15 mg/L of Ni^{2+}, 25 mg/L of $[Au(CN)_2]^-$ and other contaminated ions e.g. hydroxide (OH^-), cyanide (CN^-) and sulfate (SO_4^{2-}) anions

(Table 2.1). In Fig. 2.2, the HFSLM setup is illustrated. Both feed and stripping solutions were recirculated to each reservoir via recycling mode for 2 h. Then, 5 mL samples of feed and stripping solutions were collected to analyze the concentration of Ni^{2+} and $[Au(CN)_2]^-$ using an inductively coupled plasma (ICP) technique (Optima 2100 DV, Perkin Elmer). All experiments were controlled at T = 303±1 K for both feed and stripping solutions using a digital hotplate stirrer (DAIHAN, MSH-20D) and checked by a precision Pt-100 thermocouple having an accuracy of ±0.1 K.

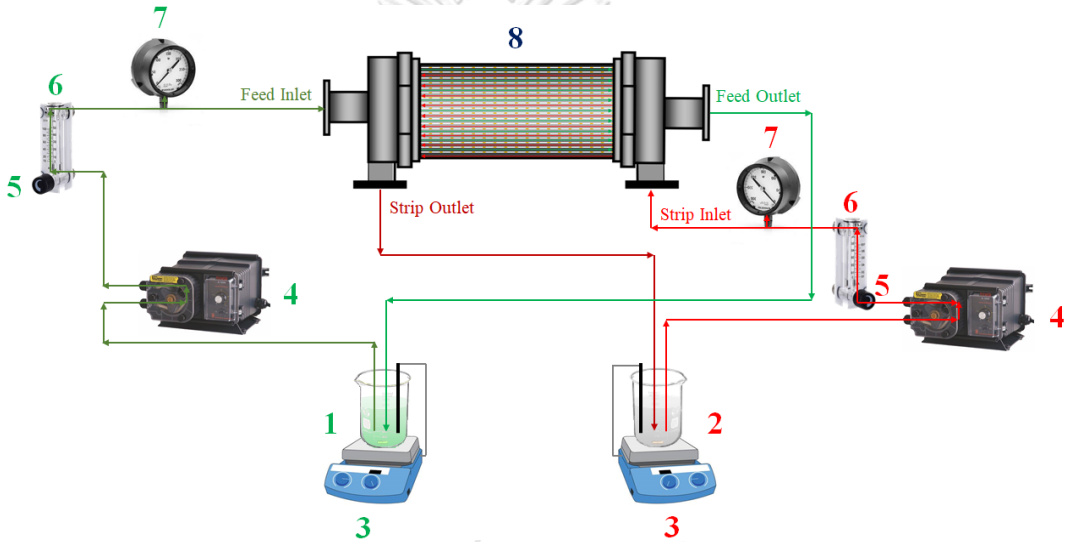

Figure 2.2 Schematic flow diagram of the separation system via HFSLM: **1** feed solution reservoir, **2** stripping solution reservoir, **3** hotplate and stirrer with Pt-100 temperature sensor, **4** peristaltic pump, **5** flow regulator valve, **6** flow meter, **7** pressure gauge, and **8** hollow fiber module.

The extractability of Ni^{2+} and $[Au(CN)_2]^-$ in this work was calculated by the percentage of extraction (*%Ex*) and stripping (*%St*) using Eqs. (2.1) and (2.2):

$$\%E = \frac{C_{(i)} - C_{(aq)}}{C_{(i)}} \times 100 \qquad (2.1)$$

$$\%St = \frac{C_{(strip)}}{C_{(org)}} \times 100 \quad (2.2)$$

The distribution ratio (D) is defined as the concentration of metal ions (Ni^{2+} and $[Au(CN)_2]^-$) in the organic phase of the liquid membrane to that in the aqueous phase after extraction and stripping. It can be determined, as expressed:

$$D = \frac{C_{(org)}}{C_{(aq)}} \quad (2.3)$$

where $C_{(i)}$ is the initial concentration of Ni^{2+} and $[Au(CN)_2]^-$ in aqueous feed solution (mg/L) before extraction, $C_{(aq)}$ is the concentration of Ni^{2+} and $[Au(CN)_2]^-$ in aqueous feed phase after extraction (mg/L), $C_{(strip)}$ is the concentration of Ni^{2+} and $[Au(CN)_2]^-$ in aqueous stripping phase after stripping (mg/L), and $C_{(org)}$ is the concentration of Ni^{2+} and $[Au(CN)_2]^-$ in organic phase after extraction (mg/L).

In the organic phase, a higher distribution ratio is proportional to higher Ni^{2+} and $[Au(CN)_2]^-$ concentrations, thus enhancing the extraction of Ni^{2+} and $[Au(CN)_2]^-$ from aqueous feed phase to organic liquid membrane phase.

The $C_{(org)}$ in the organic phase of the liquid membrane layer can be obtained by subtracting the aqueous concentration from the initial concentration, as shown [56]:

$$C_{(org)} = C_{(i)} - C_{(aq)} \quad (2.4)$$

In order to enhance extraction efficiency and selectivity, synergism of mixed extractants was used to overcome the problems from utilizing a single extractant. Synergistic extraction is defined as the cooperation of two extractants in transferring

จุฬาลงกรณ์มหาวิทยาลัย
CHULALONGKORN UNIVERSITY

metal ions from the aqueous feed phase to the organic liquid membrane phase. The synergistic coefficient (*SC*) is defined as the distribution ratio (*D*) of metal ions (Ni^{2+} and $[Au(CN)_2]^-$) by the mixture of D2EHPA and TBP extractants (D_{mix}) to the sum of the distribution ratio by the single extractants D2EHPA (D_{D2EHPA}) and TBP (D_{TBP}), as shown in Eq. (2.5):

$$SC = \frac{D_{mix}}{D_{D2EHPA} + D_{TBP}} \tag{2.5}$$

Extractant synergism is established when D_{mix} is greater when a single extractant is used (SC > 1). An antagonistic effect occurs vice versa ($SC < 1$) [57, 58].

2.5 Results and discussion

2.5.1 Effect of type of extractant

Due to their cost benefits as well as proof of performances, the two extractants viz. D2EHPA and TBP were selected as both a suitable acidic and neutral extractant for the extraction of Ni^{2+}. In Table 2.3, the extractability of Ni^{2+} and $[Au(CN)_2]^-$ by a single extractant across HFSLM are tabulated.

จุฬาลงกรณ์มหาวิทยาลัย
CHULALONGKORN UNIVERSITY

Table 2.3 Effect of a single and mixed extractants for Ni^{2+} and $[Au(CN)_2]^-$ extraction via HFSLM: feed phase; 15 mg/L Ni^{2+}, 25 mg/L $[Au(CN)_2]^-$, pH 8.6±0.05 | liquid membrane phase; 0.50 mol/L extractant in kerosene | stripping phase; 0.50 mol/L HCl, pH 0.38±0.05 | $q_F = q_S$ = 200 mL/min | t = 2 h | T = 303±1 K.

Extractants	%Extraction		Distribution ratio (D)		Selectivity ($S_{Ni/Au}$)	Synergistic Coefficients (SC)	
	Ni^{2+}	$[Au(CN)_2]^-$	Ni^{2+}	$[Au(CN)_2]^-$		Ni^{2+}	$[Au(CN)_2]^-$
0.50 mol/L D2EHPA	56.18 ±0.89	24.21 ±0.57	1.282 ±0.043	0.3194 ±0.0096	2.321 ±0.021	-	-
0.50 mol/L TBP	52.68 ±0.73	31.54 ±0.85	1.113 ±0.035	0.4607 ±0.0172	1.670 ±0.075	-	-
0.25 mol/L D2EHPA/0.25 mol/L TBP	85.70 ±1.53	15.65 ±0.62	5.993 ±0.631	0.1855 ±0.0084	5.476 ±0.143	2.502 ±0.248	0.2378 ±0.0014

As results show in Table 2.3, both D2EHPA, an acidic type extractant, and TBP, a solvating type extractant are capable of extracting Ni^{2+} and $[Au(CN)_2]^-$ from the real rinse wastewater of the ENIG plating process. However, when these two extractants are used, the distribution ratio of each ion (D_{Ni} and D_{Au}) as well as the selectivity of Ni^{2+} relative to $[Au(CN)_2]^-$ ($S_{Ni/Au}$) are found to be quite different, especially $[Au(CN)_2]^-$. At equal concentration of 0.50 mol/L, D2EHPA attained a slightly higher extraction percentage ($E_{Ni,D2EHPA}$ 56.18%) and distribution ratio ($D_{Ni,D2EHPA}$ 1.282) of Ni^{2+} more than TBP ($E_{Ni,TBP}$ 52.68% and $D_{Ni,TBP}$ 1.113). Furthermore, selective extraction in terms of selectivity of Ni^{2+} relative to $[Au(CN)_2]^-$ is improved when D2EHPA is used ($S_{Ni/Au,D2EHPA}$ 2.321), as a result of its less extractability of $[Au(CN)_2]^-$ than TBP. The non-target $[Au(CN)_2]^-$ were also extracted reaching a high percentage by D2EHPA ($E_{Au,D2EHPA}$ 24.21%) and TBP ($E_{Au,TBP}$ 31.54%). Such outcomes can affect the purity of Ni^{2+} in the aqueous stripping phase and loss of valuable Au metal, thus reduction of $[Au(CN)_2]^-$ extraction from the aqueous feed phase is needed.

D2EHPA is an acidic extractant, offering both hydrogen bond donor and acceptor sites while TBP, a neutral extractant, only offers a single acceptor site per molecule. At an organic-aqueous membrane interface of liquid membrane, the polar hydroxyl group (-OH) of D2EHPA can be deprotonated to become a negative charge on the oxygen atom ($P\text{-}O^-$) [59]. The deprotonated form of D2EHPA has high affinity to strongly interact with the positive charges on Ni^{2+}. Furthermore, Ni^{2+} prefer to substitute the hydrogen atom in the P−O-H group of D2EHPA and combined with the P=O group via the cation exchange mechanism. Thus, D2EHPA extractant was found to give better efficiency for Ni^{2+} extraction over TBP in terms of distribution ratio and selectivity.

จุฬาลงกรณ์มหาวิทยาลัย
CHULALONGKORN UNIVERSITY

The chemical reactions of Ni^{2+} with dimeric form of D2EHPA extractant via cation exchange mechanism are as follows [51, 60, 61]:

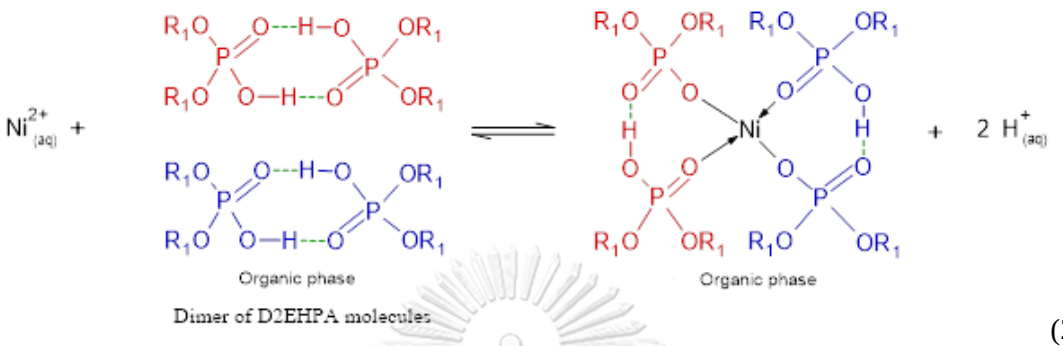

(2.6)

where R_1 denotes 2-ethylhexyl group (C_8H_{17}) as in Eq. (2.6).

In the literature, the reaction mechanism of Ni^{2+} in aqueous basic solution with the TBP extractant has never been reported. Consequently, the reactive extraction of Ni^{2+} applying TBP extractant in aqueous basic solution, mainly composed of the hydroxide ions (OH^-) with 16.2 mmol/L and 37.48 %relative molar concentration (Table 2.1), is proposed in this study.

จุฬาลงกรณ์มหาวิทยาลัย
CHULALONGKORN UNIVERSITY

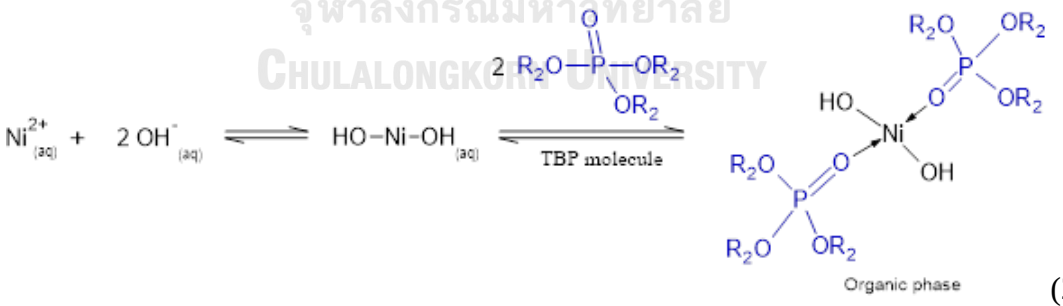

(2.7)

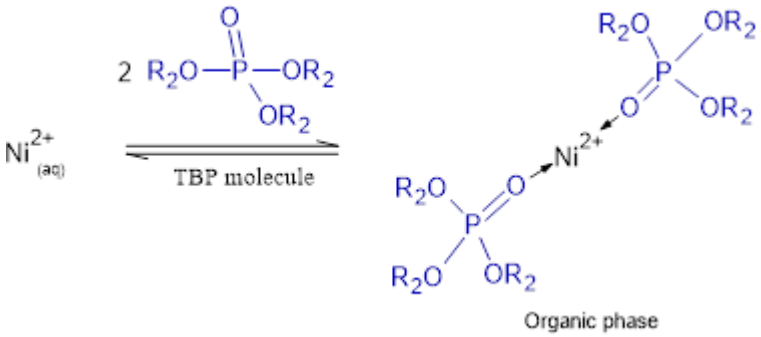

(2.8)

where R_2 denotes butyl group (C_4H_9) as in Eqs. (2.7) and (2.8).

Owing to its chemical stability, low aqueous solubility and high loading characteristics, D2EHPA proved to be the most ideal extractant for Ni^{2+} extraction [62]. Besides, since Ni^{2+} extraction is highly pH dependent, a higher acidic extractant like D2EHPA is seen to be preferable. Due to its high solubility and degree of protonation, D2EHPA provides the highest acidity constant [27]. Thus, the H-atom in the hydroxyl group (-OH) of D2EHPA is easily substituted by Ni^{2+}.

Henceforth, extraction by solvation is carried out by a solvating extractant. In nature, a solvating extractant has a weak base, extracting either neutral metal complexes or acids by forming a solvate.

In the rinse wastewater of the ENIG plating process, Au(I) is present as the complex of $[Au(CN)_2]^-$ anions whereas Ni^{2+} is found as cations. When aqueous feed solution is basic, $[Au(CN)_2]^-$ can be extracted via anion exchange with several amine extractants [63-65], quaternary ammonium compounds [66] and ionic liquids [67, 68]. It can be seen that D2EHPA and/or TBP is a suitable choice of extractant for selectively separating Ni^{2+} from $[Au(CN)_2]^-$ ions via HFSLM.

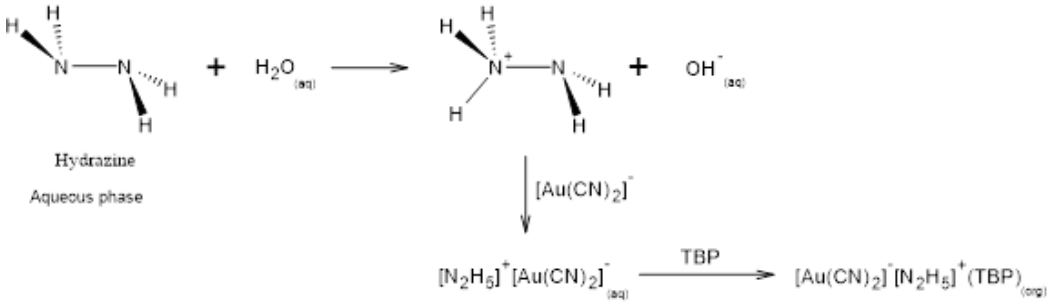

(2.9)

[69]

(2.10)

Table 2.4 Separation time of Ni^{2+} and $[Au(CN)_2]^-$ applying different extractant systems.

Extractants	Separation time (min) at $\%E_{Ni}$				Separation time (min) at $\%E_{Au}$				
	40 %	50 %	55 %	80 %	1 %	5 %	10 %	15 %	20 %
0.5 mol/L D2EHPA	9.2	64	106	-	4.2	37	49	67	97
0.5 mol/L TBP	52	107	-	-	2.9	9.4	30	54	71
0.25 mol/L D2EHPA/0.25 mol/L TBP	1.6	2.5	2.9	28	10	46	69	110	-

จุฬาลงกรณ์มหาวิทยาลัย
CHULALONGKORN UNIVERSITY

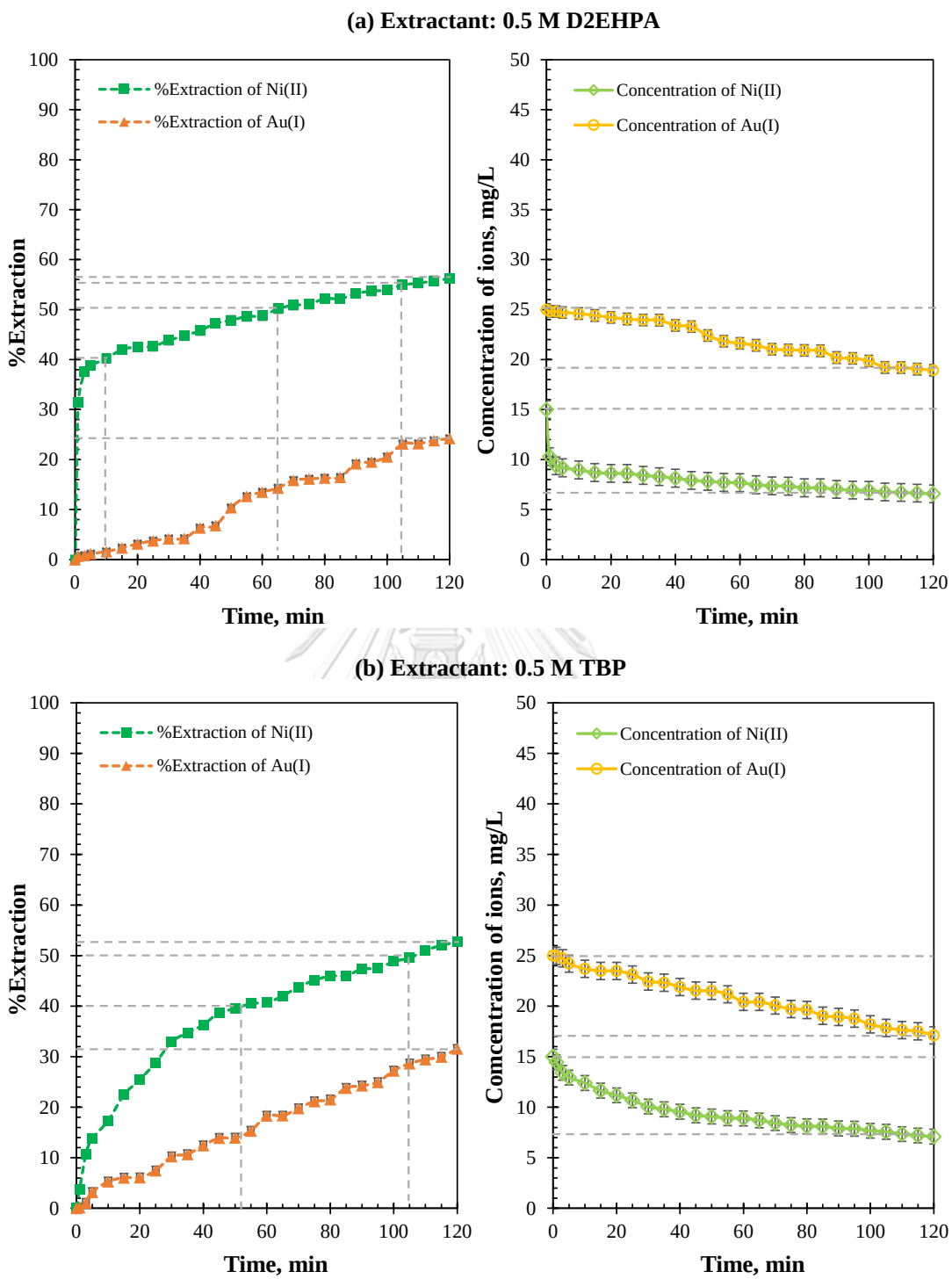

Figure 2.3 Extraction percentage and concentration of Ni^{2+} and $[Au(CN)_2]^-$ in aqueous feed phase with continuous separation time (*t*): (a) 0.50 mol/L D2EHPA extractant and (b) 0.50 mol/L TBP extractant: feed phase; 15 mg/L Ni^{2+}, 25 mg/L $[Au(CN)_2]^-$, pH

8.6±0.05 | liquid membrane phase; 0.50 mol/L D2EHPA in kerosene | stripping phase; 0.50 mol/L HCl, pH 0.38±0.05 | $q_F = q_S$ = 200 mL/min | t = 2 h | T = 303±1 K.

2.5.2 Effect of mixed extractants

Amongst the single extractant types studied in Section 2.5.1, it was found that both D2EHPA and TBP extractants were best for the extraction of Ni^{2+} via HFSLM having good selectivity of Ni^{2+} relative to $[Au(CN)_2]^-$ ($S_{Ni/Au}$). As depicted in Table 2.3 and Fig. 2.4, mixing of 0.25 mol/L D2EHPA and 0.25 mol/L TBP extractants are investigated in order to improve the extraction of Ni^{2+} and the selectivity ($S_{Ni/Au}$).

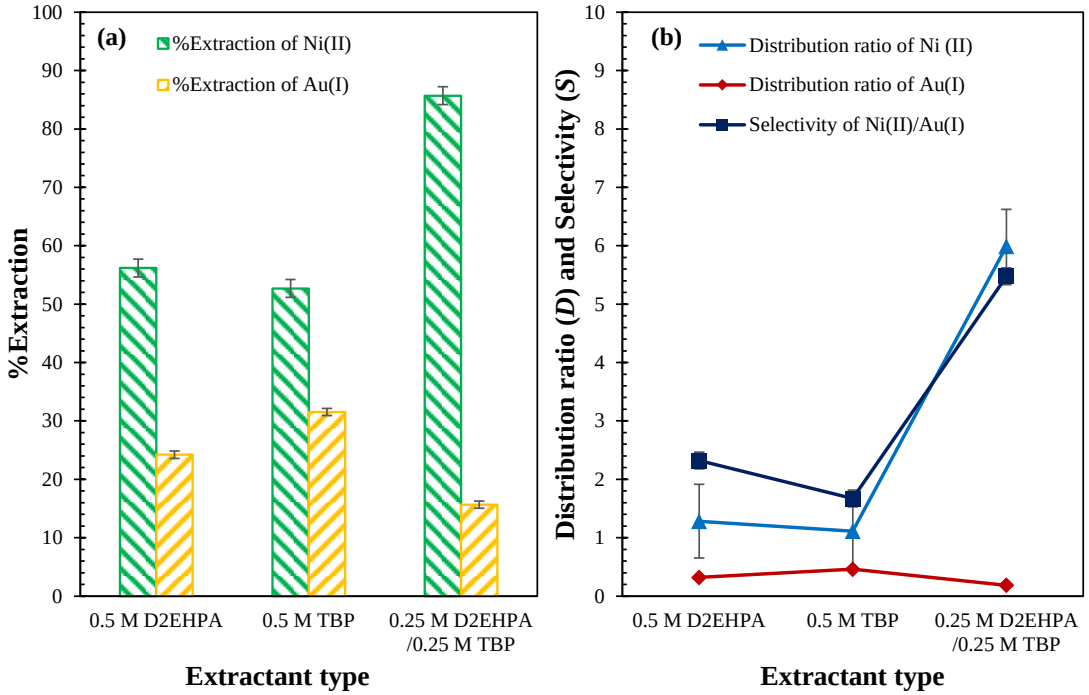

Figure 2.4 Effect of mixed extractants on Ni^{2+} and $[Au(CN)_2]^-$ extraction from aqueous feed phase via HFSLM: feed phase; 15 mg/L Ni^{2+}, 25 mg/L $[Au(CN)_2]^-$, pH 8.6±0.05 | liquid membrane phase; 0.50 mol/L of total extractant concentration in kerosene | stripping phase; 0.50 mol/L HCl, pH 0.38±0.05 | $q_F = q_S$ = 200 mL/min | t = 2 h | T = 303±1 K.

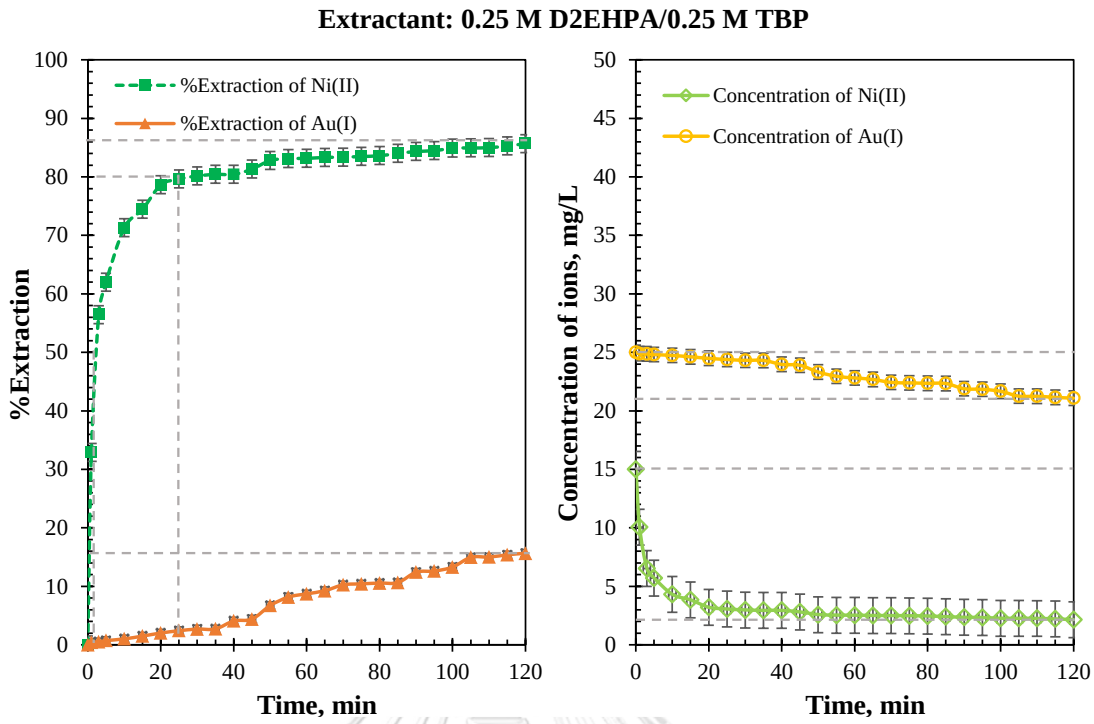

Figure 2.5 Extraction percentage and concentration of Ni^{2+} and $[Au(CN)_2]^-$ in aqueous feed phase over separation time (t): feed phase; 15 mg/L Ni^{2+}, 25 mg/L $[Au(CN)_2]^-$, pH 8.6±0.05 | liquid membrane phase 0.25 mol/L D2EHPA and 0.25 mol/L TBP extractants in kerosene | stripping phase; 0.50 M HCl, pH 0.38±0.05 | $q_F = q_S = 200$ mL/min | $t = 2$ h | $T = 303\pm1$ K.

จุฬาลงกรณ์มหาวิทยาลัย
CHULALONGKORN UNIVERSITY

According to Fig. 2.4a, it is evident that using the mixture of D2EHPA/TBP extractants yielded the highest Ni^{2+} extraction efficiency followed by the single extractants i.e. D2EHPA and TBP, respectively. In Table 2.3, the synergistic coefficient of the D2EHPA/TBP extractants for Ni^{2+} extraction ($SC_{Ni} > 1$) indicates that synergism was found to occur. Thus, maximum extraction ($\%E_{Ni}$) of 85.70%, distribution ratio ($D_{mix,\ Ni}$) of 5.993 and a selectivity ($S_{Ni/Au}$) of 5.476 were achieved (Fig. 2.4b). Furthermore, the synergistic mixture D2EHPA/TBP can transport the Ni^{2+} much faster than a single extractant as seen in Table 2.4 as well as Figs. 2.3 and 2.5. Accordingly, extraction of Ni^{2+} can rapidly reach 50% within 2.5 min, and then 80% within 28 min.

Thus, separation time of Ni^{2+} via HSFLM can be reduced compared with using D2EHPA and TBP extractant, respectively. In contrast, extraction of $[Au(CN)_2]^-$ by the mixture D2EHPA/TBP expressed an antagonistic effect behavior (synergistic coefficient, $SC_{Au} < 1$) as in Table 2.3. Transportation of $[Au(CN)_2]^-$ from the aqueous feed phase via HFSLM decreased significantly. At equal extraction percentage of 10% for $[Au(CN)_2]^-$ ($\%E_{Au}$), it took a separation time of 69 min when using the mixture D2EHPA/TBP. This outcome was clearly slower than when D2EHPA and TBP extractants were used (Table 2.4). Thus, as regards selective separation, the combination of D2EHPA/TBP extractants proved to be the most suitable ions carrier system via HFSLM as a result of their synergism to target Ni^{2+} as well as their antagonism to non-target $[Au(CN)_2]^-$ for improving $\%E_{Ni}$, D_{Ni} and $S_{Ni/Au}$.

As in Eq. (2.6), the D2EHPA molecules were strongly attracted via H-bonding in dimer form. The majority of the D2EHPA molecules are dimerized in nonpolar diluents such as kerosene, and its aqueous solubility is also extremely low [70]. The synergistic effect of the mixture D2EHPA/TBP in enhancing Ni^{2+} extraction is proposed via the replacement of two D2EHPA molecules in $Ni{\cdot}(D2EHPA)_4$ complex by two TBP molecules to form adducts with Ni complexes of $Ni{\cdot}(D2EHPA)_2(TBP)_2$ [51, 71]. The reactive extraction mechanism of Ni^{2+} by mixed D2EHPA/TBP extractants is expressed in Eq. (2.11):

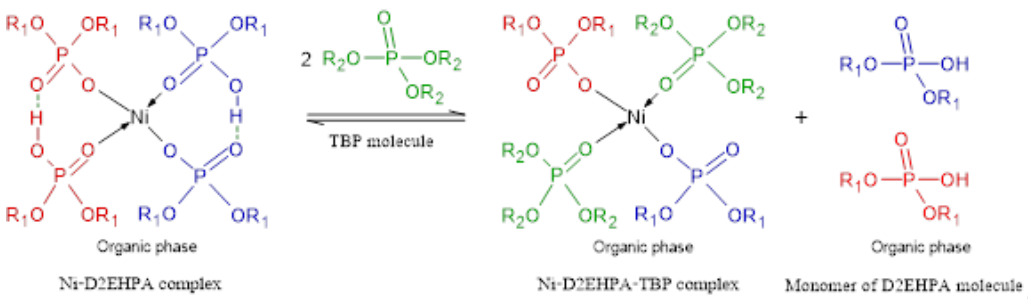

(2.11)

As calculated via Van der Waals radii, the molecular volume of the TBP molecule proved to be smaller than that of D2EHPA molecule by about 50 Å, as shown in Table 2.5 [72].

Table 2.5 Physicochemical properties of D2EHPA and TBP extractant.

Extractant	Molecular volume[1] ($Å^3$)	Negative charge on the oxygen atom of phosphoryl functional group	Dipole moment (Debye)
PA	311.3	-0.873	2.74
TBP	263.7	-0.779	3.10

Note: [1] Molecular volumes were calculated via the Van der Waals radii.

Therefore, the TBP molecule can easily replace the D2EHPA molecule in the Ni·$(D2EHPA)_4$ complex [51]. As shown in Table 2.5, the greater dipole moment of the TBP molecule indicates its greater polarity.

According to Eq. (2.11), the remaining two molecules of monomeric D2EHPA can be dissociated at the interface of the organic membrane-aqueous phases, and then form a complex with one ion of Ni^{2+} as in Eq. (2.12) [51, 70, 73]:

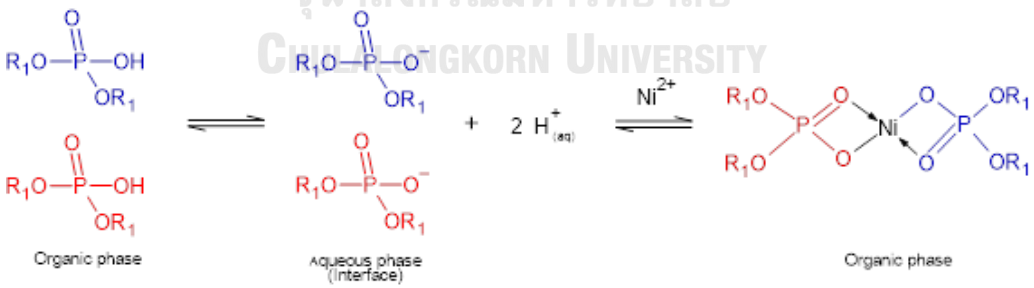

(2.12)

In this study, the rinse wastewater from the ENIG process is a slightly basic effluent having pH of 8.6±0.05. Thus, deprotonation of the monomeric D2EHPA molecules is quite favorable. It is proved that D2EHPA extractant is suitable for Ni^{2+} extraction in the basic aqueous solution [61].

As observed in Eqs. (2.11) and (2.12), when the mixture D2EHPA/TBP is used, it can be seen that four molecules of D2EHPA are able to form a complex with two ions of Ni^{2+}. Thus, this outcome increases the extractability for Ni^{2+} more than when a single D2EHPA extractant is used such that four D2EHPA molecules form a tetrameric complex with one Ni^{2+} ion as in Eq. (2.6). Furthermore, two molecules of TBP can also extract one Ni^{2+} ion via the complex of $Ni(OH)_2{\cdot}(TBP)_2$ or $Ni{\cdot}(TBP)_2$ as in Eq. (2.7).

At equal total molar concentration or number of extractant molecules, it is found that the mixed extractants of four D2EHPA and four TBP molecules (i.e. 0.25 mol/L D2EHPA/0.25 mol/L TBP) are able to extract three Ni^{2+} ions while a single type extractant of eight D2EHPA molecules (i.e. 0.50 mol/L D2EHPA) form a complex with two Ni^{2+} ions. Thus, the extractability of Ni^{2+} by the mixture D2EHPA/TBP proved to be 1.5 times more than when the single D2EHPA extractant system was used.

In the case of $[Au(CN)_2]^-$, it is noted that extraction efficiency by the mixture D2EHPA/TBP decreased. This antagonistic effect may be a result of less H^+ generated by D2EHPA dissociation as its lower concentration (i.e. from 0.50 mol/L to 0.25 mol/L) and by TBP molecules in preferring to form a $Ni{\cdot}(D2EHPA)_2(TBP)_2$ complex. The supported liquid membrane system containing the combination of D2EHPA/TBP extractants is suitable for further investigation due to their synergistic effect ($SC_{Ni} > 1$), high efficiency of Ni^{2+} extraction ($E_{Ni} > 80\%$), improved distribution ratio (D_{Ni}) as well as selectivity of Ni^{2+} relative to $[Au(CN)_2]^-$ ($S_{Ni/Au}$).

In general, D2EHPA contains mono-(2-ethylhexyl) phosphoric acid (M2EHPA) as impurities due to poor purification of the reagent and/or due to hydrolysis of D2EHPA during prolonged storage. Haghshenas et al. [52] found that the presence of M2EHPA causes the extraction curves of these metals to shift to lower pH

values depending on the physico-chemistry properties of the metal. In other words, the presence of M2EHPA changes the thermodynamic conditions of extraction and produces variable changes in the shifting of the extraction curves that for some metals are in order Cd > Cu >Co > Ni > Zn. This impurity sometimes affects separation efficiency. This antagonistic effect may cause trouble with the solvent extraction.

2.5.3 Effect of molar ratio of mixed D2EHPA/TBP extractant

As proved in Section 2.5.2, when the synergistic mixture D2EHPA/TBP increased, extraction of Ni^{2+} was found to increase significantly. Fig. 2.6 and Table 2.6 show the effect of the combination of D2EHPA/TBP extractants at various molar ratios as regards the extraction percentages (%*E*) of Ni^{2+} and $[Au(CN)_2]^-$. At equal total concentration of 0.5 mol/L, it is seen that extraction of Ni^{2+} increased from 56.18 to 85.70% when TBP concentration increased from 0.05 to 0.25 mol/L and the molar ratio of the mixture D2EHPA/TBP decreased from 9:1 to 1:1, respectively. Furthermore, the distribution ratio of Ni^{2+} (D_{Ni}) and selectivity of Ni^{2+} relative to $[Au(CN)_2]^-$ ($S_{Ni/Au}$) also increased as TBP concentration increased. Thus, the optimum combination obtained for the mixed extractants in the liquid membrane for this HFSLM studied is an equal molar concentration (1:1 ratio) of 0.25 mol/L D2EHPA and 0.25 mol/L TBP.

According to Eq. (2.11), the role of TBP extractant is to disrupt the dimers or aggregation of the D2EHPA molecules. Two D2EHPA molecules and two TBP molecules can form a complex with the Ni^{2+} as $Ni{\cdot}(D2EHPA)_2(TBP)_2$. Hence, two monomeric molecules of D2EHPA become available for complexation with other Ni^{2+} ions, which enhances the extraction efficiency (%E_{Ni}) as in Eq. (2.11). Furthermore, at equal molar concentration in comparison with D2EHPA, TBP extractant can solvate

Ni^{2+} ions by using two TBP molecules as a form of $Ni(OH)_2{\cdot}(TBP)_2$ or $Ni{\cdot}(TBP)_2$, Eq. (2.7). However, four molecules of D2EHPA are required for extraction with Ni^{2+} when the extractant is taken alone as in Eq. (2.6). For example, at equal number of extractant molecules expressed in Eqs. (2.13) and (2.14), it can be proved that the mixture of D2EHPA/TBP at 1:1 ratio provides higher extractability of Ni^{2+} in comparison with using D2EHPA/TBP ratio of 5:1.

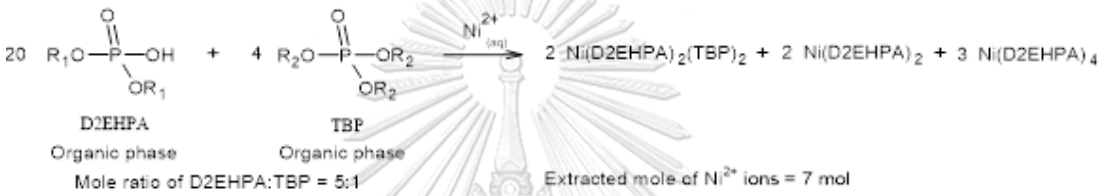

(2.13)

(2.14)

จุฬาลงกรณ์มหาวิทยาลัย
CHULALONGKORN UNIVERSITY

As for the extraction of $[Au(CN)_2]^-$, increasing the extractant TBP as well as decreasing D2EHPA in molar concentration from 9:1 to 1:1 at equal molar concentration practically decreases the degree of extraction. Results arise due to the reduction of H^+ generated after Ni^{2+} extraction with D2EHPA molecules as in Eqs. (2.6) and (2.11). Thus, the protonation mechanism of hydrazine (N_2H_4) to form hydrazinium ($N_2H_5^+$) ions, for $[Au(CN)_2]^-$ complexation as in Eq. (2.8), is decreased. Furthermore, although concentration of TBP increased, its molecule contributes to form Ni-complexes such as $Ni{\cdot}(D2EHPA)_2(TBP)_2$, $Ni(OH)_2{\cdot}(TBP)_2$ and/or $Ni{\cdot}(TBP)_2$. These

extractive reactions are competitive as in Eqs. (2.8) and (2.9), whereby the complex of $K^{+}[Au(CN)_2]^{-}$(TBP) and $[N_2H5]^{+}[Au(CN)_2]^{-}$(TBP) are formed.

จุฬาลงกรณ์มหาวิทยาลัย
CHULALONGKORN UNIVERSITY

Table 2.6 Effect of molar ratio of mixed D2EHPA/ TBP extractants for Ni^{2+} and $[Au(CN)_2]^-$ extraction via HFSLM: feed phase; 15 mg/L Ni^{2+}, 25 mg/L $[Au(CN)_2]^-$, pH 8.6±0.05 | liquid membrane phase; 0.50 mol/L total concentration of mixed D2EHPA/TBP extractants in kerosene | stripping phase; 0.50 mol/L HCl, pH 0.38±0.05 | $q_F = q_S$ = 200 mL/min | t = 2 h | T = 303±1 K.

Extractant Concentration	Molar ratio of D2EHPA/TBP	%Extraction		Distribution ratio (D)		Selectivity ($S_{Ni/Au}$)	Synergistic Coefficients (SC)	
		Ni^{2+}	$[Au(CN)_2]^-$	Ni^{2+}	$[Au(CN)_2]^-$		Ni^{2+}	$[Au(CN)_2]^-$
0.50 M D2EHPA	-	56.18 ±0.89	24.21 ±0.57	1.282 ±0.035	0.3194 ±0.0096	2.321 ±0.021	-	-
0.45 M D2EHPA/0.05 M TBP	9:1	71.32 ±0.44	28.16 ±0.28	2.487 ±0.048	0.3920 ±0.0057	2.533 ±0.038	1.038 ±0.017	0.5024 ±0.0274
0.40 M D2EHPA/0.10 M TBP	4:1	72.59 ±0.20	21.39 ±0.54	2.648 ±0.022	0.2721 ±0.0090	3.394 ±0.084	1.106 ±0.006	0.3488 ±0.0261
0.35 M D2EHPA/0.15 M TBP	2.33:1	74.83 ±0.39	19.57 ±0.19	2.973 ±0.069	0.2433 ±0.0028	3.824 ±0.064	1.241 ±0.033	0.3119 ±0.0078
0.30 M D2EHPA/0.20 M TBP	1.5:1	81.16 ±0.28	17.42 ±0.14	4.308 ±0.093	0.2109 ±0.0019	4.659 ±0.063	1.798 ±0.044	0.2704 ±0.0074
0.25 M D2EHPA/0.25 M TBP	1:1	85.70 ±0.18	15.65 ±0.62	5.993 ±0.631	0.1855 ±0.0084	5.476 ±0.143	2.502 ±0.248	0.2378 ±0.0014

CHULALONGKORN UNIVERSITY

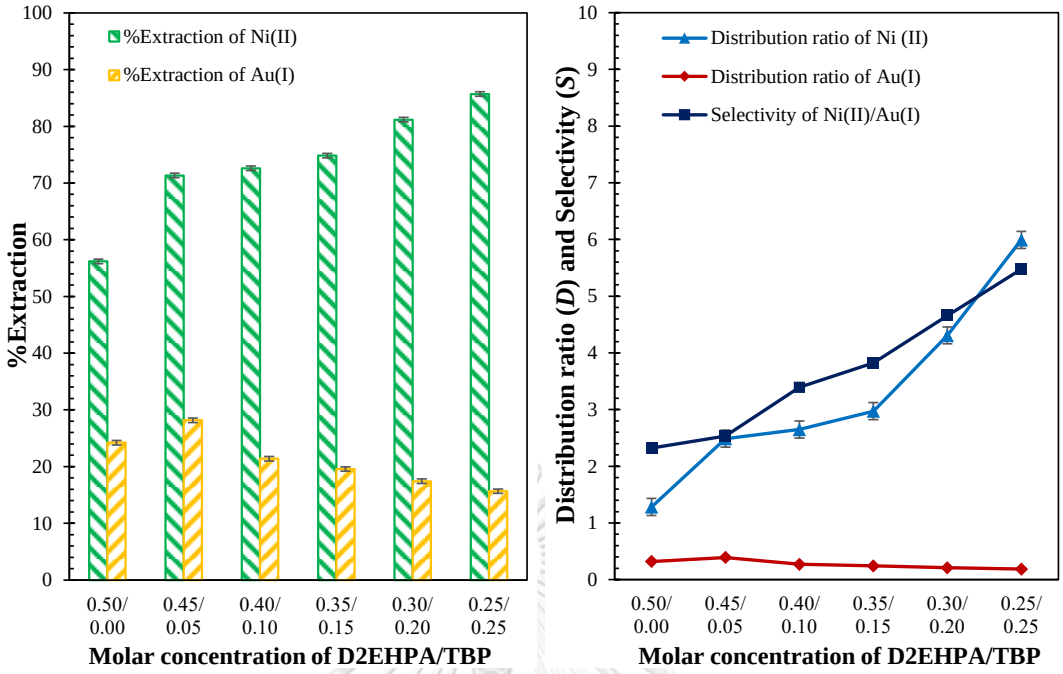

Figure 2.6 Effect of concentration and molar ratio of the D2EHPA/ TBP synergistic extractants: feed phase; 15 mg/L Ni^{2+}, 25 mg/L $[Au(CN)_2]^-$, pH 8.6±0.05 | liquid membrane phase; mixed D2EHPA/TBP extractant in kerosene | stripping phase; 0.50 mol/L HCl, pH 0.38±0.05 | $q_F = q_S$ = 200 mL/min | t = 2 h | T = 303±1 K.

2.5.4 Effect of extractant concentration

As presented in Table 2.7 and Figs. 2.7a to 7c, the effect of concentration of D2EHPA and TBP as well as the mixture D2EHPA/TBP was investigated by varying their concentration from 0.01 to 1.0 mol/L.

Table 2.7 Effect of extractant concentration for Ni^{2+} and $[Au(CN)_2]^-$ extraction via HFSLM: feed phase; 15 mg/L Ni^{2+}, 25 mg/L $[Au(CN)_2]^-$, pH 8.6±0.05 | liquid membrane phase; 0.01 to 1.0 mol/L extractant in kerosene | stripping phase; 0.50 mol/L HCl, pH 0.38±0.05 | q_F = q_S = 200 mL/min | t = 2 h | T = 303±1 K.

Extractant	Extraction, %		Distribution ratio (D)		Selectivity	Synergistic Coefficients (SC)	
	Ni^{2+}	$[Au(CN)_2]^-$	Ni^{2+}	$[Au(CN)_2]^-$	($S_{Ni/Au}$)	Ni^{2+}	$[Au(CN)_2]^-$
0.01 M D2EHPA	1.813 ±0.396	0.8402 ±0.0533	0.01846 ±0.00422	0.008473 ±0.000543	2.158 ±0.206	-	-
0.025 M D2EHPA	4.620 ±0.460	2.010 ±0.330	0.04844 ±0.00521	0.02051 ±0.00354	2.299 ±0.185	-	-
0.05 M D2EHPA	9.161 ±0.720	7.203 ±0.266	0.1008 ±0.0084	0.07762 ±0.00320	1.272 ±0.129	-	-
0.10 M D2EHPA	18.32 ±0.440	13.67 ±0.56	0.2243 ±0.0064	0.1583 ±0.0032	1.340 ±0.027	-	-
0.25 M D2EHPA	31.75 ±0.750	19.94 ±0.65	0.4652 ±0.0169	0.2491 ±0.0072	1.592 ±0.100	-	-
0.50 M D2EHPA	56.18 ±0.89	24.21 ±0.57	1.282 ±0.043	0.3194 ±0.0096	2.321 ±0.021	-	-
1.00 M D2EHPA	58.21 ±0.40	25.17 ±0.61	1.393 ±0.022	0.3364 ±0.0113	2.313 ±0.064	-	-
0.01 M TBP	0.9503±0.0832	1.040 ±0.153	0.009594 ±0.000851	0.01051 ±0.00157	0.9138 ±0.0385	-	-
0.025 M TBP	3.420 ±0.140	2.214 ±0.262	0.03541 ±0.00142	0.02264 ±0.00283	1.545 ±0.089	-	-
0.05 M TBP	5.807 ±0.398	3.541 ±0.320	0.06165 ±0.00462	0.03671 ±0.00354	1.640 ±0.009	-	-
0.10 M TBP	11.40 ±0.53	9.703 ±0.432	0.1287 ±0.0070	0.1075 ±0.0055	1.175 ±0.004	-	-
0.25 M TBP	21.45 ±0.52	15.12 ±0.29	0.2731 ±0.0087	0.1781 ±0.0042	1.419 ±0.008	-	-
0.50 M TBP	52.68 ±0.73	31.54 ±0.85	1.113 ±0.035	0.4607 ±0.0172	1.670 ±0.075	-	-
1.00 M TBP	53.05 ±0.32	33.17 ±0.39	1.130 ±0.015	0.4963 ±0.0084	1.599 ±0.030	-	-
0.005 M D2EHPA/0.005 M TBP	4.650 ±0.450	1.250 ±0.083	0.04877 ±0.09510	0.01266 ±0.00086	3.720 ±0.066	1.713 ±0.038	0.6852 ±0.0390
0.0125 M D2EHPA/0.0125 M TBP	14.11 ±0.37	3.230 ±0.293	0.1643 ±0.0048	0.03434 ±0.00324	4.250 ±0.169	1.858 ±0.035	0.8476 ±0.0251
0.025 M D2EHPA/0.025 M TBP	22.42 ±0.03	6.710 ±0.430	0.2890 ±0.0006	0.07193 ±0.00509	3.341 ±0.141	1.797 ±0.046	0.6115 ±0.0270
0.05 M D2EHPA/0.05 M TBP	39.20 ±0.60	9.710 ±0.430	0.6447 ±0.0170	0.1075 ±0.0054	4.037 ±0.082	1.820 ±0.055	0.4008 ±0.0270
0.125 M D2EHPA/0.125 M TBP	59.52 ±0.99	12.56 ±0.48	1.470 ±0.079	0.1436 ±0.0065	4.739 ±0.073	2.000 ±0.034	0.3348 ±0.0214
0.25 M D2EHPA/0.25 M TBP	85.70 ±1.53	15.65 ±0.62	5.993 ±0.631	0.1855 ±0.0084	5.476 ±0.143	2.502 ±0.248	0.2378 ±0.0014
0.50 M D2EHPA/0.50 M TBP	86.80 ±1.13	16.27 ±0.58	6.576 ±0.379	0.1943 ±0.0085	5.335 ±0.232	2.606 ±0.141	0.2323 ±0.0101

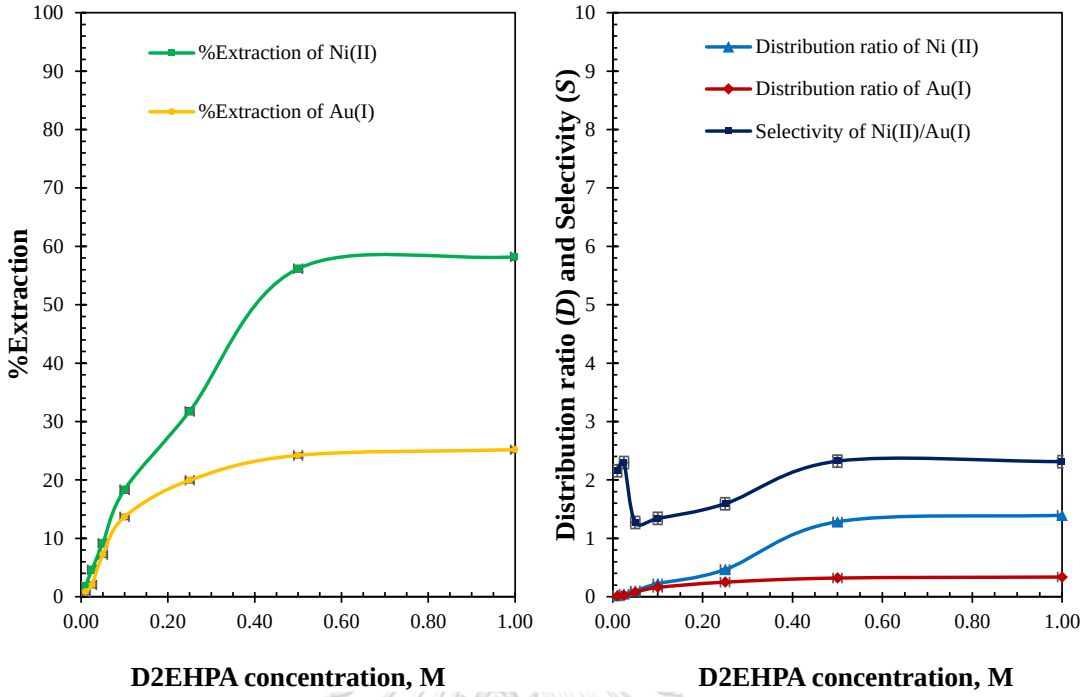

Figure 2.7a Effect of D2EHPA extractant concentrations: feed phase; 15 mg/L Ni^{2+}, 25 mg/L $[Au(CN)_2]^-$, pH 8.6±0.05 | liquid membrane phase; D2EHPA in kerosene | stripping phase; 0.50 mol/L HCl, pH 0.38±0.05 | $q_F = q_S$ = 200 mL/min | t = 2 h | T = 303±1 K.

จุฬาลงกรณ์มหาวิทยาลัย
CHULALONGKORN UNIVERSITY

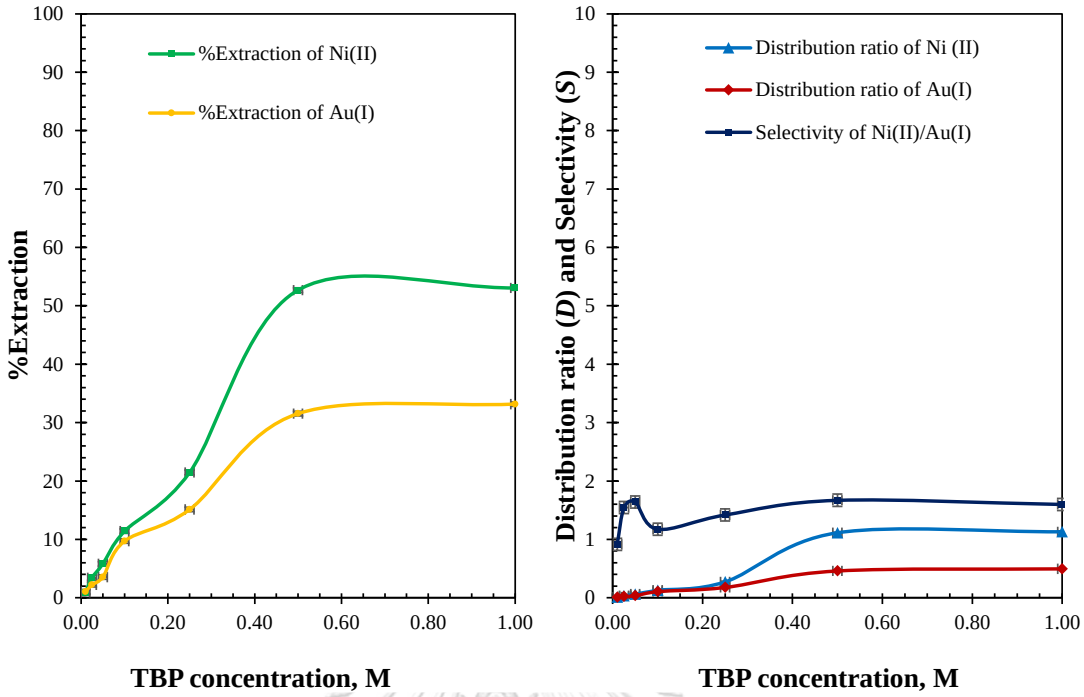

Figure 2.7b Effect of TBP extractant concentrations: feed phase; 15 mg/L Ni^{2+}, 25 mg/L $[Au(CN)_2]^-$, pH 8.6±0.05 | liquid membrane phase; TBP in kerosene | stripping phase; 0.50 mol/L HCl, pH 0.38±0.05 | $q_F = q_S$ = 200 mL/min | t = 2 h | T = 303±1 K.

จุฬาลงกรณ์มหาวิทยาลัย
CHULALONGKORN UNIVERSITY

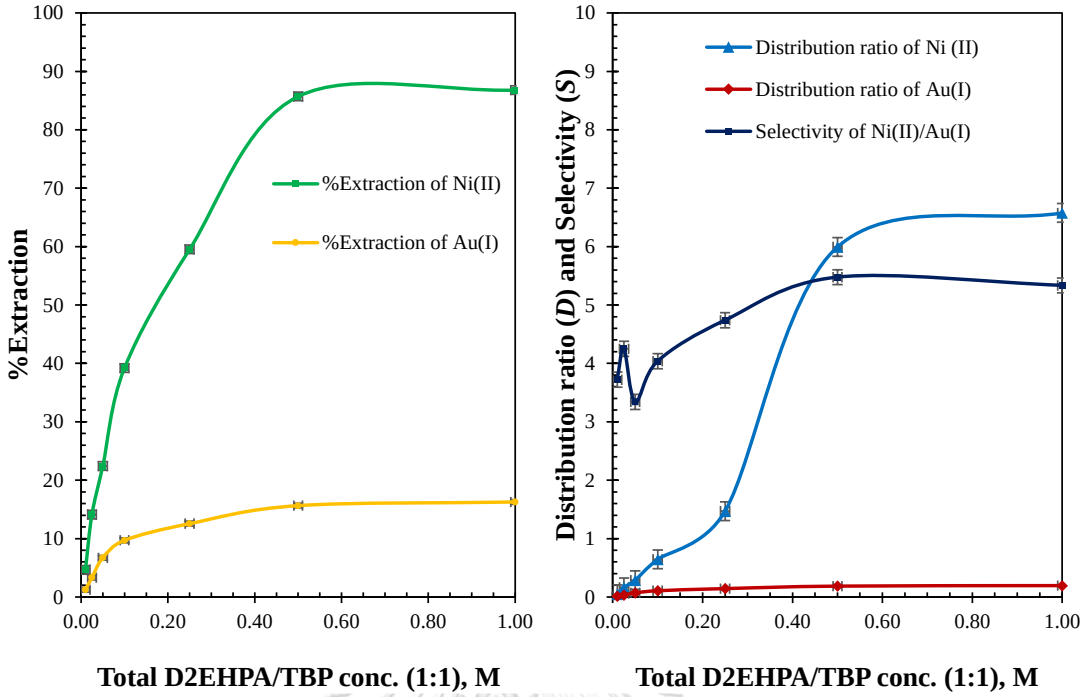

Figure 2.7c Effect of mixed D2EHPA and TBP extractant concentrations (1:1 ratio): feed phase; 15 mg/L Ni^{2+}, 25 mg/L $[Au(CN)_2]^-$, pH 8.6±0.05 | liquid membrane phase; mixed of D2EHPA and TBP extractant in kerosene | stripping phase; 0.50 mol/L HCl, pH 0.38±0.05 | $q_F = q_S$ = 200 mL/min | t = 2 h | T = 303±1 K.

Overall, results demonstrate that by increasing the concentration of the extractant from 0.01 to 1.00 mol/L, for the single D2EHPA, TBP and synergistic D2EHPA/TBP system, the extraction of Ni^{2+} and $[Au(CN)_2]^-$ increased. Beyond 0.50 mol/L and up to 1.00 mol/L, it is seen that the slight difference in extraction of Ni^{2+} and $[Au(CN)_2]^-$ reveals that the plateau stage was reached. Thus, 0.50 mol/L concentration of the extractant proved to be sufficient and economical for the extraction of Ni^{2+} and $[Au(CN)_2]^-$ in trace amount.

จุฬาลงกรณ์มหาวิทยาลัย
Chulalongkorn University

2.5.5 Effect of the type of strippant

The type of strippant or stripping agent is one of the key factors for the back extraction or stripping of metal ions from a thin layer of the organic liquid membrane. The loaded organic phase was stripped using different acidic solutions. In Table 2.8, stripping efficiencies of the various strippants i.e. distilled water (H_2O) and the strong inorganic acids (HCl, H_2SO_4 and HNO_3) are presented. In the case of the synergistic D2EHPA/TBP extractants, stripping percentages of the target Ni^{2+} when using different strippants were found to be in the order: HCl > H_2SO_4 > H_2O > HNO_3. It was difficult to strip Ni^{2+} from the loaded D2EHPA/TBP using distilled water. Furthermore, stripping performances of the non-target $[Au(CN)_2]^-$ were less than 2% for all three strong inorganic acids. Thus, HCl was selected as the most suitable strippant for use in the HFSLM system due to the results, which affirm the highest selectivity of Ni^{2+} relative to $[Au(CN)_2]^-$ in the stripping solution.

จุฬาลงกรณ์มหาวิทยาลัย
CHULALONGKORN UNIVERSITY

Table 2.8 Effect of strippants on the selective stripping of Ni^{2+} and $[Au(CN)_2]^-$: feed phase; 15 mg/L Ni^{2+}, 25 mg/L $[Au(CN)_2]^-$, pH 8.6±0.05 | stripping solution; 0.50 mol/L strippant | $q_F = q_S$ = 200 mL/min | t = 2 h | T = 303±1 K.

Strippant	pH at 303 K	pK_a	Organic extractant	%Stripping		Distribution Ratio (D)		Selectivity ($S_{Ni/Au}$)
				Ni^{2+}	$[Au(CN)_2]^-$	Ni^{2+}	$[Au(CN)_2]^-$	
HCl	0.44±0.02	-6.11	0.25 M D2EHPA/0.25 M TBP	85.70 ±0.18	15.65 ±0.62	5.993 ±0.631	0.1855 ±0.0084	5.476 ±0.143
			0.50 M D2EHPA	56.18 ±0.89	24.21 ±0.57	1.282 ±0.043	0.3194 ±0.0096	2.321 ±0.021
			0.50 M TBP	52.68 ±0.73	31.54 ±0.85	1.113 ±0.035	0.4607 ±0.0172	1.670 ±0.075
HNO_3	0.42±0.02	-1.38	0.25 M D2EHPA/0.25 M TBP	4.473 ±0.158	1.941 ±0.020	0.04682 ±0.00164	0.01979 ±0.00028	2.304 ±0.213
			0.50 M D2EHPA	7.353 ±0.549	2.220 ±0.260	0.07937 ±0.00660	0.02270 ±0.00281	3.312 ±0.288
			0.50 M TBP	2.441 ±0.520	1.554 ±0.149	0.02502 ±0.00562	0.01579 ±0.00161	1.571 ±0.412
H_2SO_4	0.43±0.02	-3.00	0.25 M D2EHPA/0.25 M TBP	23.85 ±0.38	1.284 ±0.239	0.3132 ±0.0069	0.01301 ±0.00254	18.57 ±0.41
			0.50 M D2EHPA	9.862 ±0.379	2.432 ±0.521	0.1094 ±0.0048	0.02493 ±0.00564	4.055 ±0.017
			0.50 M TBP	4.723 ±0.092	1.230 ±0.521	0.0496 ±0.0011	0.01245 ±0.00071	3.840 ±.0478
H_2O	5.86±0.02	14.0	0.25 M D2EHPA/0.25 M TBP	3.050 ±0.317	5.006 ±0.331	0.03146 ±0.00355	0.05270 ±0.00379	0.6093 ±0.0084
			0.50 M D2EHPA	4.731 ±0.090	9.403 ±0.532	0.04966 ±0.00107	0.1038 ±0.0067	0.5031 ±0.0200
			0.50 M TBP	0.9906 ±0.036	12.21 ±0.263	0.01001 ±0.00037	0.1391 ±0.0035	0.08113 ±0.00108

To understand these observations in detail, awareness of the reaction mechanism between the metal-extractant complex and strippant is indispensable. The stripping mechanisms of Ni-extractant complexes by inorganic acids (HA), which occur at the organic-aqueous interface can be represented, as in Eqs. (2.15) to (2.18).

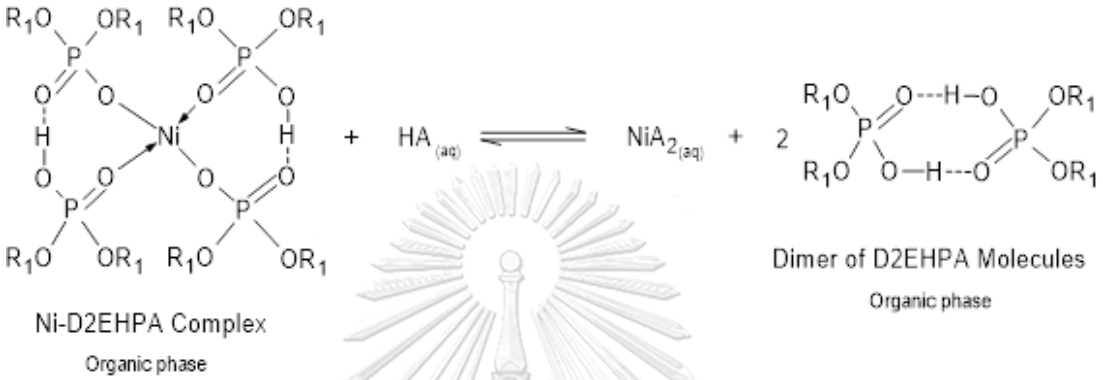

(2.15)

(2.16)

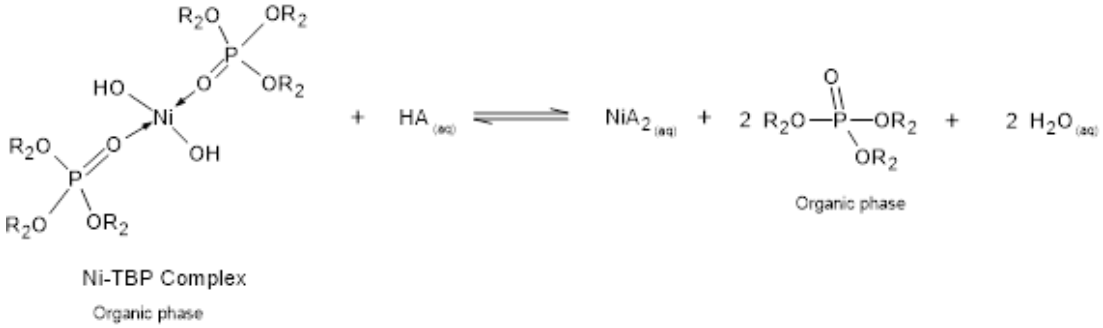

(2.17)

จุฬาลงกรณ์มหาวิทยาลัย
CHULALONGKORN UNIVERSITY

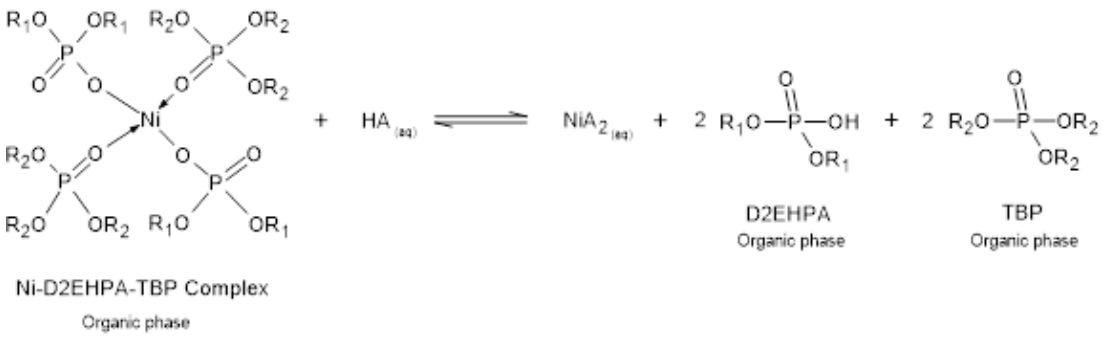

(2.18)

The case of different inorganic acids resulting in different stripping percentage of Ni-extractant complexes can be explained by the effect of pK_a of these acids. In simple terms, pK_a is a number that shows how weak or strong an acid is. A strong acid will have a pK_a of less than zero. The lower the value of pK_a, the stronger the acid and the greater its ability to donate its protons. The extraction of Ni^{2+} by D2EHPA and TBP extractants from the real rinse wastewater of the ENIG plating process is carried out in basic alkaline solution at pH 8.5±0.05. However, higher acid conditions are more favorable. D2EHPA has highly acidic properties, due to the presence of oxygen atoms bonding to the phosphorus atom and the alkyl radicals. In Eqs. (2.15) and (2.18), the strong interaction of O-Ni-O bonding between D2EHPA and Ni proved difficult for stripping in the mild acid. From Table 2.8, the order of pK_a of the three inorganic acids are listed as follows: HCl > H_2SO_4 > HNO_3. Thus, HCl is the most effective strippant.

2.5.6 Effect of stripping agent concentration

Since stripping depends on the nature of the metal complexes in the loaded organic phase, the nature and the concentration of acidic stripping solutions affect stripping efficiency. The effect of HCl concentration towards selective and synergistic stripping

of Ni^{2+} was studied in the range of 0.001 to 1.00 mol/L with pH from 3.01 to 0.1, as exhibited in Table 2.9 as well as Figs. 2.8 and 2.9.

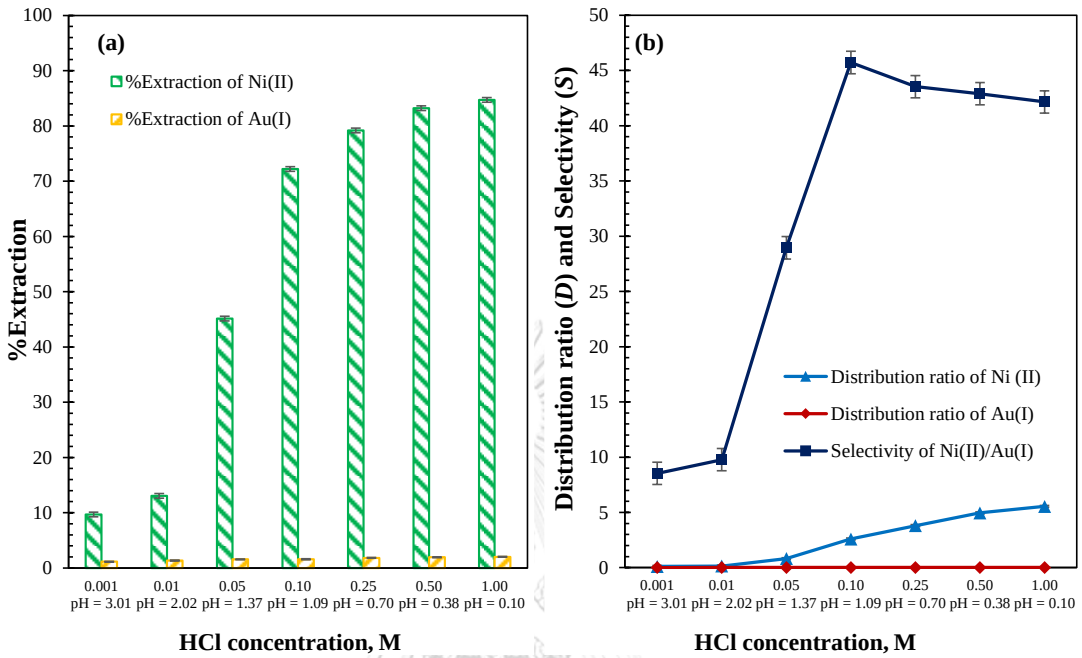

Figure 2.8 Effect of strippant concentration: feed phase; 15 mg/L Ni^{2+}, 25 mg/L $[Au(CN)_2]^-$, pH 8.6±0.05 | liquid membrane phase; mixture of 0.25 mol/L D2EHPA and 0.25 mol/L TBP extractants in kerosene | stripping phase; HCl | $q_F = q_S = 200$ mL/min | $t = 2$ h | $T = 303\pm1$ K.

จุฬาลงกรณ์มหาวิทยาลัย
CHULALONGKORN UNIVERSITY

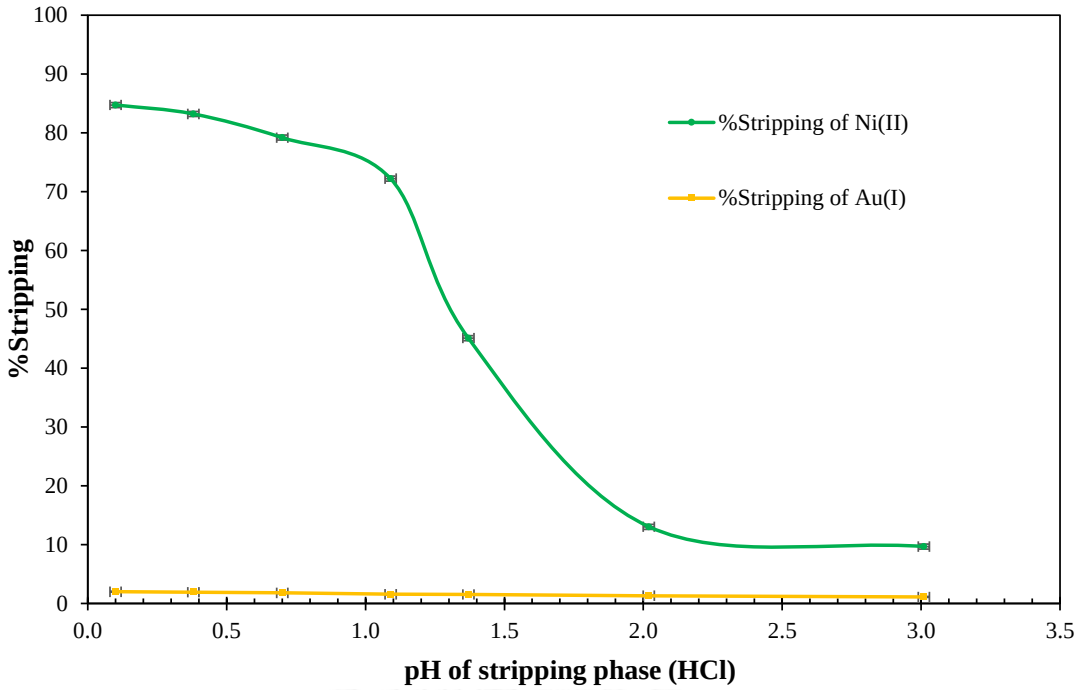

Figure 2.9 Stripping percentage of Ni^{2+} and $[Au(CN)_2]^-$ ions via HFSLM with various pH of HCl strippant: feed phase; 15 mg/L Ni^{2+}, 25 mg/L $[Au(CN)_2]^-$, pH 8.6±0.05 | liquid membrane phase; mixture of 0.25 mol/L D2EHPA and 0.25 mol/L TBP extractants in kerosene | stripping phase; HCl | $q_F = q_S$ = 200 mL/min | t = 2 h | T = 303±1 K.

จุฬาลงกรณ์มหาวิทยาลัย
CHULALONGKORN UNIVERSITY

Table 2.9 Effect of strippant concentration for Ni^{2+} and $[Au(CN)_2]^-$ extraction via HFSLM: feed phase; 15 mg/L Ni^{2+}, 25 mg/L $[Au(CN)_2]^-$, pH 8.6±0.05 | liquid membrane phase; mixture of 0.25 mol/L D2EHPA and 0.25 mol/L TBP extractants in kerosene | stripping phase; HCl | $q_F = q_S$ = 200 mL/min | t = 2 h | T = 303±1 K.

Strippant Concentration	pH at 303 K	%Stripping		Distribution Ratio (D)		Selectivity
		Ni^{2+}	$[Au(CN)_2]^-$	Ni^{2+}	$[Au(CN)_2]^-$	($S_{Ni/Au}$)
0.001 M HCl	3.01±0.02	9.683 ±0.273	1.134 ±0.255	0.1072 ±0.0035	0.01147 ±0.00262	8.536 ±1.374
0.01 M HCl	2.02±0.02	13.06 ±0.18	1.336 ±0.021	0.1502 ±0.0023	0.01354 ±0.00022	9.773 ±0.281
0.05 M HCl	1.37±0.02	45.12 ±0.63	1.558 ±0.014	0.8221 ±0.0220	0.01583 ±0.00014	28.95 ±0.20
0.10 M HCl	1.09±0.02	72.21 ±0.60	1.579 ±0.040	2.598 ±0.086	0.01605 ±0.00041	45.72 ±0.62
0.25 M HCl	0.70±0.02	79.18 ±0.61	1.819 ±0.061	3.802 ±0.161	0.01853 ±0.00063	43.53 ±0.94
0.50 M HCl	0.38±0.02	83.21 ±0.26	1.940 ±0.023	4.956 ±0.112	0.01978 ±0.00024	42.89 ±0.32
1.00 M HCl	0.10±0.02	84.73 ±0.42	2.010 ±0.137	5.549 ±0.217	0.02051 ±0.00142	42.15 ±3.33

CHULALONGKORN UNIVERSITY

As presented in Table 2.9, the increase in acid concentration increased the stripping percentage of Ni^{2+}. It is observed that Ni^{2+} stripping increased up to 85%; maximum HCl concentration was 1.00 mol/L. Beyond 0.50 mol/L HCl, stripping slightly increased. In Fig. 2.9, when pH of the stripping solution decreased, the stripping efficiency of Ni^{2+} increased. 0.50 mol/L HCl proved to be enough for selective stripping of Ni^{2+} from $[Au(CN)_2]^-$ in trace amount.

2.5.7 Equilibrium study of Ni^{2+} extraction via HFSLM

The extraction of Ni^{2+} using single extractants D2EHPA and TBP as well as the synergistic extractant mixture D2EHPA/TBP can be written as shown in Section 2.7: Supplementary information.

According to Eqs. (S2.10) and (S2.12), plots between $\ln(D_{Ni})$ in *y*-axis and $\ln([Extracant])$ in *x*-axis provide the equilibrium constant (K_{ex}) from the y-axis intersection as shown in Table 2.10.

Table 2.10 Equilibrium constant (K_{Ex}) for Ni^{2+} extraction via HFSLM.

Extractant	K_{Ex}
D2EHPA	3.719 mol/L
TBP	1.479 $(mol/L)^{-1}$
D2EHPA/TBP (1:1 ratio)	11.35

2.5.8 Mass transfer coefficient for Ni^{2+} extraction from the real rinse wastewater of the ENIG plating process via HFSLM

For the recycling mode of operation both feed and strip phases are continuously recirculated from the respective reservoirs. The resistances across the feed–membrane interface, membrane pore and strip–membrane interface are related as follows [74]. Detail calculation on mass transfer coefficients and mass balance have shown in Section 2.8 Appendix B.

Eqs. (S2.40) to (S2.42) in Section 2.8 Appendix B is applied to calculate the diffusion flux (J_D) and the mass transfer coefficient for Ni^{2+} and $[Au(CN)_2]^-$ via the liquid membrane. The results are shown in Table 2.11.

จุฬาลงกรณ์มหาวิทยาลัย
CHULALONGKORN UNIVERSITY

Table 2.11 Mass transfer coefficient of Ni^{2+} and $[Au(CN)_2]^-$ extraction via HFSLM: feed phase; 15 mg/L Ni^{2+}, 25 mg/L $[Au(CN)_2]^-$, pH 8.6±0.05 | liquid membrane phase; total extractant concentration of 0.50 mol/L in kerosene | stripping phase; 0.50 mol/L HCl, pH 0.38±0.05 | $q_F = q_S$ = 200 mL/min | t = 2 h | T = 303±1 K.

Ni^{2+} ions extraction from feed phase to liquid membrane phase		
Extractant	J_D, mmol/m^2·s	$K_{ex,}$ m/s
0.50 mol/L D2EHPA	1.42×10^{-5}	12.7×10^{-5}
0.50 mol/L TBP	1.34×10^{-5}	11.0×10^{-5}
0.25 mol/L D2EHPA/0.25 mol/L TBP	2.17×10^{-5}	59.4×10^{-5}
$[Au(CN)_2]^-$ ions extraction from feed phase to liquid membrane phase		
Extractant	J_D, mmol/m^2·s	$K_{ex,}$ m/s
0.50 mol/L D2EHPA	0.305×10^{-5}	3.17×10^{-5}
0.50 mol/L TBP	0.397×10^{-5}	4.57×10^{-5}
0.25 mol/L D2EHPA/0.25 mol/L TBP	0.197×10^{-5}	1.84×10^{-5}

2.5.9 Determination of the reaction order and the reaction rate constant for Ni^{2+} and $[Au(CN)_2]^-$ extraction from the real rinse wastewater of the ENIG plating process via HFSLM

The reaction order (n) and the reaction rate constant for Ni^{2+} and $[Au(CN)_2]^-$ extraction ($k_{ex,Ni}$) were verified by integration and graphical method, as shown in Table 2.12.

จุฬาลงกรณ์มหาวิทยาลัย
CHULALONGKORN UNIVERSITY

Table 2.12 Analysis of reaction order and rate constants: feed phase; 15 mg/L Ni^{2+}, 25 mg/L $[Au(CN)_2]^-$, pH 8.6±0.05 | liquid membrane phase; total extractant concentration of 0.50 mol/L in kerosene | stripping phase; 0.50 mol/L HCl, pH 0.38±0.05 | $q_F = q_S$ = 200 mL/min | t = 2 h | T = 303±1 K.

Ni^{2+} extraction from feed phase to liquid membrane phase					
Extractant	Rate order	Reaction rate constant		R^2	Remark
0.50 mol/L D2EHPA	0	1.6×10^{-3}	$mmol\cdot L^{-1}\cdot min^{-1}$	0.5786	
	1	9×10^{-3}	min^{-1}	0.7224	
	2	2×10^{-5}	$L\cdot mmol^{-1}\cdot min^{-1}$	0.8396	Best fit
0.50 mol/L TBP	0	1.4×10^{-3}	$mmol\cdot L^{-1}\cdot min^{-1}$	0.8574	
	1	7.4×10^{-3}	min^{-1}	0.9187	
	2	1×10^{-5}	$L\cdot mmol^{-1}\cdot min^{-1}$	0.9631	Best fit
0.25 mol/L D2EHPA/ 0.25 mol/L TBP	0	2.6×10^{-3}	$mmol\cdot L^{-1}\cdot min^{-1}$	0.3932	
	1	2.22×10^{-2}	min^{-1}	0.6043	
	2	7×10^{-5}	$L\cdot mmol^{-1}\cdot min^{-1}$	0.7927	Best fit
$[Au(CN)_2]^-$ extraction from feed phase to liquid membrane phase					
Extractant	Rate order	Reaction rate constant		R^2	Remark
0.50 mol/L D2EHPA	0	3×10^{-4}	$mmol\cdot L^{-1}\cdot min^{-1}$	0.9821	Best fit
	1	2.3×10^{-3}	min^{-1}	0.9808	
	2	5×10^{-7}	$L\cdot mmol^{-1}\cdot min^{-1}$	0.9772	
0.50 mol/L TBP	0	3×10^{-4}	$mmol\cdot L^{-1}\cdot min^{-1}$	0.9934	
	1	3.2×10^{-3}	min^{-1}	0.9958	Best fit
	2	7×10^{-7}	$L\cdot mmol^{-1}\cdot min^{-1}$	0.9928	
0.25 mol/L D2EHPA/ 0.25 mol/L TBP	0	2×10^{-4}	$mmol\cdot L^{-1}\cdot min^{-1}$	0.9821	Best fit
	1	1.4×10^{-3}	min^{-1}	0.9815	
	2	3×10^{-7}	$L\cdot mmol^{-1}\cdot min^{-1}$	0.9801	

จุฬาลงกรณ์มหาวิทยาลัย
CHULALONGKORN UNIVERSITY

2.6 Conclusions

In this study, results demonstrate that HFSLM could successfully separate Ni^{2+} and $[Au(CN)_2]^-$ from the real rinse wastewater of the ENIG plating process. It is evident that the binary mixtures having acidic/neutral extractants of D2EHPA/TBP were found to be capable of selectively extracting both Ni^{2+} and $[Au(CN)_2]^-$ at low concentrations from the feed solution viz. up to 85.70% and 15.65%, respectively. Optimum conditions proved to be 0.25 mol/L D2EHPA and 0.25 mol/L TBP in kerosene in the liquid membrane phase. Subsequently, 0.50 mol/L HCl was employed as a stripping agent (strippant) for the back extraction of Ni^{2+} and for $[Au(CN)_2]^-$ from the liquid membrane phase. The HFSLM technique illustrates the selective extraction of Ni^{2+} over other conventional techniques. The successful separation of Ni^{2+} from the real rinse wastewater of the ENIG plating process via HFSLM proved its worth that it can be a most useful technique in the integrated operation of the ENIG plating process.

2.7 Supplementary information

Calculation detail on equilibrium constant of Ni^{2+} and $[Au(CN)_2]^-$ extractant with three extractant systems can be expressed as:

$$\mathrm{Ni}^{2+}_{(aq)} + (1+x)(\mathrm{HR})_{2(org)} \overset{K_{Ex}}{\rightleftharpoons} \mathrm{NiR}_2 \cdot (\mathrm{HR})_{2x(org)} + 2\mathrm{H}^+_{(aq)} \quad \text{(S2.1)}$$

$$\mathrm{Ni}^{2+}_{(aq)} + y\mathrm{TBP}_{(org)} \overset{K_{Ex}}{\rightleftharpoons} \mathrm{Ni}^{2+} \cdot y\mathrm{TBP}_{(org)} \quad \text{(S2.2)}$$

$$\mathrm{Ni}^{2+}_{(aq)} + (1+x)(\mathrm{HR})_{2(org)} + y\mathrm{TBP}_{(org)} \overset{K_{Ex}}{\rightleftharpoons} \mathrm{NiR}_2 \cdot y\mathrm{TBP}_{(org)} + 2x\mathrm{HR}_{(org)} + 2\mathrm{H}^+_{(aq)} \quad \text{(S2.3)}$$

where HR is D2EHPA, x and y are the stoichiometric coefficients associated with the D2EHPA and TBP extractants, respectively.

Based on the above complexation reaction, the equilibrium constant (K_{Ex}) of Ni^{2+} in the aqueous feed solutions can be written as:

$$K_{Ex,\mathrm{Ni,D2EHPA}} = \frac{\left[\mathrm{NiR_2}\cdot(\mathrm{HR})_{2x(org)}\right]\left[\mathrm{H}^+_{(aq)}\right]^2}{\left[\mathrm{Ni}^{2+}_{(aq)}\right]\left[(\mathrm{HR})_{2(org)}\right]^{(1+x)}} \tag{S2.4}$$

$$K_{Ex,\mathrm{Ni,TBP}} = \frac{\left[\mathrm{Ni}^{2+}\cdot y\mathrm{TBP}_{(org)}\right]}{\left[\mathrm{Ni}^{2+}_{(aq)}\right]\left[\mathrm{TBP}_{(org)}\right]^{y}} \tag{S2.5}$$

$$K_{Ex,\mathrm{Ni,D2EHPA/TBP}} = \frac{\left[\mathrm{NiR_2}\cdot m\mathrm{TBP}_{(org)}\right]\left[\mathrm{HR}_{(org)}\right]^{2x}\left[\mathrm{H}^+_{(aq)}\right]^2}{\left[\mathrm{Ni}^{2+}_{(aq)}\right]\left[(\mathrm{HR})_{2(org)}\right]^{(1+x)}\left[\mathrm{TBP}_{(org)}\right]^{y}} \tag{S2.6}$$

Eqs. (S2.4) to (S2.66) can be written in terms of the distribution coefficient of the Ni^{2+} in the organic phase as:

$$K_{Ex,\mathrm{Ni,D2EHPA}} = \frac{D_{\mathrm{Ni,D2EHPA}}\left[\mathrm{H}^+_{(aq)}\right]^2}{\left[(\mathrm{HR})_{2(org)}\right]^{(1+x)}} \tag{S2.7}$$

$$K_{Ex,\mathrm{Ni,TBP}} = \frac{D_{\mathrm{Ni,TBP}}}{\left[\mathrm{TBP}_{(org)}\right]^{y}} \tag{S2.8}$$

$$K_{Ex,\mathrm{Ni,D2EHPA/TBP}} = \frac{D_{\mathrm{Ni,\ D2EHPA/TBP}}\left[\mathrm{HR}_{(org)}\right]^{2x}\left[\mathrm{H}^+_{(aq)}\right]^2}{\left[(\mathrm{HR})_{2(org)}\right]^{(1+x)}\left[\mathrm{TBP}_{(org)}\right]^{y}} \tag{S2.9}$$

Rearranging Eqs. (S2.7) to (S2.9) and taking the natural logarithm on both sides:

$$\ln\left(D_{\mathrm{Ni,D2EHPA}}\right) = (1+x)\ln\left(\left[(\mathrm{HR})_{2(org)}\right]\right) + \ln\left(K_{Ex,\mathrm{Ni,D2EHPA}}\right) - 2\ln\left(\left[\mathrm{H}^+_{(aq)}\right]\right) \tag{S2.10}$$

จุฬาลงกรณ์มหาวิทยาลัย
CHULALONGKORN UNIVERSITY

$$\ln\left(D_{\mathrm{Ni,TBP}}\right) = y\ln\left(\left[\mathrm{TBP}_{(org)}\right]\right) + \ln\left(K_{Ex,\mathrm{Ni,TBP}}\right) \tag{S2.11}$$

$$\ln\left(D_{\mathrm{Ni,D2EHPA/TBP}}\right) = (1+x)\ln\left(\left[(\mathrm{HR})_{2(aq)}\right]\right) + y\ln\left(\left[\mathrm{TBP}_{(aq)}\right]\right) + \ln\left(K_{Ex,\mathrm{Ni,D2EHPA/TBP}}\right) - 2x\ln\left(\left[\mathrm{HR}_{(org)}\right]\right) - 2\ln\left(\left[\mathrm{H}^{+}_{(aq)}\right]\right) \tag{S2.12}$$

Detail calculation base on mass balance for separation of Ni^{2+} ions via HFSLM [75].

$$R_T = \frac{C_f - \left(\frac{k_2}{k_1}\right)C_s}{\frac{1}{k_f} + \frac{d_0}{D_m}\left(\frac{1}{k_1}\right) + \frac{1}{k_s}\left(\frac{k_2}{k_1}\right)} = K\left(C_f - mC_s\right) \tag{S2.13}$$

where C_f is the bulk concentration of the Ni^{2+} in the feed-side (lumen-side) fluid at location "z" of the lumen (kmol/m^3), C_s is the bulk concentration of the Ni^{2+} in the strip-side (shell-side) fluid at location "z" of the shell (kmol/m^3), k_f is the feed-side film mass transfer coefficient (m/s), k_s is the strip-side film mass transfer coefficient (m/s), d_o is the hollow fiber thickness (m), D_m is the molecular diffusion coefficient of the metal-carrier complex in the HFSLM (m^2/s), k_1 is the feed-side distribution coefficient of Ni^{2+} and k_2 is the strip-side distribution coefficient of Ni^{2+}.

$$\frac{1}{K} = \frac{1}{k_f} + \frac{d_0}{D_m}\left(\frac{1}{k_1}\right) + \frac{1}{k_s}\left(\frac{k_2}{k_1}\right) \tag{S2.14}$$

Here, K is defined as the overall mass transfer coefficient of the transport process, m/s.

From the equilibrium constant (K_{Ex}) from Eqs. (S2.1) to (S2.3), the feed-membrane interface and the strip-membrane interface can be modified:

$$K_{Ex,\mathrm{Ni,D2EHPA}} = \frac{C_{imf,\overline{\mathrm{Ni\text{-}D2EHPA}}} \cdot \left(C_{hif}\right)^2}{C_{if,\mathrm{Ni}} \left[(\mathrm{HR})_{2(org)}\right]_{free,f}} \tag{S2.15}$$

$$K_{Ex,\mathrm{Ni,D2EHPA}} = \frac{C_{ims,\overline{\mathrm{Ni/D2EHPA}}} \cdot \left(C_{his}\right)^2}{C_{is,\mathrm{Ni}} \left[(\mathrm{HR})_{2(org)}\right]_{free,s}} \tag{S2.16}$$

$$K_{Ex,\mathrm{Ni,TBP}} = \frac{C_{imf,\overline{\mathrm{Ni\text{-}TBP}}}}{C_{if} \left[\mathrm{TBP}_{(org)}\right]_{free,f}} \tag{S2.17}$$

$$K_{Ex,\mathrm{Ni,TBP}} = \frac{C_{ims,\overline{\mathrm{Ni\text{-}TBP}}}}{C_{is} \left[\mathrm{TBP}_{(org)}\right]_{free,s}} \tag{S2.18}$$

$$K_{Ex,\mathrm{Ni,D2EHPA/TBP}} = \frac{C_{imf,\overline{\mathrm{Ni\text{-}D2EHPA\text{-}TBP}}} \cdot \left(C_{ihf}\right)^2}{C_{if,\mathrm{Ni}} \left[(\mathrm{HR})_{2(org)}\right]_f^{0.55} \left[\mathrm{HR}_{(org)}\right]_f^{0.9} \left[\mathrm{TBP}_{(org)}\right]_f^{0.55}} \tag{S2.19}$$

$$K_{Ex,\mathrm{Ni,D2EHPA/TBP}} = \frac{C_{ims,\overline{\mathrm{Ni\text{-}D2EHPA\text{-}TBP}}} \cdot \left(C_{ihs}\right)^2}{C_{is,\mathrm{Ni}} \left[(\mathrm{HR})_{2(org)}\right]_s^{0.55} \left[\mathrm{HR}_{(org)}\right]_s^{0.9} \left[\mathrm{TBP}_{(org)}\right]_s^{0.55}} \tag{S2.20}$$

where, C_{imf} and C_{ims} are the organic-metal complex concentration at the feed-membrane interface and the strip-membrane interface respectively, kmol/m^3. C_{ihf} and C_{his} are the concentrations of the H^+ at the feed-membrane interface and the strip-membrane interface respectively, kmol/m^3.

From the above-mentioned equations:

$$k_{1,\mathrm{Ni/D2EHPA}} = K_{Ex,\mathrm{Ni/D2EHPA}} \frac{\left[(\mathrm{HR})_{2(org)}\right]_{free,f}}{\left(C_{hif}\right)^2} = \frac{C_{imf,\overline{\mathrm{Ni\text{-}D2EHPA}}}}{C_{if,\mathrm{Ni}}} \tag{S2.21}$$

$$k_{2,\text{Ni/D2EHPA}} = K_{Ex,\text{Ni/D2EHPA}} \frac{\left[(\text{HR})_{2(org)}\right]_{free,s}}{\left(C_{his}\right)^2} = \frac{C_{ims,\overline{\text{Ni/D2EHPA}}}}{C_{is,\text{Ni}}} \tag{S2.22}$$

$$k_{1,\text{Ni/TBP}} = K_{Ex,\text{Ni/TBP}} \left[\text{TBP}_{(org)}\right]_{free,f} = \frac{C_{imf,\overline{\text{Ni-TBP}}}}{C_{if}} \tag{S2.23}$$

$$k_{2,\text{Ni/TBP}} = K_{Ex,\text{Ni/TBP}} \left[\text{TBP}_{(org)}\right]_{free,s} = \frac{C_{ims,\overline{\text{Ni-TBP}}}}{C_{is}} \tag{S2.24}$$

$$k_{1,\text{Ni/D2EHPA/TBP}} = K_{Ex,\text{Ni/D2EHPA/TBP}} \frac{\left[(\text{HR})_{2(org)}\right]_{free,f}^{0.55} \left[\text{HR}_{(org)}\right]_{free,f}^{0.9} \left[\text{TBP}_{(org)}\right]_{free,f}^{0.55}}{\left(C_{ihf}\right)^2} = \frac{C_{imf,\overline{\text{Ni-D2EHPA-TBP}}}}{C_{if,\text{Ni}}}$$

(S2.25)

$$k_{2,\text{Ni/D2EHPA/TBP}} = K_{Ex,\text{Ni/D2EHPA/TBP}} \frac{\left[(\text{HR})_{2(org)}\right]_{free,s}^{0.55} \left[\text{HR}_{(org)}\right]_{free,s}^{0.9} \left[\text{TBP}_{(org)}\right]_{free,s}^{0.55}}{\left(C_{ihs}\right)^2} = \frac{C_{ims,\overline{\text{Ni-D2EHPA-TBP}}}}{C_{is,\text{Ni}}}$$

(S2.26)

where k_1 and k_2 are the distribution coefficients on the feed and strip sides of the membrane, respectively, and C_{if} and C_{is} are the concentration of the metal ions in the feed phase at the feed-membrane interface and the concentration of metal ions in the strip phase at the strip-membrane interface, respectively, kmol/m^3.

The ratio of k_1 and k_2 can be written as:

$$m_{\text{Ni/D2EHPA}} = \frac{k_2}{k_1} = \left(\frac{C_{hif}}{C_{his}}\right)^2 \frac{\left[(\text{HR})_{2(org)}\right]_{free,s}}{\left[(\text{HR})_{2(org)}\right]_{free,f}} \tag{S2.27}$$

$$m_{\text{Ni,TBP}} = \frac{\left[\text{TBP}_{(org)}\right]_{free,s}}{\left[\text{TBP}_{(org)}\right]_{free,f}} \tag{S2.28}$$

$$m_{\mathrm{Ni,D2EHPA/TBP}} = \left(\frac{C_{ihf}}{C_{ihs}}\right)^2 \frac{\left[(\mathrm{HR})_{2(org)}\right]_{free,s}^{0.55}\left[\mathrm{HR}_{(org)}\right]_{free,s}^{0.9}\left[\mathrm{TBP}_{(org)}\right]_{free,s}^{0.55}}{\left[(\mathrm{HR})_{2(org)}\right]_{free,f}^{0.55}\left[\mathrm{HR}_{(org)}\right]_{free,f}^{0.9}\left[\mathrm{TBP}_{(org)}\right]_{free,f}^{0.55}} \tag{S2.29}$$

The high value of strip acidity or buffered feed phase or the high D2EHPA and TBP concentration results in low values of "*m*". This implies that the strip-side equilibrium reaction is instantaneous and hence strip-side film resistance may be neglected [76].

For the calculation of *m*, the organic extractant balance can be expressed as:

$$\left[(\mathrm{HR})_{2(org)}\right]_{free} = \left[(\mathrm{HR})_{2(org)}\right]_{initial} - n_1 \sum\left[\mathrm{M\text{-}Complex}_{(org)}\right]_i \tag{S2.30}$$

$$\left[\mathrm{TBP}_{(org)}\right]_{free} = \left[\mathrm{TBP}_{(org)}\right]_{initial} - n_2 \sum\left[\mathrm{M\text{-}Complex}_{(org)}\right]_i \tag{S2.31}$$

Here, n_1 and n_2 are the stoichiometric coefficients associated with the organic-metal complex, $\sum\left[\mathrm{M\text{-}Complex}_{(org)}\right]_i$ is the sum of all the metal ions complexes with the organic extractant.

Similarly, as per the complexation reaction, Eqs. (S2.1) and (S2.3), the H^+ balance is as follows:

$$C_{hf\,0(t=t)} = C_{hf\,0(t=0)} + \sum\left\{C_{f\,0(t=0)} - C_{f\,0(t=t)}\right\}_i \tag{S2.32}$$

$$C_{hs0(t=t)} = C_{hs0(t=0)} + \sum\left\{C_{s0(t=0)} - C_{s0(t=t)}\right\}_i \tag{S2.33}$$

where $C_{hf\,0}$ is the bulk concentration of the H^+ in the feed reservoir or the bulk inlet concentration of the H^+ in the feed-side fluid at the lumen inlet (kmol/m^3) at respective time (t = 0 and t = t) and C_{hs0} is the bulk concentration of the H^+ in the strip reservoir

or the bulk inlet concentration of the H^+ in the strip-side fluid at the shell inlet at respective time (t = 0 and t = t) (kmol/m^3). For the present study, the feed was buffered as the pH was maintained constant at 8.6±0.05. Hence C_{hs0} was kept constant.

The mass balance across the feed/strip reservoirs is given as:

$$V_F \frac{dC_{F,0}}{dt} = q_F \left(C_{F,z} - C_{F,0} \right) \tag{S2.34}$$

$$V_S \frac{dC_{S,0}}{dt} = q_F \left(C_{S,z} - C_{S,0} \right) \tag{S2.35}$$

Here, V is the volume of feed (V_F) and strip reservoir (V_S) (m^3), and t is the time (s).

The module exit concentrations for both feed phase and strip phase are calculated accordingly:

$$C_{F,z} = \frac{C_{F,0}\left(1 - m\frac{q_F}{q_S}\right)\exp\left[\frac{-2\varepsilon KL}{r_i u_f}\left(1 - m\frac{q_F}{q_S}\right)\right]}{1 - m\frac{q_F}{q_S}\exp\left[\frac{-2\varepsilon KL}{r_i u_f}\left(1 - m\frac{q_F}{q_S}\right)\right]} + \frac{mC_{S,0}\left\{1 - \exp\left[\frac{-2\varepsilon KL}{r_i u_f}\left(1 - m\frac{q_F}{q_S}\right)\right]\right\}}{1 - m\frac{q_F}{q_S}\exp\left[\frac{-2\varepsilon KL}{r_i u_f}\left(1 - m\frac{q_F}{q_S}\right)\right]} \tag{S2.36}$$

$$C_{S,z} = C_{S,0} + \frac{q_F}{q_S}\left(C_{F,0} - C_{F,z} \right) \tag{S2.37}$$

where $C_{F,z}$ is the bulk outlet concentration of the Ni^{2+} in the feed-side fluid at the lumen exit (kmol/m^3), $C_{F,0}$ is the bulk concentration of the Ni^{2+} in the feed reservoir or the bulk inlet concentration of the Ni^{2+} in the feed-side fluid at the lumen inlet (kmol/m^3), q_F is the volumetric flow of the feed phase through the lumen of the module (m^3/s), q_S is the volumetric flow of the strip phase through the shell of the module (m^3/s), ε

is the porosity of the membrane, L is the length of the module (m), r_i is the fiber inner radius (m), u_f is the fiber velocity (m/s), $C_{S,0}$ is the bulk concentration of the Ni^{2+} in the strip reservoir or the bulk inlet concentration of the Ni^{2+} in the strip-side fluid at the shell inlet (kmol/m^3) and $C_{S,z}$ is the bulk outlet concentration of the Ni^{2+} in the strip-side fluid at the shell exit (kmol/m^3).

Ni^{2+} and $[Au(CN_2)]^-$ transport from the feed to the organic membrane phase is given by:

$$\frac{d\left[\mathrm{Ni}^{2+}{}_{(aq)}\right]_F}{dt} = -\frac{A}{V_a} J_{D,\mathrm{Ni}} \tag{S2.38}$$

$$\frac{d\left[\left[\mathrm{Au}\left(CN\right)_2\right]^-{}_{(aq)}\right]_F}{dt} = -\frac{A}{V_a} J_{D,\mathrm{Au}} \tag{S2.39}$$

The flux through the supported liquid membrane can be described by:

$$J_D = \left(\frac{1}{A}\right)\frac{dq}{dt} = -D\frac{dC}{dx} \tag{S2.40}$$

Where J_D is diffusional flux per unit area (moles·s^{-1}·cm^{-2}); q is amount (moles); t = time (sec); D = diffusion coefficient in the region (cm^2·s^{-1}); A = area available for diffusion (cm^2). The driving force is the spatial gradient in concentration or, more properly, in activity.

The mass transfer coefficient for Ni^{2+} and $[Au(CN)_2]^-$ extraction via HFSLM can be calculated from Eqs. (B2.29) and (B2.30), respectively [77]:

$$K_{Ex,\mathrm{Ni}} = \frac{J_{D,\mathrm{Ni}}}{\left[\mathrm{Ni}^{2+}{}_{(aq)}\right]_F} \tag{S2.41}$$

$$K_{Ex,\mathrm{Au}} = \frac{J_{D,\mathrm{Au}}}{\left[\left[\mathrm{Au}\left(CN\right)_2\right]^-_{(aq)}\right]_F} \tag{S2.42}$$

2.8 Acknowledgements

This work was supported by the Research and Researcher for Industry (RRI) of Thailand Research Fund (TRF) [grant numbers PHD60I005]; Mektec Manufacturing corporation (Thailand) ltd.; the Mass Separation Laboratory, Department of Chemical Engineering, Chulalongkorn University as well as the Research Cess Fund (Malaysia–Thailand Joint Authority).

2.9 References

[1] H. Roberts, K. Johal, Lead-Free Board Surface Finishes, in: J. Bath (Ed.) Lead-Free Soldering, Springer US, Boston, MA, 2007, pp. 221-269.

[2] R. Nichols, Lead-Free Printed Wiring Board Surface Finishes, Lead-free Soldering Process Development and Reliability, (2020) 249-305.

[3] T. Osaka, T. Misato, J. Sato, H. Akiya, T. Homma, M. Kato, Y. Okinaka, O. Yoshioka, Evaluation of Substrate (Ni)-Catalyzed Electroless Gold Plating Process, Journal of The Electrochemical Society, 147 (2000) 1059.

[4] A. Accogli, E. Gibertini, G. Panzeri, A. Lucotti, L. Magagnin, Understanding the Failure Mode of Electroless Nickel Immersion Gold Process: In Situ-Raman Spectroscopy and Electrochemical Characterization, Journal of the Electrochemical Society, 167 (2020).

[5] L. Sun, E. Miznikov, L. Wang, A. Adin, Nickel removal from wastewater by electroflocculation-filtration hybridization, Desalination, 249 (2009) 832-836.

[6] H. Cangul, L. Broday, K. Salnikow, J. Sutherland, W. Peng, Q. Zhang, V. Poltaratsky, H. Yee, M.A. Zoroddu, M. Costa, Molecular mechanisms of nickel carcinogenesis, Toxicology Letters, 127 (2002) 69-75.

[7] S.K. Seilkop, A.R. Oller, Respiratory cancer risks associated with low-level nickel exposure: an integrated assessment based on animal, epidemiological, and mechanistic data, Regulatory Toxicology and Pharmacology, 37 (2003) 173-190.

[8] R. Khosravi, A. Azizi, R. Ghaedrahmati, V.K. Gupta, S. Agarwal, Adsorption of gold from cyanide leaching solution onto activated carbon originating from coconut shell—Optimization, kinetics and equilibrium studies, Journal of Industrial and Engineering Chemistry, 54 (2017) 464-471.

[9] M. Morcali, B. Zeytuncu, E. Ozlem, S. Aktas, Studies of Gold Adsorption from Chloride Media, Materials Research, 18 (2015) 660-667.

[10] C. Brooks, Metal Recovery from Industrial Waste, 2018.

[11] G. Hussain, M.A. Khan, Adsorption of Gold (III) from Aqueous Solutions on Bagasse Ash, in, 2011.

[12] T.A. Kurniawan, G.Y.S. Chan, W.-H. Lo, S. Babel, Physico–chemical treatment techniques for wastewater laden with heavy metals, Chemical Engineering Journal, 118 (2006) 83-98.

[13] F. Fu, Q. Wang, Removal of heavy metal ions from wastewaters: A review, Journal of Environmental Management, 92 (2011) 407-418.

[14] V.K. Gupta, I. Ali, T.A. Saleh, A. Nayak, S. Agarwal, Chemical treatment technologies for waste-water recycling—an overview, RSC Advances, 2 (2012) 6380-6388.

[15] M. Barakat, New Trends in Removing Heavy Metals from Industrial Wastewater, Arabian Journal of Chemistry, 4 (2011) 361-377.

[16] S. Gunatilake, Methods of Removing Heavy Metals from Industrial Wastewater, Journal of Multidiciplinary Engineering Science Studies, 1 (2015).

[17] N. Sunsandee, N. Leepipatpiboon, P. Ramakul, U. Pancharoen, The selective separation of (S)-amlodipine via a hollow fiber supported liquid membrane: Modeling and experimental verification, Chemical Engineering Journal, 180 (2012) 299-308.

[18] T. Wannachod, T. Wongsawa, P. Ramakul, U. Pancharoen, S. Kheawhom, The synergistic extraction of uranium ions from monazite leach solution via HFSLM and its mass transfer, Journal of Industrial and Engineering Chemistry, 33 (2015).

[19] Z. Es'haghi, R. Azmoodeh, Hollow fiber supported liquid membrane microextraction of Cu2+ followed by flame atomic absorption spectroscopy determination, Arabian Journal of Chemistry, 3 (2010) 21-26.

[20] A.W. Lothongkum, U. Pancharoen, T. Prapasawat, Treatment of heavy metals from industrial wastewaters using hollow fiber supported liquid membrane, Water Treatment Processes, (2013) 300-332.

[21] Z. Es'haghi, A. Nezhadali, H.A. Hosseini, S. Mohammadi-Nokhandani, Pre-concentration and determination of zinc in water samples by ligand assisted pseudo stirbar hollow fiber solid/liquid phase microextraction, Arabian Journal of Chemistry, 10 (2017) S3840-S3847.

[22] S. Panja, P.K. Mohapatra, S.C. Tripathi, V.K. Manchanda, Facilitated transport of uranium(VI) across supported liquid membranes containing T2EHDGA as the carrier extractant, Journal of Hazardous Materials, 188 (2011) 281-287.

[23] R. Vijayalakshmi, S. Chaudhury, A. Mallavarapu, D. Singh, S. Aggarwal, H. Singh, Studies on yttrium permeation through hollow fibre supported liquid membrane from nitrate medium using di-nonyl phenyl phosphoric acid as the carrier phase, International Journal of Mineral Processing, 135 (2015).

[24] S. Chaudhury, A new approach for selective Cs+ separation from simulated nuclear waste solution using electrodriven cation transport through hollow fiber supported liquid membranes, Journal of membrane science, v. 545 (2018) pp. 75-80-2018 v.2545.

[25] A.C. Ni'am, Y.-F. Wang, S.-W. Chen, G.-M. Chang, S.-J. You, Simultaneous recovery of rare earth elements from waste permanent magnets (WPMs) leach liquor by solvent extraction and hollow fiber supported liquid membrane, Chemical Engineering and Processing - Process Intensification, 148 (2020) 107831.

จุฬาลงกรณ์มหาวิทยาลัย
Chulalongkorn University

[26] C.S. Kedari, J.S. Yadav, C.P. Kaushik, TALSPEAK process on hollow fiber renewable liquid membrane apropos to the remedial maneuver of high level nuclear waste, Journal of Hazardous Materials, 399 (2020) 123050.

[27] H. Duan, S. Wang, X. Yang, X. Yuan, Q. Zhang, Z. Huang, H. Guo, Simultaneous separation of copper from nickel in ammoniacal solutions using supported liquid membrane containing synergistic mixture of M5640 and TRPO, Chemical Engineering Research and Design, 117 (2017) 460-471.

[28] P. Zaheri, T. Mohammadi, H. Abolghasemi, M. Ghannadi Maraghe, Supported liquid membrane incorporated with carbon nanotubes for the extraction of Europium using Cyanex272 as carrier, Chemical Engineering Research and Design, 100 (2015) 81-88.

[29] P. Kazemi, M. Peydayesh, A. Bandegi, T. Mohammadi, O. Bakhtiari, Stability and extraction study of phenolic wastewater treatment by supported liquid membrane using tributyl phosphate and sesame oil as liquid membrane, Chemical Engineering Research and Design, 92 (2014) 375-383.

[30] V. Mohdee, V. Parasuk, U. Pancharoen, Synergistic effect of Thiourea and HCl on Palladium (II) recovery: An investigation on Chemical structures and thermodynamic stability via DFT, Arabian Journal of Chemistry, 14 (2021) 103196.

[31] M.S. Manna, K.K. Bhatluri, P. Saha, A.K. Ghoshal, Transportation of bioactive (+)catechin from its aqueous solution using flat sheet supported liquid membrane, Journal of Membrane Science, 447 (2013) 325-334.

[32] N. Sunsandee, S. Phatanasri, U. Pancharoen, Separation of homogeneous palladium catalysts from pharmaceutical industry wastewater by using synergistic recovery phase via HFSLM system, Arabian Journal of Chemistry, 14 (2021) 103024.

[33] A. Talebi, T.T. Teng, A.F.M. Alkarkhi, I. Norli, L.W. Low, Optimization of nickel removal using liquid–liquid extraction and response surface methodology, Desalination and Water Treatment, 47 (2012) 334-340.

จุฬาลงกรณ์มหาวิทยาลัย
Chulalongkorn University

[34] S.H. Chang, T.T. Teng, N. Ismail, Extraction of Cu(II) from aqueous solutions by vegetable oil-based organic solvents, Journal of Hazardous Materials, 181 (2010) 868-872.

[35] M.K. Jha, V. Kumar, J. Jeong, J.-c. Lee, Review on solvent extraction of cadmium from various solutions, Hydrometallurgy, 111-112 (2012) 1-9.

[36] Y. Jin, Y. Ma, Y. Weng, X. Jia, J. Li, Solvent extraction of Fe3+ from the hydrochloric acid route phosphoric acid by D2EHPA in kerosene, Journal of Industrial and Engineering Chemistry, 20 (2014) 3446-3452.

[37] C.S. Sousa Junior, M. Nascimento, I.O.C. Masson, O.G.C. Cunha, Equilibrium study for manganese extraction in sulfate media with D2EHPA in Isoparaffin (17/21), Hydrometallurgy, 103 (2010) 114-117.

[38] H. Jafari, H. Abdollahi, M. Gharabaghi, A.A. Balesini, Solvent extraction of zinc from synthetic Zn-Cd-Mn chloride solution using D2EHPA: Optimization and thermodynamic studies, Separation and Purification Technology, 197 (2018) 210-219.

[39] H.G. Nowier, N. El-Said, H.F. Aly, Carrier-mediated transport of toxic elements through liquid membranes: Transport of Cd(II) from high salinity chloride medium through supported liquid membrane containing TBP/cyclohexane, Journal of Membrane Science, 177 (2000) 41-47.

[40] A. Datta, D. Datta, A. Chandra, Separation and recovery of copper from aqueous solutions using tri-n-butyl phosphate in benzene, Journal of Molecular Liquids, 221 (2016) 139-148.

[41] P. Amani, J. Asadi, E. Mohammadi, S. Akhgar, M. Esmaili, Cooperative influence of D2EHPA and TBP on the reactive extraction of cobalt from sulfuric acid leach solution in a horizontal semi-industrial column, Journal of Environmental Chemical Engineering, 5 (2017) 4716-4727.

[42] S. Chaturabul, W. Srirachat, T. Wannachod, P. Ramakul, U. Pancharoen, S. Kheawhom, Separation of mercury(II) from petroleum produced water via

จุฬาลงกรณ์มหาวิทยาลัย
CHULALONGKORN UNIVERSITY

hollow fiber supported liquid membrane and mass transfer modeling, Chemical Engineering Journal, 265 (2015) 34-46.

[43] E. Vahidi, F. Rashchi, D. Moradkhani, Recovery of zinc from an industrial zinc leach residue by solvent extraction using D2EHPA, Minerals Engineering, 22 (2009) 204-206.

[44] E. Keshavarz Alamdari, D. Moradkhani, D. Darvishi, M. Askari, D. Behnian, Synergistic effect of MEHPA on co-extraction of zinc and cadmium with DEHPA, Minerals Engineering, 17 (2004) 89-92.

[45] A.D. Sharma, N.D. Patil, A.W. Patwardhan, R.K. Moorthy, P.K. Ghosh, Synergistic interplay between D2EHPA and TBP towards the extraction of lithium using hollow fiber supported liquid membrane, Separation Science and Technology, 51 (2016) 2242-2254.

[46] A. Azizitorghabeh, F. Rashchi, A. Babakhani, M. Noori, Synergistic extraction and separation of Fe(III) and Zn(II) using TBP and D2EHPA, Separation Science and Technology, 52 (2017) 476-486.

[47] B. Shakib, R. Torkaman, M. Torab-Mostaedi, M. Asadollahzadeh, Enhancing the Vanadium Extraction Performance Using Synergistic Mixtures of D2EHPA and TBP in RDC Column with the Perforated Structure; Case Study: Evaluation Probability Density Functions, Chemical Engineering and Processing - Process Intensification, 166 (2021) 108503.

[48] X. Meng, Y. Long, Y. Tian, W. Li, T. Liu, S. Huo, Electro-membrane extraction of lithium with D2EHPA/TBP compound extractant, Hydrometallurgy, 202 (2021) 105615.

[49] R. Zheng, S. Bao, Y. Zhang, B. Chen, Synthesis of Di-(2-ethylhexyl) Phosphoric Acid (D2EHPA)-Tributyl Phosphate (TBP) Impregnated Resin and Application in Adsorption of Vanadium(IV), Minerals, 8 (2018).

[50] L. Lee, N. Morad, M. Rafatullah, Synergistic Extraction of Cd, Cu and Ni with D2EHPA/TBP: Screening of Factors by Fractional Factorial Design,

จุฬาลงกรณ์มหาวิทยาลัย
Chulalongkorn University

International Journal of Chemical Engineering and Applications, 10 (2019) 114-120.

[51] B. Gajda, M.B. Bogacki, The effect of tributyl phosphate on the extraction of nickel(ii) and cobalt(ii) ions with di(2-ethylhexyl)phosphoric acid, Physicochem. Probl. Miner. Process., 41 (2007) 145-152.

[52] D. Haghshenas Fatmehsari, D. Darvishi, S. Etemadi, A.R. Eivazi Hollagh, E. Keshavarz Alamdari, A.A. Salardini, Interaction between TBP and D2EHPA during Zn, Cd, Mn, Cu, Co and Ni solvent extraction: A thermodynamic and empirical approach, Hydrometallurgy, 98 (2009) 143-147.

[53] V. Mohdee, P. Ramakul, S. Phatanasri, U. Pancharoen, A numerical and experimental investigation on the selective separation of Pd (II) from wastewater using Aliquat 336 via hollow fiber supported liquid membrane, Journal of Environmental Chemical Engineering, 8 (2020) 104234.

[54] T. Wannachod, T. Wongsawa, P. Ramakul, U. Pancharoen, S. Kheawhom, The synergistic extraction of uranium ions from monazite leach solution via HFSLM and its mass transfer, Journal of Industrial and Engineering Chemistry, 33 (2016) 246-254.

[55] T. Pirom, T. Wongsawa, T. Wannachod, N. Sunsandee, U. Pancharoen, S. Kheawhom, Amoxicillin removal from aqueous solutions using hollow fibre supported liquid membrane: kinetic study, Chemical Papers, 71 (2017) 1291-1302.

[56] J. Aggett, T.E. Clark, R.A. Richardson, Solvent extraction of divalent metal perchlorates by tributyl phosphate, Journal of Inorganic and Nuclear Chemistry, 31 (1969) 2919-2926.

[57] S.R. R. Sarkar, S. Basu, Synergism in solvent extraction and solvent extraction kinetics, J. Chem. Biol. Phys. Sci., 4 (2014) 3156-3181.

[58] M. Špadina, K. Bohinc, T. Zemb, J.-F. Dufrêche, Synergistic Solvent Extraction Is Driven by Entropy, ACS Nano, 13 (2019) 13745-13758.

จุฬาลงกรณ์มหาวิทยาลัย
Chulalongkorn University

[59] D.U. Bapat, V.H. Dalvi, Molecular Insights into Water Clusters Formed in Tributylphosphate-Di-(2-ethylhexyl)phosphoric Acid Extractant Systems from Experiments and Molecular Dynamics Simulations, J Phys Chem B, 123 (2019) 1618-1635.

[60] S. Chauhan, T.M. Patel, A Review on Solvent Extraction of Nickel, International journal of engineering research and technology, 3 (2014).

[61] M. Gharabaghi, M. Irannajad, A.R. Azadmehr, Separation of nickel and zinc ions in a synthetic acidic solution by solvent extraction using D2EHPA and Cyanex 272, Physicochem. Probl. Miner. Process., 49 (2013) 233-242.

[62] M.T. H. Narita, Y. Sato, Structure of the extracted complex in the Ni (II)-LIX84I system and the effect of D2EHPA addition, Solvent Extr. Ion Exch., 24 (2006) 693-702.

[63] M.B. Mooiman, J.D. Miller, The chemistry of gold solvent extraction from cyanide solution using modified amines, Hydrometallurgy, 16 (1986) 245-261.

[64] G.A. Kordosky, J.M. Sierakoski, M.J. Virnig, P.L. Mattison, Gold solvent extraction from typical cyanide leach solutions, Hydrometallurgy, 30 (1992) 291-305.

[65] A.M. Sastre, A. Madi, J.L. Cortina, F.J. Alguacil, Solvent extraction of gold by LIX 79: experimental equilibrium study, Journal of Chemical Technology & Biotechnology, 74 (1999) 310-314.

[66] X. Yang, K. Huang, Q. Wei, Z. Huang, J. Chen, J. Wu, Stripping of Au(I) from a Loaded Cetyltrimethylammonium Bromide/Tributyl Phosphate Organic Solution: Conversion and Reduction, Solvent Extraction and Ion Exchange, 26 (2008) 556-569.

[67] X. Yang, R. Yang, D. Shi, S. Wang, J. Chen, H. Guo, Hydrophobic ionic liquids as novel extractants for gold(I) recovery from alkaline cyanide solutions, Journal of Chemical Technology & Biotechnology, 90 (2015) 1102-1109.

CHULALONGKORN UNIVERSITY

[68] X. Yang, C. Miao, Y. Sun, T. Lei, Q. Xie, S. Wang, Efficient extraction of gold(I) from alkaline aurocyanide solution using green ionic liquid-based aqueous biphasic systems, Journal of the Taiwan Institute of Chemical Engineers, 91 (2018) 176-185.

[69] M. Tromp, M. Burgard, M.J.F. Leroy, M. Prevost, Extraction of gold and silver cyanide complexes through supported liquid membranes containing macrocyclic extractants, Journal of Membrane Science, 38 (1988) 295-300.

[70] R.K. Biswas, M.A. Habib, M.N. Islam, Some Physicochemical Properties of (D2EHPA). 1. Distribution, Dimerization, and Acid Dissociation Constants of D2EHPA in a Kerosene/0.10 kmol m-3 (Na+,H+)Cl- System and the Extraction of Mn(II), Industrial & Engineering Chemistry Research, 39 (2000) 155-160.

[71] D.S. Flett, Principles and practices of solvent extraction. Second Edition, Revised and Expanded. Edited by J Rydberg, M Cox, C Musikas and GR Choppin. Marcel Dekker, New York, 2004. 760 pp, ISBN 0 8247 5053 2, Journal of Chemical Technology & Biotechnology, 80 (2005) 359-360.

[72] Z. Kolarik, Critical evaluation of some equilibrium constants involving acidic organophosphorus extractants, Pure and Applied Chemistry, 54 (1982) 2593-2674.

[73] A. Ghosh, D. Datta, H. Uslu, H.S. Bamufleh, S. Kumar, Separation of copper ion (Cu2+) from aqueous solution using tri-n-butyl phosphate and di-2-ethylhexyl phosphoric acid as extractants, Journal of Molecular Liquids, 258 (2018) 147-154.

[74] A. Sharma, N. Patil, A. Patwardhan, R. Moorthy, P. Ghosh, Synergistic interplay between D2EHPA and TBP towards the extraction of lithium using hollow fiber supported liquid membrane, Separation Science and Technology, 51 (2016).

[75] A. Sharma, N. Patil, A. Patwardhan, R. Moorthy, P. Ghosh, Synergistic interplay between D2EHPA and TBP towards the extraction of lithium using hollow fiber supported liquid membrane, Separation Science and Technology, 51 (2016).

จุฬาลงกรณ์มหาวิทยาลัย
Chulalongkorn University

[76] S.A. Ansari, P.K. Mohapatra, V.K. Manchanda, Recovery of Actinides and Lanthanides from High-Level Waste Using Hollow-Fiber Supported Liquid Membrane with TODGA as the Carrier, Industrial & Engineering Chemistry Research, 48 (2009) 8605-8612.

[77] T. Wannachod, N. Leepipatpiboon, U. Pancharoen, S. Phatanasri, Mass transfer and selective separation of neodymium ions via a hollow fiber supported liquid membrane using PC88A as extractant, Journal of Industrial and Engineering Chemistry, 21 (2015) 535-541.

จุฬาลงกรณ์มหาวิทยาลัย
CHULALONGKORN UNIVERSITY

CHAPTER III

Selective elimination of Ni(II) ions from rinse wastewater of ENIG plating via HFSLM, applying vegetable oils as alternative greener diluents: Experiment, kinetic and mass transfer model

Wanchalerm Srirachat[a], Natthapol Traiwongsa[a], Kittamuk Purktimatanont[a], Soorathep Kheawhom[a], Ura Pancharoen[a,*]

[a] *Department of Chemical Engineering, Faculty of Engineering, Chulalongkorn University, Patumwan, Bangkok 10330, Thailand*

* Corresponding author

จุฬาลงกรณ์มหาวิทยาลัย
CHULALONGKORN UNIVERSITY

This article has been submitted in Journal:

Journal of the Taiwan Institute of Chemical Engineers. In press.

3.1 Graphical abstract

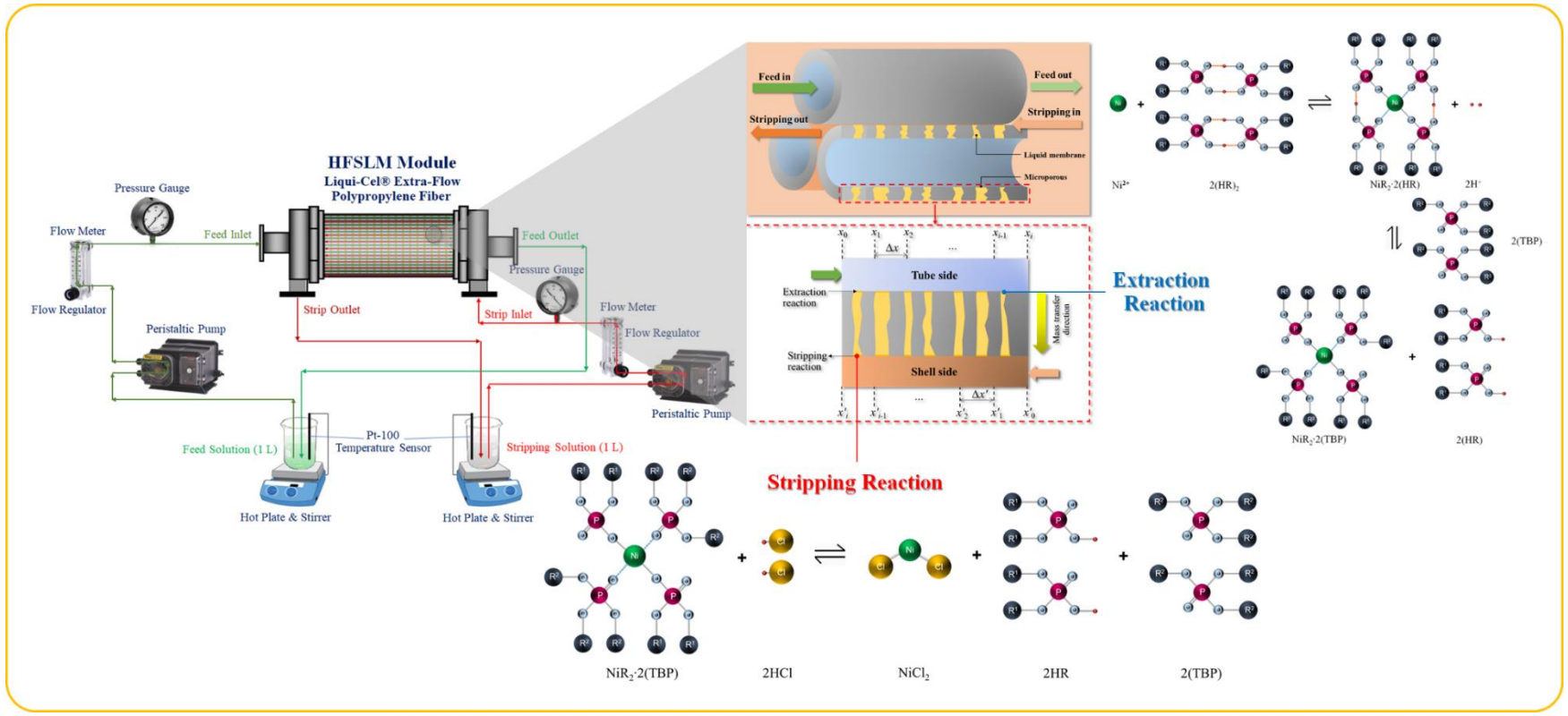

3.2 Abstract

Nowadays, electroless nickel immersion gold (ENIG) plating is the most commonly used surface finish for high-reliability printed circuit boards (PCBs). Such a process, however, generates a large quantity of wastewater containing valuable metal ions. This work highlights the performance of hollow fiber supported liquid membrane (HFSLM) for a single-step operation and selective elimination of trace Ni^{2+} from $[Au(CN)_2]^-$ in real rinse wastewater. Various types of vegetable oil (palm, sunflower, soybean, coconut and rice bran) are investigated as eco-friendly benign diluents. Herein, all vegetable oil-based diluents loaded with organophosphorus extractants: D2EHPA and TBP demonstrate their effectiveness for the selective elimination of Ni^{2+}. Optimum conditions found proved to be a mixture of 0.25 mol/L D2EHPA and 0.25 mol/L TBP dissolved in palm oil as liquid membrane, at pH 8.6 of feed solution, 0.50 mol/L HCl as strippant, and flow rates of both feed and stripping solutions of 200 mL/min. A mass transfer model, developed to predict the final concentration of Ni^{2+} in feed and stripping solutions, is seen to fit in well with the experimental results.

Keywords: Hollow fiber supported liquid membrane; Electroless nickel immersion gold plating; Rinse wastewater; Gold(I); Nickel(II)

3.3 Introduction

Nowadays, printed circuit boards (PCBs) have a most important role in electronic devices. In the metallization of PCBs by the electroless nickel immersion gold (ENIG) plating process, it is noted that rinse water baths, after use, always contain economical quantities of nickel and gold existing in the form of Ni^{2+} and $[Au(CN)_2]^-$, respectively

[1, 2]. Thus, the opportunity to recover $[Au(CN)_2]^-$ and reuse them to achieve cost reduction and sustainable wastewater treatment is paramount.

Hollow fiber supported liquid membrane (HFSLM) is a useful separation technique that can be applied on an industrial scale for the recovery of precious and toxic metal ions from wastewater. HFSLM has unique properties such as high selectivity, less consumption of extractants and diluents, low energy consumption as well as simultaneous operation within a single-step (extraction and stripping) of target ions at extremely low concentration of ppb levels. Furthermore, the high surface area of HFSLM provides high mass transfer rate of separation.

In the liquid membrane phase of HFSLM, extractants are generally dissolved in the petroleum-based organic diluents viz. kerosene, dodecane, toluene etc. However, such diluents are toxic, volatile and flammable, which are difficult to handle and can be harmful to human beings as well as the environment. It is therefore required to find alternative greener diluents in order to curb environmental problems.

As green substitutes, vegetable oils have great potential owing to their outstanding characteristics such as nontoxicity, inflammability and biodegradability. Oils such as soybeans, palm fruit, sunflower seeds, coconuts, rice grains etc. are more environmentally friendly than petroleum-based diluents. Previous works have addressed the effect of vegetable oils in liquid membrane systems in order to successfully separate and recover various compounds such as mercury [3], methylene blue [4], and copper [5].

With regard to the efficient elimination of metal ions, HFSLM strongly depends on the types of extractants and diluents used as well as the acidity of stripping solution. Hence, these parameters have been reviewed and applied in this work. This work

จุฬาลงกรณ์มหาวิทยาลัย
CHULALONGKORN UNIVERSITY

highlights the effect of various types of vegetable oils as non-toxic diluents on the elimination of a low concentration of Ni^{2+} and sets out to recover $[Au(CN)_2]^-$ from the real rinse wastewater of the ENIG plating process via HFSLM. Parameters studied are as follows: types and concentration of extractants, types of vegetable-oil based diluents used to prepare the liquid membrane, pH and concentration of the stripping solutions. Performance of separation systems are investigated in terms of efficiency of extraction and stripping of Ni^{2+}, $[Au(CN)_2]^-$, distribution ratio, selectivity and synergistic coefficient. Moreover, a mathematic model, based on conservation of mass considering axial convection, diffusion, reactions at the liquid-membrane interfaces, and mass accumulation, has been developed to predict the extraction and stripping of Ni^{2+} and $[Au(CN)_2]^-$.

3.4 Experimental

3.4.1 Chemicals and reagents

As an aqueous feed solution, the real rinse wastewater of the ENIG plating process containing Ni^{2+} and $[Au(CN)_2]^-$ was supplied by Mektec Manufacturing Corporation (Thailand) Ltd. The initial concentrations of Ni^{2+} and $[Au(CN)_2]^-$ in the inlet feed solution were 15 mg/L and 25 mg/L, respectively. In Table A3.1 of the Section 3.7: Supplementary information, details of the key components of the feed solution are given. Two types of organophosphorous extractants studied viz. di-(2-ethylhexyl) phosphoric acid (D2EHPA), as the acidic extractant, and tributyl phosphate (TBP), as the neutral extractant, were obtained from Merck. For preparation of the liquid membrane phase, both extractants were dissolved in various types of vegetable oil-based diluents such as palm oil, sunflower oil, soybean oil, coconut oil and rice bran

oil. Hydrochloric acid (HCl) was utilized as the aqueous stripping solution. As listed in Table A3.2 of the Section 3.7: Supplementary information, all chemicals along with feed solution were used without further modification and purification.

3.4.2 Apparatus and experimental procedure

The characteristics of the hollow fiber (HF) module used in this work (Liqui-Cel® Extra-Flow) are shown in Table A3.3 of the Section 3.7: Supplementary information. For all experiments, the aqueous feed solution contained 15 mg/L of Ni^{2+} and 25 mg/L of $[Au(CN)_2]^-$ at initial pH value of 8.6±0.5.

The liquid membrane (LM) solution was prepared by dissolving D2EHPA and/or TBP extractants in various types of vegetable oil-based diluents. The LM solution was circulated along the tube and shell sides of the HF module for 40 min until the HF micropores were filled in having a total volume of about 50 mL. Then, deionized (DI) water was fed through the tube and shell sides of the HF module to remove excess LM solution. After that, the separation started by pumping 1 L of the feed solution into the tube side of the HF module. Simultaneously, 1 L of the 0.50 mol/L HCl solution as strippant was countercurrently pumped into the shell side of the HF module. The HF system was operated via recycling mode (Fig. A3.1 of the Section 3.7: Supplementary information). The volumetric flow rate of feed and stripping solutions was found to be equal to 200 mL/min, as recorded in our previous work [6]. The operating temperature for both the feed solution reservoir and stripping solution reservoir was controlled at 303±1 K. During the experiment, after an interval of 5 min, samples of 5 mL were taken out from the feed and strip reservoirs. The concentration of Ni(II) and Au(I) ions was analyzed using inductively coupled plasma (ICP) technique (model Optima 2100 DV,

จุฬาลงกรณ์มหาวิทยาลัย
CHULALONGKORN UNIVERSITY

Perkin Elmer). The pH of feed and stripping solutions was measured using pH meter (model EUTECH pH 700).

3.4.3 Calculations of separation efficiency

The separability of Ni^{2+} and $[Au(CN)_2]^-$ was calculated by the extraction (%*E*) and stripping (%*St*) percentages based on mass transfer basis, using Eqs. (3.1) and (3.2):

$$\%E = \left(1-\left(\frac{C_{f,t}\times V_{f,t}}{C_{f,0}\times V_{f,0}}\right)\right)\times 100 \tag{3.1}$$

$$\%S = \left(\frac{C_{s,t}\times V_{s,t}}{C_{m,t}\times V_{m}}\right)\times 100 \tag{3.2}$$

Concentration of the ions in the liquid membrane phase ($C_{m,t}$) can be obtained by the mass balance, as shown in Eq. (3.3):

$$C_{m,t} = \frac{\left(C_{F,i}\times V_{F,i}\right) - \left(C_{F,t}\times V_{F,t}\right)}{V_m} \tag{3.3}$$

The distribution ratio (*D*) of the metal ions between the liquid membrane phase and the aqueous feed phase after separation can be determined, as expressed in Eq. (3.4):

$$D = \frac{C_{m,t}\times V_m}{C_{F,t}\times V_{F,t}} \tag{3.4}$$

The selectivity between Ni^{2+} and $[Au(CN)_2]^-$ ($S_{Ni(II)/Au(I)}$) is obtained by Eq. (3.5) based on mass transfer of metal ions from the aqueous feed phase into the liquid membrane phase:

$$S_{\mathrm{Ni(II)/Au(I)}} = \frac{C_{\mathrm{Ni(II)},F,i} - \left(C_{\mathrm{Ni(II)},F,t} \times \frac{V_{F,t}}{V_{F,i}} \right)}{C_{\mathrm{Au(I)},F,i} - \left(C_{\mathrm{Au(I)},f,t} \times \frac{V_{F,t}}{V_{F,i}} \right)} \tag{3.5}$$

To enhance extraction efficiency and selectivity, synergism of the mixed reactive extractants was applied. Synergistic extraction is proved when the synergistic coefficient (*SC*), as shown in Eq. (3.6), is more than 1; an antagonistic effect occurs vice versa (*SC* less than 1) [7]:

$$SC = \frac{D_{mix}}{D_{\mathrm{D2EHPA}} + D_{\mathrm{TBP}}} \tag{3.6}$$

3.5 Results and discussion

3.5.1 Effect of vegetable oil-based diluents on Ni^{2+} and $[Au(CN)_2]^-$ extractions

Figs. A3.2 to A3.4 of the Section 3.7: Supplementary information show the schematic mass transport of Ni^{2+} via the liquid membrane phase. The target Ni^{2+} in the feed solution reacts with the extractants (D2EHPA, TBP and mixture of D2EHPA-TBP) at the feed-liquid membrane interface, forming the Ni-extractant complex. Subsequently, the complex diffused across the liquid membrane phase to the liquid membrane-stripping interface. Then, it reacted with H^+ from HCl in the stripping phase. Finally, the Ni^{2+} ions were released into the stripping phase while the extractant diffused back toward the feed-liquid membrane interface and reacted once again with the Ni^{2+} from the feed phase. The extractions of Ni^{2+} from the feed phase by D2EHPA, TBP plus the mixture of D2EHPA-TBP are expressed in Eqs. (A3.1) to (A3.3) of the Section 3.7: Supplementary information.

Five different types of vegetable oils without extractants, vegetable oils loaded with 0.50 mol/L D2EHPA, and vegetable oils loaded with 0.50 mol/L TBP were investigated to selectively extract Ni^{2+} from $[Au(CN)_2]^-$ in the real rinse wastewater, as presented in Table 3.1 and Fig. 3.1.

จุฬาลงกรณ์มหาวิทยาลัย
CHULALONGKORN UNIVERSITY

Table 3.1 Extraction percentage (%*E*), distribution ratio (*D*), and selectivity (*S*) of Ni^{2+} and $[Au(CN)_2]^-$ separation via HFSLM using various types of vegetable oil-based diluents.

Liquid membrane phases	*%E*		*D*		$S_{Ni(II)/Au(I)}$
	Ni^{2+}	$[Au(CN)_2]^-$	Ni^{2+}	$[Au(CN)_2]^-$	
Palm oil-based diluent					
Without extractant	8.427	1.211	9.202×10^{-2}	1.226×10^{-2}	4.175
0.50 mol/L D2EHPA	53.37	21.79	1.145	2.786×10^{-1}	1.470
0.50 mol/L TBP	50.05	28.39	1.002	3.965×10^{-1}	1.058
Sunflower oil-based diluent					
Without extractant	7.303	9.684×10^{-1}	7.879×10^{-2}	9.779×10^{-3}	4.525
0.50 mol/L D2EHPA	52.25	21.30	1.094	2.707×10^{-1}	1.471
0.50 mol/L TBP	48.99	27.76	9.605×10^{-1}	3.842×10^{-1}	1.059
Soybean oil-based diluent					
Without extractant	4.494	7.263×10^{-1}	4.706×10^{-2}	7.316×10^{-3}	3.713
0.50 mol/L D2EHPA	49.44	20.09	9.778×10^{-1}	2.515×10^{-1}	1.476
0.50 mol/L TBP	46.36	26.18	8.642×10^{-1}	3.546×10^{-1}	1.062
Coconut oil-based diluent					
Without extractant	5.618	1.453	5.952×10^{-2}	1.474×10^{-2}	2.320
0.50 mol/L D2EHPA	50.56	20.58	1.023	2.591×10^{-1}	1.474
0.50 mol/L TBP	47.41	26.81	9.016×10^{-1}	3.663×10^{-1}	1.061
Rice bran oil-based diluent					
Without extractant	3.371	1.695	3.488×10^{-2}	1.724×10^{-2}	1.193
0.50 mol/L D2EHPA	47.75	19.37	9.140×10^{-1}	2.402×10^{-1}	1.479
0.50 mol/L TBP	44.78	25.23	8.109×10^{-1}	3.375×10^{-1}	1.065

CHULALONGKORN UNIVERSITY

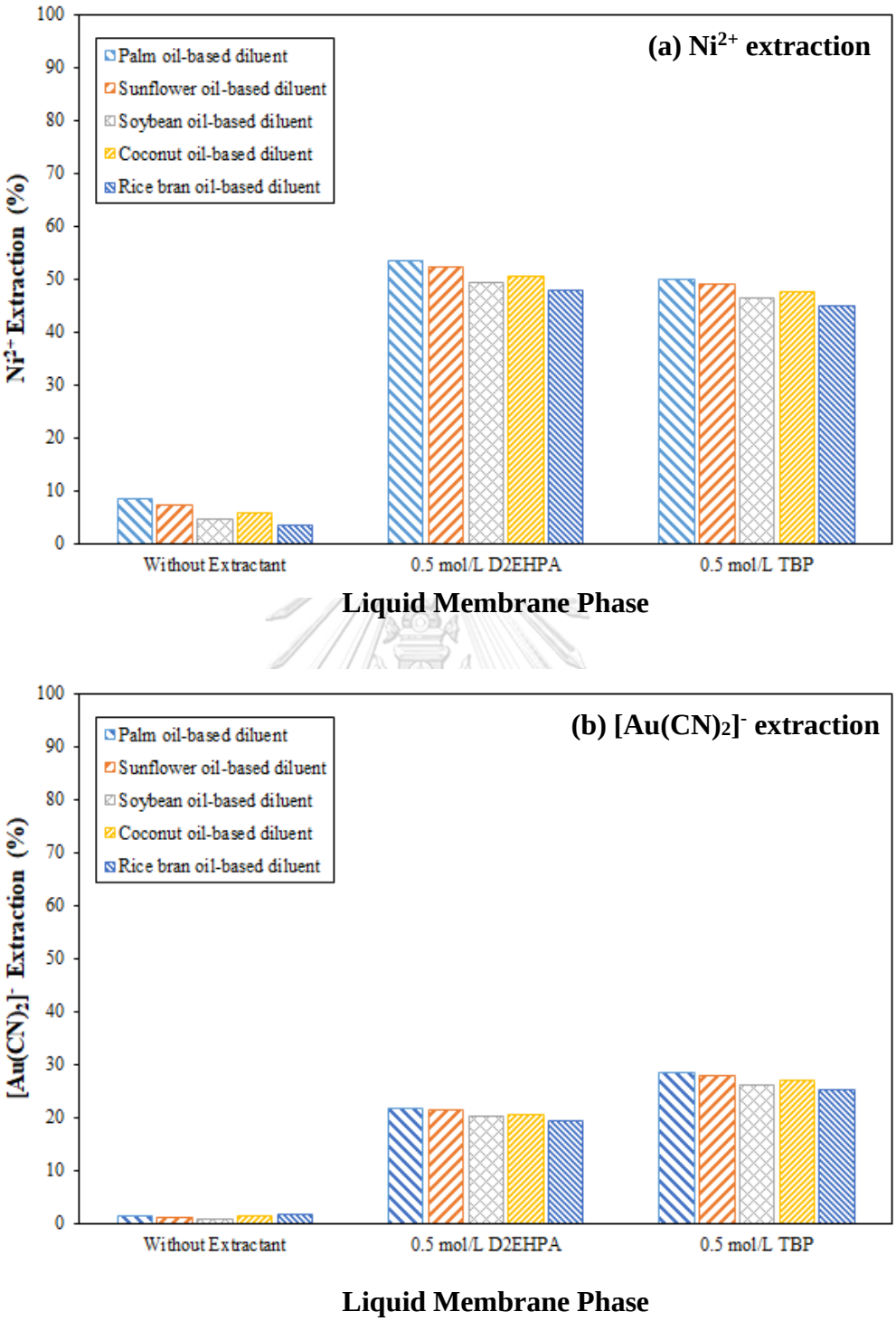

Figure 3.1 Extraction percentage (%E): (a) Ni^{2+} and (b) $[Au(CN)_2]^-$ via HFSLM with various types of vegetable oil-based diluents.

It was found that all vegetable oils in the liquid membrane phase without any organophosphorus extractants provided ≈ 3 to 8% of Ni^{2+} and 0.7 to 1.7% of $[Au(CN)_2]^-$

extraction. Results proved that the vegetable oils were poor extractants for Ni^{2+} and $[Au(CN)_2]^-$. Such results with low extractability of vegetable oils are in agreement with previous work undertaken: namely, coconut oil [5, 8] and sunflower oil [9]. Owing to the non-polarity of vegetable oils, oil molecules are inclined to interact weakly with polar compounds like Ni^{2+} and $[Au(CN)_2]^-$, thus resulting in poor solubility of Ni^{2+} and $[Au(CN)_2]^-$ in oils. The mild extraction of ≈ 3 to 8% of Ni^{2+} could be deduced as extraction by the free fatty acids contained in the vegetable oils via the cation exchange reaction between Ni^{2+} cations in the aqueous feed phase and the acidic proton (H^+) in the liquid membrane phase. This outcome occurred due to the substantial pH drop measured from the aqueous feed phase before ($pH_{feed,i}$), and after separation ($pH_{feed,f}$), as shown in Fig. 3.2.

จุฬาลงกรณ์มหาวิทยาลัย
CHULALONGKORN UNIVERSITY

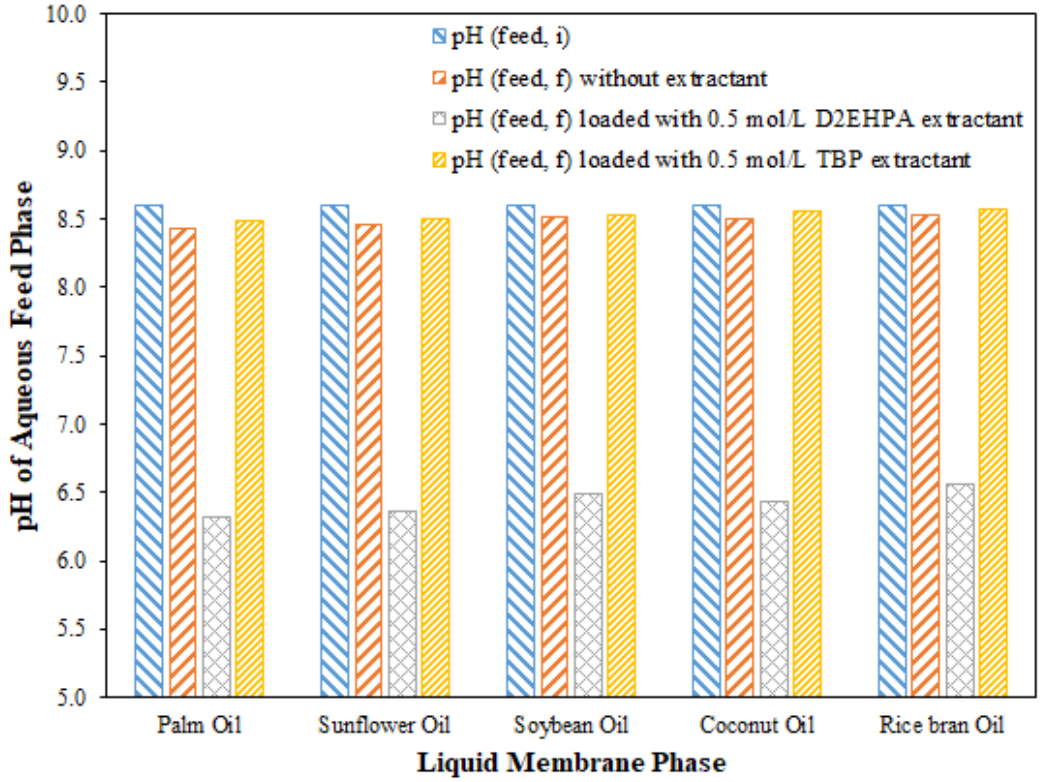

Figure 3.2 pH of aqueous feed phase before (feed,*i*) and after (feed,*f*) separation via HFSLM, using various types of vegetable oil-based diluents in the liquid membrane phase.

Triglycerides, which account for more than 90% [10] of the components in vegetable oils, are naturally occurring long-chain esters formed by glycerol molecules with three long-chain fatty acids that do not carry any acidic H^+. Hence, it is presumed that the acidic H^+ was derived from the free fatty acids, which are components in vegetable oils [10]. The small quantity of free fatty acids (<2% [10]) contained in vegetable oils justifies the low extraction percentage of Ni^{2+} and $[Au(CN)_2]^-$ attained when no extractant was added (Table 3.1, Figs. 3.1a and 3.1b). Owing to the low extractability of Ni^{2+}, vegetable oils function more as diluents than as additional extractants in the extraction of Ni^{2+} from aqueous feed solutions.

However, when vegetable oils loaded with a single extractant of 0.50 mol/L D2EHPA and 0.50 mol/L TBP were used in the liquid membrane phases, extraction percentage increased dramatically to ≈ 49% of Ni^{2+} and 24% of $[Au(CN)_2]^-$ (Table 3.1, Figs. 3.1a and 3.11b). This suggests that both D2EHPA and TBP are effective extractants for the selective extraction of Ni^{2+} from $[Au(CN)_2]^-$. Being a cation extractant, D2EHPA extracts Ni^{2+} by a process of cation exchange between Ni^{2+} from the aqueous feed phase and H^+ derived from D2EHPA in the liquid membrane phase. In Fig. 3.2, pH in the aqueous feed phase is greatly reduced from $pH_{feed,i}$ (≈ 8.6) to $pH_{feed,f}$ (≈ 6.4) for all cases, owing to the substantial amount of D2EHPA contained in the liquid membrane phase. In Fig. 3.1, when 0.50 mol/L TBP loaded vegetable oil-based diluents in the liquid membrane phase were used, extraction percentage and distribution of Ni^{2+} increased. However, pH in the aqueous feed phase after extraction slightly decreased i.e. from $pH_{feed,i}$ (≈ 8.6) to $pH_{feed,f}$ (≈ 8.5) for all cases.

In HFSLM applications, it is seen that the important property of any desirable diluent should include: low viscosity as well as low volatility and high distribution ratio with no miscibility within the aqueous phases. From Table 3.1, it is evident that the palm oil-D2EHPA combination demonstrates the highest distribution ratio for the extraction of Ni^{2+} (1.145) followed by sunflower oil (1.094), coconut oil (1.023), soybean oil (0.978) and rice bran oil (0.914).

จุฬาลงกรณ์มหาวิทยาลัย
CHULALONGKORN UNIVERSITY

3.5.2 Effect of mixed extractants D2EHPA and TBP in the liquid membrane phase

In order to increase overall extraction performance, synergistic extraction can be accomplished having any combination of extractants. D2EHPA and TBP were

investigated in order to improve the synergistic extraction of Ni^{2+} and $[Au(CN)_2]^-$. Thus, both D2EHPA and TBP concentrations were fixed at 0.25 mol/L. As depicted in Fig. 3.3a to 3.3e, it is evident that the mixture of 0.25 mol/L D2EHPA and 0.25 mol/L TBP extractants improved Ni^{2+} extraction over 70% for all vegetable oil-based diluents. Furthermore, the distribution ratios of Ni^{2+} (D_{Ni}) and selectivity ($S_{Ni/Au}$) for the mixed D2EHPA and TBP extractants in comparison with a single D2EHPA improved about 4 and 2 times, respectively. Therefore, the combination of D2EHPA and TBP was noted to have a remarkable synergistic effect in the mixed extractant system.

In contrast, extraction of the undesired $[Au(CN)_2]^-$ by the D2EHPA-TBP system significantly decreased in comparison with the single D2EHPA and TBP for all vegetable oil-based diluents.

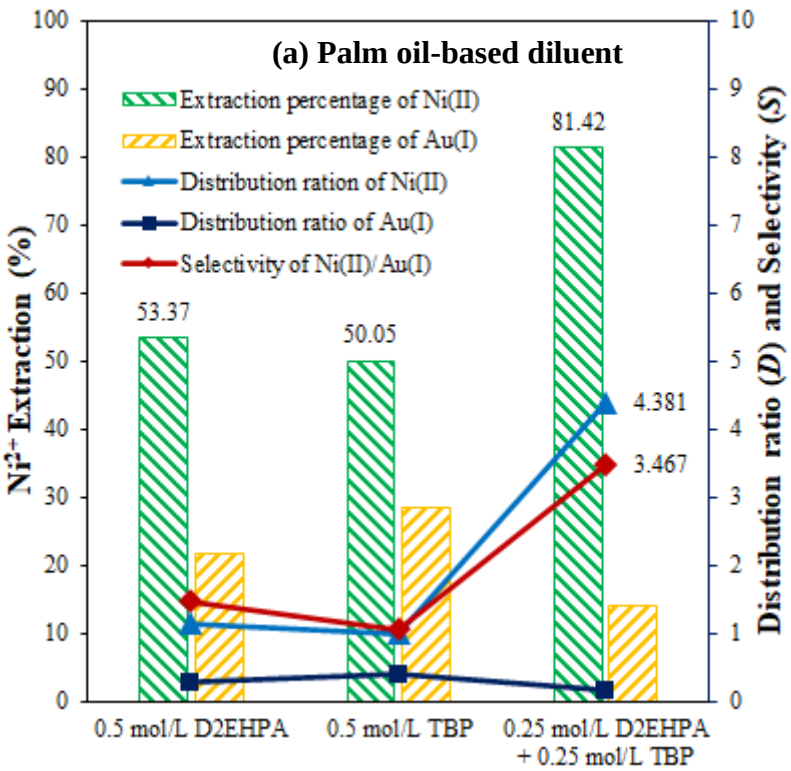

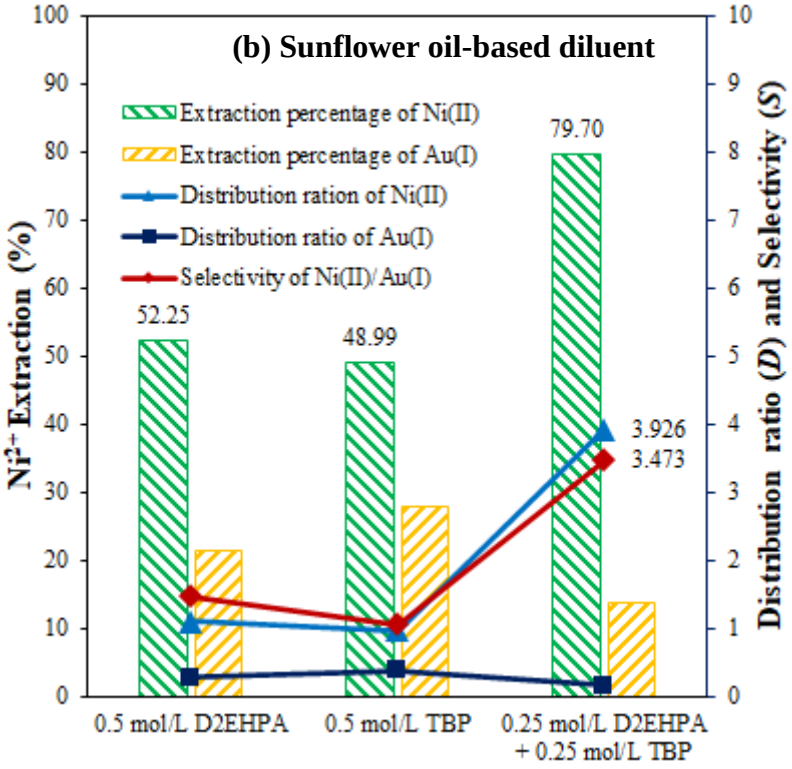
(b) Sunflower oil-based diluent
Extraction percentage of Ni(II)
Extraction percentage of Au(I)
Distribution ration of Ni(II)
Distribution ratio of Au(I)
Selectivity of Ni(II)/Au(I)
52.25
48.99
79.70
3.926
3.473
Ni2+ Extraction (%)
Distribution ratio (D) and Selectivity (S)
0.5 mol/L D2EHPA
0.5 mol/L TBP
0.25 mol/L D2EHPA + 0.25 mol/L TBP

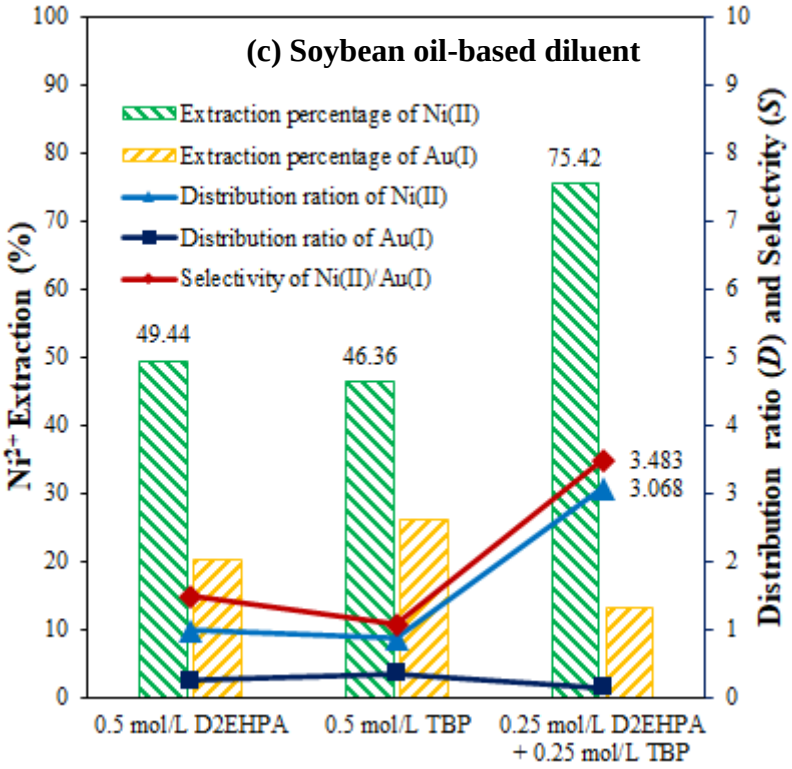
(c) Soybean oil-based diluent
Extraction percentage of Ni(II)
Extraction percentage of Au(I)
Distribution ration of Ni(II)
Distribution ratio of Au(I)
Selectivity of Ni(II)/Au(I)
49.44
46.36
75.42
3.483
3.068
Ni2+ Extraction (%)
Distribution ratio (D) and Selectivity (S)
0.5 mol/L D2EHPA
0.5 mol/L TBP
0.25 mol/L D2EHPA + 0.25 mol/L TBP

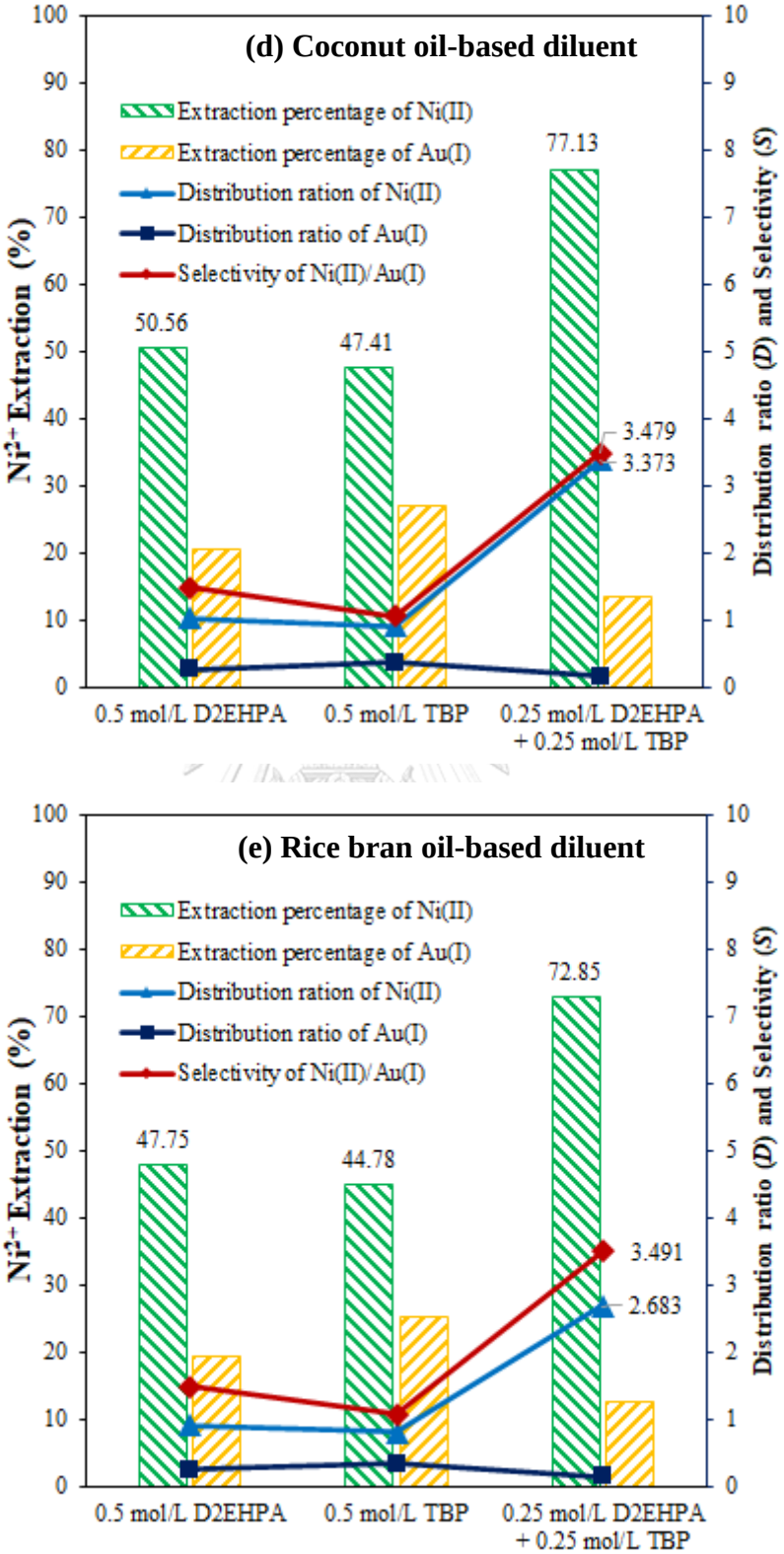

Figure 3.3 Effect of mixed extractants 0.25 M D2EHPA and 0.25 M TBP on the synergistic extraction of Ni^{2+} and antagonistic extraction of $[Au(CN)_2]^-$ with various

types of vegetable oil-based diluents: (a) palm oil, (b) sunflower oil (c) soybean oil (d) coconut oil, and (e) rice bran oil.

3.5.3 Effect of stripping phase pH

The stripping reaction of Ni-extractant complex and H^+ at the liquid membrane-stripping interface is represented, as in Eqs. (A3.4) to (A3.6) of the Section 3.7: Supplementary information. Since, in the hollow fiber operation, Ni^{2+} is stripped out continuously by H^+ at the liquid membrane-stripping interface, the overall reaction in Eqs. (A3.1) to (A3.3) Supplementary information are taken into account as the forward reaction.

In the stripping phase, pH plays an important role and is responsible for inducing the transport of Ni^{2+} from the liquid membrane phase to the stripping phase. An acidic condition is necessary for protonation of the metal-extractant complexes: Ni-D2EHPA, Ni-TBP and Ni-D2EHPA-TBP. Experiments were carried out in the stripping phase whereby pH varied from 0.1 to 3.01, thus HCl concentration decreased from 1 to 10^{-3} mol/L, respectively. Results are shown in Figs. 3.4a to 3.4e. It is clear that when a higher pH in the stripping phase is applied, stripping percentages are low due to the inadequate protonation process of the Ni-extractant complexes. A higher pH can affect the transport of Ni^{2+} from the liquid membrane phase to the stripping phase. It is observed that at pH 0.1, the stripping percentages of Ni^{2+} were at their highest.

จุฬาลงกรณ์มหาวิทยาลัย
CHULALONGKORN UNIVERSITY

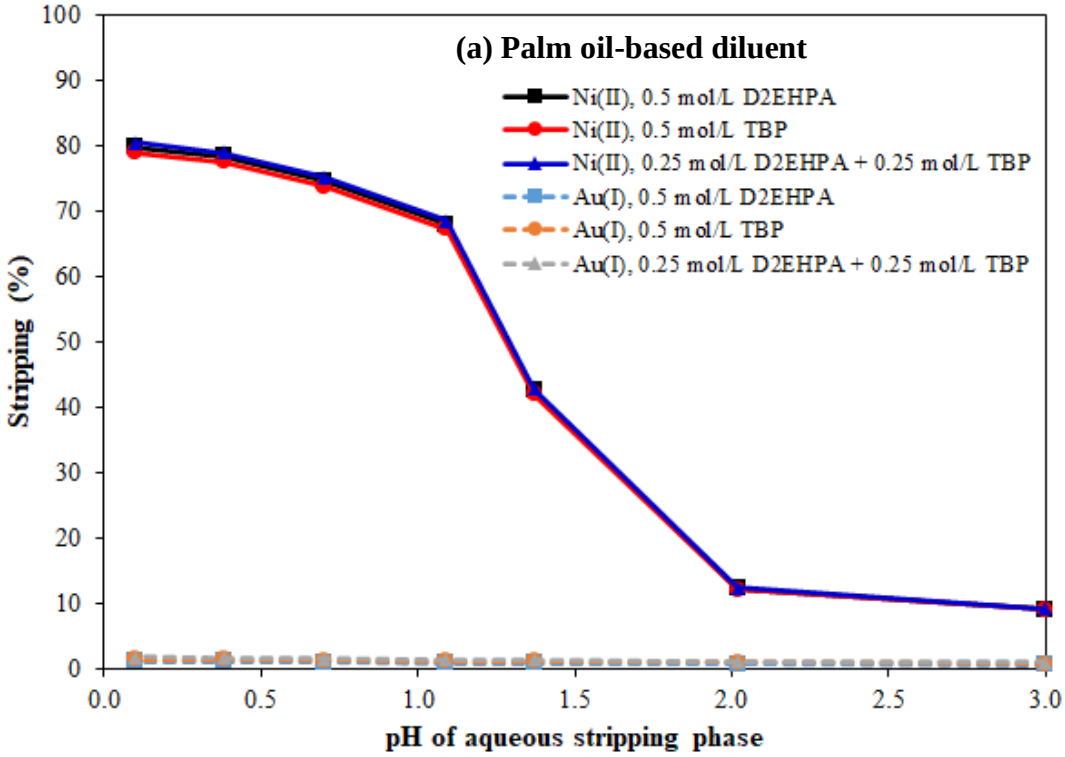
(a) Palm oil-based diluent
Ni(II), 0.5 mol/L D2EHPA
Ni(II), 0.5 mol/L TBP
Ni(II), 0.25 mol/L D2EHPA + 0.25 mol/L TBP
Au(I), 0.5 mol/L D2EHPA
Au(I), 0.5 mol/L TBP
Au(I), 0.25 mol/L D2EHPA + 0.25 mol/L TBP
Stripping (%)
pH of aqueous stripping phase
0
10
20
30
40
50
60
70
80
90
100
0.0
0.5
1.0
1.5
2.0
2.5
3.0

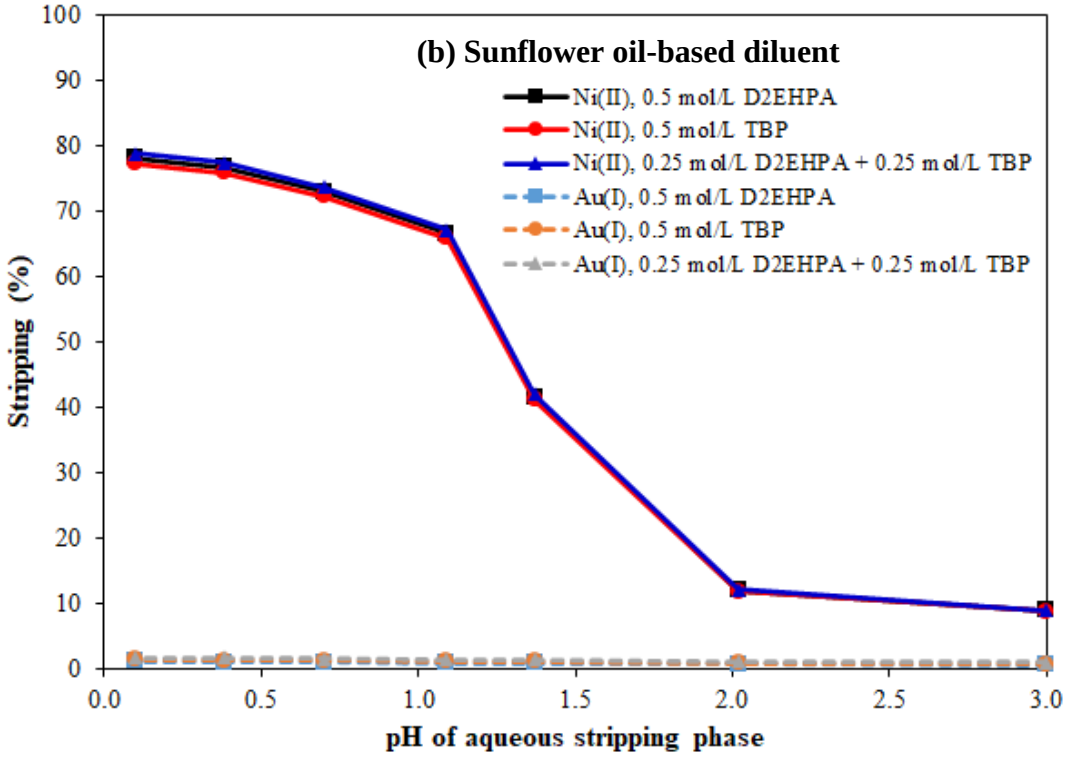
(b) Sunflower oil-based diluent
Ni(II), 0.5 mol/L D2EHPA
Ni(II), 0.5 mol/L TBP
Ni(II), 0.25 mol/L D2EHPA + 0.25 mol/L TBP
Au(I), 0.5 mol/L D2EHPA
Au(I), 0.5 mol/L TBP
Au(I), 0.25 mol/L D2EHPA + 0.25 mol/L TBP
Stripping (%)
pH of aqueous stripping phase
0
10
20
30
40
50
60
70
80
90
100
0.0
0.5
1.0
1.5
2.0
2.5
3.0

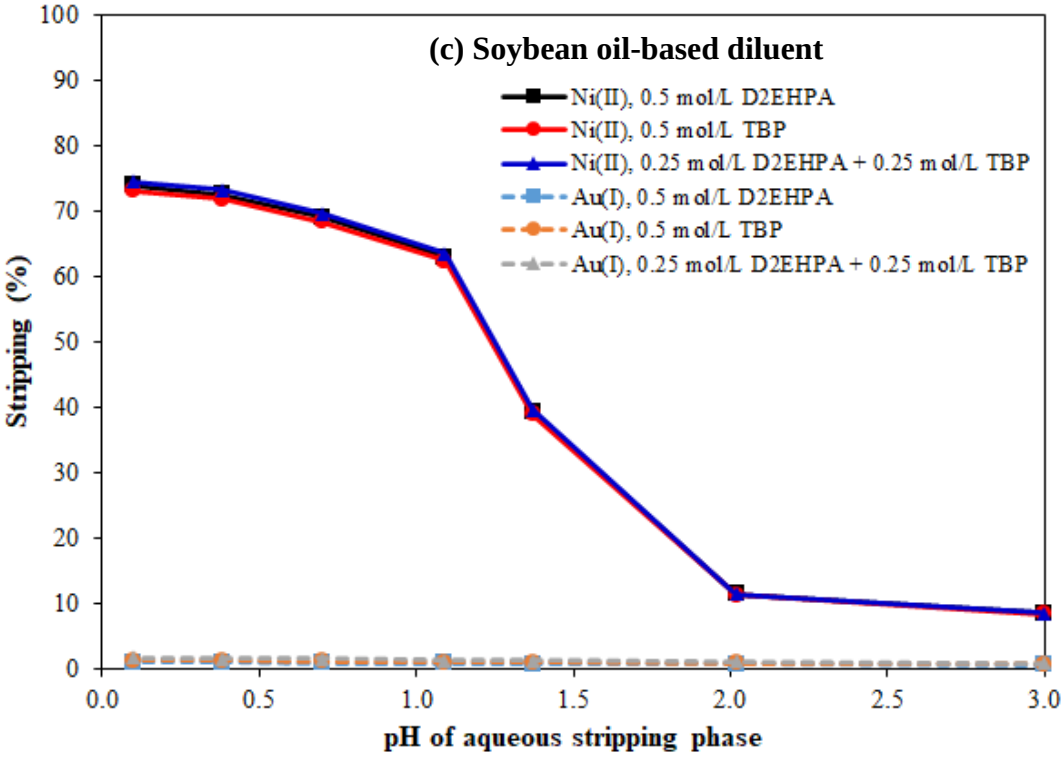
(c) Soybean oil-based diluent
Ni(II), 0.5 mol/L D2EHPA
Ni(II), 0.5 mol/L TBP
Ni(II), 0.25 mol/L D2EHPA + 0.25 mol/L TBP
Au(I), 0.5 mol/L D2EHPA
Au(I), 0.5 mol/L TBP
Au(I), 0.25 mol/L D2EHPA + 0.25 mol/L TBP
Stripping (%)
pH of aqueous stripping phase
0
10
20
30
40
50
60
70
80
90
100
0.0
0.5
1.0
1.5
2.0
2.5
3.0

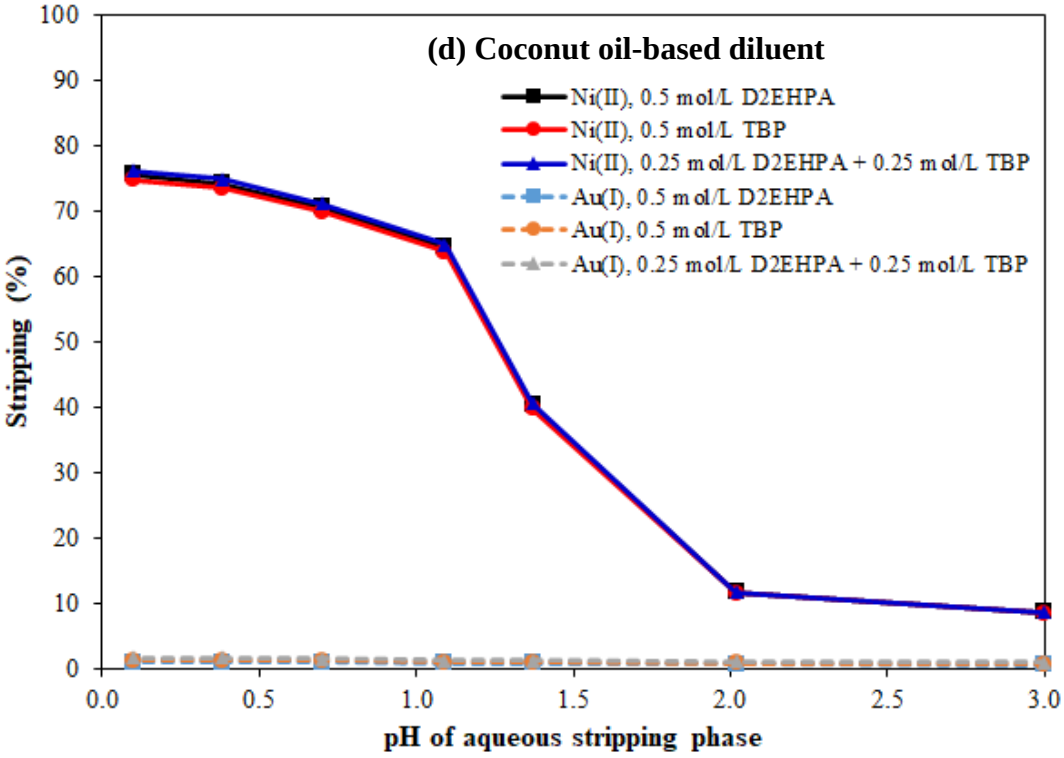
(d) Coconut oil-based diluent
Ni(II), 0.5 mol/L D2EHPA
Ni(II), 0.5 mol/L TBP
Ni(II), 0.25 mol/L D2EHPA + 0.25 mol/L TBP
Au(I), 0.5 mol/L D2EHPA
Au(I), 0.5 mol/L TBP
Au(I), 0.25 mol/L D2EHPA + 0.25 mol/L TBP
Stripping (%)
pH of aqueous stripping phase
0
10
20
30
40
50
60
70
80
90
100
0.0
0.5
1.0
1.5
2.0
2.5
3.0

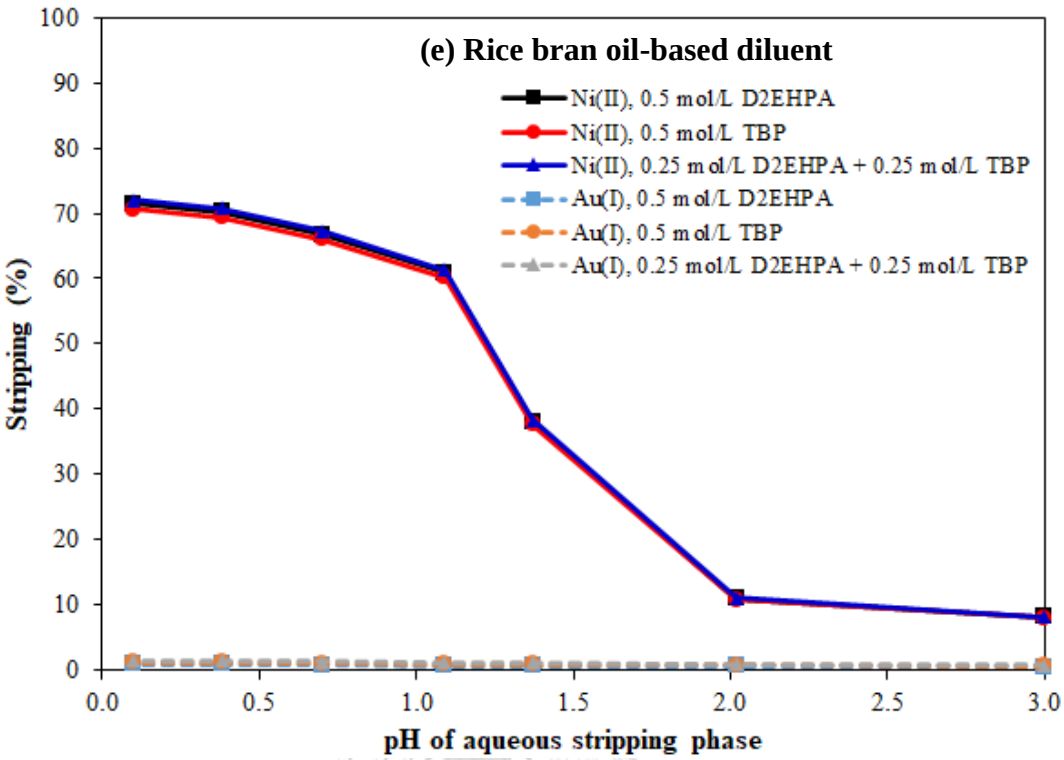

Figure 3.4 Stripping percentage (%*S*) of Ni^{2+} and $[Au(CN)_2]^-$ separation via HFSLM with various pH of stripping phase and vegetable oil-based diluents: (a) palm oil, (b) sunflower oil, (c) soybean oil, (d) coconut oil, and (e) rice bran oil.

3.5.4 Equilibrium distribution of Ni^{2+} and $[Au(CN)_2]^-$ separation via HFSLM system

A study on the change in concentration of Ni^{2+} and $[Au(CN)_2]^-$ in feed, liquid membrane and stripping phases with time was carried out in the HFSLM module. In Figs. 3.5a to 3.5e, the concentration profiles of Ni^{2+} and $[Au(CN)_2]^-$ in the three different phases with regards to time are shown. In the case of the mixed extractants viz. 0.25 mol/L D2EHPA and 0.25 mol/L TBP in the palm oil-based diluent as liquid membrane, it is evident from the feed phase concentration profile that there are three distinct zones. From the start of the experiment and up to 3 min, Ni^{2+} concentration in the feed phase dropped significantly from 15 mg/L to 7 mg/L, achieving about 54% extraction.

(a) Palm oil-based diluent

CHULALONGKORN UNIVERSITY
จุฬาลงกรณ์มหาวิทยาลัย

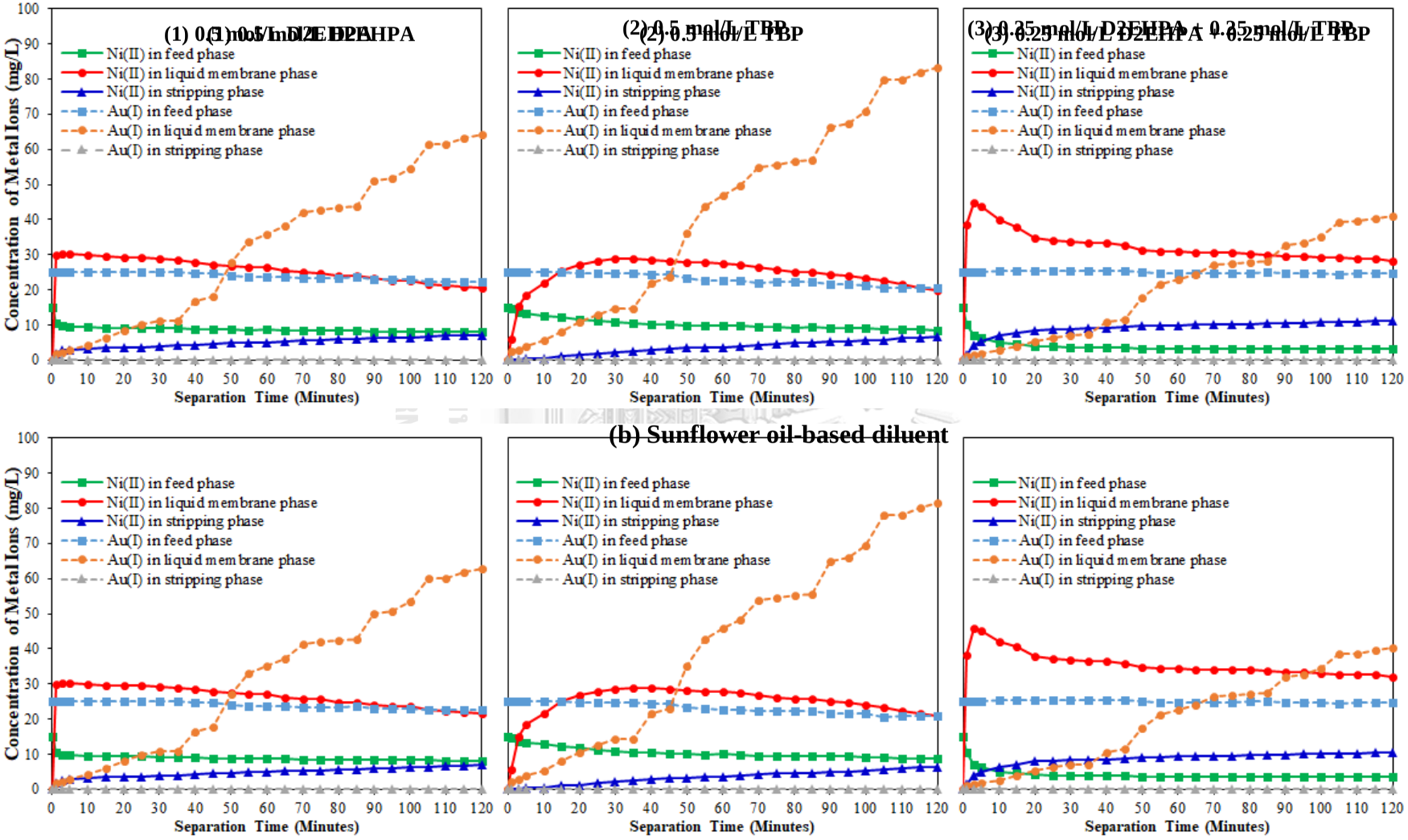
(1) 0.5 mol/L D2EHPA
(2) 0.5 mol/L TBP
(3) 0.25 mol/L D2EHPA + 0.25 mol/L TBP
(b) Sunflower oil-based diluent
Ni(II) in feed phase
Ni(II) in liquid membrane phase
Ni(II) in stripping phase
Au(I) in feed phase
Au(I) in liquid membrane phase
Au(I) in stripping phase
Concentration of Metal Ions (mg/L)
Separation Time (Minutes)

จุฬาลงกรณ์มหาวิทยาลัย
Chulalongkorn University

(c) Soybean oil-based diluent

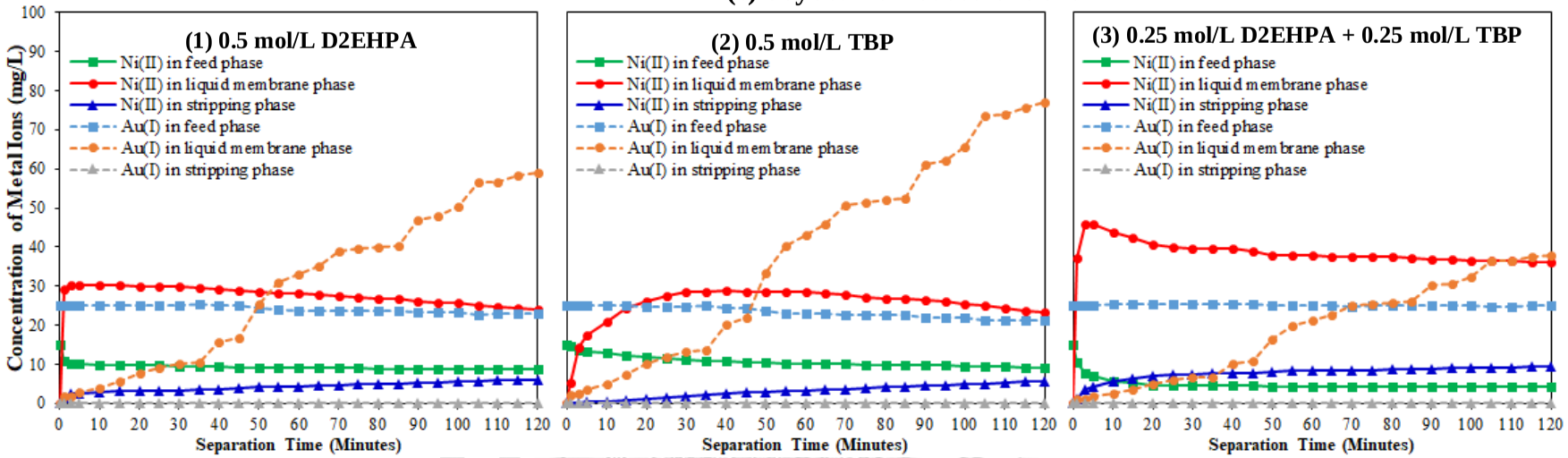

(d) Coconut oil-based diluent

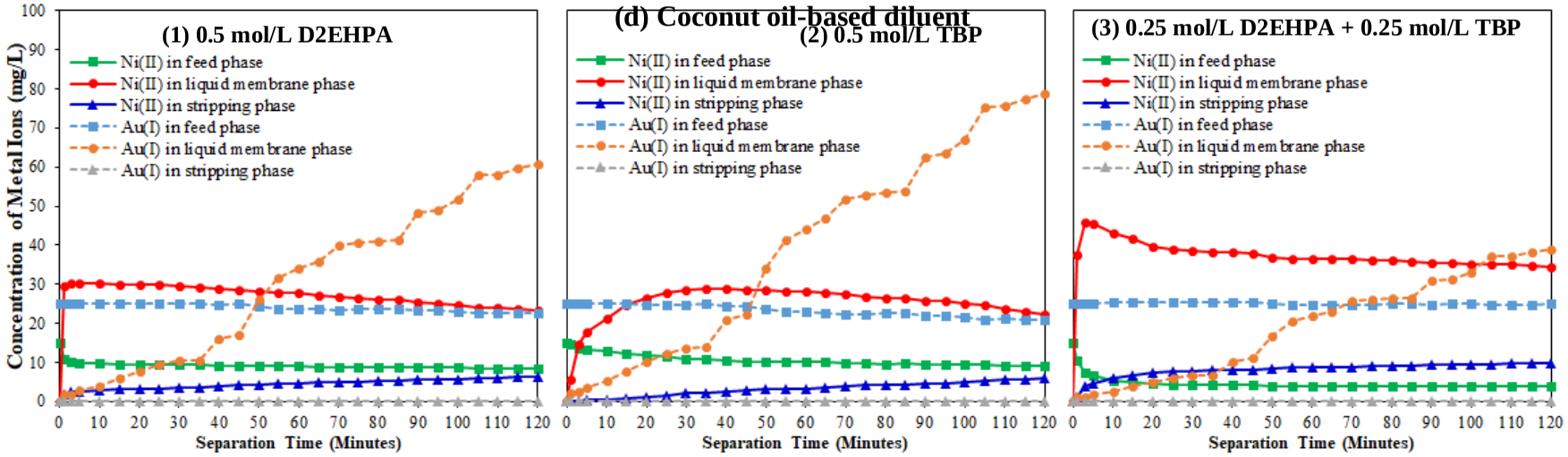

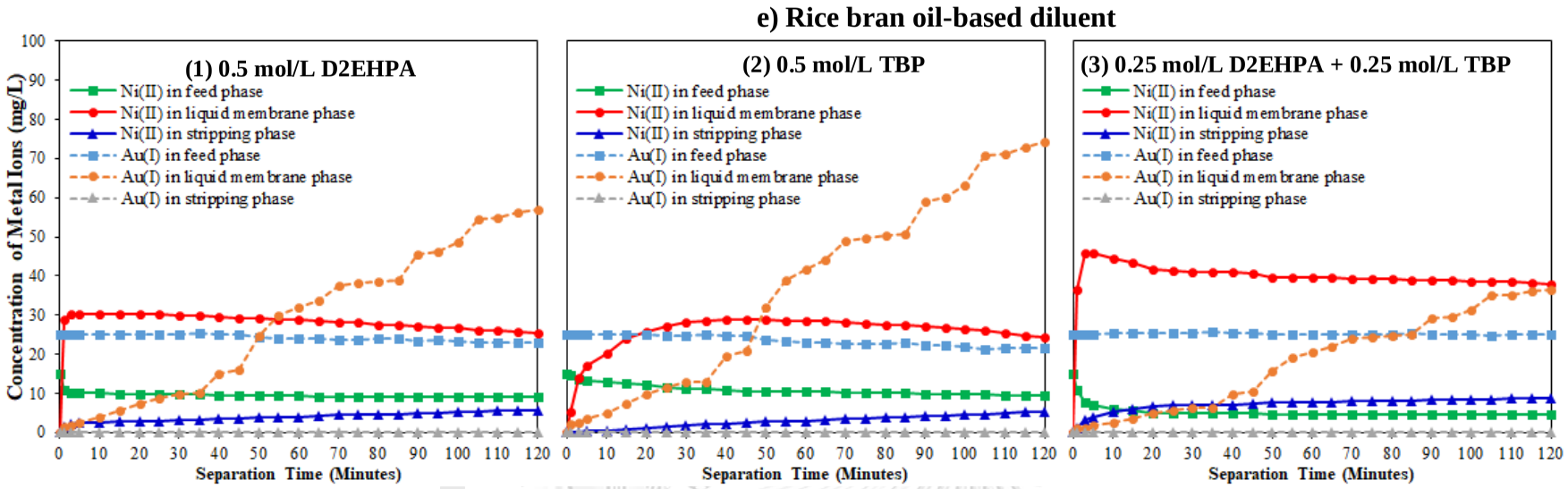

Figure 3.5 Equilibrium distribution and concentration profiles of Ni^{2+} and $[Au(CN)_2]^-$ with time in the various phases (feed, liquid membrane and stripping): (a) palm oil, (b) sunflower oil, (c) soybean oil, (d) coconut oil, and (e) rice bran oil-based diluents.

3.5.5 Reaction order and reaction rate constant

The reaction rate of Ni^{2+} extraction, $r_{\mathrm{Ni},Ex}(x,t)$, can be expressed as follows:

$$r_{\mathrm{Ni},Ex}(x,t) = -k_{Ex}\left[C_{\mathrm{Ni},F}(x,t)\right]^{m} \tag{3.7}$$

where x is the longitudinal axis of the hollow fiber in the tube side, k_{Ex} is the reaction rate constant of extraction, t is the separation time, $C_{\mathrm{Ni},F}(x,t)$ is the concentration of Ni^{2+} in the feed solution and m is the order of extraction reaction.

In order to strip Ni^{2+}, hydrogen ions (H^{+}) in the stripping solution is kept in plentiful supply higher than that in the feed solution, resulting in a higher forward reaction than a backward reaction. The overall reaction of Ni^{2+} stripping in Eqs. (A3.4) to (A3.6), therefore, can be considered as forward reaction. Thus, the reaction rate of Ni^{2+} stripping, $r_{\mathrm{Ni},St}(x',t)$ becomes:

$$r_{\mathrm{Ni},St}(x',t) = -k_{St}\left[C_{\mathrm{Ni},St}(x',t)\right]^{n} \tag{3.8}$$

where x' is the longitudinal axis of the hollow fiber in the shell side and equal to $L-x$, k_{St} is the reaction rate constant of stripping, $C_{\mathrm{Ni},St}(x',t)$ is the concentration of Ni^{2+} in the stripping solution and n is the order of stripping reaction.

Using Taylor series to linearize the reaction rates of extraction and stripping in Eqs. (3.7) and (3.8), as shown in the supplementary information, the following equations are obtained:

$$r_{\mathrm{Ni},Ex}(x_i,t) = -\left(\Omega C_{\mathrm{Ni},F}\left(x_i,t\right) + \psi\right) \tag{3.9}$$

where $\Omega = mk_{Ex}\left[C_{\mathrm{Ni},F}\left(0,t\right)\right]^{m-1}$, $\psi = \left(1-m\right)k_{Ex}\left[C_{\mathrm{Ni},F}\left(0,t\right)\right]^{m}$

$$r_{\mathrm{Ni},St}(x_i',t)=\sigma C_{\mathrm{Ni},St}\left(x_i',t\right)+\delta \tag{3.10}$$

where $\sigma = nk_{St}\left[C_{\mathrm{Ni},St}\left(0,t\right)\right]^{n-1}$, $\delta=\left(1-n\right)k_{St}\left[C_{\mathrm{Ni},St}\left(0,t\right)\right]^{n}$.

Integration and graphical methods, plotted between the integral concentration or Ni^{2+} and $[Au(CN)_2]^-$ versus time, were utilized to estimate the reaction rate constants and reaction orders of Ni^{2+} and $[Au(CN)_2]^-$ extraction and stripping. In Tables 3.2 and 3.3, results are given. Due to the highest R^2 for all vegetable oil-based diluents, reactions for both extraction and stripping of Ni^{2+} from real rinse wastewater of the ENIG process were found to be of third-order. Meanwhile, the extraction reaction of $[Au(CN)_2]^-$ was zero-order and stripping reaction was first-order.

The reaction rates of extraction and stripping of Ni^{2+} using the mixed extractants: D2EHPA and TBP in the palm-oil based diluent were 1.7574 $mmol^{-2}\cdot L^2\cdot min^{-1}$ and 0.0317 $mmol^{-2}\cdot L^2\cdot min^{-1}$, respectively. These values indicate that the rate of stripping is slower than the rate of extraction.

จุฬาลงกรณ์มหาวิทยาลัย
CHULALONGKORN UNIVERSITY

Table 3.2 Reaction rate order (*m*, *n*) and reaction rate constants of extraction and stripping of Ni^{2+} via HFSLM by mixed extractants (0.25 mol/L D2EHPA and 0.25 mol/L TBP) in various vegetable oil-based diluents with 0.50 mol/L HCl as strippant.

m, *n*	Reaction	Plot	Rate constant (k_{Ni})	R^2
Palm oil-based diluent				
3	Extraction	$\left(\frac{1}{2\left(C_{Ni,F}\right)^2}-\frac{1}{2\left(C_{Ni,0}\right)^2}\right)$ vs *t*	1757.4× $mmol^{-2}\cdot L^2\cdot min^{-1}$	0.8979
3	Stripping	$\left(\frac{1}{2\left(C_{Ni,Org}-C_{Ni,St}\right)^2}-\frac{1}{2\left(C_{Ni,Org}\right)^2}\right)$ vs *t*	31.7×10^{-3} $mmol^{-2}\cdot L^2\cdot min^{-1}$	0.9898
Sunflower oil-based diluent				
3	Extraction	$\left(\frac{1}{2\left(C_{Ni,F}\right)^2}-\frac{1}{2\left(C_{Ni,0}\right)^2}\right)$ vs *t*	1485×10^{-3} $mmol^{-2}\cdot L^2\cdot min^{-1}$	0.8873
3	Stripping	$\left(\frac{1}{2\left(C_{Ni,Org}-C_{Ni,St}\right)^2}-\frac{1}{2\left(C_{Ni,Org}\right)^2}\right)$ vs *t*	18.4×10^{-3} $mmol^{-2}\cdot L^2\cdot min^{-1}$	0.9762
Soybean oil-based diluent				
3	Extraction	$\left(\frac{1}{2\left(C_{Ni,F}\right)^2}-\frac{1}{2\left(C_{Ni,0}\right)^2}\right)$ vs *t*	1019.7×10^{-3} $mmol^{-2}\cdot L^2\cdot min^{-1}$	0.8636
3	Stripping	$\left(\frac{1}{2\left(C_{Ni,Org}-C_{Ni,St}\right)^2}-\frac{1}{2\left(C_{Ni,Org}\right)^2}\right)$ vs *t*	10.7×10^{-3} $mmol^{-2}\cdot L^2\cdot min^{-1}$	0.9551
Coconut oil-based diluent				
3	Extraction	$\left(\frac{1}{2\left(C_{Ni,F}\right)^2}-\frac{1}{2\left(C_{Ni,0}\right)^2}\right)$ vs *t*	1177.2×10^{-3} $mmol^{-2}\cdot L^2\cdot min^{-1}$	0.8727
3	Stripping	$\left(\frac{1}{2\left(C_{Ni,Org}-C_{Ni,St}\right)^2}-\frac{1}{2\left(C_{Ni,Org}\right)^2}\right)$ vs *t*	13.1×10^{-3} $mmol^{-2}\cdot L^2\cdot min^{-1}$	0.9637
Rice bran oil-based diluent				
3	Extraction	$\left(\frac{1}{2\left(C_{Ni,F}\right)^2}-\frac{1}{2\left(C_{Ni,0}\right)^2}\right)$ vs *t*	833.4×10^{-3} $mmol^{-2}\cdot L^2\cdot min^{-1}$	0.8511
3	Stripping	$\left(\frac{1}{2\left(C_{Ni,Org}-C_{Ni,St}\right)^2}-\frac{1}{2\left(C_{Ni,Org}\right)^2}\right)$ vs *t*	8.2×10^{-3} $mmol^{-2}\cdot L^2\cdot min^{-1}$	0.9422

CHULALONGKORN UNIVERSITY

Table 3.3 Reaction order (*m*, *n*) and reaction rate constants of extraction and stripping of $[Au(CN)_2]^-$ via HFSLM by mixed extractants (0.25 mol/L D2EHPA and 0.25 mol/L TBP) in various vegetable oil-based diluents with 0.50 mol/L HCl as strippant.

m, *n*	Reaction	Plot	Rate constant (k_{Au})	R^2
Palm oil-based diluent				
0	Extraction	$C_{Ni,F}$ vs t	9×10^{-6} mmol·L^{-1}·min^{-1}	0.5955
1	Stripping	$\ln\left(\frac{C_{Ni,Org}-C_{Ni,St}}{C_{Ni,Org}}\right)$ vs t	1×10^{-5} min^{-1}	0.9913
Sunflower oil-based diluent				
0	Extraction	$C_{Ni,F}$ vs t	6×10^{-6} mmol·L^{-1}·min^{-1}	0.5368
1	Stripping	$\ln\left(\frac{C_{Ni,Org}-C_{Ni,St}}{C_{Ni,Org}}\right)$ vs t	1×10^{-5} min^{-1}	0.9914
Soybean oil-based diluent				
0	Extraction	$C_{Ni,F}$ vs t	1×10^{-6} mmol·L^{-1}·min^{-1}	0.3395
1	Stripping	$\ln\left(\frac{C_{Ni,Org}-C_{Ni,St}}{C_{Ni,Org}}\right)$ vs t	1×10^{-5} min^{-1}	0.9914
Coconut oil-based diluent				
0	Extraction	$C_{Ni,F}$ vs t	2×10^{-6} mmol·L^{-1}·min^{-1}	0.4276
1	Stripping	$\ln\left(\frac{C_{Ni,Org}-C_{Ni,St}}{C_{Ni,Org}}\right)$ vs t	1×10^{-5} min^{-1}	0.9914
Rice bran oil-based diluent				
0	Extraction	$C_{Ni,F}$ vs t	6×10^{-6} mmol·L^{-1}·min^{-1}	0.1877
1	Stripping	$\ln\left(\frac{C_{Ni,Org}-C_{Ni,St}}{C_{Ni,Org}}\right)$ vs t	1×10^{-5} min^{-1}	0.9914

จุฬาลงกรณ์มหาวิทยาลัย
Chulalongkorn University

3.5.6 Validation of the mathematical Model

A mathematical model based on the conservation of mass was developed in order to predict the concentration of Ni^{2+} in both feed and stripping solutions. Parameters considered in the model were axial convection, diffusion, mass accumulation and reactions at the liquid membrane interfaces.

In the feed phase, the mathematical model was developed under the following assumptions:

1. Temperature, pressure and volume of the feed phase, inside the tube, are constant.
2. The inside radius of the hollow-fiber is very small. Therefore, the concentration profile of Ni^{2+} in the radial direction is constant, meaning that the diffusion fluxes of the ions in the feed phase occur only in the axial direction.
3. The extractant in the liquid membrane phase is kept at excess concentration and Ni^{2+} are transferred into the strippant solution continuously. Therefore, extraction reaction can be considered as forward reaction.
4. Extraction reaction takes place at the feed-liquid membrane interface along the length of the hollow fiber.
5. Only the Ni-extractant complex, which is formed due to the extraction reaction, not Ni^{2+}, can transport into the liquid membrane phase.

For the stripping phase, the mathematical model was developed as follows:

1. Temperature, pressure and volume of the strippant phase, inside the shell, are constant.
2. Stripping reaction occurs at the liquid membrane-strippant interface along the length of the hollow fiber.

จุฬาลงกรณ์มหาวิทยาลัย
Chulalongkorn University

3. Only Ni^{2+} according to the stripping reaction at the interface, not the Ni-extractant complex, can be stripped into the stripping solution.
4. The strippant is kept at excess concentration. Therefore, stripping reaction can be considered as forward reaction.

In order to determine the model equation, the tube and shell sides of the hollow fiber were dissected into segments. Each segment is very small as shown in Fig. A3.5 in Section 3.7 Appendix A.

Upon examining a small segment in the tube side of the hollow fiber, the conservation of mass for Ni^{2+} can be expressed as:

$$q_F C_{\mathrm{Ni},F}\left(x_{i-1},t\right)-q_F C_{\mathrm{Ni},F}\left(x_i,t\right)+\frac{A_{c,F}D_{\mathrm{Ni},F}}{\Delta x_i}\left(C_{\mathrm{Ni},F}\left(x_i,t\right)-C_{\mathrm{Ni},F}\left(x_{i-1},t\right)\right)+r_{\mathrm{Ni},Ex}\left(x_i,t\right)V_F=V_F\frac{dC_{\mathrm{Ni},F}\left(x_i,t\right)}{dt}$$

(3.11)

where

q_F is the volumetric flow rate of the feed solution.

i is the number of divided tiny segments.

$A_{c,F}$ is the cross-sectional area of the tube $=\pi r_i^2$

V_F is the volume of a tiny segment of the hollow fiber in the tube side $=\pi r_i^2 \Delta x_i$

$\Delta x_i = L/i$

r_i and L refer to the inside radius and effective length of the hollow fibers, respectively.

$D_{\mathrm{Ni},f}$ is the mass diffusivity of Ni^{2+} in the feed solution, which can be estimated by Eq. (A3.11) in Section 3.7 Appendix A.

Eq. (3.11) is solved through Euler's method, as described in Section 3.7 Appendix A. Thus, the concentration of Ni^{2+} in the outlet feed solution, $C_{\mathrm{Ni},F}(x_{i+1},t_{i+1})$, can be calculated:

$$C_{\mathrm{Ni},F}(x_{i+1},t_{i+1}) = C_{\mathrm{Ni},F}(x_i,t_i)\left(1-\frac{q_F\left(t_{i+1}-t_i\right)}{V_F}-\Omega\left(t_{i+1}-t_i\right)+\alpha\left(t_{i+1}-t_i\right)\right) + C_{\mathrm{Ni},F}\left(x_{i-1},t_i\right)\left(\frac{q_F\left(t_{i+1}-t_i\right)}{V_F}-\alpha\left(t_{i+1}-t_i\right)\right)-\psi\left(t_{i+1}-t_i\right) \quad (3.12)$$

where $\alpha = \dfrac{A_{c,F}D_{\mathrm{Ni},F}}{\Delta x_i V_F}$

For the stripping phase, mass conservation of Ni^{2+} was examined for each small segment in the shell side of the hollow fiber, as shown below:

$$q_{St}C_{\mathrm{Ni},St}\left(x'_{i-1},t\right)-q_{St}C_{\mathrm{Ni},St}\left(x'_i,t\right)+\frac{A_{c,St}D_{\mathrm{Ni},St}}{\Delta x'_i}\left(C_{\mathrm{Ni},St}\left(x'_i,t\right)-C_{\mathrm{Ni},St}\left(x'_{i-1},t\right)\right)+r_{\mathrm{Ni},St}\left(x'_i,t\right)V_{St}=V_{St}\frac{dC_{\mathrm{Ni},St}\left(x'_i,t\right)}{dt}$$

(3.13)

where

q_{St} is the volumetric flow rate of the stripping solution.

$A_{c,St}$ is the cross-sectional area of the shell side of the hollow fiber = $\dfrac{\sqrt{3}}{4}d_o^2-\dfrac{\pi r_o^2}{2}$

V_{St} is the volume of a tiny segment of the shell side of the hollow fiber = $A_{c,St}\Delta x'_i$

d_o and r_o are the outside diameter and outside radius of the hollow fibers.

$D_{\mathrm{Ni},St}$ is the mass diffusivity of Ni^{2+} in the stripping solution, which is calculated using Eq. (A3.11) of the Section 3.7: Supplementary information.

Solving Eq. (3.13) using Euler's method, as described in detail in Section 3.7 Appendix A, results in an equation for the calculation of Ni^{2+} concentration in the outlet stripping solution, $C_{\mathrm{Ni},St}(x'_{i+1},t_{i+1})$, as shown below:

$$C_{\mathrm{Ni},St}(x'_{i+1},t_{i+1}) = C_{\mathrm{Ni},St}(x'_i,t_i)\left(1-\frac{q_{St}\left(t_{i+1}-t_i\right)}{V_{St}}+\sigma\left(t_{i+1}-t_i\right)+\beta\left(t_{i+1}-t_i\right)\right) + C_{\mathrm{Ni},St}\left(x'_{i-1},t_i\right)\left(\frac{q_{St}\left(t_{i+1}-t_i\right)}{V_{St}}-\beta\left(t_{i+1}-t_i\right)\right)+\delta\left(t_{i+1}-t_i\right) \quad (3.14)$$

where $\beta = \dfrac{A_{c,St}D_{\mathrm{Ni},St}}{\Delta x'_i V_{St}}$

In Fig. 3.6, concentrations of Ni^{2+} for extraction and stripping obtained from the model and the experiment are compared. Results clearly show that the mathematical model developed in this work agreed well with the experimental results. Values obtained confirm that the chemical reactions at the liquid-membrane interfaces as well as diffusion are significant factors governing the rate of Ni^{2+} transport across the liquid membrane.

จุฬาลงกรณ์มหาวิทยาลัย
CHULALONGKORN UNIVERSITY

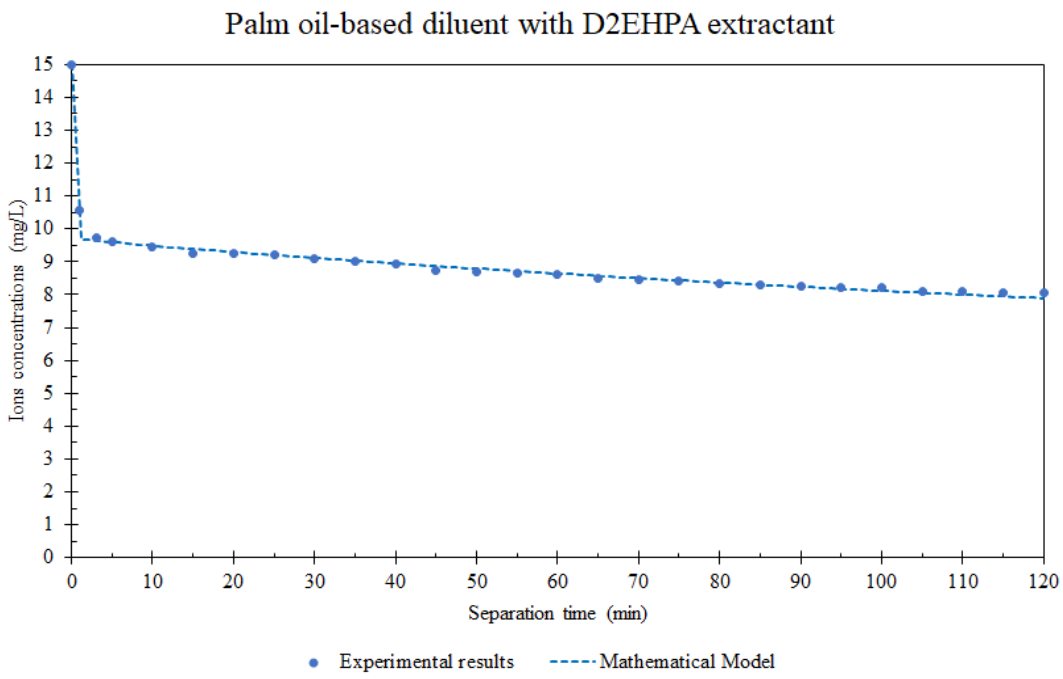

Figure 3.6 Adaptability of the mathematical model to predict the extraction.

3.6 Conclusions

In conclusion, it is evident that the binary mixtures of D2EHPA-TBP were found to be capable of selectively extracting both Ni^{2+} and $[Au(CN)_2]^-$ from the real ENIG rinse wastewater up to 85.7% and 15.6%, respectively. Optimum conditions proved to be 0.25 M D2EHPA and 0.25 M TBP. Maximum distribution ratio for Ni^{2+} and for $[Au(CN)_2]^-$ reached 5.99 and 0.19, respectively. Subsequently, 0.5 M hydrochloric acid was employed as a stripping agent for the back extraction of Ni^{2+} and for $[Au(CN)_2]^-$ in the organic phase.

3.7 Appendix A

Table A3.1 Properties of real rinse wastewater from ENIG plating process as feed solution.

Components	Chemical formula	Concentration	
		mg/L	mol/L
Nickel(II) ion	Ni^{2+}	15	0.3×10^{-3}
Aurodicyanate ion	$[Au(CN)_2]^-$	25	0.1×10^{-3}
Lead(II) ion	Pb^{2+}	1	0.01×10^{-3}
Potassium ion	K^+	667	17.1×10^{-3}
Sodium ion	Na^+	59	2.6×10^{-3}
Cyanide ion	CN^-	18	0.7×10^{-3}
Sulfate ion	SO_4^{2-}	25	0.3×10^{-3}
Hydroxide ion	OH^-	276	16.2×10^{-3}
Hypophosphate ion	H_2PO_{3-}	45	0.6×10^{-3}
Acetate ion	CH_3COO^-	0.4	0.01×10^{-3}
Pyrophosphate	$P_2O_7^{4-}$	88	0.5×10^{-3}
Hydrazine	N_2H_4	163	5.1×10^{-3}

จุฬาลงกรณ์มหาวิทยาลัย
CHULALONGKORN UNIVERSITY

Table A3.2 Chemicals used in this study.

Chemicals	Chemical formula	Molar mass	CAS No.	Purity, %wt.	Purification method	Source
Organic extractants in the liquid membrane phase						
Di-(2-ethylhexyl) phosphoric acid, D2EHPA	$C_{16}H_{35}O_4P$	322.42	298-07-7	>97.0 (Synthesis Grade)	None	Merck
Tributyl Phosphate, TBP	$C_{12}H_{27}O_4P$	266.31	126-73-8	>99.0 (Synthesis Grade)	None	Merck
Vegetable oil based-diluents in the liquid membrane phase						
Palm Oil	N/A	N/A	8002-75-3	N/A (Analytical Grade)	None	Sigma Aldrich
Sunflower oil	N/A	N/A	8001-21-6	N/A (Analytical Grade)	None	Sigma Aldrich
Soybean oil	N/A	N/A	8001-22-7	N/A (Analytical Grade)	None	Sigma Aldrich
Coconut oil	N/A	N/A	8001-31-8	N/A (Analytical Grade)	None	Sigma Aldrich
Rice bran oil	N/A	N/A	68553-81-1	N/A (Analytical Grade)	None	Sigma Aldrich
Inorganic strippant in the stripping phase						
				Concentration, %wt.		
Hydrochloric acid	HCl	36.46	7647-01-0	37.0-38.0 (Analytical Grade)	None	Merck

Table A3.3 Typical characteristics of Liqui-Cel® Extra-Flow hollow fiber module.

Properties	Units	Values
Material		Polypropylene
Module diameter	m	6.3×10^{-2}
Module length	m	2.03×10^{-1}
Number of hollow fibers	fibers	35,000
Effective length of a hollow fiber	m	1.5×10^{-1}
Inside diameter of a hollow fiber	m	2.4×10^{-4}
Outside diameter of a hollow fiber	m	3×10^{-4}
Average pore size	m per fiber	3×10^{-8}
Pore size	m per fiber	5×10^{-8}
Porosity	-	3×10^{-2}
Effective surface area	m^2 per fiber	1.4
Area per unit volume	$m^2 \cdot m^{-3}$	2.93×10^{3}
Tortuosity factor	-	2.6
Maximum pressure difference	$kg\cdot m^{-2}$	4.2×10^{4}
Operating temperature	K	273-333

จุฬาลงกรณ์มหาวิทยาลัย
CHULALONGKORN UNIVERSITY

Table A3.4 Reaction rate order (*m*, *n*) and reaction rate constants of extraction and stripping of Ni^{2+} via HFSLM by mixed extractants (0.25 M D2EHPA and 0.25 M TBP) in various vegetable oil-based diluents with 0.50 M HCl as strippant.

m, *n*	Reaction	Plot	Rate constant (k_{Ni})	R^2
Palm oil-based diluent				
0	Extraction	$C_{Ni,F}$ vs t	2.4×10^{-3} mmol·L^{-1}·min^{-1}	0.3614
	Stripping	$\left(C_{Ni,Org}-C_{Ni,St}\right)$ vs t	2.7×10^{-3} mmol·L^{-1}·min^{-1}	0.7707
1	Extraction	$\ln\left(\frac{C_{Ni,F}}{C_{Ni,0}}\right)$ vs t	18.2×10^{-3} min^{-1}	0.8185
	Stripping	$\ln\left(\frac{C_{Ni,Org}-C_{Ni,St}}{C_{Ni,Org}}\right)$ vs t	5.2×10^{-3} min^{-1}	0.9249
2	Extraction	$\left(\frac{1}{C_{Ni,F}}-\frac{1}{C_{Ni,0}}\right)$ vs t	164.7×10^{-3} mmol^{-1}·L·min^{-1}	0.8605
	Stripping	$\left(\frac{1}{C_{Ni,Org}-C_{Ni,St}}-\frac{1}{C_{Ni,Org}}\right)$ vs t	12.6×10^{-3} mmol^{-1}·L·min^{-1}	0.9674
3	Extraction	$\left(\frac{1}{2\left(C_{Ni,F}\right)^2}-\frac{1}{2\left(C_{Ni,0}\right)^2}\right)$ vs t	1757.4× mmol^{-2}·L^{2}·min^{-1}	0.8979
	Stripping	$\left(\frac{1}{2\left(C_{Ni,Org}-C_{Ni,St}\right)^2}-\frac{1}{2\left(C_{Ni,Org}\right)^2}\right)$ vs t	31.7×10^{-3} mmol^{-2}·L^{2}·min^{-1}	0.9898
Sunflower oil-based diluent				
0	Extraction	$C_{Ni,F}$ vs t	2.4×10^{-3} mmol·L^{-1}·min^{-1}	0.3572
	Stripping	$\left(C_{Ni,Org}-C_{Ni,St}\right)$ vs t	2.3×10^{-3} mmol·L^{-1}·min^{-1}	0.7841
1	Extraction	$\ln\left(\frac{C_{Ni,F}}{C_{Ni,0}}\right)$ vs t	17.3×10^{-3} min^{-1}	0.8145
	Stripping	$\ln\left(\frac{C_{Ni,Org}-C_{Ni,St}}{C_{Ni,Org}}\right)$ vs t	4.2×10^{-3} min^{-1}	0.9118
2	Extraction	$\left(\frac{1}{C_{Ni,F}}-\frac{1}{C_{Ni,0}}\right)$ vs t	148.5×10^{-3} mmol^{-1}·L·min^{-1}	0.8527
	Stripping	$\left(\frac{1}{C_{Ni,Org}-C_{Ni,St}}-\frac{1}{C_{Ni,Org}}\right)$ vs t	8.7×10^{-3} mmol^{-1}·L·min^{-1}	0.9506

CHULALONGKORN UNIVERSITY

3	Extraction	$\left(\frac{1}{2\left(C_{\mathrm{Ni},F}\right)^2}-\frac{1}{2\left(C_{\mathrm{Ni},0}\right)^2}\right)$ vs t	1485×10^{-3} $\mathrm{mmol^{-2}\cdot L^{2}\cdot min^{-1}}$	0.8873
	Stripping	$\left(\frac{1}{2\left(C_{\mathrm{Ni},Org}-C_{\mathrm{Ni},St}\right)^2}-\frac{1}{2\left(C_{\mathrm{Ni},Org}\right)^2}\right)$ vs t	18.4×10^{-3} $\mathrm{mmol^{-2}\cdot L^{2}\cdot min^{-1}}$	0.9762
Soybean oil-based diluent				
0	Extraction	$C_{\mathrm{Ni},F}$ vs t	2.2×10^{-3} $\mathrm{mmol\cdot L^{-1}\cdot min^{-1}}$	0.3456
	Stripping	$\left(C_{\mathrm{Ni},Org}-C_{\mathrm{Ni},St}\right)$ vs t	1.7×10^{-3} $\mathrm{mmol\cdot L^{-1}\cdot min^{-1}}$	0.7906
1	Extraction	$\ln\left(\frac{C_{\mathrm{Ni},F}}{C_{\mathrm{Ni},0}}\right)$ vs t	15.1×10^{-3} $\mathrm{min^{-1}}$	0.8054
	Stripping	$\ln\left(\frac{C_{\mathrm{Ni},Org}-C_{\mathrm{Ni},St}}{C_{\mathrm{Ni},Org}}\right)$ vs t	3.3×10^{-3} $\mathrm{min^{-1}}$	0.8978
2	Extraction	$\left(\frac{1}{C_{\mathrm{Ni},F}}-\frac{1}{C_{\mathrm{Ni},0}}\right)$ vs t	117.1×10^{-3} $\mathrm{mmol^{-1}\cdot L\cdot min^{-1}}$	0.8357
	Stripping	$\left(\frac{1}{C_{\mathrm{Ni},Org}-C_{\mathrm{Ni},St}}-\frac{1}{C_{\mathrm{Ni},Org}}\right)$ vs t	5.9×10^{-3} $\mathrm{mmol^{-1}\cdot L\cdot min^{-1}}$	0.9302
3	Extraction	$\left(\frac{1}{2\left(C_{\mathrm{Ni},F}\right)^2}-\frac{1}{2\left(C_{\mathrm{Ni},0}\right)^2}\right)$ vs t	1019.7×10^{-3} $\mathrm{mmol^{-2}\cdot L^{2}\cdot min^{-1}}$	0.8636
	Stripping	$\left(\frac{1}{2\left(C_{\mathrm{Ni},Org}-C_{\mathrm{Ni},St}\right)^2}-\frac{1}{2\left(C_{\mathrm{Ni},Org}\right)^2}\right)$ vs t	10.7×10^{-3} $\mathrm{mmol^{-2}\cdot L^{2}\cdot min^{-1}}$	0.9551
Coconut oil-based diluent				
0	Extraction	$C_{\mathrm{Ni},F}$ vs t	2.3×10^{-3} $\mathrm{mmol\cdot L^{-1}\cdot min^{-1}}$	0.3504
	Stripping	$\left(C_{\mathrm{Ni},Org}-C_{\mathrm{Ni},St}\right)$ vs t	1.9×10^{-3} $\mathrm{mmol\cdot L^{-1}\cdot min^{-1}}$	0.7909
1	Extraction	$\ln\left(\frac{C_{\mathrm{Ni},F}}{C_{\mathrm{Ni},0}}\right)$ vs t	15.9×10^{-3} $\mathrm{min^{-1}}$	0.8089
	Stripping	$\ln\left(\frac{C_{\mathrm{Ni},Org}-C_{\mathrm{Ni},St}}{C_{\mathrm{Ni},Org}}\right)$ vs t	3.6×10^{-3} $\mathrm{min^{-1}}$	0.9030
2	Extraction	$\left(\frac{1}{C_{\mathrm{Ni},F}}-\frac{1}{C_{\mathrm{Ni},0}}\right)$ vs t	128.4×10^{-3} $\mathrm{mmol^{-1}\cdot L\cdot min^{-1}}$	0.8422
	Stripping	$\left(\frac{1}{C_{\mathrm{Ni},Org}-C_{\mathrm{Ni},St}}-\frac{1}{C_{\mathrm{Ni},Org}}\right)$ vs t	6.8×10^{-3} $\mathrm{mmol^{-1}\cdot L\cdot min^{-1}}$	0.9381

CHULALONGKORN UNIVERSITY

3	Extraction	$\left(\frac{1}{2\left(C_{\mathrm{Ni},F}\right)^2}-\frac{1}{2\left(C_{\mathrm{Ni},0}\right)^2}\right)$ vs t	1177.2×10^{-3} $\mathrm{mmol^{-2}\cdot L^{2}\cdot min^{-1}}$	0.8727
	Stripping	$\left(\frac{1}{2\left(C_{\mathrm{Ni},Org}-C_{\mathrm{Ni},St}\right)^2}-\frac{1}{2\left(C_{\mathrm{Ni},Org}\right)^2}\right)$ vs t	13.1×10^{-3} $\mathrm{mmol^{-2}\cdot L^{2}\cdot min^{-1}}$	0.9637
Rice bran oil-based diluent				
0	Extraction	$C_{\mathrm{Ni},F}$ vs t	2.1×10^{-3} $\mathrm{mmol\cdot L^{-1}\cdot min^{-1}}$	0.3380
	Stripping	$\left(C_{\mathrm{Ni},Org}-C_{\mathrm{Ni},St}\right)$ vs t	1.4×10^{-3} $\mathrm{mmol\cdot L^{-1}\cdot min^{-1}}$	0.7754
1	Extraction	$\ln\left(\frac{C_{\mathrm{Ni},F}}{C_{\mathrm{Ni},0}}\right)$ vs t	14×10^{-3} $\mathrm{min^{-1}}$	0.8004
	Stripping	$\ln\left(\frac{C_{\mathrm{Ni},Org}-C_{\mathrm{Ni},St}}{C_{\mathrm{Ni},Org}}\right)$ vs t	2.8×10^{-3} $\mathrm{min^{-1}}$	0.8908
2	Extraction	$\left(\frac{1}{C_{\mathrm{Ni},F}}-\frac{1}{C_{\mathrm{Ni},0}}\right)$ vs t	102.7×10^{-3} $\mathrm{mmol^{-1}\cdot L\cdot min^{-1}}$	0.8267
	Stripping	$\left(\frac{1}{C_{\mathrm{Ni},Org}-C_{\mathrm{Ni},St}}-\frac{1}{C_{\mathrm{Ni},Org}}\right)$ vs t	4.8×10^{-3} $\mathrm{mmol^{-1}\cdot L\cdot min^{-1}}$	0.9191
3	Extraction	$\left(\frac{1}{2\left(C_{\mathrm{Ni},F}\right)^2}-\frac{1}{2\left(C_{\mathrm{Ni},0}\right)^2}\right)$ vs t	833.4×10^{-3} $\mathrm{mmol^{-2}\cdot L^{2}\cdot min^{-1}}$	0.8511
	Stripping	$\left(\frac{1}{2\left(C_{\mathrm{Ni},Org}-C_{\mathrm{Ni},St}\right)^2}-\frac{1}{2\left(C_{\mathrm{Ni},Org}\right)^2}\right)$ vs t	8.2×10^{-3} $\mathrm{mmol^{-2}\cdot L^{2}\cdot min^{-1}}$	0.9422

จุฬาลงกรณ์มหาวิทยาลัย
CHULALONGKORN UNIVERSITY

Table A3.5 Reaction order (*m/n*) and reaction rate constants of extraction and stripping of $[Au(CN)_2]^-$ via HFSLM by mixed extractants (0.25 mol/L D2EHPA and 0.25 mol/L TBP) in various vegetable oil-based diluents with 0.50 mol/L HCl as strippant.

m/n	Reaction	Plot	Rate constant (k_{Au})	R^2
Palm oil-based diluent				
0	Extraction	$C_{Ni,F}$ vs t	9×10^{-6} mmol·L^{-1}·min^{-1}	0.5955
	Stripping	$\left(C_{Ni,Org}-C_{Ni,St}\right)$ vs t	1.5×10^{-3} mmol·L^{-1}·min^{-1}	0.9821
1	Extraction	$\ln\left(\frac{C_{Ni,F}}{C_{Ni,0}}\right)$ vs t	9×10^{-5} min^{-1}	0.2572
	Stripping	$\ln\left(\frac{C_{Ni,Org}-C_{Ni,St}}{C_{Ni,Org}}\right)$ vs t	1×10^{-5} min^{-1}	0.9913
2	Extraction	$\left(\frac{1}{C_{Ni,F}}-\frac{1}{C_{Ni,0}}\right)$ vs t	9×10^{-4} mmol^{-1}·L·min^{-1}	0.2629
	Stripping	$\left(\frac{1}{C_{Ni,Org}-C_{Ni,St}}-\frac{1}{C_{Ni,Org}}\right)$ vs t	1×10^{-4} mmol^{-1}·L·min^{-1}	0.7569
3	Extraction	$\left(\frac{1}{2\left(C_{Ni,F}\right)^2}-\frac{1}{2\left(C_{Ni,0}\right)^2}\right)$ vs t	9.3×10^{-3} mmol^{-2}·L^{2}·min^{-1}	0.2687
	Stripping	$\left(\frac{1}{2\left(C_{Ni,Org}-C_{Ni,St}\right)^2}-\frac{1}{2\left(C_{Ni,Org}\right)^2}\right)$ vs t	1.6×10^{-3} mmol^{-2}·L^{2}·min^{-1}	0.0322
Sunflower oil-based diluent				
0	Extraction	$C_{Ni,F}$ vs t	6×10^{-6} mmol·L^{-1}·min^{-1}	0.5368
	Stripping	$\left(C_{Ni,Org}-C_{Ni,St}\right)$ vs t	1.4×10^{-3} mmol·L^{-1}·min^{-1}	0.9821
1	Extraction	$\ln\left(\frac{C_{Ni,F}}{C_{Ni,0}}\right)$ vs t	6×10^{-5} min^{-1}	0.1369
	Stripping	$\ln\left(\frac{C_{Ni,Org}-C_{Ni,St}}{C_{Ni,Org}}\right)$ vs t	1×10^{-5} min^{-1}	0.9914
2	Extraction	$\left(\frac{1}{C_{Ni,F}}-\frac{1}{C_{Ni,0}}\right)$ vs t	6×10^{-4} mmol^{-1}·L·min^{-1}	0.1409

จุฬาลงกรณ์มหาวิทยาลัย
CHULALONGKORN UNIVERSITY

	Stripping	$\left(\frac{1}{C_{\mathrm{Ni},Org}-C_{\mathrm{Ni},St}}-\frac{1}{C_{\mathrm{Ni},Org}}\right)$ vs t	1×10^{-4} mmol^{-1}·L·min^{-1}	0.7563
3	Extraction	$\left(\frac{1}{2\left(C_{\mathrm{Ni},F}\right)^2}-\frac{1}{2\left(C_{\mathrm{Ni},0}\right)^2}\right)$ vs t	6.2×10^{-3} mmol^{-2}·L^{2}·min^{-1}	0.1451
	Stripping	$\left(\frac{1}{2\left(C_{\mathrm{Ni},Org}-C_{\mathrm{Ni},St}\right)^2}-\frac{1}{2\left(C_{\mathrm{Ni},Org}\right)^2}\right)$ vs t	1.5×10^{-3} mmol^{-2}·L^{2}·min^{-1}	0.0321
Soybean oil-based diluent				
0	Extraction	$C_{\mathrm{Ni},F}$ vs t	1×10^{-6} mmol·L^{-1}·min^{-1}	0.3395
	Stripping	$\left(C_{\mathrm{Ni},Org}-C_{\mathrm{Ni},St}\right)$ vs t	1.4×10^{-3} mmol·L^{-1}·min^{-1}	0.9821
1	Extraction	$\ln\left(\frac{C_{\mathrm{Ni},F}}{C_{\mathrm{Ni},0}}\right)$ vs t	1×10^{-5} min^{-1}	0.0087
	Stripping	$\ln\left(\frac{C_{\mathrm{Ni},Org}-C_{\mathrm{Ni},St}}{C_{\mathrm{Ni},Org}}\right)$ vs t	1×10^{-5} min^{-1}	0.9914
2	Extraction	$\left(\frac{1}{C_{\mathrm{Ni},F}}-\frac{1}{C_{\mathrm{Ni},0}}\right)$ vs t	1×10^{-4} mmol^{-1}·L·min^{-1}	0.0084
	Stripping	$\left(\frac{1}{C_{\mathrm{Ni},Org}-C_{\mathrm{Ni},St}}-\frac{1}{C_{\mathrm{Ni},Org}}\right)$ vs t	1×10^{-4} mmol^{-1}·L·min^{-1}	0.7557
3	Extraction	$\left(\frac{1}{2\left(C_{\mathrm{Ni},F}\right)^2}-\frac{1}{2\left(C_{\mathrm{Ni},0}\right)^2}\right)$ vs t	1.3×10^{-3} mmol^{-2}·L^{2}·min^{-1}	0.0080
	Stripping	$\left(\frac{1}{2\left(C_{\mathrm{Ni},Org}-C_{\mathrm{Ni},St}\right)^2}-\frac{1}{2\left(C_{\mathrm{Ni},Org}\right)^2}\right)$ vs t	1.6×10^{-3} mmol^{-2}·L^{2}·min^{-1}	0.0320
Coconut oil-based diluent				
0	Extraction	$C_{\mathrm{Ni},F}$ vs t	2×10^{-6} mmol·L^{-1}·min^{-1}	0.4276
	Stripping	$\left(C_{\mathrm{Ni},Org}-C_{\mathrm{Ni},St}\right)$ vs t	1.4×10^{-3} mmol·L^{-1}·min^{-1}	0.9821
1	Extraction	$\ln\left(\frac{C_{\mathrm{Ni},F}}{C_{\mathrm{Ni},0}}\right)$ vs t	2×10^{-5} min^{-1}	0.0113
	Stripping	$\ln\left(\frac{C_{\mathrm{Ni},Org}-C_{\mathrm{Ni},St}}{C_{\mathrm{Ni},Org}}\right)$ vs t	1×10^{-5} min^{-1}	0.9914
2	Extraction	$\left(\frac{1}{C_{\mathrm{Ni},F}}-\frac{1}{C_{\mathrm{Ni},0}}\right)$ vs t	2×10^{-4} mmol^{-1}·L·min^{-1}	0.0121

จุฬาลงกรณ์มหาวิทยาลัย
Chulalongkorn University

	Stripping	$\left(\frac{1}{C_{\mathrm{Ni},Org}-C_{\mathrm{Ni},St}}-\frac{1}{C_{\mathrm{Ni},Org}}\right)$ vs t	1×10^{-4} mmol^{-1}·L·min^{-1}	0.7559
3	Extraction	$\left(\frac{1}{2\left(C_{\mathrm{Ni},F}\right)^2}-\frac{1}{2\left(C_{\mathrm{Ni},0}\right)^2}\right)$ vs t	1.7×10^{-3} mmol^{-2}·L^{2}·min^{-1}	0.0129
	Stripping	$\left(\frac{1}{2\left(C_{\mathrm{Ni},Org}-C_{\mathrm{Ni},St}\right)^2}-\frac{1}{2\left(C_{\mathrm{Ni},Org}\right)^2}\right)$ vs t	1.6×10^{-3} mmol^{-2}·L^{2}·min^{-1}	0.0321

Rice bran oil-based diluent

0	Extraction	$C_{\mathrm{Ni},F}$ vs t	6×10^{-6} mmol·L^{-1}·min^{-1}	0.1877
	Stripping	$\left(C_{\mathrm{Ni},Org}-C_{\mathrm{Ni},St}\right)$ vs t	1.3×10^{-3} mmol·L^{-1}·min^{-1}	0.9821
1	Extraction	$\ln\left(\frac{C_{\mathrm{Ni},F}}{C_{\mathrm{Ni},0}}\right)$ vs t	6×10^{-5} min^{-1}	0.1446
	Stripping	$\ln\left(\frac{C_{\mathrm{Ni},Org}-C_{\mathrm{Ni},St}}{C_{\mathrm{Ni},Org}}\right)$ vs t	1×10^{-5} min^{-1}	0.9914
2	Extraction	$\left(\frac{1}{C_{\mathrm{Ni},F}}-\frac{1}{C_{\mathrm{Ni},0}}\right)$ vs t	6×10^{-4} mmol^{-1}·L·min^{-1}	0.1450
	Stripping	$\left(\frac{1}{C_{\mathrm{Ni},Org}-C_{\mathrm{Ni},St}}-\frac{1}{C_{\mathrm{Ni},Org}}\right)$ vs t	1×10^{-4} mmol^{-1}·L·min^{-1}	0.7553
3	Extraction	$\left(\frac{1}{2\left(C_{\mathrm{Ni},F}\right)^2}-\frac{1}{2\left(C_{\mathrm{Ni},0}\right)^2}\right)$ vs t	5.7×10^{-3} mmol^{-2}·L^{2}·min^{-1}	0.1453
	Stripping	$\left(\frac{1}{2\left(C_{\mathrm{Ni},Org}-C_{\mathrm{Ni},St}\right)^2}-\frac{1}{2\left(C_{\mathrm{Ni},Org}\right)^2}\right)$ vs t	1.7×10^{-3} mmol^{-2}·L^{2}·min^{-1}	0.0320

จุฬาลงกรณ์มหาวิทยาลัย
CHULALONGKORN UNIVERSITY

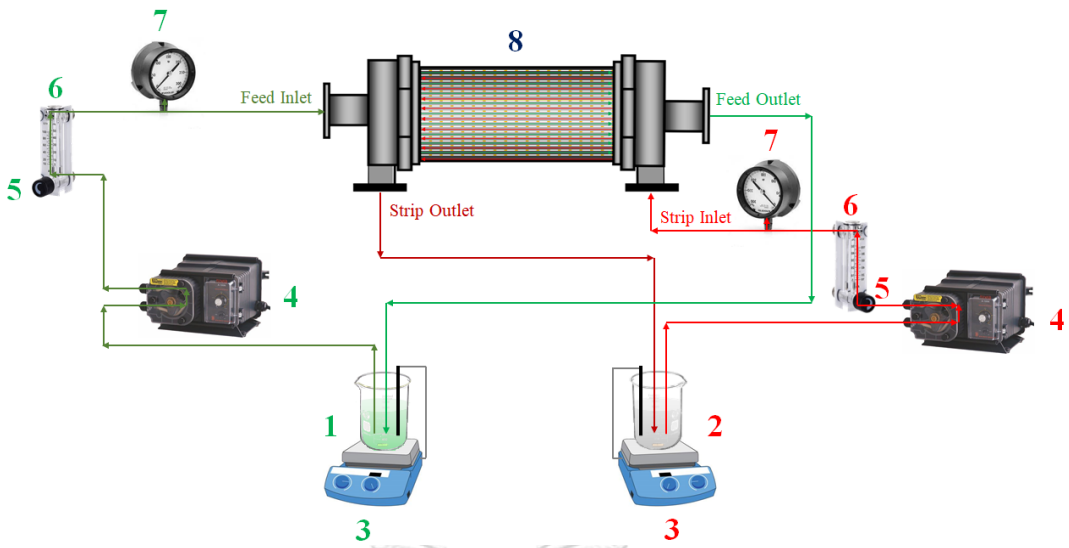

Figure A3.1 The separation system via HFSLM: **1** feed solution reservoir, **2** stripping solution reservoir, **3** hotplate and stirrer with Pt-100 temperature sensor, **4** peristaltic pump, **5** flow regulator valve, **6** flow meter, **7** pressure gauge, and **8** hollow fiber module.

3.7.1 Transport mechanism of Ni^{2+} across the liquid membrane phase

Nickel in the real rinse wastewater from the ENIG plating process exists in Ni^{2+} form at pH 8.6±0.05. The HFSLM system is comprised of a feed phase (an aqueous solution containing Ni^{2+}), a strippant phase, and a supported liquid membrane phase embedded with an organic extractant, which separates both the feed and strippant phase. In Figs. A3.2 to A3.4, schematic diagrams of mass transport of Ni^{2+} via the liquid membrane with different extractants are shown. Ni^{2+} react with extractants (D2EHPA, TBP and mixed D2EHPA/TBP) at the feed-liquid membrane interface (feed side film) forming a Ni-extractant complex species. Then, the Ni-extractant complex diffuses across the liquid membrane to the liquid membrane-strippant interface (strip side film) to react with HCl as the strippant. Subsequently, Ni^{2+} are stripped into the strippant phase. Thus, Ni^{2+} can be simultaneously extracted and stripped in a single-step operation. The rate

of transport of Ni^{2+} is governed by the concentration gradient between the feed and strippant phase.

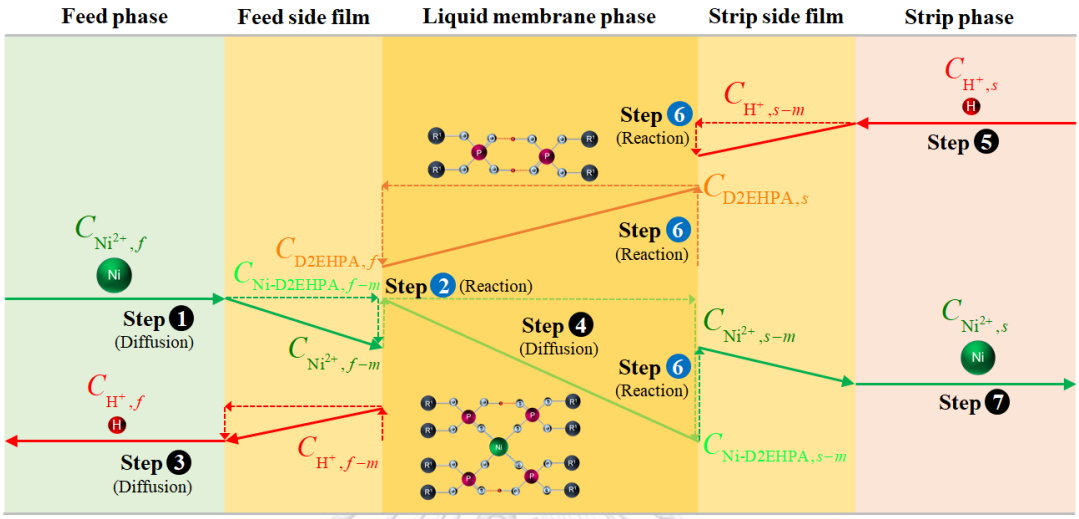

Figure A3.2 Concentration profiles at steady-state of Ni^{2+} and other species across the supported liquid membrane using D2EHPA extractant.

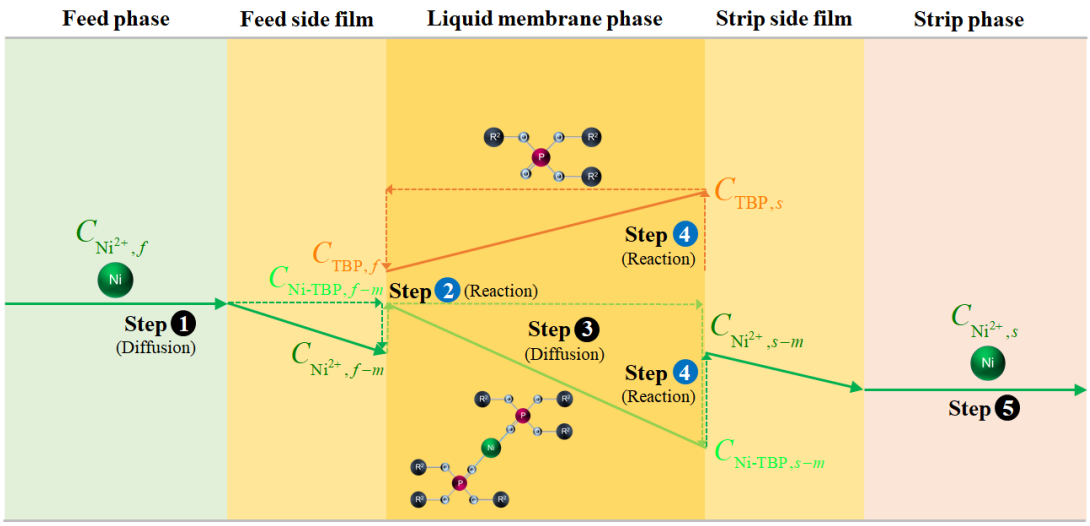

Figure A3.3 Concentration profiles at steady-state of Ni^{2+} and other species across the supported liquid membrane using TBP extractant.

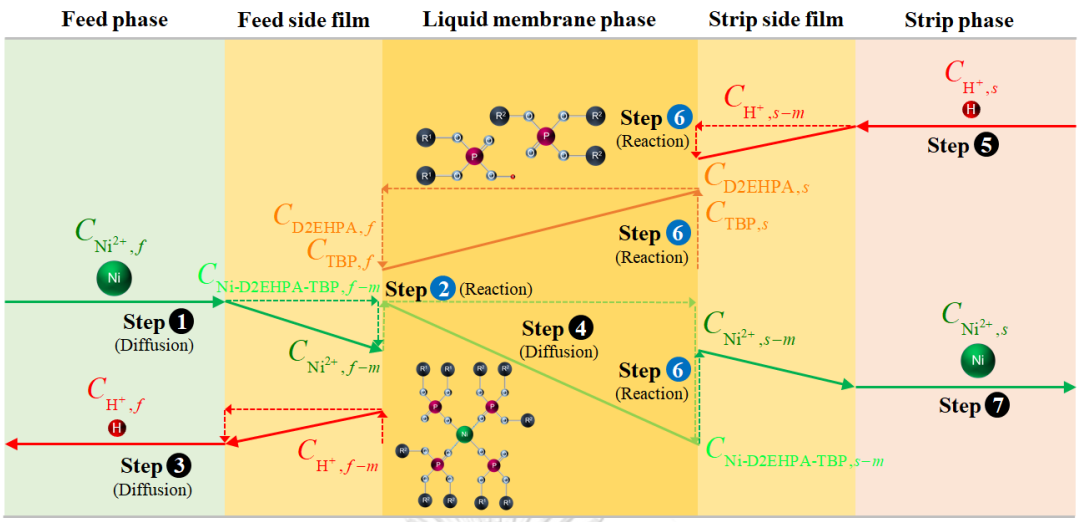

Figure A3.4 Concentration profiles at steady state of Ni^{2+} ions and other species across liquid membrane using mixed extractants of D2EHPA and TBP.

The extraction reaction of Ni^{2+} and extractants (D2EHPA, TBP and mixed D2EHPA-TBP) can be expressed, as in Eqs. (A3.1) to (A3.3):

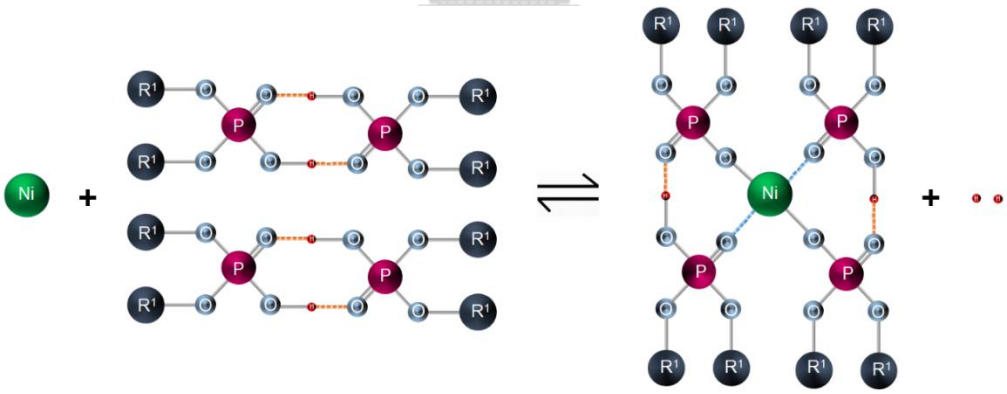

Ni^{2+} $2(HR)_2$ $NiR_2{\cdot}2HR$ $2H^+$ (A3.1)

The dimer of D2EHPA is represented by $(HR)_2$ where R^1 is 2-ethylhexyl group (C_8H_{17}). $NiR_2{\cdot}2HR$ represents the D2EHPA-Ni complex in the liquid membrane phase.

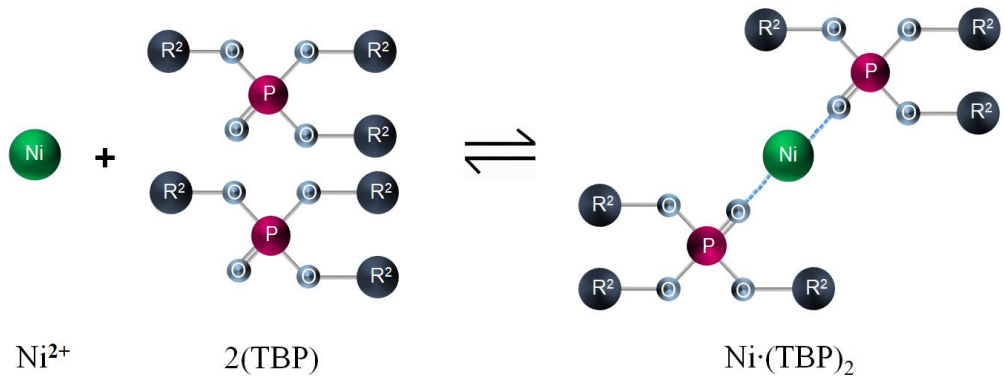

(A3.2)

where R^2 is butyl group (C_4H_9) of TBP molecule.

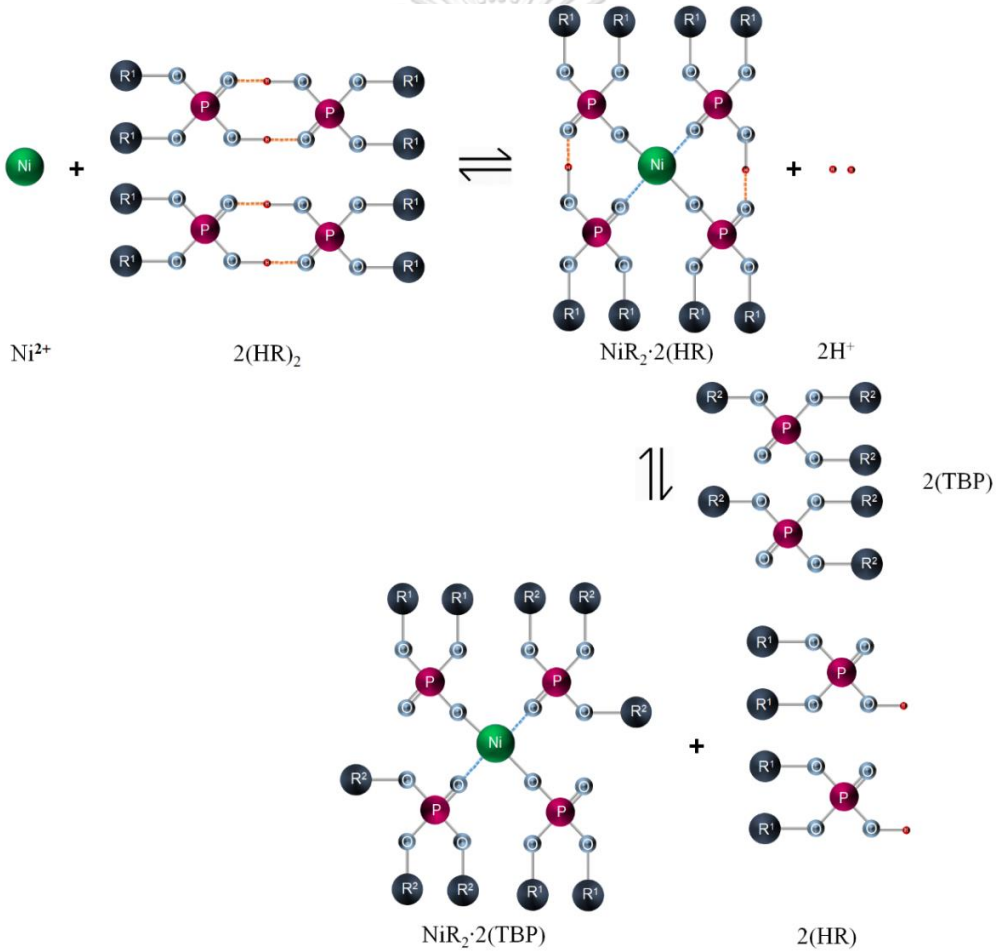

(A3.3)

The stripping reaction of the Ni-extractant complexes and HCl as the strippant can be expressed, as in Eqs. (A3.4) to (A3.6):

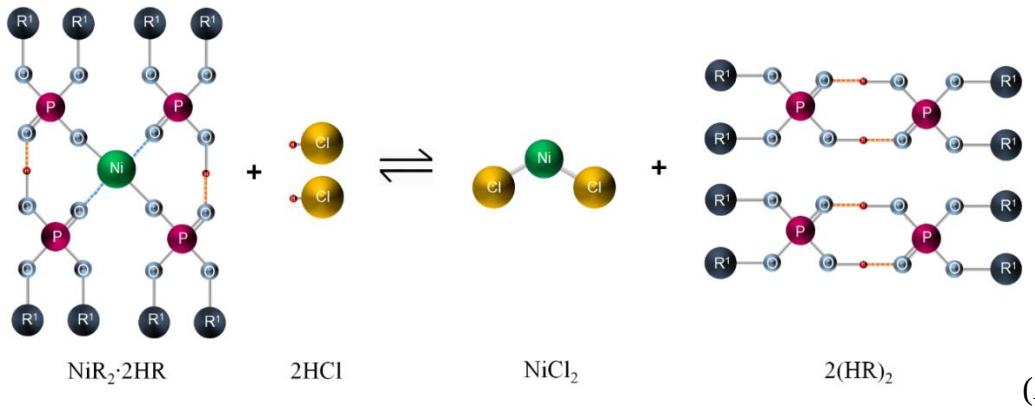

(A3.4)

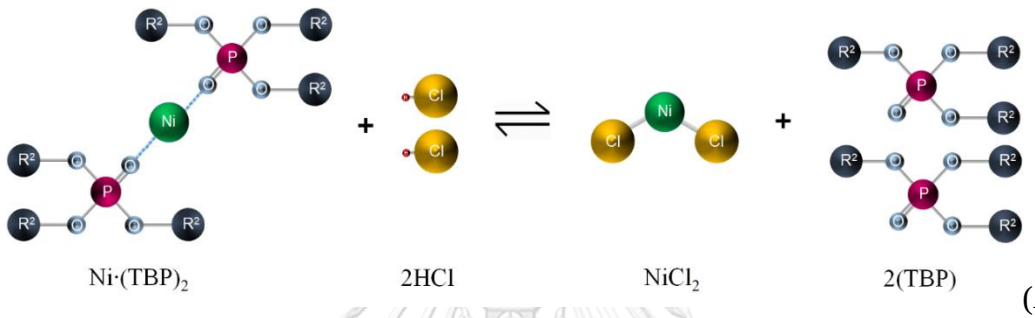

(A3.5)

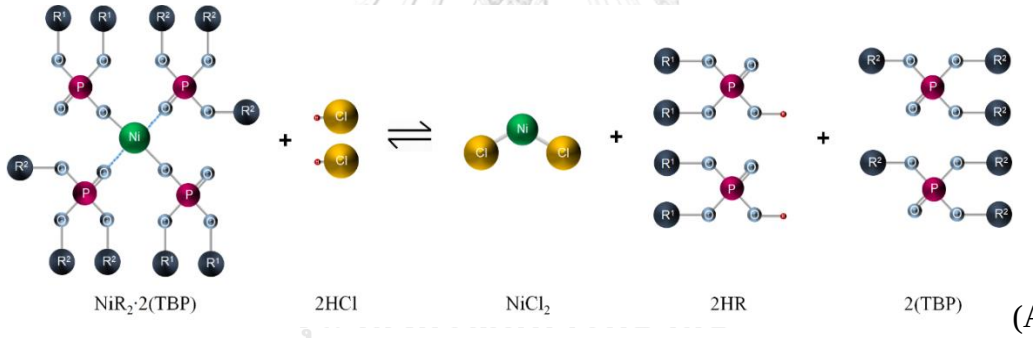

(A3.6)

CHULALONGKORN UNIVERSITY

The reaction rate of extraction of Ni^{2+} ions ($r_{\mathrm{Ni,Ex}}$) can be expressed as:

$$r_{\mathrm{Ni,Ex}}(x,t) = -k_{\mathrm{Ex}} C_{\mathrm{Ni},f}^{m}(x,t) \tag{A3.7}$$

where x is the longitudinal axis of the hollow fiber in the feed phase, k_{Ex} is the reaction rate constant of extraction, t is the elimination time, $C_{\mathrm{Ni},f}$ is the concentration of Ni^{2+} in the feed phase (mg/L) and m is the reaction order of extraction.

In the strippant phase, the strippant is kept at excess concentration. Hence, the total reaction of Ni^{2+} ions stripping in Eqs. (A3.4) to (A3.6) can be considered as forward reaction. Thus, the reaction rate of Ni^{2+} ions stripping ($r_{Ni,St}$) becomes:

$$r_{Ni,St}(x',t) = k_{St} C^{n}_{Ni,St}(x',t) \tag{S3.8}$$

where x' is the longitudinal axis of the hollow fiber in the strippant phase, k_{St} is the reaction rate constant of stripping, $C_{Ni,s}$ is the concentration of Ni^{2+} in the strippant phase (mg/L) and n is the reaction order of extraction.

3.7.2 Development of the mathematical model

A mathematical model for predicting the extraction and stripping of Ni^{2+} across HFSLM is generated from the conservation of mass at tiny segments of the hollow fibers, as shown in Fig. (A3.5). Parameters in the model include axial convection, diffusion, reactions at the liquid-membrane interfaces, and mass accumulation.

จุฬาลงกรณ์มหาวิทยาลัย
CHULALONGKORN UNIVERSITY

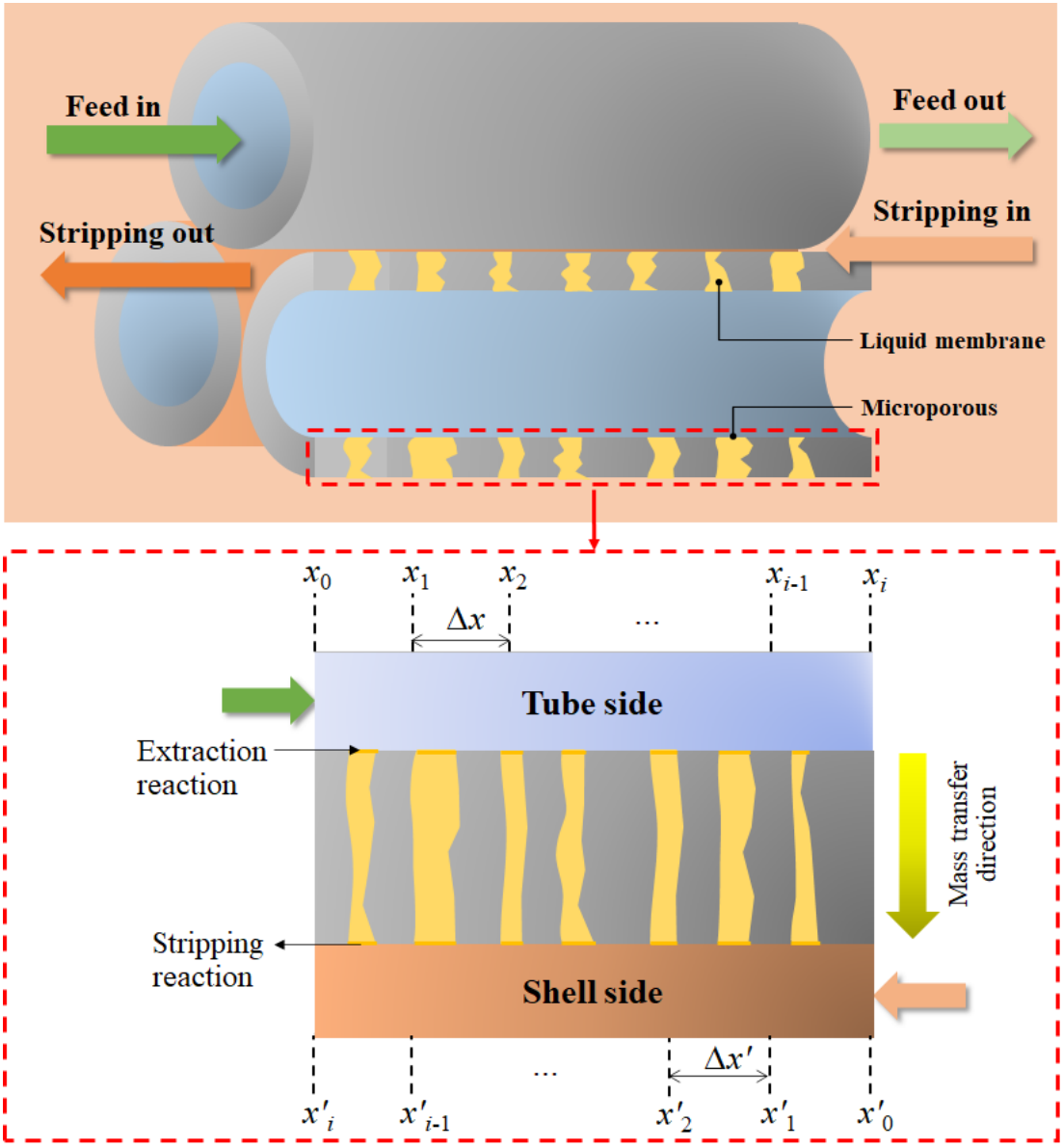

Figure A3.5 Schema of metal ions transport across tube and shell sides of the hollow fibers.

The mathematical model for extraction on the feed side is generated based on the following hypotheses:

1. Temperature, pressure and volume of the feed phase, inside the tube, are const ant.
2. The inside radius of the hollow-fiber is tiny. Thus, the concentration profile of Ni^{2+} in the radial direction is constant, meaning that the diffusion fluxes of the

ions in the feed phase occur only in the axial direction.

3. The extractant in the liquid membrane phase is kept at excess concentration an d Ni^{2+} are transferred into the strippant solution continuously. Thus, extractio n reaction can be considered as forward reaction.
4. Extraction reaction takes place at the feed-liquid membrane interface along the length of the hollow fiber.
5. Only the Ni-extractant complex, which is formed due to the extraction reaction , not Ni^{2+}, can transport into the liquid membrane phase.

In the case of a mathematical model for the stripping of Ni^{2+} into the strippant phase, a model is generated based on the hypotheses as follows:

1. Temperature, pressure and volume of the strippant phase, inside the shell, are c onstant
2. Stripping reaction occurs at the liquid membrane-strippant interface along the l ength of the hollow fiber.
3. Only Ni^{2+} according to the stripping reaction at the interface, not the Ni-extract ant complex, can be stripped into the stripping solution.
4. The strippant is kept at excess concentration. Therefore, stripping reaction can be considered as forward reaction.

In the feed phase, the conservation of mass for Ni^{2+} in each tiny segment (Δx), see Fig. (A3.5), is defined, as in Eqs. (A3.9) and (A3.10):

[Rate of mass transport into the system by convection] – [Rate of mass transport out of the system by convection] + [Rate of mass transport through the system by diffusion]

– [Rate of mass extracted by extraction reaction] = [Rate of mass accumulation within the system] (A3.9)

$$q_F C_{\mathrm{Ni},F}\left(x_{i-1},t\right)-q_F C_{\mathrm{Ni},F}\left(x_i,t\right)+\frac{A_{c,F}D_{\mathrm{Ni},F}}{\Delta x_i}\left(C_{\mathrm{Ni},F}\left(x_i,t\right)-C_{\mathrm{Ni},F}\left(x_{i-1},t\right)\right)+r_{\mathrm{Ni},Ex}\left(x_i,t\right)V_F=V_F\frac{dC_{\mathrm{Ni},F}\left(x_i,t\right)}{dt}$$

(A3.10)

where

q_F is the volumetric flow rate of the feed solution.

i is the number of divided tiny segments.

$A_{c,F}$ is the cross-sectional area of the tube $=\pi r_i^2$

V_F is the volume of a tiny segment of the hollow fiber in the tube side $=\pi r_i^2\Delta x_i$

$\Delta x_i = L/i$

r_i and L refer to the inside radius and effective length of the hollow fibers, respectively.

$D_{\mathrm{Ni},f}$ is the mass diffusivity of Ni^{2+} ions in the feed solution, which can be estimated by Eq. (A3.11):

$$D_{\mathrm{Ni}}=\frac{7.4\times10^{-8}\left(\phi M\right)^{1/2}T}{\eta V_A^{0.6}} \qquad \text{(A3.11)}$$

where ϕ is the solvent association factor and is equal to 2.6, M is the solvent molecular weight (g/mol), T is the temperature (K), η is the dynamic viscosity of the solvent (cP), and V_A is the molar volume of solute A at its boiling temperature (cm^3/mol).

By linearizing the reaction rate, $r_{\mathrm{Ni,Ex}}(x,t)$ in Eq. (A3.7), using the Taylor series, the following equations are obtained:

$$r_{\mathrm{Ni},Ex}(x_i,t) = -k_{Ex}\left[C_{\mathrm{Ni},F}(0,t)\right]^m - mk_{Ex}\left[C_{\mathrm{Ni},F}(0,t)\right]^{m-1}\left[C_{\mathrm{Ni},F}(x_i,t) - C_{\mathrm{Ni},F}(0,t)\right] \quad \text{(A3.12)}$$

$$r_{\mathrm{Ni},Ex}(x_i,t) = -k_{Ex}\left[C_{\mathrm{Ni},F}(0,t)\right]^m - mk_{Ex}\left[C_{\mathrm{Ni},F}(0,t)\right]^{m-1} C_{\mathrm{Ni},F}(x_i,t) + mk_{Ex}\left[C_{\mathrm{Ni},F}(0,t)\right]^m \quad \text{(A3.13)}$$

$$r_{\mathrm{Ni},Ex}(x_i,t) = -mk_{Ex}\left[C_{\mathrm{Ni},F}(0,t)\right]^{m-1} C_{\mathrm{Ni},F}(x_i,t) - (1-m)k_{Ex}\left[C_{\mathrm{Ni},F}(0,t)\right]^m \quad \text{(A3.14)}$$

$$r_{\mathrm{Ni},Ex}(x_i,t) = -\left(mk_{Ex}\left[C_{\mathrm{Ni},F}(0,t)\right]^{m-1} C_{\mathrm{Ni},F}(x_i,t) + (1-m)k_{Ex}\left[C_{\mathrm{Ni},F}(0,t)\right]^m\right) \quad \text{(A3.15)}$$

$$r_{\mathrm{Ni},Ex}(x_i,t) = -\left(\Omega C_{\mathrm{Ni},F}(x_i,t) + \psi\right) \quad \text{(A3.16)}$$

where $\Omega = mk_{Ex}\left[C_{\mathrm{Ni},F}(0,t)\right]^{m-1}$, $\psi = (1-m)k_{Ex}\left[C_{\mathrm{Ni},F}(0,t)\right]^m$.

and then substituting Eq. (A3.16) into Eq. (A3.10) yields:

$$\frac{V_f}{q_f}\frac{dC_{\mathrm{Ni},f}(x_i,t)}{dt} = \left(1 - \frac{A_{c,f}D_{\mathrm{Ni},f}}{\Delta x_i q_f}\right)C_{\mathrm{Ni},f}(x_{i-1},t) - \left(1 + \frac{V_f\Omega}{q_f} - \frac{A_{c,f}D_{\mathrm{Ni},f}}{\Delta x_i q_f}\right)C_{\mathrm{Ni},f}(x_i,t) - \frac{V_f\psi}{q_f} \quad \text{(A3.17)}$$

The conservation of mass of Ni^{2+} in the tiny segments 1, 2, 3, …, i in the feed side based on Eq. (A3.12) is as follows:

$$\frac{V_f}{q_f}\frac{dC_{\mathrm{Ni},f}(x_1,t)}{dt} = \left(1 - \frac{A_{c,f}D_{\mathrm{Ni},f}}{\Delta x_1 q_f}\right)C_{\mathrm{Ni},f}(x_0,t) - \left(1 + \frac{V_f\Omega}{q_f} - \frac{A_{c,f}D_{\mathrm{Ni},f}}{\Delta x_1 q_f}\right)C_{\mathrm{Ni},f}(x_1,t) - \frac{V_f\psi}{q_f} \quad \text{(A3.18)}$$

$$\frac{V_f}{q_f}\frac{dC_{\mathrm{Ni},f}(x_2,t)}{dt} = \left(1 - \frac{A_{c,f}D_{\mathrm{Ni},f}}{\Delta x_2 q_f}\right)C_{\mathrm{Ni},f}(x_1,t) - \left(1 + \frac{V_f\Omega}{q_f} - \frac{A_{c,f}D_{\mathrm{Ni},f}}{\Delta x_2 q_f}\right)C_{\mathrm{Ni},f}(x_2,t) - \frac{V_f\psi}{q_f} \quad \text{(A3.19)}$$

$$\frac{V_f}{q_f}\frac{dC_{\mathrm{Ni},f}(x_3,t)}{dt} = \left(1 - \frac{A_{c,f}D_{\mathrm{Ni},f}}{\Delta x_3 q_f}\right)C_{\mathrm{Ni},f}(x_2,t) - \left(1 + \frac{V_f\Omega}{q_f} - \frac{A_{c,f}D_{\mathrm{Ni},f}}{\Delta x_3 q_f}\right)C_{\mathrm{Ni},f}(x_3,t) - \frac{V_f\psi}{q_f} \quad \text{(A3.20)}$$

.

.

.

จุฬาลงกรณ์มหาวิทยาลัย
Chulalongkorn University

$$\frac{V_f}{q_f}\frac{dC_{\mathrm{Ni},f}(x_i,t)}{dt}=\left(1-\frac{A_{c,f}D_{\mathrm{Ni},f}}{\Delta x_i q_f}\right)C_{\mathrm{Ni},f}(x_{i-1},t)-\left(1+\frac{V_f\Omega}{q_f}-\frac{A_{c,f}D_{\mathrm{Ni},f}}{\Delta x_i q_f}\right)C_{\mathrm{Ni},f}(x_i,t)-\frac{V_f\psi}{q_f} \quad \text{(A3.21)}$$

$$\frac{dC_{\mathrm{Ni},f}(x_i,t)}{dt}=\left(1-\frac{A_{c,f}D_{\mathrm{Ni},f}}{\Delta x_i q_f}\right)C_{\mathrm{Ni},f}(x_{i-1},t)\left(\frac{q_f}{V_f}\right)-\left(1+\frac{V_f\Omega}{q_f}-\frac{A_{c,f}D_{\mathrm{Ni},f}}{\Delta x_i q_f}\right)C_{\mathrm{Ni},f}(x_i,t)\left(\frac{q_f}{V_f}\right)-\psi \quad \text{(A3.22)}$$

Solving the series of differential equations i.e. Eqs. (A3.13) to (A3.16) using the concept of Euler's method yields:

$$y_{n+1}=y_n+f(t_n,y_n)\cdot(t_{n+1}-t_n) \quad \text{(A3.18)}$$

$$\begin{aligned}C_{\mathrm{Ni},f}(x_{i+1},t_{i+1})&=C_{\mathrm{Ni},f}(x_i,t_i)\\&+\left(\left(1-\frac{A_{c,f}D_{\mathrm{Ni},f}}{\Delta x_i q_f}\right)C_{\mathrm{Ni},f}(x_{i-1},t_i)\left(\frac{q_f}{V_f}\right)-\left(1+\frac{V_f\Omega}{q_f}-\frac{A_{c,f}D_{\mathrm{Ni},f}}{\Delta x_i q_f}\right)C_{\mathrm{Ni},f}(x_i,t_i)\left(\frac{q_f}{V_f}\right)-\psi\right)\cdot(t_{i+1}-t_i)\end{aligned}$$

(A3.19)

$$\begin{aligned}C_{\mathrm{Ni},f}(x_{i+1},t_{i+1})&=C_{\mathrm{Ni},f}(x_i,t_i)+\frac{C_{\mathrm{Ni},f}(x_{i-1},t_i)q_f(t_{i+1}-t_i)}{V_f}-\frac{A_{c,f}D_{\mathrm{Ni},f}C_{\mathrm{Ni},f}(x_{i-1},t_i)(t_{i+1}-t_i)}{\Delta x_i V_f}\\&-\frac{C_{\mathrm{Ni},f}(x_i,t_i)q_f(t_{i+1}-t_i)}{V_f}-C_{\mathrm{Ni},f}(x_i,t_i)\Omega(t_{i+1}-t_i)\\&+\frac{A_{c,f}D_{\mathrm{Ni},f}C_{\mathrm{Ni},f}(x_i,t_i)(t_{i+1}-t_i)}{\Delta x_i V_f}-\psi(t_{i+1}-t_i)\end{aligned} \quad \text{(A3.20)}$$

$$\begin{aligned}C_{\mathrm{Ni},f}(x_{i+1},t_{i+1})&=C_{\mathrm{Ni},f}(x_i,t_i)\left(1-\frac{q_f(t_{i+1}-t_i)}{V_f}-\Omega(t_{i+1}-t_i)+\frac{A_{c,f}D_{\mathrm{Ni},f}(t_{i+1}-t_i)}{\Delta x_i V_f}\right)\\&+C_{\mathrm{Ni},f}(x_{i-1},t_i)\left(\frac{q_f(t_{i+1}-t_i)}{V_f}-\frac{A_{c,f}D_{\mathrm{Ni},f}(t_{i+1}-t_i)}{\Delta x_i V_f}\right)-\psi(t_{i+1}-t_i)\end{aligned} \quad \text{(A3.21)}$$

$$\begin{aligned}C_{\mathrm{Ni},F}(x_{i+1},t_{i+1})&=C_{\mathrm{Ni},F}(x_i,t_i)\left(1-\frac{q_F(t_{i+1}-t_i)}{V_F}-\Omega(t_{i+1}-t_i)+\alpha(t_{i+1}-t_i)\right)\\&+C_{\mathrm{Ni},F}(x_{i-1},t_i)\left(\frac{q_F(t_{i+1}-t_i)}{V_F}-\alpha(t_{i+1}-t_i)\right)-\psi(t_{i+1}-t_i)\end{aligned} \quad \text{(A3.22)}$$

จุฬาลงกรณ์มหาวิทยาลัย
CHULALONGKORN UNIVERSITY

where $\alpha = \dfrac{A_{c,F} D_{\mathrm{Ni},F}}{\Delta x_i V_F}$

In the strippant phase, based on Eq. (A3.9), the conservation of mass of Ni^{2+} in the tiny segment ($\Delta x'$), see Fig. (A3.5), is written as:

$$q_{St} C_{\mathrm{Ni},St}\left(x'_{i-1},t\right) - q_{St} C_{\mathrm{Ni},St}\left(x'_i,t\right) + \frac{A_{c,St} D_{\mathrm{Ni},St}}{\Delta x'_i}\left(C_{\mathrm{Ni},St}\left(x'_i,t\right) - C_{\mathrm{Ni},St}\left(x'_{i-1},t\right)\right) + r_{\mathrm{Ni},St}\left(x'_i,t\right) V_{St} = V_{St} \frac{dC_{\mathrm{Ni},St}\left(x'_i,t\right)}{dt}$$

(A3.23)

where

q_{St} is the volumetric flow rate of the stripping solution.

$A_{c,St}$ is the cross-sectional area of the shell side of the hollow fiber = $\dfrac{\sqrt{3}}{4} d_o^2 - \dfrac{\pi r_o^2}{2}$

V_{St} is the volume of a tiny segment of the shell side of the hollow fiber = $A_{c,St} \Delta x'_i$

r_o is the outside radius.

d_o is the outside diameter of the hollow fibers.

$D_{\mathrm{Ni},St}$ is the mass diffusivity of Ni^{2+} ions in the stripping solution, which is calculated using Eq. (A3.11).

The reaction rate of stripping of Ni^{2+}, $r_{\mathrm{Ni},St}(x',t)$ in Eq. (A3.8), can be linearized using the Taylor series. The linearized equations are shown below:

$$r_{\mathrm{Ni},St}(x'_i,t) = k_{St}\left[C_{\mathrm{Ni},St}(0,t)\right]^n + nk_{St}\left[C_{\mathrm{Ni},St}(0,t)\right]^{n-1}\left[C_{\mathrm{Ni},St}(x'_i,t) - C_{\mathrm{Ni},St}(0,t)\right] \quad \text{(A3.24)}$$

$$r_{\mathrm{Ni},St}(x'_i,t) = k_{St}\left[C_{\mathrm{Ni},St}(0,t)\right]^n + nk_{St}\left[C_{\mathrm{Ni},St}(0,0)\right]^{n-1} C_{\mathrm{Ni},St}(x'_i,t) - nk_{St}\left[C_{\mathrm{Ni},St}(0,t)\right]^n \quad \text{(A3.25)}$$

$$r_{\mathrm{Ni},St}(x'_i,t) = nk_{St}\left[C_{\mathrm{Ni},St}(0,t)\right]^{n-1} C_{\mathrm{Ni},St}(x'_i,t) + (1-n)k_{St}\left[C_{\mathrm{Ni},St}(0,t)\right]^n \quad \text{(A3.26)}$$

CHULALONGKORN UNIVERSITY

$$r_{\mathrm{Ni},St}(x_i',t)=\sigma C_{\mathrm{Ni},St}\left(x_i',t\right)+\delta \tag{A3.27}$$

where $\sigma = nk_{St}\left[C_{\mathrm{Ni},St}\left(0,t\right)\right]^{n-1}$, $\delta=\left(1-n\right)k_{St}\left[C_{\mathrm{Ni},St}\left(0,t\right)\right]^{n}$.

Merging Eqs. (A3.23) and (A3.27) and rearranging the equation achieves:

$$V_{St}\frac{dC_{\mathrm{Ni},St}\left(x_i',t\right)}{dt}=q_{St}C_{\mathrm{Ni},St}\left(x_{i-1}',t\right)-q_{St}C_{\mathrm{Ni},St}\left(x_i',t\right)+\frac{A_{c,St}D_{\mathrm{Ni},St}}{\Delta x_i'}\left(C_{\mathrm{Ni},St}\left(x_i',t\right)-C_{\mathrm{Ni},St}\left(x_{i-1}',t\right)\right)+\sigma C_{\mathrm{Ni},St}\left(x_i',t\right)V_{St}+\delta V_{St}$$

(A3.28)

$$\frac{dC_{\mathrm{Ni},St}\left(x_i',t\right)}{dt}=\frac{q_{St}}{V_{St}}C_{\mathrm{Ni},St}\left(x_{i-1}',t\right)-\frac{q_{St}}{V_{St}}C_{\mathrm{Ni},St}\left(x_i',t\right)+\frac{A_{c,St}D_{\mathrm{Ni},St}}{V_{St}\Delta x_i'}\left(C_{\mathrm{Ni},St}\left(x_i',t\right)-C_{\mathrm{Ni},St}\left(x_{i-1}',t\right)\right)+\sigma C_{\mathrm{Ni},St}\left(x_i',t\right)+\delta$$

(A3.29)

$$\frac{dC_{\mathrm{Ni},St}\left(x_i',t\right)}{dt}=\left(1-\frac{A_{c,St}D_{\mathrm{Ni},St}}{\Delta x_i' q_{St}}\right)C_{\mathrm{Ni},St}\left(x_{i-1}',t\right)\left(\frac{q_{St}}{V_{St}}\right)-\left(1-\frac{V_{St}\sigma}{q_{St}}-\frac{A_{c,St}D_{\mathrm{Ni},St}}{\Delta x_i' q_{St}}\right)C_{\mathrm{Ni},St}\left(x_i',t\right)\left(\frac{q_{St}}{V_{St}}\right)+\delta$$

(A3.30)

The conservation of mass of Ni^{2+} in the tiny segments 1, 2, 3, …, *i* based on Eq. (A3.30) is as follows:

$$\frac{dC_{\mathrm{Ni},St}\left(x_1',t\right)}{dt}=\left(1-\frac{A_{c,St}D_{\mathrm{Ni},St}}{\Delta x_1' q_{St}}\right)C_{\mathrm{Ni},St}\left(x_0',t\right)\left(\frac{q_{St}}{V_{St}}\right)-\left(1-\frac{V_{St}\sigma}{q_{St}}-\frac{A_{c,St}D_{\mathrm{Ni},St}}{\Delta x_1' q_{St}}\right)C_{\mathrm{Ni},St}\left(x_1',t\right)\left(\frac{q_{St}}{V_{St}}\right)+\delta$$

(A3.31)

$$\frac{dC_{\mathrm{Ni},St}\left(x_2',t\right)}{dt}=\left(1-\frac{A_{c,St}D_{\mathrm{Ni},St}}{\Delta x_2' q_{St}}\right)C_{\mathrm{Ni},St}\left(x_1',t\right)\left(\frac{q_{St}}{V_{St}}\right)-\left(1-\frac{V_{St}\sigma}{q_{St}}-\frac{A_{c,St}D_{\mathrm{Ni},St}}{\Delta x_2' q_{St}}\right)C_{\mathrm{Ni},St}\left(x_2',t\right)\left(\frac{q_{St}}{V_{St}}\right)+\delta$$

(A3.32)

$$\frac{dC_{\mathrm{Ni},St}\left(x_3',t\right)}{dt}=\left(1-\frac{A_{c,St}D_{\mathrm{Ni},St}}{\Delta x_3' q_{St}}\right)C_{\mathrm{Ni},St}\left(x_2',t\right)\left(\frac{q_{St}}{V_{St}}\right)-\left(1-\frac{V_{St}\sigma}{q_{St}}-\frac{A_{c,St}D_{\mathrm{Ni},St}}{\Delta x_3' q_{St}}\right)C_{\mathrm{Ni},St}\left(x_3',t\right)\left(\frac{q_{St}}{V_{St}}\right)+\delta$$

(A3.33)

.

จุฬาลงกรณ์มหาวิทยาลัย
CHULALONGKORN UNIVERSITY

.

.

$$\frac{dC_{\mathrm{Ni},St}\left(x_i',t\right)}{dt}=\left(1-\frac{A_{c,St}D_{\mathrm{Ni},St}}{\Delta x_i' q_{St}}\right)C_{\mathrm{Ni},St}\left(x_{i-1}',t\right)\left(\frac{q_{St}}{V_{St}}\right)-\left(1-\frac{V_{St}\sigma}{q_{St}}-\frac{A_{c,St}D_{\mathrm{Ni},St}}{\Delta x_i' q_{St}}\right)C_{\mathrm{Ni},St}\left(x_i',t\right)\left(\frac{q_{St}}{V_{St}}\right)+\delta$$

(A3.34)

Solving the series of differential equation i.e. Eqs. (A3.31) to (A3.34), using the concept of Euler's method, yields Eqs. (A3.35) to (A3.38) which are used to determine the concentration of Ni^{2+} in the outlet stripping solution, $C_{\mathrm{Ni},St}(x',t)$.

$$\begin{aligned}C_{\mathrm{Ni},St}(x_{i+1}',t_{i+1})&=C_{\mathrm{Ni},St}(x_i',t_i)\\&+\left(\left(1-\frac{A_{c,f}D_{\mathrm{Ni},St}}{\Delta x_i' q_{St}}\right)C_{\mathrm{Ni},St}\left(x_{i-1}',t_i\right)\left(\frac{q_{St}}{V_{St}}\right)-\left(1-\frac{V_{St}\sigma}{q_{St}}-\frac{A_{c,St}D_{\mathrm{Ni},St}}{\Delta x_i' q_{St}}\right)C_{\mathrm{Ni},St}\left(x_i',t_i\right)\left(\frac{q_{St}}{V_{St}}\right)+\delta\right)\cdot\left(t_{i+1}-t_i\right)\end{aligned}$$

(A3.35)

$$\begin{aligned}C_{\mathrm{Ni},St}(x_{i+1}',t_{i+1})&=C_{\mathrm{Ni},St}(x_i',t_i)+\frac{C_{\mathrm{Ni},St}\left(x_{i-1}',t_i\right)q_{St}\left(t_{i+1}-t_i\right)}{V_{St}}-\frac{A_{c,St}D_{\mathrm{Ni},St}C_{\mathrm{Ni},St}\left(x_{i-1}',t_i\right)\left(t_{i+1}-t_i\right)}{\Delta x_i' V_{St}}\\&-\frac{C_{\mathrm{Ni},St}\left(x_i',t_i\right)q_{St}\left(t_{i+1}-t_i\right)}{V_{St}}+C_{\mathrm{Ni},St}\left(x_i',t_i\right)\sigma\left(t_{i+1}-t_i\right)\\&+\frac{A_{c,St}D_{\mathrm{Ni},St}C_{\mathrm{Ni},St}\left(x_i',t_i\right)\left(t_{i+1}-t_i\right)}{\Delta x_i' V_{St}}+\delta\left(t_{i+1}-t_i\right)\end{aligned}$$

(A3.36)

$$\begin{aligned}C_{\mathrm{Ni},St}(x_{i+1}',t_{i+1})&=C_{\mathrm{Ni},St}(x_i',t_i)\left(1-\frac{q_{St}\left(t_{i+1}-t_i\right)}{V_{St}}+\sigma\left(t_{i+1}-t_i\right)+\frac{A_{c,St}D_{\mathrm{Ni},St}\left(t_{i+1}-t_i\right)}{\Delta x_i' V_{St}}\right)\\&+C_{\mathrm{Ni},St}\left(x_{i-1}',t_i\right)\left(\frac{q_{St}\left(t_{i+1}-t_i\right)}{V_{St}}-\frac{A_{c,St}D_{\mathrm{Ni},St}\left(t_{i+1}-t_i\right)}{\Delta x_i' V_{St}}\right)+\delta\left(t_{i+1}-t_i\right)\end{aligned}$$

(A3.37)

$$C_{\mathrm{Ni},St}(x'_{i+1},t_{i+1}) = C_{\mathrm{Ni},St}(x'_i,t_i)\left(1-\frac{q_{St}\left(t_{i+1}-t_i\right)}{V_{St}}+\sigma\left(t_{i+1}-t_i\right)+\beta\left(t_{i+1}-t_i\right)\right)$$
$$+C_{\mathrm{Ni},St}\left(x'_{i-1},t_i\right)\left(\frac{q_{St}\left(t_{i+1}-t_i\right)}{V_{St}}-\beta\left(t_{i+1}-t_i\right)\right)+\delta\left(t_{i+1}-t_i\right)$$

(A3.38)

where $\beta = \dfrac{A_{c,St}D_{\mathrm{Ni},St}}{\Delta x'_i V_{St}}$

The validity of the mathematical model is verified by the experimental results, and the percent average relative deviation (%ARD) is as shown in Eq. (A3.39):

$$\%ARD = \frac{1}{N}\sum_{i=1}^{N}\left|\frac{C_{Exptl.}-C_{Model}}{C_{Exptl.}}\right|\times 100 \qquad \text{(A3.39)}$$

where N is the number of experimental data, $C_{Exptl.}$ and C_{Model} represent the concentration of Ni^{2+} ions obtained from the experiment and the mathematical model, respectively.

จุฬาลงกรณ์มหาวิทยาลัย
CHULALONGKORN UNIVERSITY

3.8 Acknowledgements

This work was supported by the Research and Researcher for Industry (RRI) of Thailand Research Fund (TRF) [grant numbers PHD60I005]; Mektec Manufacturing corporation (Thailand) ltd.; the Mass Separation Laboratory, Department of Chemical Engineering, Chulalongkorn University as well as the Research Cess Fund (Malaysia–Thailand Joint Authority).

3.9 Nomenclatures

$C_{f,0}$	Initial concentration of ions in the aqueous feed phase at time = 0
$C_{f,t}$	Concentration of ions in the aqueous feed phase after separation at time = t
$C_{s,t}$	Concentration of ions in the aqueous stripping phase after separation at time
$= t\, C_{m,t}$	Concentration of ions in the liquid membrane phase at time = t
D	Distribution ratio
D_{mix}	Distribution ratio of ions using mixed extractants: D2EHPA-TBP
D_{D2EHPA}	Distribution ratio of ions using a single extractant: D2EHPA
D_{TBP}	Distribution ratio of ions using a single extractant: TBP
Q_f	Volumetric flow rate of the feed solution
Q_s	Volumetric flow rate of the stripping solution
$S_{\mathrm{Ni(II)/Au(I)}}$	Selectivity between Ni^{2+} and $[Au(CN)_2]^-$
SC	Synergistic coefficient
$V_{f,0}$	Total volume of the aqueous feed phase in the reservoir at initial (1 L)
$V_{f,t}$	Total volume of the aqueous feed phase in the reservoir at time = t
$V_{s,t}$	Total volume of the stripping phase at time = t
V_m	Total volume of the liquid membrane phase (8.4×10^{-2} L)

3.10 References

[1] T. Osaka, T. Misato, J. Sato, H. Akiya, T. Homma, M. Kato, Y. Okinaka, O. Yoshioka, Evaluation of Substrate (Ni)-Catalyzed Electroless Gold Plating Process, Journal of The Electrochemical Society, 147 (2000) 1059.

[2] A. Accogli, E. Gibertini, G. Panzeri, A. Lucotti, L. Magagnin, Understanding the Failure Mode of Electroless Nickel Immersion Gold Process: In Situ-Raman Spectroscopy and Electrochemical Characterization, Journal of the Electrochemical Society, 167 (2020).

[3] K. Chakrabarty, P. Saha, A.K. Ghoshal, Separation of mercury from its aqueous solution through supported liquid membrane using environmentally benign diluent, Journal of Membrane Science, 350 (2010) 395-401.

[4] P. Kazemi, M. Peydayesh, A. Bandegi, T. Mohammadi, O. Bakhtiari, Pertraction of methylene blue using a mixture of D2EHPA/M2EHPA and sesame oil as a liquid membrane, Chemical Papers, 67 (2013) 722-729.

[5] P. Venkateswaran, A.N. Gopalakrishnan, K. Palanivelu, Di(2-ethylhexyl)phosphoric acid-coconut oil supported liquid membrane for the separation of copper ions from copper plating wastewater, Journal of Environmental Sciences, 19 (2007) 1446-1453.

[6] W. Srirachat, P. Usapein, S. Kheawhom, U. Pancharoen, Selective separation of trace nickel(II) and gold(I) ions via hollow fiber supported liquid membrane enhanced by synergistic extractants D2EHPA/TBP, Arabian Journal of Chemistry, 14 (2021) 103427.

[7] M. Špadina, K. Bohinc, T. Zemb, J.-F. Dufrêche, Synergistic Solvent Extraction Is Driven by Entropy, ACS Nano, 13 (2019) 13745-13758.

[8] K.P. P. Venkateswaran, Vegetable oil as greener liquid membrane, in: New Research on Hazardous Materials, Nova Science Publishers, Inc., The United States of America, 2007, pp. 347–369.

[9] V. Kumar, R.K. Singh, P. Chowdhury, Efficient extraction and recovery of Lignosulfonate using sunflower oil as green solvent in liquid membrane

จุฬาลงกรณ์มหาวิทยาลัย
Chulalongkorn University

transport: Equilibrium and kinetic study, Journal of Industrial and Engineering Chemistry, 67 (2018) 109-122.

[10] F. Gunstone, Vegetable Oils in Food Technology: Composition, Properties and Uses, Second Edition, in, 2011, pp. 1-24.

จุฬาลงกรณ์มหาวิทยาลัย
CHULALONGKORN UNIVERSITY

CHAPTER IV

An investigation of saturated vapor pressure regarding low-volatility organophosphorus extractants Di-(2-Ethylhexyl) Phosphoric Acid and Tributyl Phosphate: Correlation and thermodynamics study

Wanchalerm Srirachat[a], Ura Pancharoen[a,*], Soorathep Kheawhom[a,*]

[a] *Department of Chemical Engineering, Faculty of Engineering, Chulalongkorn University, Patumwan, Bangkok 10330, Thailand*

* Corresponding author

จุฬาลงกรณ์มหาวิทยาลัย
CHULALONGKORN UNIVERSITY

This article has been published in Journal: Vacuum.

Volume: 156. Year: 2018. https://doi.org/10.1016/j.vacuum.2018.07.036.

4.1 Graphical abstract

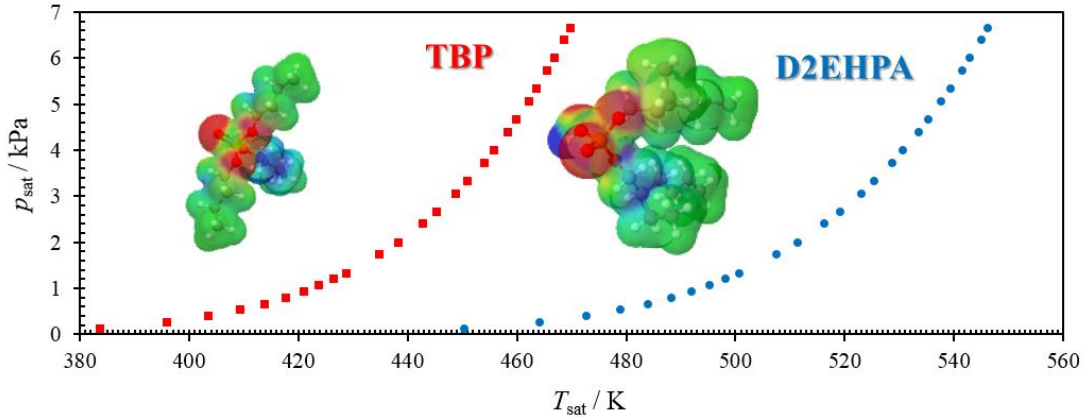

4.2 Abstract

New saturated vapor pressure data of low volatility organophosphorus extractants, namely di-(2-ethylhexyl) phosphoric acid (D2EHPA) and tributyl phosphate (TBP), were investigated in the temperature range T = (383.8-546.2) K using a vacuum distillation method. The experimental saturated vapor pressure data for both extractants in the range of p_{sat} = (0.13-6.67) kPa were compared with the literature data. The data was found to be a good fit with Antoine, August, Riedel vapor pressure and Wagner equation with a relative average deviation (*RAD*) less than 1 %. Regression constants prove to be very useful in estimating saturated vapor pressure at operating temperature. Intermolecular hydrogen bonding affected D2EHPA having lower saturated vapor pressure in comparison with TBP. Additionally, the thermodynamic properties of both molar enthalpy and molar entropy of vaporization of these two organophosphorus extractants were obtained from the experimental data using the Clausius-Clapeyron equation. As temperature increased, molar enthalpy and molar entropy of vaporization decreased showing a positive deviation from Trouton's rule. Using the relations of molar enthalpy and temperature based on the first law of thermodynamics, saturated liquid heat capacity was obtained. All data obtained can be usefully employed for the

design of a distillation column or evaporator for recycling of both extractants from organic wastewater.

Keywords: Saturated vapor pressure; Enthalpy of vaporization; Entropy of vaporization; Saturated liquid heat capacity; Acentric factor

4.3 Introduction

Phosphate esters comprise a large group of commercially important compounds as diverse as pesticides, nerve gases, plasticizers, solvents, and hydraulic fluids. Di-(2-ethyl hexyl) phosphoric acid (D2EHPA, Fig. 4.1) and tributyl phosphate (TBP, Fig. 4.2) are important organophosphorus extractants for many industrial separation processes such as absorption process used for removal of components from process or waste gases [1] and liquid-liquid extraction for fuel reprocessing [2]. These extractants are also extensively used in the recovery of zinc, nickel, beryllium, cobalt and rare-earths [3, 4]. When reactive liquid-liquid separations are applied, hazardous organic wastes are generated. These wastes are toxic and mainly composed of organophosphorus extractants dissolved in organic diluents. Inhalation of their vapors and/or aerosols, even at low levels, causes headaches, nausea, general discomfort and sometimes mental imbalance in humans. The concentration level of these species in the discharge waste is strictly regulated by the environmental aspect. One of the methodological treatments is the purification of mixed organic waste into each pure species to enable recycling and reuse in the process. Current efforts to address challenges in the green industry include the reuse or recycling of hazardous waste. In order to assess the most suitable method, detailed fundamental studies are necessary.

จุฬาลงกรณ์มหาวิทยาลัย
CHULALONGKORN UNIVERSITY

In the design of multicomponent separation processes, thermodynamic and transport properties of fluids play a vital role [5]. Of equal importance, the thermophysical properties of D2EHPA and TBP extractants have been studied as summarized in Table S4.1 of the Section 4.8: Supplementary information such as density, viscosity and refractive index. However, saturated vapor pressure (p_{sat}) and boiling temperature (T_b) data of these compounds have not been investigated sufficiently or collected by the well-known databank of NIST. Vapor pressure of liquids is important properties of compound with regard to their industrial application in separation/distillation processes or as solvents. Such data can be useful in the simulation and optimization of the recycling process of hazardous extractants from organic wastewater.

The p_{sat} of fluids have been extensively investigated [6-10]. The data of p_{sat} and T_b have directly influenced distillation as well as evaporation processes [11-13]. According to literature reviews, the normal boiling temperature (T_b) of both D2EHPA [14, 15] and TBP [16-20] under atmospheric pressure of 101.3 kPa are above 563.15 K (290 ^{o}C). For high boiling compounds, discrimination between evaporation and thermal decomposition is difficult. The determination of these properties is troublesome, and one has to take into account that the evaporation may be superimposed by thermal degradation. The direct measurement of normal boiling point for D2EHPA and TBP is an extremely laborious, time-consuming and expensive process. High molecular weight phosphates decompose prior to reaching their normal boiling points and necessitate measurements under reduced pressure. To prevent decomposition of the compounds, it

must be carefully distilled or evaporated under reduced pressure. Hence, p_{sat} and T_b data under reduced pressure conditions are vital for industrial application.

As regards D2EHPA, an early p_{sat} was reported by Härtel [1] whereby p_{sat} was equal to 1 kPa at 482 K (209 ^{o}C). However, the density of D2EHPA at 293.15 K proved equal to 1,022 kg/m^3 which deviates from recently reported density values of 970 kg/m^3 [21]. This definitely indicates an impurity of the experimental D2EHPA. Thus, it is strongly recommended that the reported p_{sat} be revised. Next, Kumar et al [14] used a group contribution method to estimate the normal boiling point (T_b) of D2EHPA. The estimated T_b equaled 625.15 K (352.00 ^{o}C) at 101.3 kPa. However, this estimated T_b was not compared with any experimental values or validated with thermodynamic equations of p_{sat}. In Kumar's work, the experimentally observed flash point was quite different from the predicted value indicating a degree of reliability of the data. Furthermore, the p_{sat} and T_{sat} properties under reduced pressure were not reported. The p_{sat} of D2EHPA has been reported in the CRC handbook by Lide [22] which stated that p_{sat} was equal to 0.0020 kPa at 428 K (155 ^{o}C). However, it is noted that the p_{sat} was too low and not practical for reduced pressure on an industrial scale. Recently, Wongsawa et al [15] had reported the T_b of D2EHPA as 533 K (260 ^{o}C) using atmospheric distillation method. Since T_b was found to be high, the atmospheric distillation may result in the decomposition of D2EHPA molecule. Thus, the measured T_b will be lower.

In the case of the TBP extractant, the p_{sat} which was reported by Härtel [1] as equal to 3 kPa at 453 K (180 ^{o}C) had a density of 977 kg/m^3 at 293.15 K; the density

value being similar with recently reported values of 976.72 kg/m^3 [23-26]. Thus, the purity of TBP of that work was found to be acceptable. However, the only one point of p_{sat} and T_{sat} as recorded by Härtel is limited. The work of Skene and Krzymien [27] as well as other previous works [28-32] determined the p_{sat} of TBP from gas chromatographic techniques and from measurement of the equilibrium vapor concentration. Reported values were in a range of p_{sat} = (0.000004 – 0.0319) kPa and T_{sat} = (273 – 353) K (0 – 80 ^{o}C). However, these p_{sat} were found to be too low and not practical for reduced pressure on an industrial scale. Although, Panneerselvam et al [16], Huang et al [17] and Edmundson [18] reported T_b of TBP, their work is also limited at a pressure of 101.3 kPa. Kumar et al [20] estimated p_{sat} and T_{sat} of TBP using a group contribution method. Though the estimated values were in a range of p_{sat} = (0.000004 – 101.3) kPa and T_{sat} = (273.15 – 562.15) K (0 – 289 ^{o}C), these values did not compare with the experimental values. Thus, the experimental values of p_{sat} and T_{sat} in those ranges should be interesting to investigate.

In view of these shortcomings, it is most essential for this work to investigate the new experimental p_{sat} and T_{sat} values under low reduced pressure conditions as well as to estimate the reliable T_b values of D2EHPA and TBP extractants. Normal boiling point is an indispensable parameter for synthesis. It is an important input for computing critical temperature, flash point, enthalpy of vaporization, etc. Good quality thermodynamic data for the compound such as vapor pressure, vaporization enthalpy and critical parameters are the basis for the development of their equations of state. Reliable thermodynamic properties for the single component D2EHPA and TBP

extractants are further used for evaluation and validation of the reuse and recycling mechanisms and finally, for the application of this knowledge to multicomponent mixtures related to hazardous organic waste.

This work extends our previous studies [15, 33-35] on the thermodynamic investigation of organophosphorus extractants. We focus on measuring the new experimental p_{sat} and T_{b} (or saturated temperature: T_{sat}) data of the pure organophosphorus extractants, namely D2EHPA and TBP by vacuum distillation apparatus. The sample is distilled at an accurately controlled pressure between 0.13 and 6.7 kPa under conditions that are designed to provide approximately one theoretical plate fractionation. Data are obtained from which the initial boiling point (IBP), the final boiling point (FBP), and distillation curve relating volume percent distilled and atmospheric equivalent boiling point temperature can be prepared [36]. The obtained new experimental p_{sat} and T_{sat} data are correlated with Antoine, August, Riedel vapor pressure and Wagner equation to obtain practical equations that can be used to predict values for as yet unmeasured p_{sat} and T_{sat}. Normal boiling points of these organophosphorus extractants were also evaluated and compared with available literature values. Further, the thermodynamic properties of the acentric factor (ω), molar enthalpy of vaporization ($\Delta_{\mathrm{vap}}H$), molar entropy of vaporization ($\Delta_{\mathrm{vap}}S$) as well as saturated liquid heat capacity (C_{σ}^{l}) were calculated to fulfill the necessary design parameters. The influences of alkyl chain length and polarity of the molecule are discussed.

จุฬาลงกรณ์มหาวิทยาลัย
Chulalongkorn University

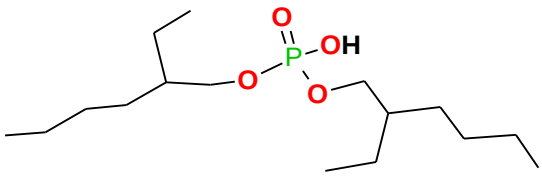

Di-(**2**-**E**thyl**h**exyl) **P**hosphoric **A**cid (D2EHPA)

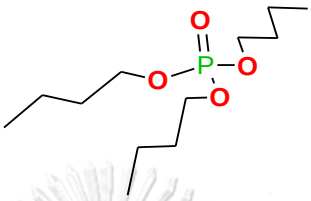

Tri**b**utyl **P**hosphate (TBP)

Figure 4.1 Structures of the organophosphorus extractants of this study.

4.4 Experimental

4.4.1 Chemicals

The name, source and purity of chemicals used in this work are shown in Table 4.1. The organophosphorus extractants D2EHPA and TBP were purchased from Merck Co. with a minimum assured purity of 97.0 % and 99.0 %, respectively. D2EHPA was further purified by extracting $Cu(OH)_2$ into a solution of D2EHPA and precipitating the resulting salt with acetone. Then, diluted HCl converts the $Cu(D2EHPA)_2$ salt back to D2EHPA and aqueous Cu(II) [37]. The chemicals used in the test method validation, namely *n*-tetradecane, *n*-hexadecane and toluene, were also obtained from Merck Co. To protect the contamination of water, both extractants were kept in a round-bottom flask containing dried molecular sieves and tightly sealed under inert atmosphere of argon gas. Before being used, the water content of all chemicals was examined by coulometric Karl Fischer titration method (Mettler Toledo, C30S). The results showed that the water contents were lower than 100 mg/kg (0.01 % wt.) which were acceptable.

Table 4.1 Source and purity of the chemicals used in this work.

Chemical name	Chemical formula	CAS number	Source	Mass fraction purity[a]	Mass fraction purity[b]	Purification method	Analysis method	Water content / mass fraction[c]
Di-(2-ethyl hexyl) phosphoric acid (D2EHPA)	$C_{16}H_{35}O_4P$	298-07-7	Merck	> 0.97	0.995±0.002	Partridge and Jensen [37]	GC	0.000060
Tributyl phosphate (TBP)	$C_{12}H_{27}O_4P$	126-73-8	Merck	> 0.99	0.996±0.001	none	GC	0.000040
n-Tetradecane	$C_{13}H_{28}$	629-59-4	Merck	> 0.99	0.996±0.001	Distillation	GC	0.000005
n-Hexadecane	$C_{16}H_{34}$	544-76-3	Merck	> 0.990	0.995±0.001	Distillation	GC	0.000003
Toluene	C_7H_8	108-88-3	Merck	> 0.999	0.999±0.001	Distillation	GC	0.000008

[a] Mass-fraction purity data were in certificate of analysis (COA) from manufacturer.

[b] Mass-fraction purity data were measured in this work by gas chromatography (GC) method.

[c] Water content data were measured in this work by coulometric Karl Fischer method.

4.4.2 Saturated vapor pressure determination

The p_{sat} and T_{sat} of pure D2EHPA and TBP were determined on the basis of boiling temperature and boiling pressure measurements. At boiling point, the vapor pressure of substance was equal to the pressure of the operating system; then the substance boiled. The p_{sat} and T_{sat} of pure liquid were measured by the vacuum distillation instrument (i-Fischer Engineering GmbH, AUTODEST® 851 AC) as illustrated in Fig. 4.2. The calibration data of experimental instruments are shown in Table S4.2 and S4.3 of the Section 4.8: Supplementary information. To confirm the method of measurement, the deviation between the measured values of reference standard, namely *n*-tetradecane and *n*-hexadecane, and literature values are summarized in Table 4.2. In Fig. 4.2, the digital temperature indicator (No. 1) was calibrated using a digital thermometer with sensor (Fluke, Model 1521, Serial No. A66705) with the uncertainty of 0.060 ^{o}C as in Table S4.2 of the Section 4.8: Supplementary information. Meanwhile, the pressure sensor (No. 2) was calibrated using the standard reagent toluene and *n*-hexadecane as shown in Table S4.3 of the Section 4.8: Supplementary information.

In brief, 200 mL of pure liquid was placed into a 500 mL round-bottom distillation flask which was connected with the rest of the apparatus. After that, the vacuum pump was started in order to evacuate the internal system until the pressure reached the level prescribed for distillation at p = (0.13- 6.7) kPa. Then, the heater was turned on and heat was applied as rapidly as possible to the flask. The heating rate for increasing temperature of the liquid sample was 5 ^{o}C/min. When vapor or refluxing liquid appeared at the neck of the flask, the heating rate was adjusted to recover the distillate at a uniform rate of (6-8) mL/min. At the 50-percentage volume fractions of the distillate collected in the receiver, the vapor temperature and pressure were recorded

and reported as T_{sat} and p_{sat}, respectively. Each experimental value was measured three times on average with a repeatability (*r*) and reproducibility (*R*) as shown in Table S4.4 of the Section 4.8: Supplementary information. The low values of reproducibility indicated the thermal stability of the studied compounds D2EHPA and TBP. The test method was validated using *n*-tetradecane and *n*-hexadecane as reference materials. The standard uncertainties of measurement were $u(T)/\mathrm{K} = 0.1$ and $u(p)/\mathrm{kPa} = 0.01 + 0.03p$, and are provided in Table S4.4 of the Section 4.8: Supplementary information. The aspects that affected the uncertainties of measurement were purity of the compounds, heating rate and distillation rate. Details of verification results of n-tetradecane and n-hexadecane compared with the literature data are described in Table 4.2.

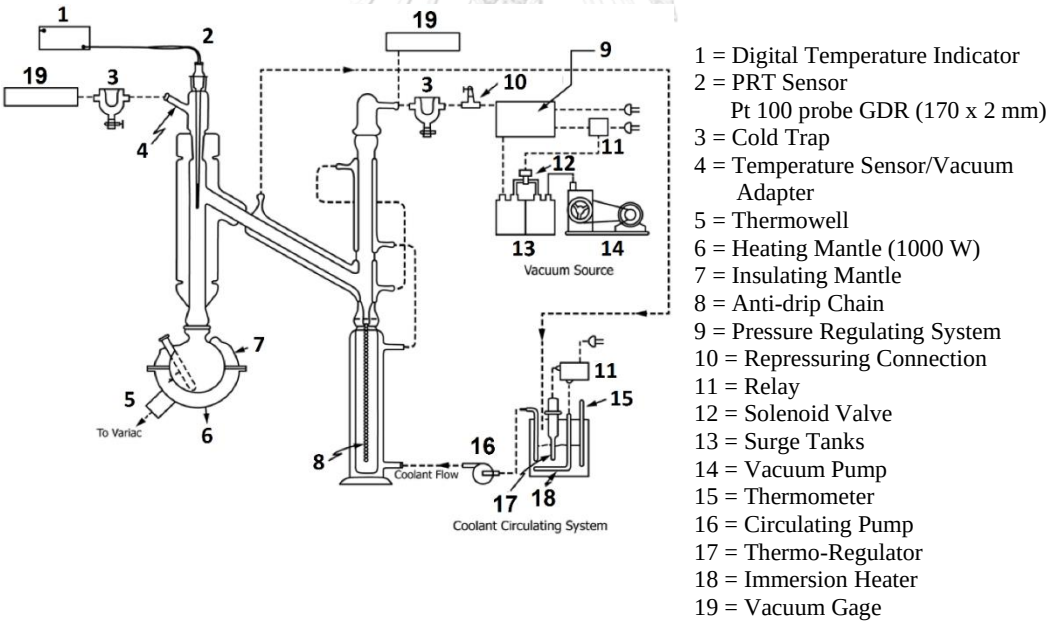

Figure 4.2 Schematic diagram of the vacuum distillation apparatus (i-Fischer Engineering GmbH, AUTODEST® 851 AC) [36].

Table 4.2 Verification results for distillation temperatures T of n-tetradecane and n-hexadecane at system pressure range of p = (0.13-6.7) kPa.

p (kPa)	*n*-Tetradecane T (K)				*n*-Hexadecane T (K)			
	ASTM[a]	Literature [68]	This work[b]	%Dev.	ASTM[a]	Literature [69]	This work[b]	%Dev.
0.13	352.05-355.05	353.3	354.4	0.31	377.45-380.75	378.5	379.8	0.34
0.67	379.55-382.55	381.3	381.6	0.08	406.25-409.55	407.8	407.4	-0.10
1.3	393.35-396.35	394.4	394.6	0.05	420.65-423.95	421.7	422.4	0.17
2.7	408.65-411.65	410.5	411.0	0.12	436.45-439.85	438.5	438.8	0.07
5.3	425.65-428.65	427.0	426.6	0.09	454.25-457.55	455.8	456.8	0.22
6.7	431.45-434.45	433.1	433.2	0.02	460.35-463.75	462.2	461.6	0.13

[a] The range of temperatures were recommended by ASTM D1160 [36].

[b] Standard uncertainty (u): $u(T)/\mathrm{K} = 0.1$ and $u(p)/\mathrm{kPa} = 0.01 + 0.03p$.

4.5 Mathematical modeling and parameter estimation

4.5.1 Saturated vapor pressure correlation

The experimental p_{sat} data of D2EHPA and TBP were correlated with the following equations:

(1) Antoine equation [38]

$$\ln p_{\text{sat}} = A - \frac{B}{T + C} \tag{4.1}$$

(2) August equation

$$\ln p_{\text{sat}} = A - \frac{B}{T} \tag{4.2}$$

(3) Riedel vapor pressure equation [39]

$$\ln p_{\text{sat}} = A + \frac{B}{T} + C \ln T + DT^{E} \tag{4.3}$$

(4) Wagner equation [40]

$$\ln\left(\frac{p_{\text{sat}}}{P_{\text{c}}}\right) = \frac{A(1-T_{\text{r}}) + B(1-T_{\text{r}})^{1.5} + C(1-T_{\text{r}})^{2.5} + D(1-T_{\text{r}})^{5}}{T_{\text{r}}} \tag{4.4}$$

where p_{sat} is the saturated vapor pressure (Pa), T is any temperature (K). The alphabets *A*, *B*, *C*, *D* and E are the regression constants. T_{r} is the reduced temperature and equal to T / T_{c}. The critical properties, namely P_{c}, T_{c} and V_{c} of D2EHPA [14] and TBP [20] were obtained from previous works of Kumar et al.

4.5.2 Acentric factor estimation

Acentric factor (ω) is a measure of the non-sphericity of molecules which can be determined from the experimental p_{sat} data. It is defined as:

(1) Pitzer [41, 42]

$$\omega = -\log\left(\frac{p_{\text{sat}}}{P_{\text{c}}}\right) - 1 \quad \text{, at } T_r = 0.7 \tag{4.5}$$

(2) Edmister [43]

$$\omega = \frac{3}{7}\left(\frac{\theta}{1-\theta}\right)\log P_{\text{c}} - 1 \tag{4.6}$$

(3) Lee-Kester [44]

$$\omega = \frac{-\ln P_{\text{c}} - 5.92714 + 6.09648\theta^{-1} + 1.28862\ln\theta - 0.169347\theta^{6}}{15.2518 - 15.6875\theta^{-1} - 13.4721\ln\theta + 0.435770\theta^{6}} \tag{4.7}$$

(4) Chen et al. [45]

$$\omega = \frac{0.3(0.2803 + 0.4789\theta)\log P_{\text{c}}}{(1-\theta)(0.9803 - 0.5211\theta)} - 1 \tag{4.8}$$

where θ is equal to $T_{\text{b}}/T_{\text{c}}$ and T_{b} is boiling temperature at 101.3 kPa.

4.5.3 Enthalpy or latent heat of vaporization

The slope of the saturation curve between p_{sat} and T_{sat} can be used to calculate $\Delta_{\text{vap}}H$ from the Clausius-Clapeyron equation according to Eq. (4.9):

$$\Delta_{\text{vap}}H = T\Delta V\left(\frac{dp_{\text{sat}}}{dT}\right) \tag{4.9}$$

where ΔV is the difference between the saturated vapor and liquid volumes ($V_g - V_l$).

For this work, the saturated vapor volumes (V_g) for both extractants D2EHPA and TBP were calculated using the Elliott-Suresh-Donohue equation of state (ESD EOS) [46] whereas the saturated liquid volumes (V_l) were calculated using the liquid density correlation. When compared to the larger molar volume of the gas phase, V_l can be neglected.

Additionally, the calculated $\Delta_{vap}H$ were fitted with the exponential function as shown in Eq. (4.10):

$$\Delta_{vap}H = A(1-T_r)^B \tag{4.10}$$

4.5.4 Entropy of vaporization

In the phase transition of vaporization, both phases of vapor and liquid coexist in equilibrium, so the difference in Gibbs free energy between vapor and liquid is equal to zero. Then, $\Delta_{vap}S$ can be calculated from $\Delta_{vap}H$ and T_{sat} as shown in Eq. (4.11):

$$\Delta_{vap}S = \frac{\Delta_{vap}H}{T_{sat}} \tag{4.11}$$

The calculated $\Delta_{vap}S$ were fitted with fourth-order polynomial function as in Eq. (4.12):

$$\Delta_{vap}S = A + B\ln T + CT + DT^2 + ET^3 \tag{4.12}$$

จุฬาลงกรณ์มหาวิทยาลัย
CHULALONGKORN UNIVERSITY

Furthermore, the calculated $\Delta_{\text{vap}}S$ from Eq. (4.11) were compared with the $\Delta_{\text{vap}}S$ obtained by Trouton's theoretical rule as expressed in Eq. (4.13):

$$\Delta_{\text{vap}}S = 4.5R + R\ln T_{\text{sat}} \tag{4.13}$$

4.5.5 Saturated liquid heat capacity

Along the saturation curve, C_{σ}^{l} is the slope of enthalpy with temperature. In this work, the derivative method was used to calculate C_{σ}^{l} by taking the temperature derivative of $\Delta_{\text{vap}}H$ as shown in Eqs. (4.14) and (4.15) [47]:

$$\frac{d\Delta_{\text{vap}}H}{dT} = \left(\frac{d_{\text{vapor}}H}{dT}\right)_{\text{sat}} - \left(\frac{d_{\text{liquid}}H}{dT}\right)_{\text{sat}} = C_{\text{sat}}^{V} - C_{\text{sat}}^{l} \approx C_{p}^{ig} - C_{\sigma}^{l} \tag{4.14}$$

$$C_{\sigma}^{l} = C_{p}^{ig} - \frac{d\Delta_{\text{vap}}H}{dT} \tag{4.15}$$

where C_{p}^{ig} is the isobaric heat capacity of ideal gas. C_{sat}^{V} and C_{sat}^{l} are the vapor and liquid heat capacity along the saturation curve, respectively.

For polyatomic ideal-gas state, the temperature dependent of C_{p}^{ig} can be derived from statistical mechanics [48] as in Eq. (4.16):

$$C_{p}^{ig} = 4R + R\sum_{j}^{3m-6}\left(\frac{\Theta_{vj}}{T}\right)^{2}\frac{\exp\left(\frac{\Theta_{vj}}{T}\right)}{\left(\exp\left(\frac{\Theta_{vj}}{T}\right)-1\right)^{2}} \tag{4.16}$$

where m is the number of atoms in the molecule. Θ_{vj} is the jth vibrational temperature which is defined as:

$$\Theta_{vj} = \frac{hcv}{k_B} \tag{4.17}$$

where h is Planck constant, c is velocity of light, v is molecular vibrational frequency, and k_B is Boltzmann's constant.

The obtained C_σ^l were fitted according to Eq. (4.18):

$$C_\sigma^l = A + B\ln T + CT + DT^2 + ET^3 \tag{4.18}$$

4.6. Results and discussion

4.6.1 Saturated vapor pressure

The measured p_{sat} and T_{sat} of pure D2EHPA and TBP are presented in Table 4.3 and plotted pressure-temperature relationship as the $p-T$ saturation curves in Figs. 4.3 and 4.4. In both compounds, the p_{sat} increased nonlinearity as temperature increased according to the rate of evaporation. Because these compounds are low in volatility, the lowest p_{sat} at 0.13 kPa was obtained at relatively high temperatures, namely D2EHPA at T = 450.5 K and TBP at T = 383.8 K. As a result of molecular structure, strength of intermolecular attraction and molar mass, the p_{sat} of D2EHPA was lower than TBP. Polar molecules tend to have a higher boiling point but lower vapor pressure than nonpolar molecules.

จุฬาลงกรณ์มหาวิทยาลัย
CHULALONGKORN UNIVERSITY

Fig. 4.5 presents the electrostatic charge potential surface as simulated by Jmol software for the polar covalent molecule of D2EHPA and TBP. Regarding the D2EHPA molecule, the presence of a large partial positive charge on H-atom and partial negative charge on O-atom of hydroxyl (-OH) group can engage in H-bonding to other molecules. The stronger electrostatic attraction by H-bonding resulted in a lower p_{sat}. Furthermore, the D2EHPA molecules were strongly attracted via H-bonding in dimer form as in Fig. 4.6 [49-51] while the TBP molecules were not. As regards the TBP molecule, the H-atoms were all bonded to the C-atoms, so H-bonding was not possible. Hence, its average cohesive force was weaker than that in the D2EHPA molecule whereas its p_{sat} was higher. This also explains that D2EHPA has such a higher boiling temperature than TBP.

The p_{sat} of nonpolar side chain is related to molar mass and size of the molecule. A bigger side chain with more surface area is more polarizable giving rise to increased attractive dispersion force and higher boiling temperature. The D2EHPA molecule has two groups of 2-ethylhexyl side chain with molar mass of 226.44 g·mol^{-1} whereas the TBP molecule has three groups of butyl side chain with molar mass of 171.34 g·mol^{-1}. The high molar mass in D2EHPA and TBP accounted for their low p_{sat} and high boiling temperature.

The *A*, *B*, *C*, *D* and E constants of Eqs. (4.1) to (4.4) were calculated by regression analysis in accordance with Antoine, August, Riedel vapor pressure and Wagner equation as represented in Table 4.4. The relative average deviations (RAD) between the calculated and the experimental p_{sat} can be calculated using Eq. (4.19):

$$\mathrm{RAD}(\%) = \left(\frac{p_{\mathrm{sat}}^{\mathrm{cal}} - p_{\mathrm{sat}}^{\mathrm{exp}}}{p_{\mathrm{sat}}^{\mathrm{exp}}} \right) \times 100 \tag{4.19}$$

The RAD percentages for Antoine, August, Riedel vapor pressure and Wagner equation were found to be (0.0089-0.0230)%, (0.2191-0.2193)%, (0.0321-0.1305)% and (0.0076-0.0080)%, respectively. Since errors in the calculated p_{sat} were relatively small, the Wagner equation was the most appropriate model for calculating the p_{sat} of D2EHPA and TBP at different temperatures. Further, the normal boiling temperature (T_{b}) for each compound was calculated by extrapolating to p_{sat} at 101.3 kPa using Wagner equation Eq. (4.4) and derived constants. The calculated T_{b} of DEHPA is 654.4 K and T_{b} of TBP is 569.1 K. In our previous work [15], the T_{b} of D2EHPA was obtained by atmospheric distillation method under the pressure of 101.3 kPa and reported as 533 K. Because of high T_{b}, the atmospheric distillation may result in the decomposition of D2EHPA molecule. Thus, the measured T_{b} will be lower. Kumar et al. [14] determined the T_{b} of 625.15 K for D2EHPA which differs from T_{b} found in this study by 29.25 K (4.68%). The p_{sat} values of D2EHPA given by Härtel [1] in the overlapping temperature was 1 kPa at 482 K while the investigated values in this work were 1.00 kPa at 493.7 K and 0.61 kPa at 482 K. It can be seen that the differences in p_{sat} and T_{sat} are 0.39 kPa and 11.7 K (2.43 %), respectively. In the CRC Handbook of Chemistry and Physics, Lide [22] reported the p_{sat} value for D2EHPA of 0.002 kPa at 428 K, while the corresponding extrapolated p_{sat} values obtained in this work by Eq.

จุฬาลงกรณ์มหาวิทยาลัย
CHULALONGKORN UNIVERSITY

(4.8) were 0.002 kPa at 386.4 K with a deviation of 9.72% and 0.04 kPa at 428 K with a deviation of 0.038 kPa. These large deviations may result from a large uncertainties of measurement at very low pressure condition of the literature.

The T_b of 569.1 K of TBP was closed to reported values of previous works such as Kumar et al [20] of 562.15 K, Panneerselvam et al [16] of 561.34 K and Edmundson [18] of 562 K with a deviation of 1.25%. The comparison with all other literature data is presented graphically in Fig. 4.4. As it can be seen from the figure, the experimental p_{sat} data agree satisfactorily with the previous results by Härtel [1] of 3 kPa at 453.15 K with a deviation of 0.62 kPa, Vogel [24] of 0.80 kPa at 411.65 K (diff. 0.20 kPa), Kumar et al [20] of 0.8 kPa at 411.65 K (diff. 0.20 kPa), 1.07 kPa at 418.15 K (diff. 0.25 kPa) and 4.67 kPa at 455.15 K (diff. 0.77 kPa). However, there is a noticeable difference from Hammer and Lydersen [28], Perry and Weber [29], Small et al [30] as well as Dean [31]. The T_b of D2EHPA and TBP reported in this work approximates the literature values. Thereby, the T_b calculated by Wagner equation is acceptable.

จุฬาลงกรณ์มหาวิทยาลัย
CHULALONGKORN UNIVERSITY

The values of ω were estimated by Eqs. (4.5) to (4.8). Comparison of these values are presented in Table 4.5. The ω of D2EHPA is higher than that of TBP. This is because ω increases with carbon chain length and generally rises with increasing polarity. In this work, ω values obtained from Edmister method as in Eq. (4.6) were used in ESD EOS.

Table 4.3 Experimental saturated vapor pressures p_{sat} and calculated enthalpy $\Delta_{vap}H$, entropy $\Delta_{vap}S$ of vaporization and saturated liquid heat capacity C_{σ}^{l} for D2EHPA and TBP at different temperatures T.[a]

D2EHPA					TBP				
p / kPa	T / K	$\Delta_{vap}H$ /kJ · mol^{-1}	$\Delta_{vap}S$ /kJ · mol^{-1} · K^{-1}	C_{σ}^{l} /kJ · mol^{-1} · K^{-1}	p / kPa	T / K	$\Delta_{vap}H$ /kJ · mol^{-1}	$\Delta_{vap}S$ /kJ · mol^{-1} · K^{-1}	C_{σ}^{l} /kJ · mol^{-1} · K^{-1}
0.13	450.5	88.98	0.1975	0.1475	0.13	383.8	72.34	0.1885	0.1361
0.27	464.1	86.91	0.1873	0.1501	0.27	396.0	70.78	0.1788	0.1381
0.40	472.7	86.00	0.1819	0.1518	0.40	403.6	69.93	0.1733	0.1393
0.53	479.0	85.10	0.1777	0.1530	0.53	409.3	69.24	0.1692	0.1403
0.67	484.1	84.42	0.1744	0.1541	0.67	413.8	68.78	0.1662	0.1410
0.80	488.3	83.92	0.1719	0.1549	0.80	417.7	68.50	0.1640	0.1417
0.93	492.0	83.59	0.1699	0.1557	0.93	421.0	68.17	0.1620	0.1422
1.07	495.3	83.26	0.1681	0.1564	1.07	423.8	67.70	0.1597	0.1427
1.20	498.2	82.91	0.1664	0.1570	1.20	426.5	67.55	0.1584	0.1432
1.33	500.8	82.66	0.1651	0.1575	1.33	428.8	67.26	0.1568	0.1436
1.73	507.6	81.99	0.1615	0.1590	1.73	434.9	66.65	0.1533	0.1446
2.00	511.3	81.52	0.1594	0.1598	2.00	438.3	66.34	0.1514	0.1452
2.40	516.2	80.96	0.1568	0.1609	2.40	442.7	65.98	0.1490	0.1460
2.67	519.1	80.67	0.1554	0.1615	2.67	445.3	65.70	0.1475	0.1465
3.07	523.0	80.25	0.1534	0.1624	3.07	448.9	65.44	0.1458	0.1471
3.33	525.4	80.10	0.1525	0.1629	3.33	451.0	65.27	0.1447	0.1475
3.73	528.7	79.74	0.1508	0.1637	3.73	454.0	65.01	0.1432	0.1480
4.00	530.7	79.50	0.1498	0.1641	4.00	455.8	64.80	0.1422	0.1484
4.40	533.5	79.32	0.1487	0.1648	4.40	458.3	64.59	0.1409	0.1488
4.67	535.3	79.13	0.1478	0.1652	4.67	459.9	64.48	0.1402	0.1491
5.07	537.7	78.81	0.1466	0.1658	5.07	462.2	64.30	0.1391	0.1495
5.33	539.3	78.76	0.1460	0.1662	5.33	463.6	64.25	0.1386	0.1498
5.73	541.5	78.49	0.1450	0.1667	5.73	465.6	64.05	0.1376	0.1502
6.00	543.0	78.46	0.1445	0.1671	6.00	466.9	64.00	0.1371	0.1504
6.40	545.0	78.23	0.1435	0.1675	6.40	468.7	63.78	0.1361	0.1508
6.67	546.2	78.02	0.1428	0.1678	6.67	469.9	63.65	0.1355	0.1510

[a] Standard uncertainty (u): $u(T)/\mathrm{K} = 0.1$ and $u(p)/\mathrm{kPa} = 0.01 + 0.03p$.

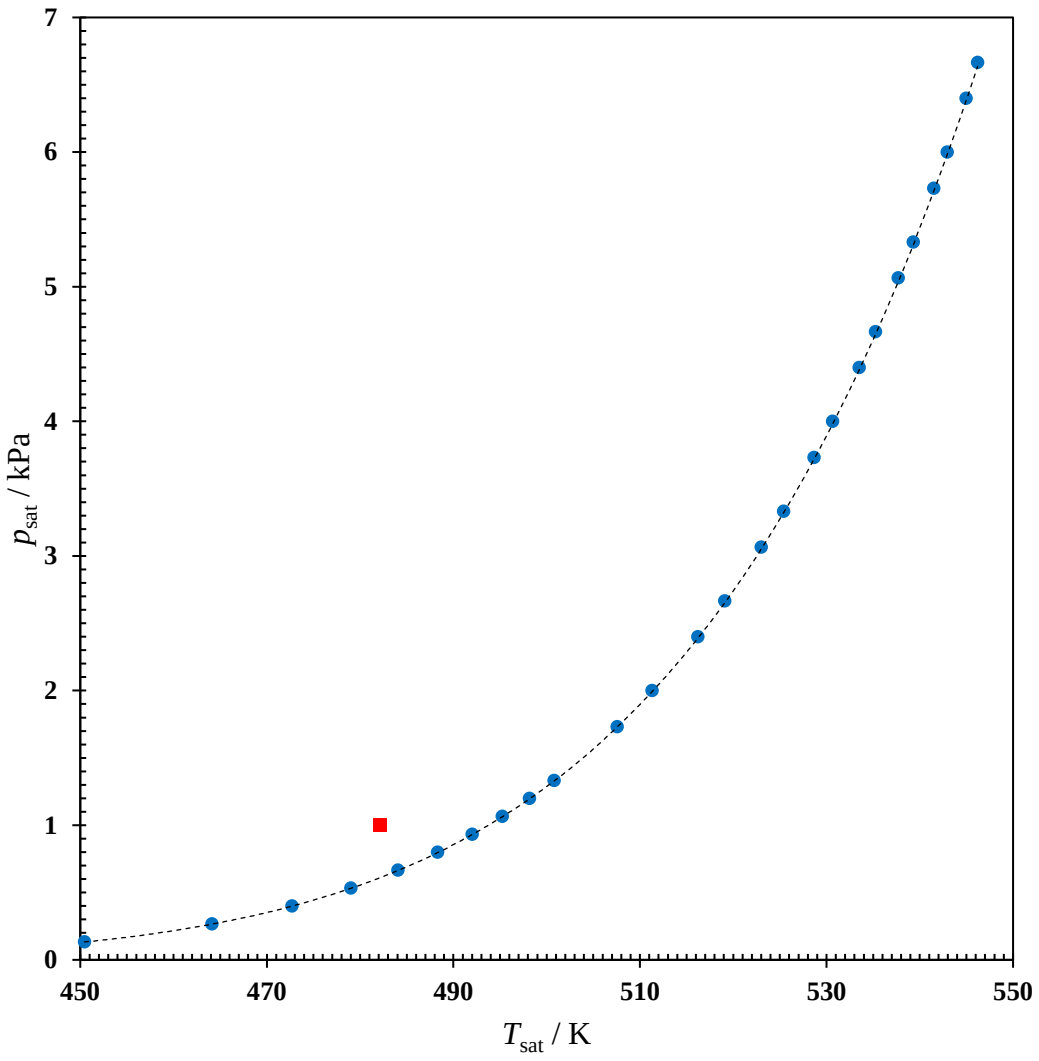

Figure 4.3 Experimental saturated vapor pressures p_{sat} of D2EHPA in temperature range T = (450-550) K. ●, This work; ■, ref [1]; and ---, fitted by Eq. (4.4).

CHULALONGKORN UNIVERSITY

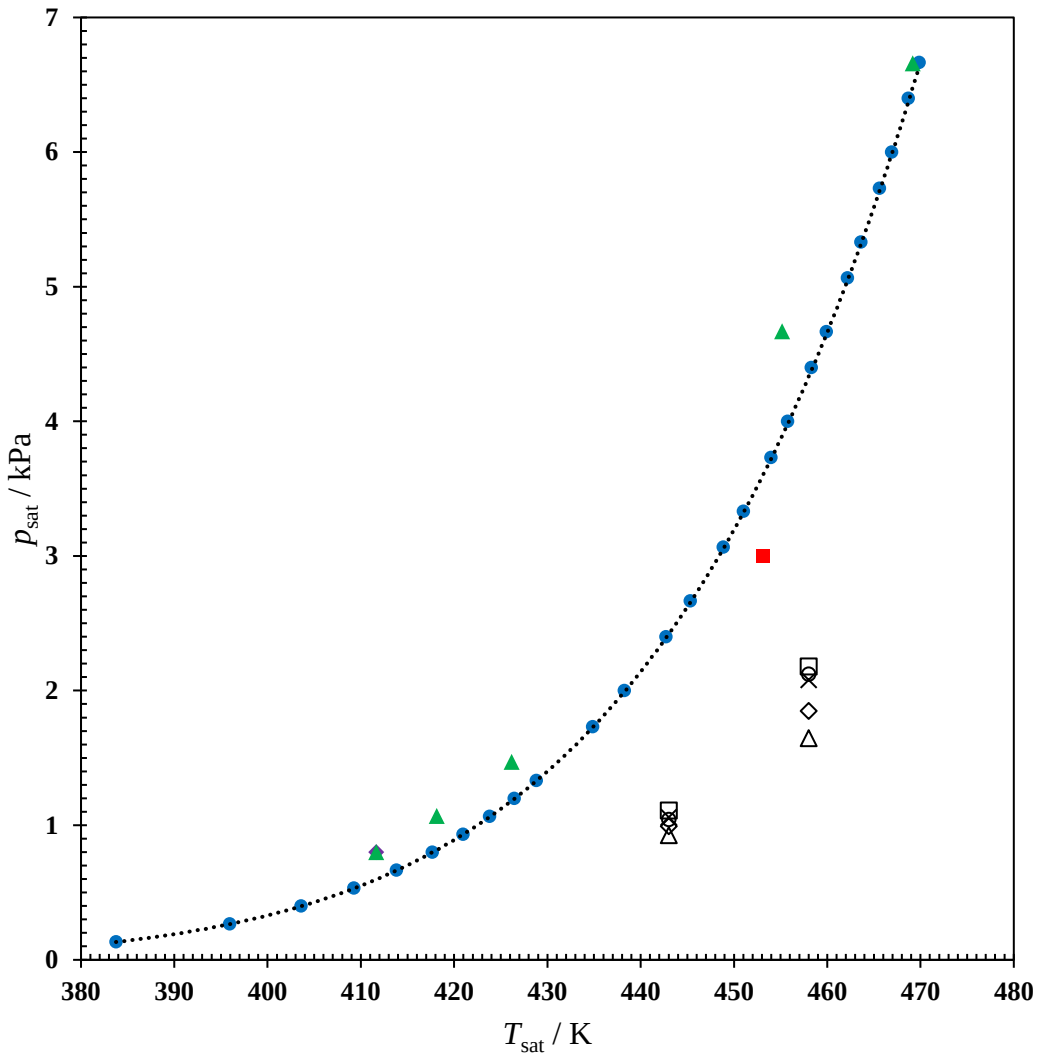

Figure 4.4 Experimental saturated vapor pressures p_{sat} of TBP in the temperature range T = (380-480) K. ●, This work; ■, ref [1]; ▲, ref [20]; ♦, ref [24]; ○, ref [28]; Δ, ref [29]; □, ref [30]; x, ref [31]; ◊, ref [52]; and ---, fitted by Eq. (4.4).

CHULALONGKORN UNIVERSITY

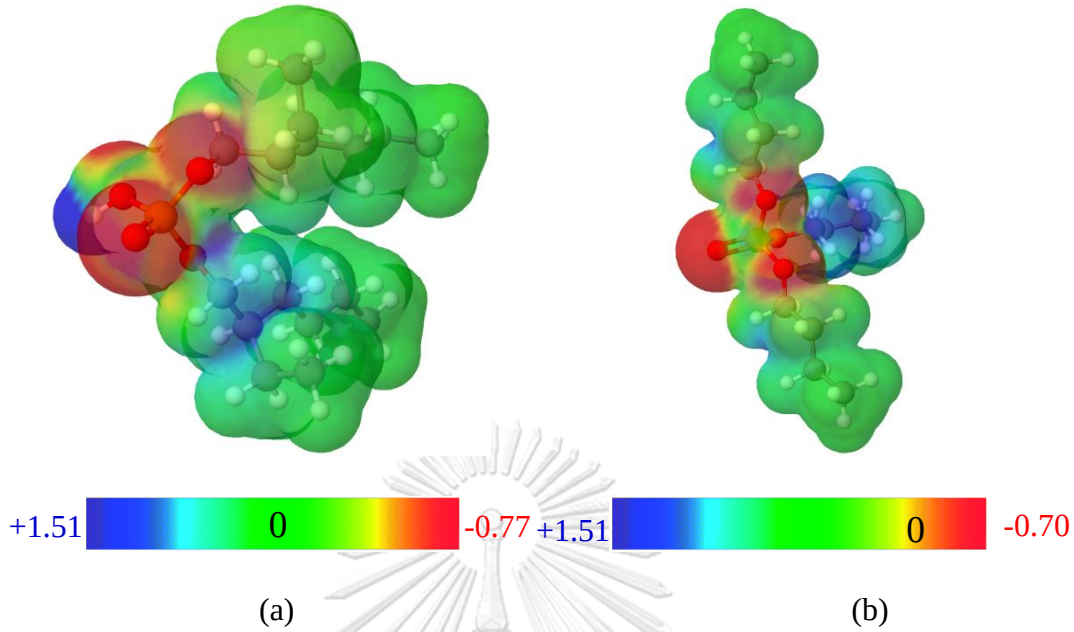

Figure 4.5 The electrostatic charge potential surface for molecule (a) D2EHPA and (b) TBP.

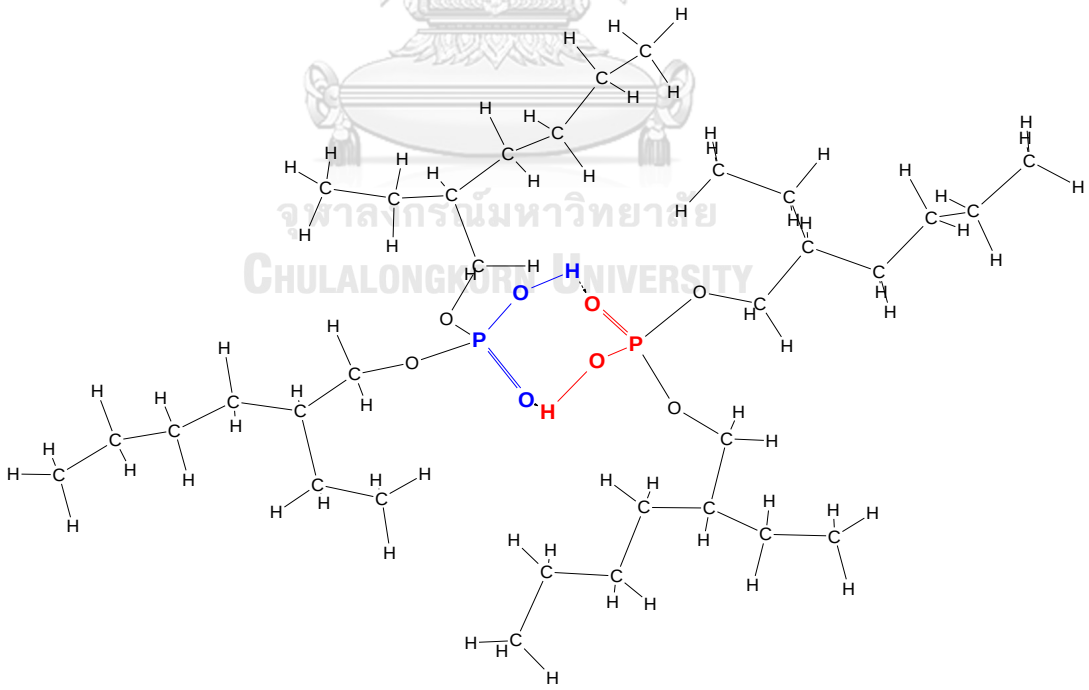

Figure 4.6 Dimers of D2EHPA

Table 4.4 Regression constants for the correlation of saturated vapor pressure p_{sat}.

	Regression constants					R^2	%RAD
	A	*B*	*C*	*D*	*E*		
D2EHPA							
Antoine, Eq. (4.1)	22.197	5673.9	-122.57	-	-	1.00000	0.0089
August, Eq. (4.2)	27.053	9955	-	-	-	0.99968	0.2193
Riedel vapor pressure, Eq. (4.3)	360.41	-28497	-48.595	2.2982e-5	2	0.99990	0.1305
Wagner, Eq. (4.4)	-11.292	1.6462	0.27717	-16.549	-	1.00000	0.0080
TBP							
Antoine, Eq. (4.1)	21.669	4749.6	-100.69	-	-	1.00000	0.0230
August, Eq. (4.2)	26.105	8117.8	-	-	-	0.99968	0.2191
Riedel vapor pressure, Eq. (4.3)	226.36	-18260	-29.625	1.6198e-5	2	1.00000	0.0321
Wagner, Eq. (4.4)	-8.6861	0.026462	0.95846	-11.543	-	1.00000	0.0076

Table 4.5 Estimated acentric factor values ω of D2EHPA and TBP.

D2EHPA		TBP	
Method	ω	Method	ω
Pitzer	0.955529	Pitzer	0.600475
Edmister	0.982000	Edmister	0.608714
Lee-Kesler	1.026421	Lee-Kesler	0.606968
Chen et al.	1.010901	Chen et al.	0.607643

4.6.2 Enthalpy and entropy of vaporization

The $\Delta_{vap}H$ for pure liquid D2EHPA and TBP was evaluated through the Clusius-Clapeyron equation from a fit of experimental p_{sat} data and presented as in Table 4.4. Generally, $\Delta_{vap}H$ can be calculated by a Clausius-Clapeyron plot of $\ln p_{sat}$ versus $1/T$ which results in a straight line whose slope is $-\Delta_{vap}H/R$ where R is the gas constant [29]. The obtained $\Delta_{vap}H$ is constant over a wide range of temperature, however, $\Delta_{vap}H$ is theoretical temperature-dependent. Recently, the technique of correlation gas chromatography (CGC) was applied to measure the $\Delta_{vap}H$ of various organic compounds [16, 53-55]. Nevertheless, the $\Delta_{vap}H$ are limited only at 298.15 K and normal boiling point (T_b). In view of these limitations, this work calculated the $\Delta_{vap}H$ of both D2EHPA and TBP by Eq. (4.8) with a temperature interval of 1 K in order to get the $\Delta_{vap}H$ at each individual temperature.

In Fig. 4.8, all values of $\Delta_{vap}H$ of both D2EHPA and TBP at T = (383.8-546.2) K were positive. As temperature increased, it was observed that $\Delta_{vap}H$ decreased. The derivative values of $d\left(\Delta_{vap}H\right)/dT$ also became more and more negative with increasing temperature as shown in Fig. 4.8 which known as Waring criterion. According to thermodynamic point of view, $\Delta_{vap}H$ is the summation of increased internal energy and work done against ambient pressure. As temperature increases, the increase in internal energy can be viewed as the energy required to overcome the intermolecular interactions in the liquid. The $\Delta_{vap}H$ is the energy required to remove

จุฬาลงกรณ์มหาวิทยาลัย
Chulalongkorn University

a molecule from the highly interacting and associated liquid phase into the vapor phase, wherein interactions almost cease to exist.

The number of carbon atoms and their arrangement in space determine the physical properties of the organic compounds. For polar compounds of phosphate esters, the main intermolecular interactions result from the dispersive forces as well as dispersive and induced dipole forces, respectively. As the carbon chain length in the phosphates increases, its size increases and hence the energy required to transfer a molecule from the liquid to vapor state also increases. As mentioned previously, the molecules of D2EHPA held together by relative strong H-bonding. In the liquid state, each molecule of D2EHPA was closer than that of TBP so the molecular interactions in D2EHPA can be more than that in TBP. In the D2EHPA, branching progressively away from the phosphoryl carbon oxygen also increases the $\Delta_{vap}H$. This may explain the reason why the $\Delta_{vap}H$ of D2EHPA, namely (78-89) kJ·mol^{-1} at T = (450.5-546.2) K was found to be higher than the $\Delta_{vap}H$ of TBP, namely (64-72) kJ·mol^{-1} at T = (383.8-469.9) K.

จุฬาลงกรณ์มหาวิทยาลัย
CHULALONGKORN UNIVERSITY

For each compound, it was noted that the $\Delta_{vap}H$ fitted in well with Eq. (4.10) since the coefficients of determination (R^2) were close to 1. The regression constants of A and B together with the RAD are listed in Table 4.6. The calculated $\Delta_{vap}H$ of TBP by Eq. (4.10) are in good agreement with the reported $\Delta_{vap}H$ in previous works of Stephenson and Malanowski [56] as well as Panneerselvam et al [55]. The published values of $\Delta_{vap}H$ of TBP was 61.4 kJ·mol^{-1} at temperature of 515 K [56] while the extrapolated $\Delta_{vap}H$ by this work was 58.74 kJ·mol^{-1} at the same temperature with a

deviation of 4.33%. Further, the standard enthalpy of vaporization ($\Delta_{vap}H^o$) by this work of 79.22 kJ·mol^{-1} at 298.15 K is very close to the reported $\Delta_{vap}H^o$ by Panneerselvam et al [55] of 80.6 kJ·mol^{-1} with a deviation of 1.71%. These indicate that the calculated $\Delta_{vap}H$ data as well as regression parameters presented by this work are definitely reliable. The obtained $\Delta_{vap}H$ data of D2EHPA and TBP proved useful in calculating the heat required to evaporate a certain quantity of liquid in the heat exchanger or evaporator units.

For both D2EHPA and TBP, the calculated values of $\Delta_{vap}S$ were positive as in Fig. 4.9 since the degree of disorder was increased by the transition from a liquid in a relatively small volume to a vapor or gas occupying a much larger space. The $\Delta_{vap}S$ of D2EHPA were seen to be higher than that of TBP as a result of its higher $\Delta_{vap}H$. As temperature increased, the trend of $\Delta_{vap}S$ decreased. This is because the heat needed to vaporize a unit mass of a substance decreased as the starting temperature increased. Further, the calculated $\Delta_{vap}S$ of D2EHPA and TBP showed a positive deviance from the predicted values by Trouton's rule (Eq. (4.13)), namely (0.088-0.090) kJ·mol^{-1}·K^{-1} due to its polar and nonquasi-spherical molecules [57]. The $\Delta_{vap}S$ of D2EHPA were in the range of (0.1428-0.1975) kJ·mol^{-1}·K^{-1} while that of TBP were (0.1355-0.1885) kJ·mol^{-1}·K^{-1}. Further, the $\Delta_{vap}S$ proved to be an excellent fit with Eq. (4.12). The regression constants of *A, B, C, D* and *E* are listed in Table 4.7.

Table 4.6 Regression constants for the correlation of enthalpy of vaporization $\Delta_{vap}H$

.

	T (K)	Regression Constants		T_c (K)	R^2	%RAD
		A	B			
D2EHPA	450.5 – 546.2	125.04	0.47542	864.80 [14]	0.99267	0.2405
TBP	383.8 – 469.9	101.82	0.55277	817.04 [20]	0.99250	0.2354

จุฬาลงกรณ์มหาวิทยาลัย
CHULALONGKORN UNIVERSITY

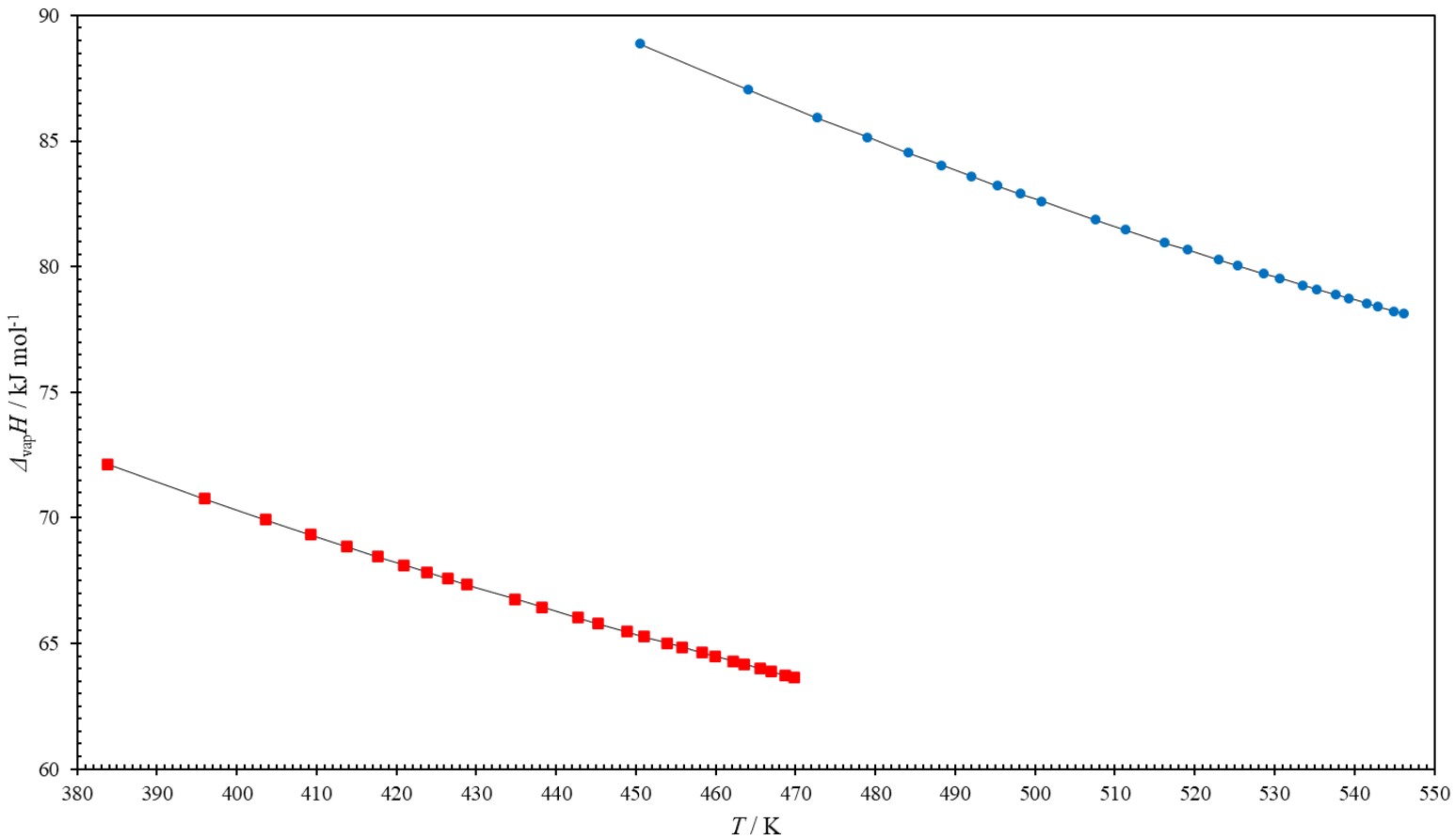

Figure 4.7 Enthalpy of vaporization $\Delta_{vap}H$ in the temperature range T = (380-550) K. ●, D2EHPA; ■, TBP; and ---, fitted by Eq. (4.10).

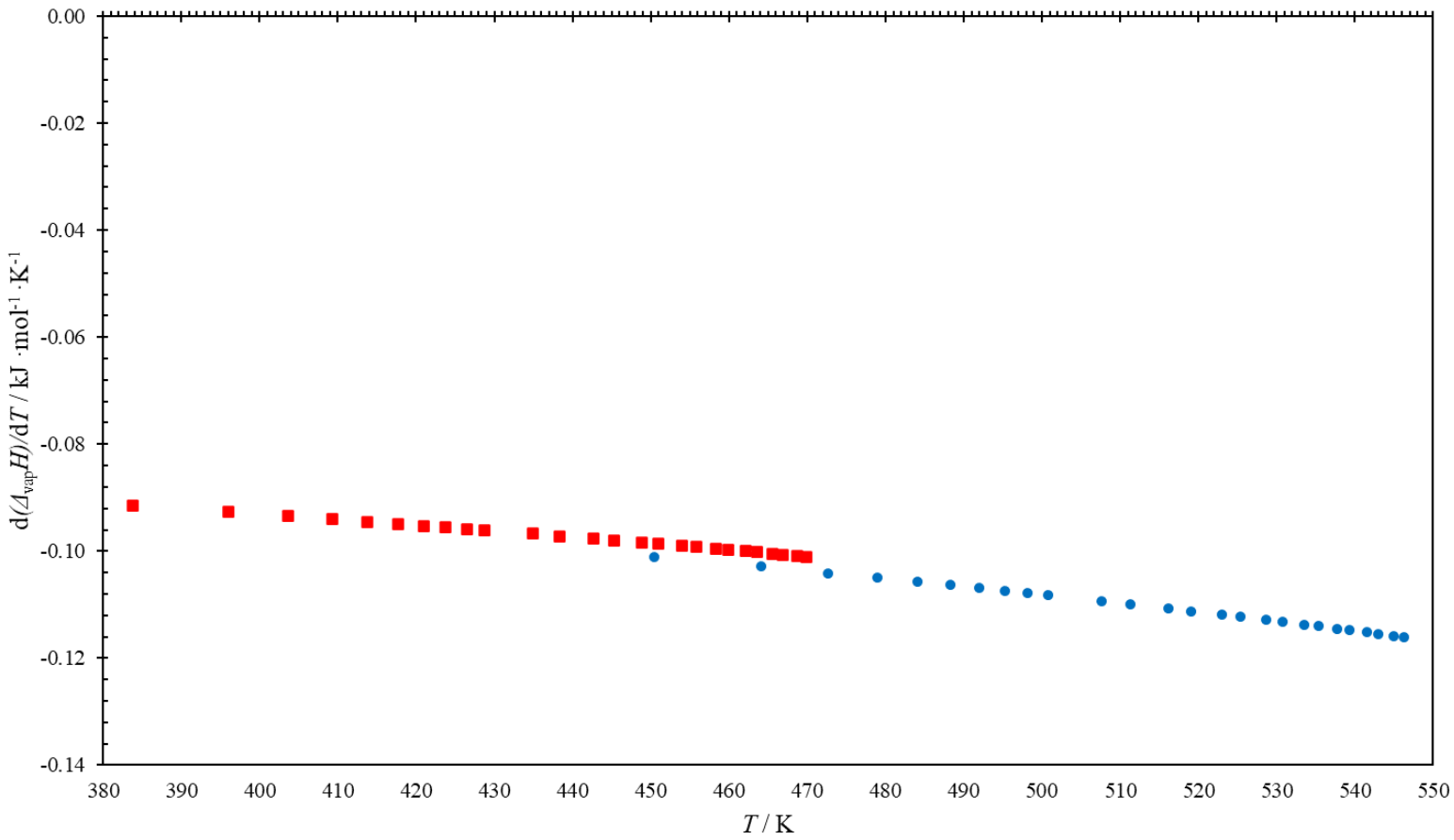

Figure 4.8 Plots of $\frac{\mathrm{d}\left(\Delta_{\mathrm{vap}}H\right)}{\mathrm{d}T}$ versus T for pure D2EHPA and TBP in this work. ΔT = 1.0 K; ●, D2EHPA; ■, TBP.

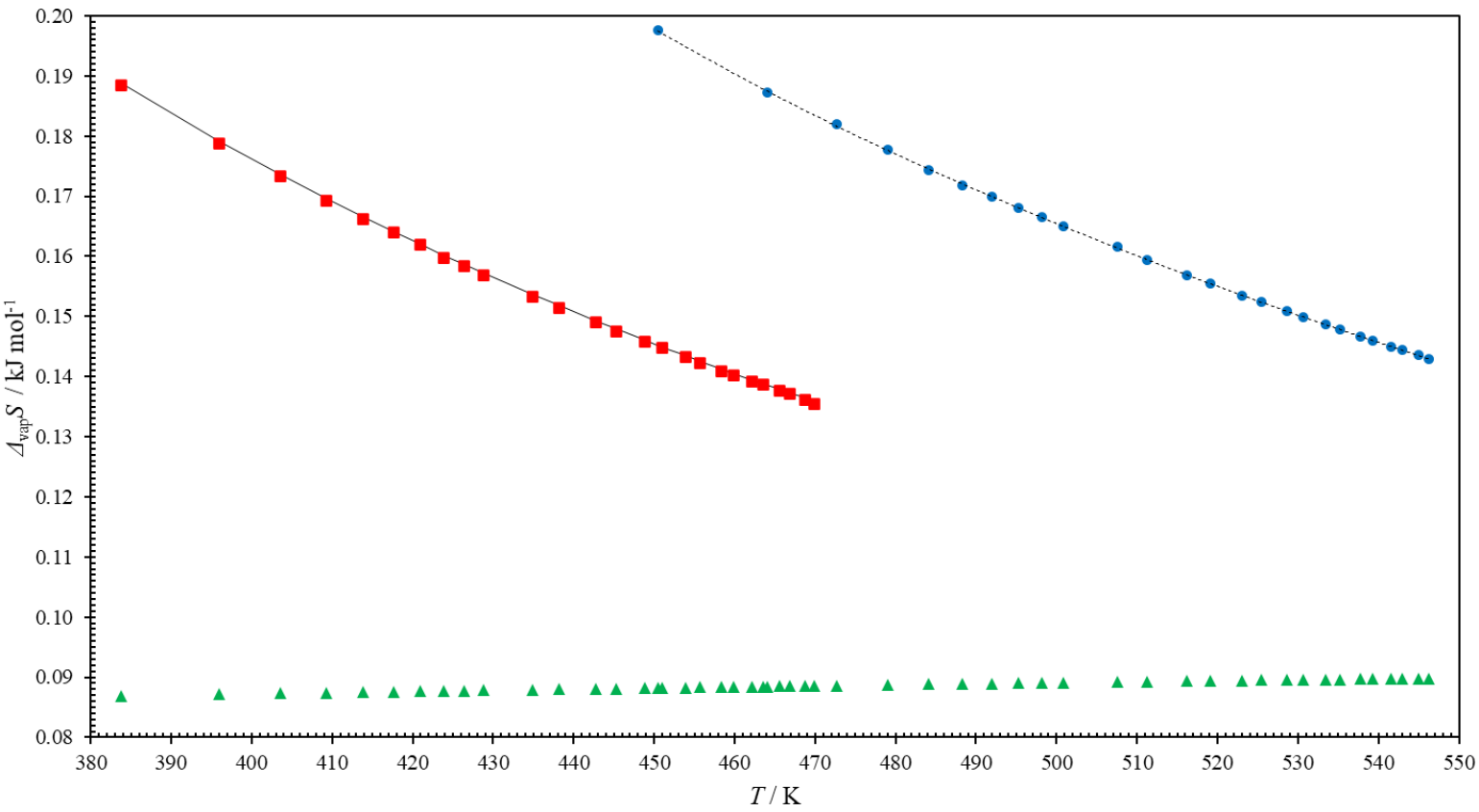

Figure 4.9 Entropy of vaporization ΔS_{vap} in the temperature range T = (380-550) K. ●, D2EHPA; ■, TBP; ▲, Trouton's rule; and ---, fitted by Eq. (4.12).

Table 4.7 Regression constants for the correlation of entropy of vaporization $\Delta_{vap}S$ and saturated liquid heat capacity C_{σ}^{l}.

	$\Delta_{vap}S$						
	Regression constants					R^2	%RAD
	A	*B*	*C*	*D*	*E*		
D2EHPA	84.695	-18.96	0.10684	-1.025E-04	4.4044E-08	0.99995	0.7046
TBP	37.027	-8.4756	0.054079	-6.04E-05	3.0544E-08	0.99968	0.2193
	C_{σ}^{l}						
	A	*B*	*C*	*D*	*E*		
D2EHPA	4.0028	-0.90882	0.0059862	-6.3734E-6	3.2218E-9	0.99998	0.0358
TBP	4.3255	-1.0165	0.0076456	-9.2974E-6	5.2041E-9	0.99996	0.1072

4.6.3 Saturated Liquid Heat Capacity

The C_{σ}^{l} were calculated using Eq. (4.15) and reported in Table 4.4. Thus, it was found that the C_{σ}^{l} of pure liquid D2EHPA and TBP linearly increased with increasing temperatures over the studied temperature range as presented in Fig. 4.10. The regression constants for Eq. (4.18) are shown in Table 4.8. Heat capacity is related to the internal energy and temperature. Internal energy is a combination of the translational and vibrational energy a molecule possesses. At low temperature, thermal motion consists chiefly of vibration but increasing temperature causes more translational and vibrational energy levels which become excited and so the internal energy increased. As a result, more and more degrees of freedom occur, so heat capacity increased. In comparison, the C_{σ}^{l} of TBP almost equaled that of D2EHPA as can be seen for example, for D2EHPA at T = 450.5 K, C_{σ}^{l} = 0.1475 kJ·mol^{-1}·K^{-1} and for TBP at T = 451.0 K, C_{σ}^{l} = 0.1475 kJ·mol^{-1}·K^{-1} or for D2EHPA at T = 464.1 K, C_{σ}^{l} = 0.1501

kJ·mol^{-1}·K^{-1} and for TBP at T = 463.6, C_{σ}^{l} = 0.1498 kJ·mol^{-1}·K^{-1}. Saturated heat capacity of liquid is important in the engineering design of chemical processes. Alternatively, it is essential when designing the size of heat exchangers and energy balance design calculations.

The new thermodynamic data of D2EHPA and TBP obtained from this work, namely saturated vapor pressure (p_{sat}), acentric factor (ω), enthalpy or heat of vaporization ($\Delta_{\text{vap}}H$), entropy of vaporization ($\Delta_{\text{vap}}S$) and saturated liquid heat capacity (C_{σ}^{l}), can be widely applied in many separation fields, especially vacuum distillation and evaporation processes over large temperature T = (383.8-546.2) K and pressure p_{sat} = (0.13-6.67) kPa ranges. On further investigation, these data can be directly used in the computing design and development for the recovery and recycling of organic wastewater via vacuum distillation or evaporation technique, for example, the reactive metal ions separation processes containing D2EHPA, TBP and organic solvents such as kerosene, toluene and other solvents [53, 54]. According to ecological considerations, this waste consisting of high boiling point compounds is hazardous and difficult to treat before discharge to the environment. In the engineering economic point of view, reusing of valuable extractants and solvents is cost saving. Thus, one of the remedies for these wastes to be handled is via a recovery or recycling process. Due to the large difference in boiling temperature but nearly chemical polarity between these extractants and the organic solvent, separation as carried out by distillation was found to be the most suitable [6, 7]. However, for designing distillation and evaporation equipment, the p_{sat} , $\Delta_{\text{vap}}H$ and C_{σ}^{l} of the pure D2EHPA and TBP as well as vapor-liquid equilibrium (VLE) data are the necessary basic data [3, 15, 37, 55]. Since there

จุฬาลงกรณ์มหาวิทยาลัย
CHULALONGKORN UNIVERSITY

is no reported on VLE systems of D2EHPA/TBP + various organic solvents, so the thermodynamic data of p_{sat} and ω over wide pressure and temperature by this work also provide a very useful in further VLE calculation without time-consuming experiment.

จุฬาลงกรณ์มหาวิทยาลัย
CHULALONGKORN UNIVERSITY

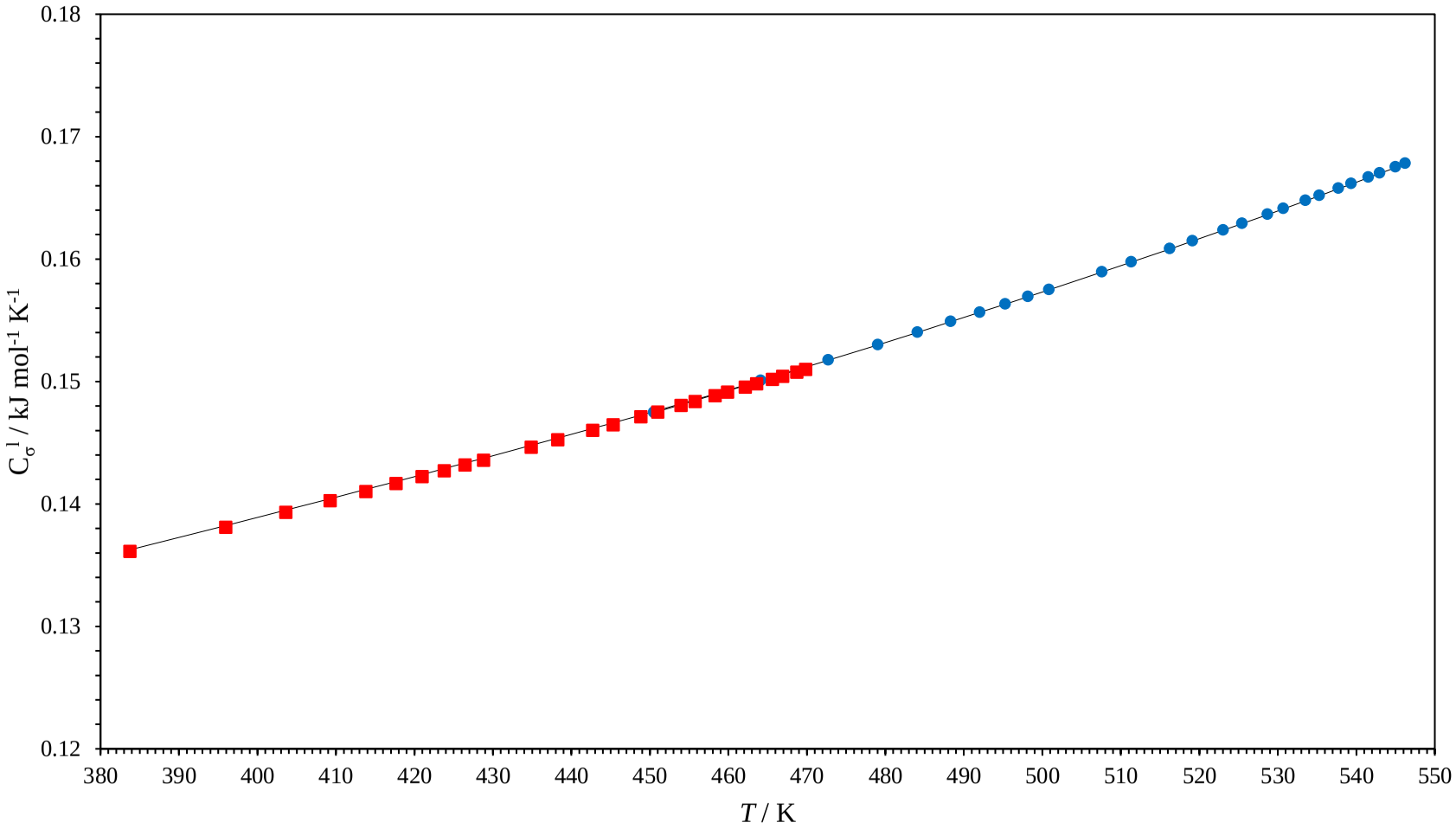

Figure 4.10 Saturated liquid heat capacity C_σ^l in the temperature range T = (380-550) K. ●, D2EHPA; ■, TBP; and ---, fitted by Eq. (4.18).

4.7. Conclusions

In this work, the p_{sat} for the low volatility organophosphorus extractants over the temperature range T = (450.5 – 546.2) K for D2EHPA and T = (383.8 – 469.9) K for TBP were determined by vacuum distillation method. Despite reaching high temperatures, the measured p_{sat} of these two extractants were relatively low, in the range of p_{sat} = (0.13 – 6.67) kPa. On investigation, it was observed that the p_{sat} values of D2EHPA were lower than that of TBP due to stronger intermolecular H-bonding. The correlation results of the experimental p_{sat} were found to be in good agreement with the estimated values as indicated by the low percentage of RAD for these models, namely Antoine (0.0089 – 0.0230) %, August (0.2191 – 0.2193) %, Riedel vapor pressure (0.0321 – 0.1305) % and Wagner equation (0.0076 – 0.0080) %. Then, the thermodynamic properties of $\Delta_{vap}H$ and $\Delta_{vap}S$ were calculated. Thus, it was observed that when temperature increased the $\Delta_{vap}H$ and $\Delta_{vap}S$ decreased. The calculated ΔS_{vap} also showed positive departures from Trouton's rule. Furthermore, the C_{σ}^{l} were determined within the experimental temperature ranges. On further investigation, the relevant data may provide some useful information for the design and development of vacuum distillation and evaporation processes for the recovery and recycling of organic waste.

4.8 Supplementary Information

Table S4.1 Previous works on thermophysical properties of pure D2EHPA and TBP.

Thermophysical properties[a]	D2EHPA			TBP		
	p / kPa	T / K	Values	p / kPa	T / K	Values
ρ / $\mathrm{kg \cdot m^{-3}}$	101.3	293.15	1,022 [1]; 1,024 [2]; 970 [3]	101.3	288.04	981.14 [4]
					288.15	981.0 [5]
	101.3	303.15	1,010 [2]; 1,009.6 [6]; 964.0 [7]; 1,009.4 [8]; 961.3 [9-11]; 965.3 [12]	101.3	289.75	979.4 [13]
	101.3	308.15	1,008 [2]; 1.008.2 [6]; 1,008.5 [8]	101.3	293.15	977 [1, 14]; 976.6 [13]; 976.72 [14]; 964.6 [15]; 976.8 [5]; 976 [16]
				101.32	293.2	972.70 [17]
	101.3	313.15	1,005 [2]; 1.0049 [6]; 957.0 [7]; 961 [18]; 1,004.6 [8]; 957.9 [12]	101.3	298.0	972 [19]; 975 [20]
	101.3	318.15	1,003 [2]; 1.0031 [6]; 1,002.6 [8]	101.3	298.15	975 [21]; 972.49 [4]; 970.83 [22]; 961.6 [15]; 973.85 [23]; 972.77 [24]; 972.82 [15]; 972.5 [5]; 972.69 [26-28]; 972.7 [29, 30]; 971.8 [31]; 972.67 [32]
	101.3	323.15	949.5 [7]; 950.4 [12]	101.3	299.0.	971 [19]
	101.3	333.15	942.0 [7]; 942.0 [12]	101.3	300.0	971 [19]
	101.3	343.15	934.5 [7]	101.3	301.0	970 [19]
				101.3	302.0	969 [19]
				101.3	303.0	968 [19, 20, 33]
				101.3	303.15	968 [21]; 968.19 [4]; 966.46 [22]; 958.4 [15]; 969.44 [23]; 968.46 [24]; 968.50 [25]; 968.2 [5]; 968.7 [34]; 967.4 [31]; 968.39 [32]

				101.3	304.0	967 [19]
				101.3	305.0	966 [19]
				101.3	306.0	965 [19]
				101.3	307.0	964 [19]
				101.3	308.0	963 [20, 33]

Table S4.1 (Con't) Previous works on thermophysical properties of pure D2EHPA and TBP.

Thermophysical properties[a]	D2EHPA			TBP		
	p / kPa	T / K	Values	p / kPa	T / K	Values
ρ / $\mathrm{kg \cdot m^{-3}}$				101.3	308.15	963 [21]; 963.88 [4]; 962.06 [22]; 955.4 [15]; 965.04 [23]; 964.15 [24]; 964.18 [25]; 963.9 [5]; 964.3 [31]; 964.11 [32]
				101.3	310.0	962 [19]
				101.3	311.0	961 [19]
				101.3	312.0	960 [19]
				101.3	313.0	959 [19]; 961 [20, 33]
				101.3	313.15	961 [21]; 959.70 [4]; 957.77 [22]; 949.6 [15]; 960.62 [23]; 959.84 [24]; 959.86 [25]; 958.6 [31]; 959.82 [32]
				101.3	314.0	958 [19]
				101.3	315.0	957 [19]
				101.3	316.0	957 [19]
				101.3	317.0	956 [19]
				101.3	318.0	955 [19]; 954 [20, 33]

101.3	318.15	954 [21]; 955.37 [4]; 953.58 [22]; 944.7 [15]; 956.19 [23]; 955.52 [24]; 955.53 [25]; 955.54 [32]
101.3	319.0	954 [19]
101.3	322.0	951 [19]
101.3	322.8	951.3 [4]
101.3	323.0	950 [19]
101.3	323.15	949.22 [22]; 940.9 [15]; 951.75 [23]; 951.20 [24]; 952.10 [25]; 951.26 [32]
101.3	324.0	950 [19]
101.3	325.0	949 [19]
101.3	326.0	948 [19]

Table S4.1 (Con't) Previous works on thermophysical properties of pure D2EHPA and TBP.

Thermophysical properties[a]	D2EHPA			TBP		
	p / kPa	T / K	Values	p / kPa	T / K	Values
ρ / $kg \cdot m^{-3}$				101.3	327.0	947 [19]
				101.3	327.9	946.9 [4]
				101.3	328.15	944.88 [22]
				101.3	329.0	945 [19]
				101.3	330.0	944 [19]
				101.3	331.0	943 [19]
				101.3	332.7	942.7 [4]

101.3	334.0	941 [19]
101.3	335.0	940 [19]
101.3	335.45	947.2 [13]
101.3	336.0	939 [19]
101.3	337.0	938 [19]
101.3	337.8	938.5 [4]
101.3	338.0	937 [19]
101.3	339.0	936 [19]
101.3	340.0	936 [19]
101.3	341.0	935 [19]
101.3	342.0	934 [19]
101.3	342.3	934.5 [4]
101.3	347.3	930.9 [4]
101.3	352.2	926.8 [4]
101.3	357.2	922.6 [4]
101.3	360.25	922.6 [13]

Table S4.1 (Con't) Previous works on thermophysical properties of pure D2EHPA and TBP.

Thermophysical properties[a]	D2EHPA			TBP		
	p / kPa	T / K	Values	p / kPa	T / K	Values
ρ / $\mathrm{kg \cdot m^{-3}}$				101.3	393.65	894.1 [13]

L_f / nm	101.3	303.15	0.049418 [8]; 0.05271 [10]; 0.0527 [11]	101.3	298.15	0.0519 [31]
	101.3	308.15	0.050629 [8]	101.3	303.15	0.0531 [31]
	101.3	313.15	0.05177 [18]; 0.051932 [8]	101.3	308.15	0.0544 [31]
	101.3	318.15	0.053166 [8]	101.3	313.15	0.0560 [31]
β_s / $m \cdot s^2 \cdot kg^{-1}$	101.3	303.15	5.6720×10^{10} [8]; 6.222×10^{10} [9]; 6.222×10^{10} [10]	101.3	298.15	63×10^{11} [23]; 64×10^{11} [24, 25]; 0.636×10^{11} [31]
	101.3	308.15	5.8474×10^{10} [8]	101.3	303.15	65×10^{11} [23]; 66×10^{11} [24, 25]; 0.656×10^{11} [31]; 66.365×10^{11} [32]
	101.3	313.15	6.225×10^{10} [18]; 6.0434×10^{10} [8]	101.3	308.15	68×10^{11} [23-25]; 0.675×10^{11} [31]; 68.503×10^{11} [32]
	101.3	318.15	6.2230×10^{10} [8]	101.3	313.15	70×10^{11} [23]; 71×10^{11} [24, 25]; 0.703×10^{11} [31]; 70.716×10^{11} [32]
				101.3	318.15	72×10^{11} [23]; 73×10^{11} [24, 25]; 73.004×10^{11} [32]
				101.13	323.15	74×10^{11} [23]; 75×10^{11} [24, 25]; 75.319×10^{11} [32]
n	101.3	293.15	1.443 [35]	101.3	288.4	1.4260 [4]
				101.3	293.15	1.42496 [13]; 1.4240 [4]; 1.3989 [16]; 1.3993 [14]
				101.32	293.2	1.4235 [17]
				101.3	298.15	1.42252 [26, 27]; 1.4224 [28, 29]
				101.3	298.2	1.4224 [4]
				101.3	303.15	1.4210 [32]

Table S4.1 (Con't) Previous works on thermophysical properties of pure D2EHPA and TBP.

Thermophysical properties[a]	D2EHPA			TBP		
	p / kPa	T / K	Values	p / kPa	T / K	Values
n				101.3	303.3	1.4202 [4]
				101.3	308.15	1.4190 [32]
				101.3	308.2	1.4183 [4]
				101.3	313.15	1.4171 [32]
				101.3	313.4	1.4163 [4]
				101.3	317.9	1.4145 [4]
				101.3	318.15	1.4146 [32]
				101.3	322.6	1.4127 [4]
				101.3	323.15	1.4131 [32]
z / kg · m^{-2} · s^{-1}	101.3	303.15	1.3340×10^{-6} [8]; 1.243×10^{-6} [10]; 1.243×10^{-6} [11]	101.3	298.15	0.124×10^{-6} [31]
	101.3	308.15	1.3132×10^{-6} [8]	101.3	303.15	0.121×10^{-6} [31]; 1.2080×10^{-6} [32]
	101.3	313.15	1.243×10^{-6} [18]; 1.2893×10^{-6} [8]	101.3	308.15	0.119×10^{-6} [31]; 1.1863×10^{-6} [32]
	101.3	318.15	1.2692×10^{-6} [8]	101.3	313.15	0.116×10^{-6} [31]; 1.1650×10^{-6} [32]
				101.3	318.15	1.1441×10^{-6} [32]
				101.3	323.15	1.1238×10^{-6} [32]

CHULALONGKORN UNIVERSITY

v / cm^3 · mol^{-1}	101.3	303.15	319.427 [8]; 337.164 [12]	101.3	298.15	273.47 [23]; 273.77 [24]; 274.0 [31]
	101.3	308.15	319.712 [8]	101.3	303.15	274.72 [23]; 274.99 [24]; 275.2 [31]
	101.3	313.15	320.953 [8]; 336.6001 [12]	101.3	308.15	275.97 [23]; 276.22 [24]; 276.1 [31]
	101.3	318.15	321.593 [8]	101.3	313.15	277.24 [23]; 277.46 [24]; 277.8 [31]

Table S4.1 (Con't) Previous works on thermophysical properties of pure D2EHPA and TBP.

Thermophysical properties[a]	D2EHPA			TBP		
	p / kPa	T / K	Values	p / kPa	T / K	Values
v / cm^3 · mol^{-1}	101.3	323.15	339.257 [12]	101.3	318.15	278.52 [23]; 278.72 [24]
	101.3	333.15	341.956 [12]	101.3	323.15	279.82 [23]; 279.98 [24]
α / K^{-1}	101.3	313.15	7.7×10^{-4} [12]	101.3	298.15	8.85×10^{-4} [24]
	101.3	323.15	7.8×10^{-4} [12]	101.3		8.9247×10^{-4} [32]
	101.3	333.15	7.9×10^{-4} [12]			
p / kPa		428	0.0019998 [36]		273	0.000004 [37]; 0.000002 [38]; 0.000001 [39]; 0.000002 [40]; 0.000002 [41]; 0.000001 [42]
		482.15	1 [1]		273.15	0.000004 [43]
		625.15	101.3 [44]		278	0.00001 [37]; 0.000003 [38]; 0.000001 [39]; 0.000004 [40]; 0.000003 [41]; 0.000002 [42]
		533.15	101.3 [45]		278.15	0.00001 [43]

	283	0.000018 [37]; 0.000006 [38]; 0.000003 [39]; 0.00007 [40]; 0.000006 [41]; 0.000004 [42]
	288	0.00004 [37]; 0.000010 [38]; 0.000005 [39]; 0.000012 [40]; 0.000010 [41]; 0.000007 [42]
	288.15	0.00004 [43]
	293	0.000077 [37]; 0.000018 [38]; 0.000009 [39]; 0.000021 [40]; 0.000018 [41]; 0.000012 [42]
	298	0.00015 [37]; 0.000031 [38]; 0.000015 [39]; 0.000036 [40]; 0.000030 [41]; 0.000022 [42]
	298.15	0.000149 [43]

Table S4.1 (Con't) Previous works on thermophysical properties of pure D2EHPA and TBP.

Thermophysical properties[a]	D2EHPA			TBP		
	p / kPa	T / K	Values	p / kPa	T / K	Values
p / kPa					303	0.000278 [37]; 0.000053 [38]; 0.000026 [39]; 0.000061 [40]; 0.000051 [41]; 0.000037 [42]
					308	0.00039 [37]; 0.000088 [38]; 0.000045 [39]; 0.000101 [40]; 0.000085 [41]; 0.000062 [42]
					308.15	0.000389 [43]
					313	0.000871 [37]; 0.000144 [38]; 0.000075 [39]; 0.000164 [40]; 0.000140 [41]; 0.000103 [42]
					323	0.00159 [37]
					323.15	0.00159 [43]

338	0.00717 [37]
338.15	0.00716 [43]
353	0.0319 [37]
411.65	0.799 [13]; 0.800 [43]
418.15	1.07 [43]
426.15	1.47 [43]
443	1.042 [38]; 0.927 [39]; 1.109 [40]; 1.060 [41]; 0.993 [42]
453.15	3 [1]
455.15	4.67 [43]
458	2.122 [38]; 1.646 [39]; 2.179 [40]; 2.080 [41]; 1.849 [42]
469.15	6.66 [43]
473	4.442 [38]; 3.030 [39]; 4.408 [40]; 4.102 [41]; 3.559 [42]
484.15	13.3 [43]
500.15	20.0 [43]

Table S4.1 (Con't) Previous works on thermophysical properties of pure D2EHPA and TBP.

Thermophysical properties[a]	D2EHPA			TBP		
	p / kPa	T / K	Values	p / kPa	T / K	Values
p / kPa					529	101.3 [46]
					558.60	101.3 [47]
					561.34	101.3 [47]
					562	101.3 [48]

					562.15	101.3 [14, 43]
					817.04	4371 [43]
η / mPa · s^{-1}	101.3	293.15	34.77 [3]	101.3	288.15	4.304 [5]
	101.3	303.15	186.921 [2]; 186.9211 [6]; 21.22 [7]; 19.288 [9-11]; 20.26 [12]	101.3	292.88	3.8156 [4]
	101.3	308.15	148.745 [2, 6]	101.3	293.0	3.882 [19]
					293.15	3.770 [5]
	101.3	313.15	124.1 [1]; 112.462 [2]; 112.4621 [6]; 13.315 [7]; 19.3 [18]; 16.32 [12]	101.3	294.0	3.797 [19]
	101.3	318.15	96.204 [2]; 96.2042 [6]	101.3	295.0	3.708 [19]
	101.3	323.15	8.559 [7, 12]	101.3	296.0	3.614 [19]
	101.3	333.15	56.8 [1]; 5.830 [7, 12]	101.3	297.0	3.521 [19]
	101.3	343.15	4.089 [7]	101.3	298.0	3.429 [19]; 3.388 [20]
	101.3	353.15	29.21 [1]	101.3	298.15	3.388 [21]; 3.3440 [4]; 3.399 [22]; 3.341 [5]; 3.32; 3.377 [31]; 3.45 [46]
				101.3	299.0	3.340 [19]
				101.3	300.0	3.255 [19]
				101.3	301.0	3.171 [19]
				101.3	302.0	3.091 [19]

Table S4.1 (Con't) Previous works on thermophysical properties of pure D2EHPA and TBP.

Thermophysical properties[a]	D2EHPA			TBP		
	p / kPa	T / K	Values	p / kPa	T / K	Values
η / mPa · s^{-1}				101.3	303.0	3.016 [19]; 2.970 [20, 33]
				101.3	303.15	2.970 [21]; 2.9726 [4]; 3.012 [22]; 2.969 [5]; 3.021 [31]
				101.3	304.0	2.944 [19]
				101.3	305.0	2.876 [19]
				101.3	306.0	2.811 [19]
				101.3	307.0	2.749 [19]
				101.3	308.0	2.691 [19]; 2.680 [20, 33]
				101.3	308.15	2.680 [21]; 2.6603 [4]; 2.702 [22]; 2.651 [5]; 2.698 [31]
				101..3	309.0	2.635 [19]
				101.3	310.0	2.583 [19]
				101.3	311.0	2.533 [19]
				101.3	312.0	2.485 [19]
				101.3	313.0	2.440 [19]; 2.430 [20, 33]
				101.3	313.15	2.5 [1]; 2.430 [21]; 2.4027 [4]; 2.441 [22]; 2.423 [31]
				101.3	314.0	2.397 [19]
				101.3	315.0	2.356 [19]
				101.3	316.0	2.317 [19]
				101.3	317.0	2.280 [19]
				101.3	318.0	2.245 [19]; 2.210 [20, 33]
				101.3	318.15	2.210 [21]; 2.1757 [4]; 2.220 [22]
				101.3	319.0	2.211 [19]

CHULALONGKORN UNIVERSITY

				101.3	320.0	2.179 [19]
				101.3	321.0	2.148 [19]

Table S4.1 (Con't) Previous works on thermophysical properties of pure D2EHPA and TBP.

Thermophysical properties[a]	D2EHPA			TBP		
	p / kPa	T / K	Values	p / kPa	T / K	Values
η / mPa · s^{-1}				101.3	322.0	2.119 [19]
				101.3	322.92	1.9734 [4]
				101.3	323.0	2.091 [19]
				101.3	323.15	2.022 [22]
				101.3	324.0	2.064 [19]
				101.3	325.0	2.038 [19]
				101.3	326.0	2.013 [19]
				101.3	327.0	1.989 [19]
				101.3	327.89	1.8038 [4]
				101.3	328.0	1.966 [19]
				101.3	328.15	1.842 [22]
				101.3	329.0	1.944 [19]
				101.3	330.0	1.923 [19]
				101.3	331.0	1.903 [19]
				101.3	332.0	1.883 [19]
				101.3	333.0	1.865 [19]
				101.3	333.15	1.8 [1]; 1.6576 [4]

CHULALONGKORN UNIVERSITY

				101.3	334.0	1.846 [19]
				101.3	335.0	1.829 [19]
				101.3	336.0	1.812 [19]
				101.3	337.0	1.796 [19]
				101.3	338.0	1.780 [19]
				101.3	338.30	1.5164 [4]

Table S4.1 (Con't) Previous works on thermophysical properties of pure D2EHPA and TBP.

Thermophysical properties[a]	D2EHPA			TBP		
	p / kPa	T / K	Values	p / kPa	T / K	Values
η / mPa · s^{-1}				101.3	339.0	1.765 [19]
				101.3	340.0	1.750 [19]
				101.3	341.0	1.736 [19]
				101.3	342.0	1.722 [19]
				101.3	343.28	1.4012 [4]
				101.3	348.09	1.3039 [4]
				101.3	353.15	1.35 [1]; 1.2001 [4]
				101.3	359.05	1.1212 [4]
u / m · s^{-1}	101.3	303.15	1,321.6 [8]; 1,293 [9]; 1,293 [10]; 1,293 [11]; 1,293 [49]	101.3	298.15	1272 [23, 31]; 1265 [24, 25]; 1264.4 [32]
	101.3	308.15	1,302.2 [8]	101.3	303.15	1255 [23, 31]; 1248 [24, 25]; 1247.4 [32]; 1240 [50]

101.3	313.15	1,293 [18]; 1283.4 [8]
101.3	318.15	1266.0 [8]

101.3	308.15	1238 [23]; 1231 [24]; 1232 [25]; 1239 [31]
101.3	313.15	1221 [23]; 1214 [24]; 1215 [25]; 1218 [31]; 1230.5 [32]
101.3	318.15	1204 [23]; 1198 [24, 25]; 1213.8 [32]
101.3	323.15	1188 [23]; 1181 [24]; 1182 [25]; 1197.3 [32]

[a] ρ = Density; L_f = Intermolecular free length; β_s = Isentropic (or adiabatic) compressibility; n = Refractive index; z = Specific acoustic impedance; v = Specific volume; α = Thermal expansion coefficient; p = Vapor pressure; η = Dynamic Viscosity; u = Ultrasonic velocity.

CHULALONGKORN UNIVERSITY

Table S4.2 Calibration results of temperature T measurements.

Immersion Depth (mm)	Standard Temperature (°C)	UUC Reading (°C)	Error (°C)	Uncertainty of Measurement (±°C)
120	0.0025	0.025	0.0225	0.060
120	37.8071	37.827	0.0199	0.060
120	39.9926	40.018	0.0254	0.060
120	60.0051	60.026	0.0209	0.060
120	100.0018	100.018	0.0162	0.060
120	149.9988	150.017	0.0182	0.060
120	200.0033	200.035	0.0317	0.060

Table S4.3 Calibration results of pressure p measurements.

Reagent	Standard Condition		UUC Reading		Error	
	T (K)	p (kPa)	T (K)	p (kPa)	T (K)	p (kPa)
Toluene	383.15	101.30	383.35	101.29	0.10	0.01
n-Hexadecane	149.2	0.67	149.3	0.67	0.10	0.00

จุฬาลงกรณ์มหาวิทยาลัย
CHULALONGKORN UNIVERSITY

Table S4.4 Repeatability (r), Reproducibility (R) and standard uncertainty $u(p)$ of vapor pressure measurement.

p_{sat} (kPa)	r (kPa)	R (kPa)	$u(p)$ (kPa)
0.13	0.01	0.01	0.01
0.27	0.01	0.02	0.02
0.40	0.01	0.02	0.02
0.53	0.01	0.02	0.03
0.67	0.01	0.02	0.03
0.80	0.01	0.02	0.03
0.93	0.01	0.03	0.04
1.07	0.01	0.03	0.04
1.20	0.01	0.03	0.05
1.33	0.01	0.03	0.05
1.73	0.02	0.06	0.06
2.00	0.02	0.06	0.07
2.40	0.02	0.06	0.08
2.67	0.03	0.07	0.09
3.07	0.03	0.07	0.10
3.33	0.03	0.07	0.11
3.73	0.04	0.09	0.12
4.00	0.04	0.09	0.13
4.40	0.04	0.09	0.14
4.67	0.05	0.11	0.15
5.07	0.05	0.11	0.16
5.33	0.05	0.11	0.17
5.73	0.06	0.13	0.18
6.00	0.06	0.13	0.19
6.40	0.06	0.13	0.20
6.67	0.07	0.15	0.21

จุฬาลงกรณ์มหาวิทยาลัย
CHULALONGKORN UNIVERSITY

4.8.1 References for the supplementary information

[1] G.H. Hartel, Low-volatility polar organic solvents for sulfur dioxide hydrogen sulfide and carbonyl sulfide, J. Chem. Eng. Data 30 (1985) 57-61.

[2] N. Swain, S.K. Singh, D. Panda, V. Chakravortty, Viscosities and densities of ternary liquid mixtures of DEHPA, benzene and ortho-xylene, J. Mol. Liq. 85 (2000) 321-330.

[3] W. Shuo, Q. Wei, D. Youyuan, Separation of oil phase from dilute oil/water emulsion in confined space apparatus, Chin. J. Chem. Eng. 20 (2012) 239-245.

[4] L.D. Lorenzi, M. Fermeglia, G. Torriano, Density, refractive index, kinematic viscosity of diesters and triesters, J. Chem. Eng. Data 42 (1997) 919-923.

[5] S. Fang, C.X. Zhao, C.H. He, Densities and viscosities of binary mixtures of tri-n-butyl phosphate + cyclohexane, + n-heptane at T = (288.15, 293.15, 298.15, 303.15, and 308.15) K, J. Chem. Eng. Data 53 (2008) 2244-2246.

[6] N. Swain, S.K. Singh, D. Panda, V. Chakravortty, Viscosities, densities and excess properties of binary mixtures of di-(2-ethyl hexyl) phosphoric acid (DEHPA) with benzene, toluene and ortho-xylene, J. Mol. Liq. 94 (2001) 233-248.

[7] L.R. Koekemoer, M.J.G. Badenhorst, R.C. Everson, Determination of viscosity and density of di-(2-ethylhexyl) phosphoric acid + aliphatic kerosene, J. Chem. Eng. Data 50 (2005) 587-590.

[8] M. Sujata, P. Rita, Ultrasonic and theoretical study of binary mixture of two polar liquids at different temperatures, Res. J. Chem. Sci. 3 (2013) 24-31.

[9] B. Dalai, S.K. Dash, S.K. Singh, Viscometric, volumetric and acoustic properties of binary mixtures of a nuclear extractant with monocarboxylic acids (C1-C3) at 303.15 K, Indian J. Pure Appl. Phys. 52 (2014) 24-29.

จุฬาลงกรณ์มหาวิทยาลัย
CHULALONGKORN UNIVERSITY

[10] B. Dalai, S.K. Dash, S.K. Singh, B.B. Swain, 1H NMR and acoustic response of binary mixtures of an organophosphorous extractant with 1-alkanols (C1–C4, C8), J. Mol. Liq. 208 (2015) 151–159.

[11] B. Dalai, S.K. Dash, S.K. Singh, N. Swain, B.B. Swain, Ultrasonic and 31P NMR investigations of an acidic nuclear extractant with some monosubstituted benzenes, J. Chem. Thermodyn. 93 (2016) 143–150.

[12] W. Srirachat, T. Wannachod, U. Pancharoen, S. Kheawhom, Effect of polarity and temperature on the binary interaction between D2EHPA extractant and organic solvents (kerosene, n-heptane, chlorobenzene and 1-octanol): Experimental and thermodynamics," Fluid Phase Equilib. 434 (2017) 117-129.

[13] A.I. Vogel, D.M. Cowan, Physical properties and chemical constitution VII. Alkyl sulfides, disulfides, sulfites, sulfates, and orthophosphates, J. Chem. Soc. (1943) 16-24.

[14] J.A. Dean, Lange's Handbook of Chemistry, 15th ed., McGraw-Hill Book Co., 1999.

[15] J. Wang, C. Li, C. Shen, Z. Wang, Towards understanding the effect of electrostatic interactions on the density of ionic liquids, Fluid Phase Equilib. 279 (2009) 87-91.

[16] S. Mo, J. Li, Y. Jin, J. Luo, X. Jia, X. Chen, Liquid-liquid equilibrium of 1-butanol + water +tri-n-butyl phosphate + ammonium chloride system, Fluid Phase Equilib. 378 (2014) 73-77.

[17] A. Senol, M. Lalikoglu, M. Bilgin, Modeling extraction equilibria of butyric acid distributed between water and tri-n-butyl amine/diluent or tri-n-butyl phosphate/diluent system: Extension of the LSER approach, Fluid Phase Equilib. 385 (2015) 153-165.

[18] B. Dalai, S.K. Dash, S.K. Singh, N. Swain, B.B. Swain, Physico-chemical properties of di-(2-ethylhexyl) phosphoric acid with apolar solvents from ultrasonic studies, Phys. Chem. Liq. 50 (2012) 242-253.

จุฬาลงกรณ์มหาวิทยาลัย
CHULALONGKORN UNIVERSITY

[19] S. Kannan, K. Kishore, Absolute viscosity and density of trisubstituted phosphoric esters, J. Chem. Eng. Data 44 (1999) 649-655.

[20] N. Swain, D. Panda, S.K. Singh, V. Chakravortty, Viscosity and density of tri-n-butyl phosphate + benzene + o-xylene from 30 oC to 45 oC," J. Chem. Eng. Data 42 (1997) 1235-1237.

[21] N. Swain, Viscosity and density of tri-n-butyl phosphate + benzene + toluene from 30 °C to 45 °C, J. Chem. Eng. Data 44 (1999) 32-34.

[22] Q. Tian, H. Liu, Densities and viscosities of binary mixtures of tributyl phosphate with hexane and dodecane from (298.15 to 328.15) K, J. Chem. Eng. Data 52 (2007) 892-897.

[23] M.A. Basu, T. Samanta, D. Das, Volumetric and acoustic properties of binary mixtures of tri-n-butyl phosphate with n-hexane, cyclohexane, and n-heptane from T = (298.15 to 323.15) K, J. Chem. Thermodyn. 57 (2013) 335-343.

[24] M.A. Basu, T. Samanta, D. Das, Volumetric and compressibility studies on tri-n-butyl phosphate (TBP)-phase modifier (1-octanol, 1-decanol and isodecanol) interactions from T = (298.15 to 323.15) K, J. Chem. Thermodyn. 70 (2014) 1-12.

[25] M.A. Basu, T. Samanta, D. Das, Thermodynamics of mixing for binary mixtures of 1-octanol and 1-decanol with n-dodecane and ternary mixture of (TBP + 1-octanol + dodecane) at T = (298.15 to 323.15) K, J. Chem. Thermodyn. 90 (2015) 158-168.

[26] J.I. Kim, Y.Y. Choi, S.J. Park, Solid-liquid equilibria, excess molar volumes, and molar refractivity deviations for extractive solvents of molybdenum, J. Chem. Eng. Data 55 (2010) 1179-1185.

[27] Y.Y. Choi, I.C. Hwang, S.H. Shin, S.J. Park, Liquid-liquid equilibria, excess molar volume and deviations of the refractive indices at 298.15 K for mixtures of solvents used in themolybdenum extraction process, Fluid Phase Equilib. 354 (2013) 59-65.

CHULALONGKORN UNIVERSITY

[28] S. Shin, S.J. Park, Y.Y. Choi, Liquid-liquid equilibria for aqueous sulfuric acid solutions with undecane, dodecane, or 1-dodecanol, trioctylamine or tributyl phosphate and excess and deviation properties for sub-binary systems at 298.15 K, Fluid Phase Equilib. 343 (2013) 36-42.

[29] J.I. Kim, S.J. Park, S.B. Kim, Y.Y. Choi, The liquid–liquid equilibria for low pH aqueous acid solution + tri-octylamine (or tri-butylphosphate) + 1-decane and the binary and ternary excess molar volumes and deviations of the refractive indices, Fluid Phase Equilib. 314 (2012) 7– 12.

[30] A.K. Pyartman, V.A. Keskinov, V.V. Lishuk, Y.A. Reshetko, Phase equilibria in the liquid ternary system [Th(NO3)4(TBP)2]-[Gd(NO3)3(TBP)3]-TBP-isooctane at different temperatures, Zh. Prikl. Khim. (Leningrad) 80 (2007) 907-910.

[31] M. Mishra, U.N. Dash, N. Swain, Acoustical and thermo dynamical studies of binary liquid mixtures of tri-n-butyl phosphate and benzene at different temperatures, J. Chem. Pharm. Res. 8 (2016) 909-914.

[32] M.N. Hossain, M.M.H. Rocky, S. Akhtar, Density, refractive index, and sound velocity for the binary mixtures of tri-n-butyl phosphate and n-butanol between 303.15 K and 323.15 K, J. Chem. Eng. Data 61 (2016) 124-131.

[33] N. Swain, D. Panda, S.K. Singh, V. Chakrovortty, Viscosities and densities of binary liquid mistures of TBP with benzene, toluene and ortho-xylene, J. Mol. Liq. 75 (1998) 211-218.

[34] L. Tsimering, A.S. Kertes, Excess enthalpies of tri-n-butylphosphate + hydrocarbons, J. Chem. Thermodyn. 6 (1974) 411-415.

[35] Technical Information: Baysolvex® D2EHPA [Online].

[36] D.R. Lide, CRC Handbook of Chemistry and Physics, 86 th ed., CRC Press, Boca Raton: , Taylor & Francis, 2005.

[37] W.G. Skene, M.E. Krzymien, Vapor pressure of tri-n-butyl phosphate, J. Chem. Eng. Data 40 (1995) 394-397.

จุฬาลงกรณ์มหาวิทยาลัย
Chulalongkorn University

[38] E. Hammer, A.L. Lydersen, The vapour pressure of di-n-butylphthalate, di-n-butylsebacate, lauric acid and myristic acid, Chem. Eng. Sci. 7 (1967) 66-72.

[39] E.S. Perry, W.H. Weber, Vapor pressures of phlegmatic liquids. II. High molecular weight esters and silicone oils, J. Am. Chem. Soc. 71 (1949) 3726-3730.

[40] P.A. Small, K.W. Small, P. Cowley, The vapour pressures of some high boiling esters, Trans. Faraday Soc. 44 (1948) 810-816.

[41] J.A. Dean, Lange's Handbook ofchemistry, 13 ed., McGraw-Hill, New York, 1985.

[42] Perry's Chemical Engineers' Handbook, 6th ed., McGraw-Hill, New York, 1984.

[43] S. Kumar, U.K. Mudali, R. Natarajan, PVT properties of PUREX/UREX solvent tri-n-butyl phosphate, J. Radioanal. Nucl. Chem. 289 (2011) 587–589.

[44] S. Kumar, S. Balasubramonian, D. Sivakumar, U.K. Mudali, R. Natarajan, PVT properties of di-(2-ethyl hexyl) phosphoric acid, J. Radioanal. Nucl. Chem. 289 (2011) 883-884.

[45] T. Wongsawa, N. Sunsandee, A.W. Lothongkum, U. Pancharoen, S. Phatanasri, The role of organic diluents in the aspects of equilibrium, kinetics and thermodynamic model for silver ion extraction using an extractant D2EHPA, Fluid Phase Equilib. 388 (2015) 22-30.

[46] M. Huang, B. Zhong, J. Li, Viscosity of the tributyl phosphate + methyl isobutyl ketone + phosphoric acid system, J. Chem. Eng. Data 53 (2008) 2029-2032.

[47] K. Panneerselvam, M.P. Antony, T.G. Srinivasan, P.R.V. Rao, Estimation of normal boiling points of trialkyl phosphates using retention indices by gas chromatography, Thermochim. Acta 511 (2010) 107-111.

[48] R.S. Edmundson, Dictionary of Organophosphorus Compounds, New York, London, Chapman and Hall Ltd., 1988.

[49] R.K. Mishra, B. Dalai, N. Swain, S.K. Dash, Prediction of ultrasonic velocity in binary mixtures of a nuclear extractant and monocarboxylic acids using several theoretical models, IJETT 41 (2016) 304-308.

[50] K. Tiwari, C. Patra, S. Padhy, V. Chakravortty, Molecular interaction study on binary mixtures of dimethyl sulphoxide + isobutyl methyl ketone (IBMK), + acetylacetone and + tri-n-butylphosphate (TBP) from the excess properties of ultrasonic velocity, viscosity and density, Phys. Chem. Liq. 32 (1996) 149-157.

4.9 Acknowledgements

This work was supported by the Research and Researcher for Industry (RRI) of Thailand Research Fund (TRF) grant number PHD60I0050 as well as partially supported by Mektec Manufacturing corporation (Thailand) Ltd. together with the Mass Separation Laboratory, Department of Chemical Engineering, Chulalongkorn University.

4.10 References

[1] G. H. Hartel, "Low-Volatility Polar Organic Solvents For Sulfur Dioxide Hydrogen Sulfide And Carbonyl Sulfide," J. Chem. Eng. Data, vol. 30, pp. 57-61, 1985.

[2] L. L. Burger and E.D. McClanahan, Gamma Radiol. , vol. 50, pp. 153-154, 1958.

[3] C. Musikas, W. W. Schulz, and J. O. Liljenzin, Solvent Extraction in Nuclear Science and Technology. In Solvent Extraction Principles and Practice, 2nd ed. New York: Marcel Dekker, 2004.

[4] K. C. Sole, Solvent Extraction in the Hydrometallurgical Processing and Purification of Metals: Process Design and Selected Applications. In Solvent Extraction and Liquid Membranes: Fundamentals and Applications in New Materials. Boca Raton, FL 33487-2742: CRC Press, 2008.

จุฬาลงกรณ์มหาวิทยาลัย
CHULALONGKORN UNIVERSITY

[5] D. R. Woods, A. N. Hrymak, and J. R. Couper, Conceptual Process Design, Process Improvement, and Troubleshooting. In Albright's Chemical Engineering Handbook. Boca Raton, FL 33487-2742: CRC Press, 2009.

[6] R. B. Evans and D. Harris, "Hydrocarbon Mixture Containing Two Concentrations of Heptanes and Heavier Fraction," J. Chem. Eng. Data, vol. 1, pp. 45-50, 1956.

[7] R. S. DePablo, "Determination of saturated vapor pressure in range 10-1-10-4 torr by effusion method," J. Chem. Eng. Data, vol. 21, pp. 141-143, 1976.

[8] K. Aim, "Saturated Vapor Pressure Measurements on Isomeric Mononitrotoluenes at Temperatures between 380 and 460 K," J. Chem. Eng. Data, vol. 39, pp. 591-594, 1994.

[9] V. Roháč, V. Růžička, K. Růžička, and K. Aim, "Measurements of Saturated Vapor Pressure above the Liquid Phase for Isomeric Dichlorobenzenes and 1,2,4-Trichlorobenzene," J. Chem. Eng. Data, vol. 43, pp. 770-775, 1998.

[10] X. Wu, H. Dong, X. Wang, Z. Zeng, and C. Wu, "Measurement and Correlation of Saturated Vapor Pressure of Ethylphenyldimethoxysilane and Ethylphenyldiethoxysilane," J. Chem. Eng. Data, vol. 60, p. 3106−3112, 2015.

[11] J. G. Brennan, "Evaporation and Dehydration," in Food Processing Handbook, J. G. Brennan, Ed., ed Wienheim: Wiley-VCH, 2006, pp. 71-124.

[12] L. Ribbins, "Distillation Control Variables," in Distillation Control, Optimization, and Tuning, ed Boca Raton, FL 33487-2742: CRC Press, 2011, pp. 7-11.

[13] L. Zhang, Z. Zhang, D. Shen, and M. Lan, "2-Propanol Dehydration via Extractive Distillation Using a Renewable Glycerol−Choline Chloride Deep Eutectic Solvent: Vapor−Liquid Equilibrium," J. Chem. Eng. Data, vol. 62, p. 872−877, 2017.

[14] S. Kumar, S. Balasubramonian, D. Sivakumar, U. K. Mudali, and R. Natarajan, "PVT Properties of Di-(2-Ethyl Hexyl) Phosphoric Acid," J. Radioanal. Nucl. Chem., vol. 289, pp. 883-884, 2011.

[15] T. Wongsawa, N. Sunsandee, A. W. Lothongkum, U. Pancharoen, and S. Phatanasri, "The Role of Organic Diluents in the Aspects of Equilibrium, Kinetics and Thermodynamic Model for Silver Ion Extraction Using an Extractant D2EHPA," Fluid Phase Equilib., vol. 388, pp. 22-30, 2015.

[16] K. Panneerselvam, M. P. Antony, T. G. Srinivasan, and P. R. V. Rao, "Estimation of Normal Boiling points of Trialkyl Phosphates using Retention indices by Gas Chromatography," Thermochim. Acta, vol. 511, pp. 107-111, 2010.

[17] M. Huang, B. Zhong, and J. Li, "Viscosity of the Tributyl Phosphate + Methyl Isobutyl Ketone + Phosphoric Acid System," J. Chem. Eng. Data, vol. 53, pp. 2029-2032, 2008.

[18] R. S. Edmundson, Dictionary of Organophosphorus Compounds. New York, London: Chapman and Hall Ltd., 1988.

[19] J. A. Dean, Lange's Handbook of Chemistry, 15th ed. ed.: McGraw-Hill Book Co,. 1999.

[20] S. Kumar, U. K. Mudali, and R. Natarajan, "PVT Properties of PUREX/UREX Solvent Tri-n-Butyl Phosphate," J. Radioanal. Nucl. Chem., vol. 289, pp. 587–589, 2011.

[21] W. Shuo, Q. Wei, and D. Youyuan, "Separation of Oil Phase from Dilute Oil/Water Emulsion in Confined Space Apparatus," Chin. J. Chem. Eng., vol. 20, pp. 239-245, 2012.

[22] D. R. Lide, CRC Handbook of Chemistry and Physics, 86 th ed. Boca Raton: CRC Press, Taylor & Francis, 2005.

[23] L. D. Lorenzi, M. Fermeglia, and G. Torriano, "Density, Refractive Index, and Kinematic Viscosity of Diesters and Triesters," J. Chem. Eng. Data, vol. 42, pp. 919-923, 1997.

CHULALONGKORN UNIVERSITY

[24] A. I. Vogel and D. M. Cowan, "Physical Properties and Chemical Constitution VII. Alkyl Sulfides, Disulfides, Sulfites, Sulfates, and Orthophosphates," J. Chem. Soc., pp. 16-24, 1943.

[25] J. Wang, C. Li, C. Shen, and Z. Wang, "Towards understanding the effect of electrostatic interactions on the density of ionic liquids," Fluid Phase Equilib., vol. 279, pp. 87-91, 2009.

[26] S. Mo, J. Li, Y. Jin, J. Luo, X. Jia, and X. Chen, "Liquid-liquid equilibrium of 1-butanol + water +tri-n-butyl phosphate + ammonium chloride system," Fluid Phase Equilib., vol. 378, pp. 73-77, 2014.

[27] W. G. Skene and M. E. Krzymien, "Vapor Pressure of Tri-n-butyl Phosphate," J. Chem. Eng. Data, vol. 40, pp. 394-397, 1995.

[28] E. Hammer and A. L. Lydersen, "The vapour pressure of di-n-butylphthalate, di-n-butylsebacate, lauric acid and myristic acid," Chem. Eng. Sci., vol. 7, pp. 66-72, 1967.

[29] E. S. Perry and W. H. Weber, "Vapor Pressures of Phlegmatic Liquids. II. High Molecular Weight Esters and Silicone Oils," J. Am. Chem. Soc., vol. 71, pp. 3726-3730, 1949.

[30] P. A. Small, K. W. Small, and P. Cowley, "The vapour pressures of some high boiling esters," Trans. Faraday Soc., vol. 44, pp. 810-816, 1948.

[31] J. A. Dean, Lange’s Handbook ofchemistry, 13 ed. New York: McGraw-Hill, 1985.

[32] Perry's Chemical Engineers' Handbook 6ed. New York: McGraw-Hill, 1984.

[33] W. Srirachat, T. Wongsawa, N. Sunsandee, U. Pancharoen, and S. Kheawhom, "Phase equilibrium for ternary liquid systems of water + di-(2-ethylhexyl) phosphoric acid + organic diluents: Thermodynamic study," Fluid Phase Equilib., vol. 401, pp. 34-47, 2015.

[34] W. Srirachat, T. Wannachod, U. Pancharoen, and S. Kheawhom, "Effect of polarity and temperature on the binary interaction between D2EHPA extractant

CHULALONGKORN UNIVERSITY

and organic solvents (kerosene, n-heptane, chlorobenzene and 1-octanol): Experimental and thermodynamics," Fluid Phase Equilib., vol. 434, pp. 117-129, 2017.

[35] T. Wongsawa, T. Koonsang, N. Kunthakudee, T. Prapasawat, K. Maneeintr, and U. Pancharoen, "The experimental investigations on viscosity, surface tension, interfacial tension and solubility of the binary and ternary systems for tributyl phosphate (TBP) extractant in various organic solvents with water: Thermodynamic NRTL model and molecular interaction approach," J. Mol. Liq., vol. 251, pp. 229-237, 2018.

[36] "ASTM D1160-15, Standard Test Methods for Distillation of Petroleum Products at Reduced Temperature. ASTM International, , West Conshohocken, PA, 2015, www.astm.org. doi:10.1520/D1160-15."

[37] J. A. Partridge and R. C. Jensen, "Purification of di-(2-ethylhexyl) phosphoric acid by precipitation of copper(II) di-(2-ethylhexyl) phosphate," J. Inorg. Nucl. Chem., vol. 31, pp. 2587-2589, 1969.

[38] C. Antoine, "Vapor Pressure: a new relationship between pressure and temperature," Comptes Rendus des Séances de l'Académie des Sciences, vol. 107, pp. 681–684, 778–780, 836–837, 1888.

[39] L. Riedel, "Eine neue universelle Dampfdruckformel Untersuchungen über eine Erweiterung des Theorems der übereinstimmenden Zustände," Teil I Chem. Ing. Tech. , vol. 26, pp. 83– 89, 1954.

[40] W. Wagner, "New vapour pressure measurements for argon and nitrogen and an new method for establishing rational vapour pressure equations," Cryogenics, vol. 13, pp. 470-482, 1973.

[41] K. S. Pitzer, "The Volumetric and Thermodynamic Properties of Fluids. I. Theoretical Basic and Virial Coefficients," J. Am. Chem. SOC., vol. 77, p. 3427, 1955.

[42] K. S. Pitzer, D. M. Lippmann, R. F. Curl, C. M. Husgins, and D. E. Peterson, "The Volumetric and Thermodynamic Properties of Fluids. II. Compressibility

จุฬาลงกรณ์มหาวิทยาลัย
Chulalongkorn University

Factor, Vapor Pressure and Entropy of Vaporization," J. Am. Chem. SOC., vol. 77, p. 3433, 1956.

[43] W. C. Edmister, "Applied Hydrocarbon Thermodynamics, Part 4: Compressibility Factors and Equations of State," Pet. Refin., vol. 37, p. 173, 1938.

[44] B. I. Lee and M. G. Kesler, "A Generalized Thermodynamic Correlation Based on Three-Parameter Corresponding States," AIChE J., vol. 21, p. 510, 1975.

[45] D. H. Chen, M. V. Dinivahi, and C. Y. Jeng, "New Acentric Factor Correlation Based on the Antoine Equation," Ind. Eng. Chem. Res. , vol. 32, pp. 241-244, 1993.

[46] J. R. ElliottJr., S. J. Suresh, and M. D. Donohue, "A simple equation of state for non-spherical and associating molecules," Ind. Eng. Chem. Res., vol. 29, pp. 1476–1485, 1990.

[47] J. W. Hogge, R. Messerly, N. Giles, T. Knotts, R. Rowley, and W. V. Wilding, "Improving thermodynamic consistency among vapor pressure, heat of vaporization, and liquid and ideal gas isobaric heat capacities through multi-property optimization," Fluid Phase Equilib., vol. 418, pp. 37-43, 2016.

[48] D. McQuarrie, Statistical Mechanics. New York: Harper & Row, 1983.

[49] M. Sujata and P. Rita, "Ultrasonic and Theoretical study of Binary Mixture of two Polar Liquids at Different Temperatures," Res. J. Chem. Sci., vol. 3, pp. 24-31, 2013.

[50] B. Dalai, S. K. Dash, S. K. Singh, N. Swain, and B. B. Swain, "Ultrasonic and 31P NMR investigations of an acidic nuclear extractant with some monosubstituted benzenes," J. Chem. Thermodyn., vol. 93, pp. 143–150, 2016.

[51] N. Swain, S. K. Singh, D. Panda, and V. Chakravortty, "Viscosities, densities and excess properties of binary mixtures of di-(2-ethyl hexyl) phosphoric acid (DEHPA) with benzene, toluene and ortho-xylene," J. Mol. Liq., vol. 94, pp. 233-248, 2001.

[52] R. H. Perry and D. W. Green, Perry's Chemical Engineerings' Handbook. Sydney: McGraw-Hill, 1998.

[53] J. S. Chickos, S. Hosseini, and D. G. Hesse, "Determination of vaporization enthalpies of simple organic molecules by correlations of changes in gas chromatographic net retention times," Thermochim. Acta, vol. 249, pp. 41-62, 1995.

[54] G. Nichols, J. Orf, S. M. Reiter, J. Chickos, and G. W. Gokel, "The vaporization enthalpies of some crown and polyethers by correlation gas chromatography," Thermochim. Acta, vol. 346, pp. 15-28, 2000.

[55] K. Panneerselvam, M. P. Antony, T. G. Srinivasan, and P. R. V. Rao, "Measurement of enthalpies of vaporization of trialkyl phosphates using correlation gas chromatography," Thermochim. Acta, vol. 466, pp. 49-56, 2007.

[56] R. M. Stephenson and S. Malanowski, Handbook of the Thermodynamics of Organic Compounds, 1st ed. 52 Vanderbilt Avenue. New York. New York 10017 Elsevier Science Publishing, 1987.

[57] J. K. Fink, Trouton's Rule in Physical Chemistry in Depth: Springer Berlin Heidelberg, 2009.

จุฬาลงกรณ์มหาวิทยาลัย
CHULALONGKORN UNIVERSITY

CHAPTER V

Isobaric Vapor-Liquid Equilibrium for Binary System Related to the Organophosphoric Extractant of D2EHPA + n-Dodecane and TBP + n-Dodecane at 0.13, 2.40 and 6.67 kPa

Wanchalerm Srirachat[a], Kreangkrai Maneeintr[b], Ura Pancharoen[a,*], Soorathep Kheawhom[a,*]

[a] *Department of Chemical Engineering, Faculty of Engineering, Chulalongkorn University, Patumwan, Bangkok 10330, Thailand*

[b] *Carbon Capture, Storage and Utilization Research Group, Department of Mining and Petroleum Engineering, Faculty of Engineering, Chulalongkorn University, Patumwan, Bangkok 10330, Thailand*

* Corresponding author

This article has been published in Journal: Vacuum.

Volume: 160. Year: 2019. https://doi.org/10.1016/j.vacuum.2018.11.011.

5.1 Graphical abstract

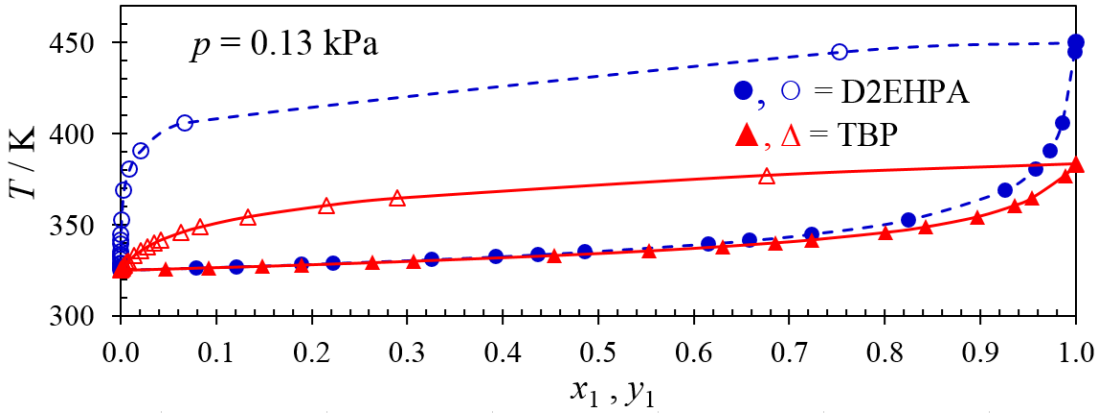

5.2 Abstract

Vacuum distillation is selected as a technique for recycling in order to separate the mixture of a hydrometallurgical organophosphoric extractant from an organic diluent because of their low volatility and high selectivity. The experimental isobaric vapor-liquid equilibrium (VLE) data for the binary systems of di-(2-ethylhexyl) phosphoric acid (D2EHPA) + n-dodecane and tri-butyl phosphate (TBP) + n-dodecane were measured at pressures of 0.13, 2.40 and 6.67 kPa, using a glass vapor-liquid equilibrium ebulliometer. VLE data were generated in the form of $T-x-y$ diagrams and checked for thermodynamic consistency via Herington area test and Van Ness point test. Data for all mixtures met the criteria of thermodynamic consistency and were found suitable for process modeling. At each pressure point, no azeotropic phenomenon was observed. Reduction in pressure of the system can significantly enhance the relative volatility and separation efficiency of both mixtures. At all pressure points, D2EHPA was noted to be more separable than TBP. Additionally, the experimental VLE results for all systems were found to have a good correlation with Raoult's law, Wilson and nonrandom two-liquid (NRTL) models. The corresponding binary interaction parameters were obtained by minimizing the deviation between the experimental and the calculated vapor phase composition and total pressure.

Keywords: D2EHPA; TBP; n-Dodecane; Vapor-liquid equilibrium; Vacuum distillation

5.3 Introduction

At present, di-(2-ethylhexyl) phosphoric acid (D2EHPA) and tributyl phosphate (TBP) are important chemicals usually used as extractants in the reactive separation process of metal ions [1, 2]. One of the most popular diluents is kerosene. After completion of the reactive separation process, organic waste is generated. This waste, containing high boiling point compounds such as D2EHPA or TBP as well as kerosene, is hazardous and difficult to treat before being discharged to the environment. Therefore, more research needs to be done to find a better method to treat the waste.

Both D2EHPA and TBP are organophosphoric extractants which belong to a high polar reactive phosphate group and a large non-polar hydrocarbon chain. These extractants have low volatility and a rating of 3 out of a maximum 4 (health hazard) in accordance with the Hazardous Materials Identification System (HMIS). In the case of kerosene, it is composed of a mixture of petroleum hydrocarbons (C_9 to C_{16}) which can cause adverse health and environmental effects. In this study, n-dodecane (C_{12}), a diluent for TBP in reprocessing plants, was selected as a representative for kerosene. According to ecological considerations, disposal of such hazardous waste should be prevented from entering drains, sewers, streams etc. Thus, one of the remedies for managing waste is via a recovery or recycling process.

Due to the large difference in boiling temperatures between these extractants and organic solvents, separation as carried out by distillation was found to be the most suitable method e.g. as in the industrial treatment of harmful noble lead [3, 4] and

bismuth (Bi) from crude tin (Sn) [5]. Under atmospheric pressure, the boiling points of D2EHPA, TBP and n-dodecane reached 654 K, 569 K, and 489 K respectively. However, at such high temperatures, these compounds will decompose. Thus, they must be carefully distilled under reduced pressure. Regarding the optimum design of distillation equipment, the vapor pressures of pure compounds and VLE data need to be taken into account. A literature survey on thermophysical properties, especially vapor-liquid equilibrium, showed that previously published studies concerning VLE data for the binary systems of D2EHPA + n-dodecane and TBP + n-dodecane are still greatly lacking [6-8]. So, for a more comprehensive study of these organophosphoric extractants, it becomes a necessity to study the VLE of these binary systems.

In this study, the new experimental isobaric VLE data for the binary systems of D2EHPA + n-dodecane and TBP + n-dodecane were determined at pressures of 0.13, 2.40, and 6.67 kPa by a vapor liquid equilibrium apparatus. Besides, the VLE data was verified for thermodynamic consistency by means of the Herington area test and Van Ness point test. Furthermore, the experimental data was correlated by Raoult's law, NTRL and Wilson activity coefficient models. For theoretical research and industrial applications, the obtained VLE data can provide a very important reference for the recycling of reactive extractants and its diluents via the distillation process.

จุฬาลงกรณ์มหาวิทยาลัย
CHULALONGKORN UNIVERSITY

5.4. Experimental

5.4.1 Chemical

The organophosphoric extractants, namely D2EHPA and TBP are commercially available from Merck Co. Anhydrous n-dodecane was acquired from Sigma Aldrich Co. D2EHPA was further purified by extracting $Cu(OH)_2$ into a solution of D2EHPA

and the resulting salt was precipitated with acetone. Then, diluted HCl converts the $Cu(D2EHPA)_2$ salt back to D2EHPA and aqueous Cu(II) [59]. To protect contamination from water, both extractants were kept in a round-bottom flask containing dried molecular sieves and were tightly sealed under inert atmosphere of argon gas. Before being used, the water content of all chemicals was examined by the coulometric Karl Fischer titration method (Mettler Toledo, C30S). Results showed that the water contents were lower than 100 ppm (0.01 % wt.) which were acceptable. The purity of these chemicals was analyzed by gas chromatography (Shimadzu, GC-2010 Plus). The obtained mass fraction purity was applied in stoichiometric calculation. A summary of all chemicals is seen in Table 5.1.

จุฬาลงกรณ์มหาวิทยาลัย
CHULALONGKORN UNIVERSITY

Table 5.1 Chemicals used in this study.

Chemicals	CAS No.	Formula	Molar Mass / $g \cdot mol^{-1}$	Mass fraction Purity[a]	Mass Fraction Purity[b]	Analysis Method	Source	Water Content / Mass Fraction[c]
D2EHPA	298-07-7	$C_{16}H_{35}O_4P$	322.42	> 0.97	0.995±0.002	GC	Merck	0.000060
TBP	126-73-8	$C_{12}H_{27}O_4P$	266.31	> 0.99	0.996±0.001	GC	Merck	0.000040
n-Dodecane	112-40-3	$C_{12}H_{26}$	170.33	> 0.99	0.998±0.001	GC	Sigma Aldrich	0.000004
n-Hexadecane	544-76-3	$C_{16}H_{34}$	226.41	> 0.990	0.995±0.001	GC	Merck	0.000003

[a] Mass-fraction purity data were in certificate of analysis (COA) from manufacturer.

[b] Mass-fraction purity data were measured in this work by gas chromatography (GC) method.

[c] Water content data were measured in this work by coulometric Karl Fischer method.

CHULALONGKORN UNIVERSITY

5.4.2 Apparatus and procedure

The experimental isobaric VLE data were determined by a glass vapor- liquid equilibrium ebulliometer (Fischer Engineering, Labodest ® VLE 602). Details of the VLE apparatus used in this study are described in Fig. 5.1. Briefly, it is composed of a heating cell, an equilibrium cell and two water- cooled condensers/ coolers. Initial samples, approximately 30.0 g, of the binary mixture of extractant + n-dodecane were prepared by mass fraction ranging from 0.01 to 0.90 using an electronic balance (Sartorius, model 11222-546) with a precision of ± 0.0001 g. Then, the obtained samples were loaded into a mixing chamber and vaporized by an electrical immersion heater arranged concentrically in a flow heater. Consequently, the vapor-liquid mixture passes upwards through a lengthened contact path (Cottrell pump) which ensures that the liquid and vapor phases are in intimate contact during boiling. In the separation chamber, the pressure system was fixed at constant. However, temperatures varied. After entering the chamber, the mixture separated into liquid and vapor phase. The temperature was determined by a Pt-100 resistance sensor with an accuracy of ±0.1 K. The desired pressures of 0.13, 2.40 and 6.67 kPa were obtained by a pressure controller and measured with an accuracy of ±0.01 kPa. To safely prevent the carrying over of liquid into the vapor phase and in order to ensure a quick equilibrium adjustment, both vapor and liquid streams flowed once again into a mixing chamber. Then, the heating power of the immersion heater was adjusted to an appropriate level to reach a sufficient reflux rate of the condensed vapor of 1 or 2 drops per second. Once equilibrium was achieved, the temperatures of the vapor and liquid did not vary over 0.1 K for a period of 30 min. After that, the two samples i.e. the liquid and condensed vapor were taken off from the sampling vessel.

จุฬาลงกรณ์มหาวิทยาลัย
CHULALONGKORN UNIVERSITY

To quantify the compositions of D2EHPA, TBP and n-dodecane in the liquid (x_i) phase and condensed vapor (y_i) phase, the Fourier Transform Infrared (FTIR) technique was applied via the spectrometer: *Spectrum One* model of *PerkinElmer Co.* The fingerprint regions of the FTIR spectrum for D2EHPA, TBP and n-dodecane are presented in Figs. S5.1 to S5.3 of the Section 5.7: Supplementary information, respectively. In comparison with the FTIR spectrum of n-dodecane, it can be seen that the characteristic peak of the organophosphoric compounds, D2EHPA and TBP, was the P=O vibration band at wave numbers 1,229 [10] and 1,235 cm^{-1} [11], respectively. These P=O bands were found to be suitable for quantifying the concentrations (mass fraction) of both D2EHPA and TBP mixed with n-dodecane. The calibration curves for calculating the concentrations of the binary mixtures of D2EHPA + n-dodecane and TBP + n-dodecane were plotted between the mass fraction on the x-axis and the peak areas on the y-axis. Then, the obtained mass fractions were used to calculate the mole fractions for each component as in Eqs. (5.1) and (5.2):

$$x_i = \frac{m_i / M_i}{m_i / M_i + m_j / M_j} \tag{5.1}$$

$$y_i = \frac{m_i / M_i}{m_i / M_i + m_j / M_j} \tag{5.2}$$

where x_i, y_i, m_i and M_i are the mole fraction in liquid phase, mole fraction in vapor phase, mass and molar mass of component i, respectively, and i, j are the indices for all components.

The experimental data were repeatedly tested three times with a re-set up of chemicals and equipment. The results were reported as average values with standard

uncertainties of $u(x_i)$ and $u(y_i)$ equal to 0.0009. The standard uncertainty of the experimental values of x_i and y_i as expressed in the respective footnote tables was calculated based on Eq. (5.3) as follows [12]:

$$u(x_i) = \sqrt{\frac{1}{n(n-1)} \sum_{k=1}^{n} \left(X_{i,k} - \frac{1}{n} \sum_{k=1}^{n} X_{i,k} \right)} \tag{5.3}$$

where n is the number of independent observations, $X_{i,k}$ is the input quantity as obtained under the same conditions of measurement and $k = 1, 2, \ldots, n$.

The test method was validated using pure n-dodecane and n-hexadecane as reference chemicals. Details of the verification results of both pure n-dodecane and n-hexadecane compared with the literature data are described in Table 5.2.

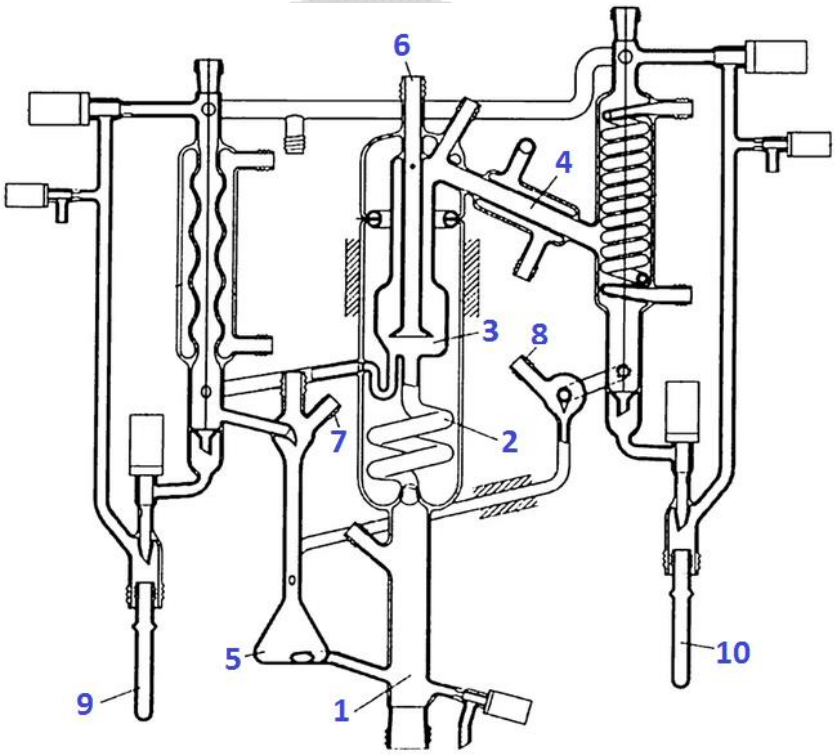

Figure 5.1 Schematic diagram of the experimental glass vapor-liquid equilibrium ebulliometer apparatus: **1** Heating bulb (inside immersion heater and outside flow heater) **2** Cottrell pump **3** Separation Chamber **4** Condenser **5** Mixing chamber **6** Vapor-phase temperature sensor (Pt-100) **7** Liquid-phase sampling point **8** Vapor-phase sampling point **9** Liquid-phase sampling vessel **10** Vapor-phase sampling vessel [13].

Table 5.2 Verification results for distillation temperatures T of n-dodecane and n-hexadecane at system pressure range of p = (0.13 – 6.7) kPa.

p (kPa)	n-Dodecane T (K)			n-Hexadecane T (K)		
	Literature [14]	This work[a]	% Dev.	Literature [15]	This work[a]	% Dev.
0.13	325.4	326.1	0.34	378.5	379.8	0.34
0.67	351.8	352.2	-0.10	407.8	407.4	-0.10
1.3	364.2	364.5	0.17	421.7	422.4	0.17
2.7	379.4	379.0	0.07	438.5	438.8	0.07
5.3	395.0	396.3	0.22	455.8	456.8	0.22
6.7	400.8	401.5	0.13	462.2	461.6	0.13

[a] Standard uncertainty (u): $u(T)/\mathrm{K} = 0.1$ and $u(p)/\mathrm{kPa} = 0.01 + 0.03p$.

จุฬาลงกรณ์มหาวิทยาลัย
Chulalongkorn University

5.5. Results and discussion

5.5.1 Experimental results

The p_{sat} values of the pure components of D2EHPA, TBP and n- dodecane were calculated according to Antoine equation: the constants A, B and C are listed in Table 5.3. Further, the normal boiling temperatures (T_b) of D2EHPA and TBP were calculated by extrapolating to p_{sat} at 101.3 kPa, using Antoine equation, according to Eq. (S5.1) of the Section 5.7: Supplementary information. The calculated T_b of

DEHPA was found to be 654.4 K and the T_b of TBP was 569.1 K. In previous work [16], the T_b of D2EHPA was obtained by the atmospheric distillation method under the pressure of 101.3 kPa and reported as 533 K. Because of high T_b, atmospheric distillation can lead to the decomposition of the D2EHPA molecule. Thus, the measured T_b will be lower. Kumar et al. [17] observed that the T_b of D2EHPA was 625.15 K. This differed from the T_b found in this study by 29.25 K or 4.68%. However, in this study, the T_b of TBP was observed to be 569.1 K. This was found to be close to values as reported in previous works such as those stated by Kumar et al. [18] which measured 562.15 K, Panneerselvam et al. [19] 561.34 K and Edmundson [20] 562 K with a deviation of 1.25 %.

Comparisons of p_{sat} and T_b of pure compounds used in this work (D2EHPA, TBP, n-dodecane and n-hexadecane) with the literature data are provided graphically in Figs. 5.2 to 5.5.

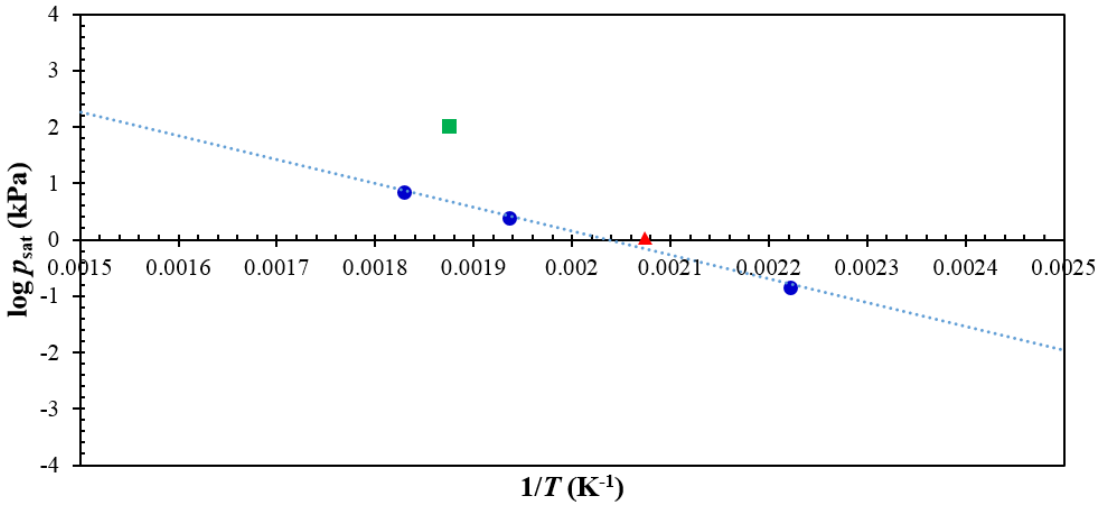

Figure 5.2 Comparison of saturated vapor pressure of pure D2EHPA. ●, this work; ▲ [21]; ■, [16].

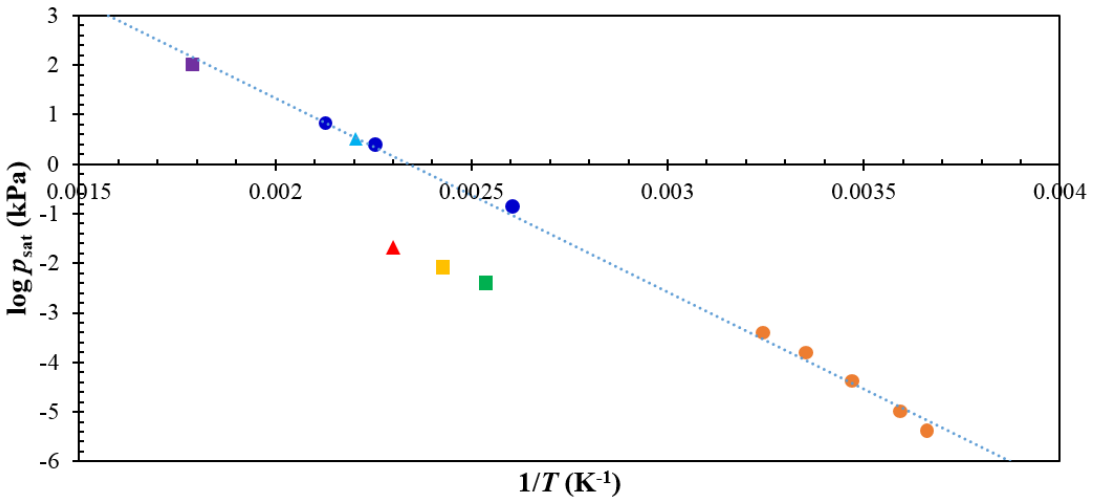

Figure 5.3 Comparison of saturated vapor pressure of pure TBP. ●, this work; ▲, [21]; ■, [22]; ▲, [23]; ■, [24]; ●, [25]; ■, [19].

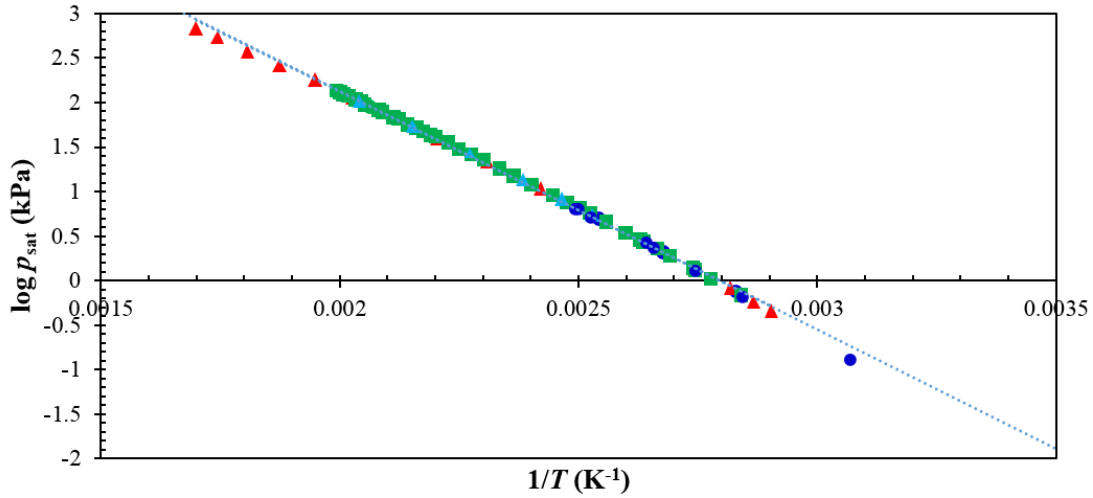

Figure 5.4 Comparison of saturated vapor pressure of pure n-dodecane. ●, this work; ▲, [26]; ■, [27]; ▲, [28].

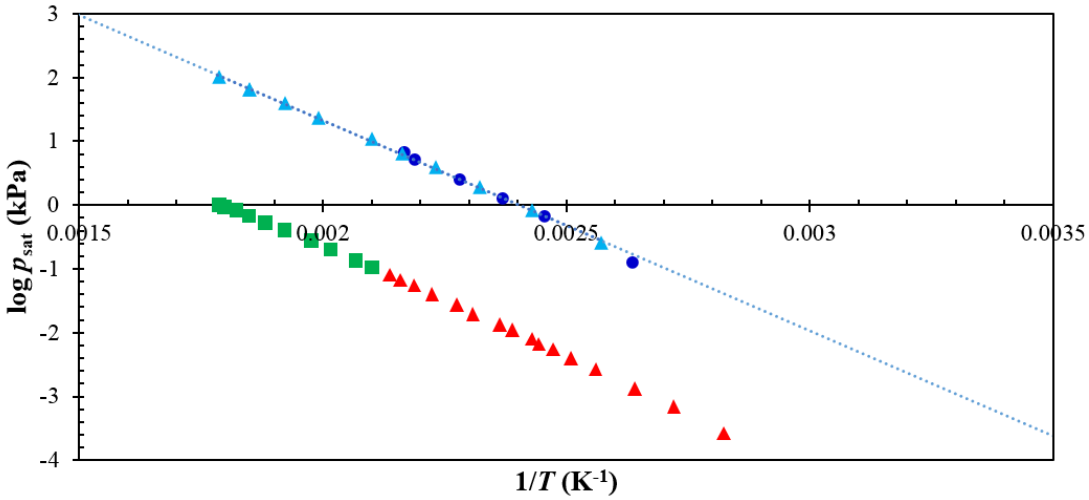

Figure 5.5 Comparison of saturated vapor pressure of pure n-hexadecane. ●, this work; ▲, [29]; ■, [26]; ▲, [15].

Table 5.3 Antoine equation parameters of pure components, namely D2EHPA, TBP and n-dodecane.

Compound	Antoine parameters			Temperature	
	A	B	C	T_{min} (K)	T_{max} (K)
D2EHPA [30]	22.197	5673.9	-122.57	450.5	546.2
TBP [30]	21.669	4749.6	-100.69	383.8	469.9
n-Dodecane [15]	20.966	3743.9	-92.839	325.8	490.5

จุฬาลงกรณ์มหาวิทยาลัย
Chulalongkorn University

The results of the isobaric VLE data for the binary systems of D2EHPA + n-dodecane and TBP + n-dodecane are listed in Tables 5.4 and 5.5 respectively, at pressures of 0.13, 2.40 and 6.67 kPa. The corresponding $T-x-y$ phase diagrams are shown in Figs. 5.6 to 5.8. In both systems, no azeotropic phenomenon was found. Further, the relative volatilities (α_{21}) for both systems were all > 3 which means that n-dodecane could be separated practically from both D2EHPA and TBP by vacuum distillation.

Table 5.4 Isobaric experimental VLE data of liquid phase (x_1) and vapor phase (y_1) mole fractions, activity coefficient (γ_1 and γ_2) of the system D2EHPA (1) + n-dodecane (2) at pressures of 0.13, 2.40 and 6.67 kPa[a]

$p = 0.13$ kPa						$p = 2.40$ kPa						$p = 6.67$ kPa					
T / K	x_1	y_1	γ_1	γ_2	α_{21}	T / K	x_1	y_1	γ_1	γ_2	α_{21}	T / K	x_1	y_1	γ_1	γ_2	α_{21}
325.2	0.0000	0.0000	1.049	1.000		376.5	0.0000	0.0000	1.040	1.000		400.4	0.0000	0.0000	1.036	1.000	
326.4	0.0793	0.0000	1.042	1.000	∞	380.7	0.1729	0.0001	1.029	1.001	2.27×10^{3}	403.0	0.0991	0.0001	1.031	1.000	1.01×10^{3}
327.1	0.1211	0.0000	1.039	1.001	∞	379.2	0.1147	0.0001	1.032	1.000	2.41×10^{3}	404.7	0.1558	0.0002	1.028	1.001	9.55×10^{2}
328.2	0.1895	0.0000	1.034	1.001	∞	381.4	0.1989	0.0001	1.027	1.001	2.22×10^{3}	406.2	0.2039	0.0003	1.025	1.001	9.12×10^{2}
328.9	0.2222	0.0000	1.032	1.002	∞	383.1	0.2586	0.0002	1.024	1.002	2.08×10^{3}	408.5	0.2712	0.0004	1.021	1.002	8.51×10^{2}
331.0	0.3259	0.0000	1.025	1.004	2.87×10^{4}	385.4	0.3311	0.0003	1.020	1.004	1.91×10^{3}	410.7	0.3295	0.0006	1.019	1.003	7.97×10^{2}
332.5	0.3931	0.0000	1.021	1.007	2.62×10^{4}	388.0	0.4033	0.0004	1.017	1.006	1.74×10^{3}	413.5	0.3977	0.0009	1.015	1.005	7.34×10^{2}
333.7	0.4374	0.0000	1.018	1.008	2.44×10^{4}	389.4	0.4392	0.0005	1.015	1.007	1.66×10^{3}	415.6	0.4410	0.0011	1.013	1.006	6.91×10^{2}
335.1	0.4862	0.0000	1.016	1.011	2.25×10^{4}	391.9	0.4964	0.0006	1.012	1.009	1.52×10^{3}	418.7	0.5013	0.0016	1.011	1.008	6.33×10^{2}
339.6	0.6153	0.0001	1.009	1.018	1.74×10^{4}	394.3	0.5459	0.0009	1.010	1.011	1.40×10^{3}	420.7	0.5350	0.0019	1.010	1.010	5.99×10^{2}
341.4	0.6577	0.0001	1.007	1.021	1.57×10^{4}	397.8	0.6085	0.0012	1.008	1.014	1.25×10^{3}	425.8	0.6119	0.0030	1.007	1.013	5.21×10^{2}
344.9	0.7229	0.0002	1.005	1.026	1.30×10^{4}	405.5	0.7127	0.0025	1.004	1.020	9.70×10^{2}	435.7	0.7222	0.0064	1.004	1.019	4.02×10^{2}
352.8	0.8251	0.0005	1.002	1.035	8.58×10^{3}	420.6	0.8361	0.0082	1.001	1.028	6.17×10^{2}	448.9	0.8173	0.0151	1.002	1.024	2.92×10^{2}
369.0	0.9262	0.0031	1.000	1.044	4.00×10^{3}	434.6	0.8998	0.0207	1.001	1.033	4.21×10^{2}	465.6	0.8896	0.0382	1.001	1.029	2.02×10^{2}
380.9	0.9587	0.0093	1.000	1.046	2.43×10^{3}	449.4	0.9382	0.0493	1.000	1.035	2.92×10^{2}	480.6	0.9281	0.0796	1.000	1.030	1.49×10^{2}
390.8	0.9731	0.0212	1.000	1.047	1.66×10^{3}	458.0	0.9531	0.0780	1.000	1.035	2.40×10^{2}	493.6	0.9515	0.1422	1.000	1.031	1.17×10^{2}

406.0	0.9869	0.0669	1.000	1.046	9.83×10^{2}	478.8	0.9779	0.2150	1.000	1.035	1.55×10^{2}	514.6	0.9768	0.3309	1.000	1.031	8.22×10
444.7	0.9990	0.7522	1.000	1.042	3.29×10^{2}	506.0	0.9955	0.6773	1.000	1.034	9.48×10	532.8	0.9916	0.6381	1.000	1.031	6.24×10
450.0	1.0000	1.0000	1.000	1.041		516.2	1.0000	1.0000	1.000	1.033		546.3	1.0000	1.0000	1.000	1.031	

[a] Standard uncertainty (u): $u(x_i) = u(y_i) = 0.0009$, $u(T) = 0.1$ K and $u(p) = 0.01 + 0.03p$ kPa .

Table 5.5 Isobaric experimental VLE data of liquid phase (x_1) and vapor phase (y_1) mole fractions, activity coefficient (γ_1 and γ_2) of the system TBP (1) + n-dodecane (2) at pressures of 0.13, 2.40 and 6.67 kPa[a]

$p = 0.13$ kPa						$p = 2.40$ kPa						$p = 6.67$ kPa					
T / K	x_1	y_1	γ_1	γ_2	α_{21}	T / K	x_1	y_1	γ_1	γ_2	α_{21}	T / K	x_1	y_1	γ_1	γ_2	α_{21}
325.2	0.0000	0.0000		1.000		376.5	0.0000	0.000		1.000		400.4	0.0000	0.0000		1.000	
325.9	0.0475	0.0008	1.308	1.000	58.44	377.9	0.0623	0.0029	1.208	1.000	22.68	402.3	0.0771	0.0051	1.186	1.001	16.28
326.6	0.0921	0.0017	1.290	1.001	58.30	378.9	0.1095	0.0054	1.196	1.001	22.58	404.3	0.1531	0.0111	1.167	1.003	16.14
327.4	0.1484	0.0030	1.267	1.004	58.31	380.5	0.1754	0.0094	1.178	1.004	22.42	405.6	0.2017	0.0154	1.155	1.005	16.07
328.1	0.1898	0.0040	1.251	1.006	58.24	382.1	0.2401	0.0140	1.160	1.007	22.30	406.8	0.2426	0.0196	1.145	1.007	16.01
329.4	0.2630	0.0061	1.221	1.013	58.20	384.4	0.3241	0.0212	1.137	1.015	22.13	410.0	0.3404	0.0315	1.121	1.015	15.84
330.2	0.3067	0.0075	1.204	1.018	58.23	386.4	0.3902	0.0282	1.119	1.023	22.01	412.7	0.4165	0.0433	1.102	1.025	15.73
333.3	0.4541	0.0140	1.146	1.048	58.60	389.3	0.4769	0.0399	1.096	1.039	21.86	415.0	0.4743	0.0544	1.088	1.035	15.65
335.8	0.5532	0.0205	1.108	1.082	59.08	390.4	0.5067	0.0448	1.088	1.045	21.82	416.7	0.5150	0.0637	1.078	1.043	15.60
338.2	0.6308	0.0279	1.081	1.120	59.43	393.1	0.5719	0.0578	1.071	1.063	21.69	418.4	0.5501	0.0729	1.070	1.052	15.53
340.2	0.6856	0.0352	1.063	1.155	59.69	395.6	0.6278	0.0722	1.057	1.082	21.61	422.2	0.6259	0.0975	1.053	1.074	15.43
341.8	0.7237	0.0418	1.051	1.185	59.81	402.0	0.7376	0.1164	1.033	1.134	21.28	427.4	0.7092	0.1376	1.035	1.108	15.26

345.9	0.8014	0.0632	1.029	1.261	59.67	407.1	0.8030	0.1629	1.020	1.178	20.94	434.0	0.7928	0.2023	1.020	1.154	15.02
348.9	0.8433	0.0834	1.019	1.313	59.04	416.6	0.8884	0.2833	1.007	1.252	20.05	440.6	0.8544	0.2847	1.011	1.198	14.70
354.4	0.8979	0.1328	1.009	1.393	56.85	421.1	0.9173	0.3611	1.004	1.282	19.55	451.6	0.9271	0.4752	1.003	1.264	14.03
360.6	0.9360	0.2150	1.004	1.461	53.38	429.9	0.9595	0.5592	1.001	1.330	18.44	460.1	0.9668	0.6792	1.001	1.305	13.42
364.6	0.9540	0.2894	1.002	1.493	50.91	432.3	0.9685	0.6254	1.001	1.341	18.12	462.4	0.9756	0.7464	1.000	1.315	13.25
377.1	0.9892	0.6761	1.000	1.553	43.07	437.4	0.9858	0.7901	1.000	1.362	17.45	467.3	0.9924	0.9058	1.000	1.335	12.89
383.4	1.0000	1.0000	1.000			442.7	1.0000	1.0000	1.000			469.9	1.0000	1.0000	1.000		

[a] Standard uncertainty (u): $u(x_i) = u(y_i) = 0.0009$, $u(T) = 0.1$ K and $u(p) = 0.01 + 0.03p$ kPa.

CHULALONGKORN UNIVERSITY

Table 5.6 Experimental and calculated infinite dilution activity coefficient γ_1^{∞} and γ_2^{∞} for all systems.

	$\gamma_{1,\text{exptl}}^{\infty}$	$\gamma_{2,\text{exptl}}^{\infty}$	$\gamma_1^{\infty,a}$	$\gamma_2^{\infty,a}$	$\gamma_1^{\infty,b}$	$\gamma_2^{\infty,b}$
	$p = 0.13$ kPa					
D2EHPA (1) + n-dodecane (2)	1.050	1.050	1.049	1.072	1.068	1.044
TBP (1) + n-dodecane (2)	1.336	1.530	1.308	2.212	1.368	1.548
	$p = 2.40$ kPa					
D2EHPA (1) + n-dodecane (2)	1.041	1.039	1.040	1.057	1.059	1.028
TBP (1) + n-dodecane (2)	1.233	1.361	1.226	1.675	1.281	1.347
	$p = 6.67$ kPa					
D2EHPA (1) + n-dodecane (2)	1.038	1.035	1.037	1.051	1.057	1.021
TBP (1) + n-dodecane (2)	1.214	1.926	1.208	1.603	1.263	1.308

[a] NRTL, [b] Wilson

จุฬาลงกรณ์มหาวิทยาลัย
CHULALONGKORN UNIVERSITY

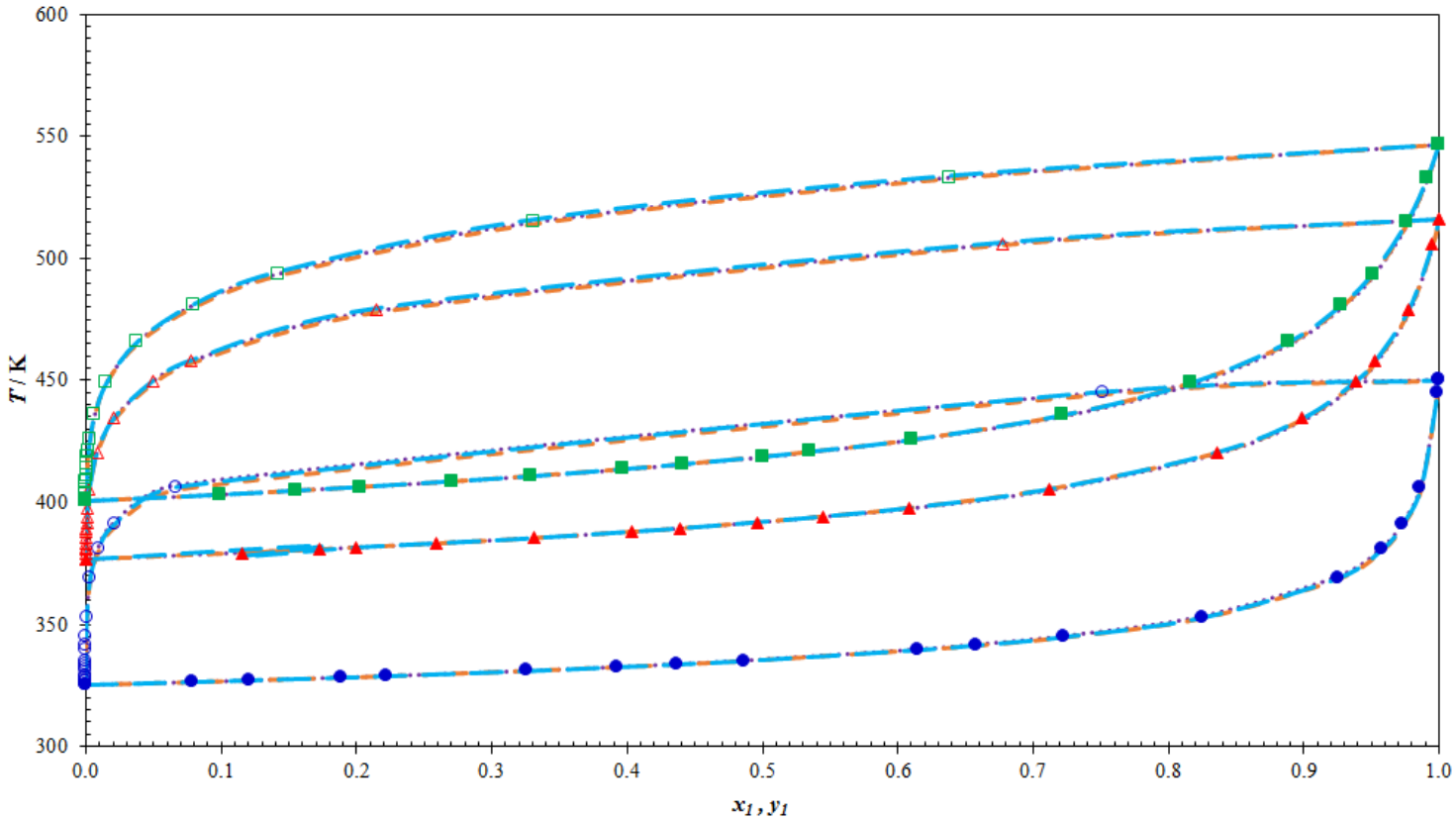

Figure 5.6 VLE phase diagrams for D2EHPA (1) + n-dodecane (2). ●, ▲, ■: experimental data for $T-x$ plot at 0.13, 2.40 and 6.67 kPa, respectively; ○, Δ, □: experimental data for $T-y$ plot at 0.13, 2.40 and 6.67 kPa, respectively; ******: Raoult's law, ▬ ▬ ▬: NRTL, ▬ ▬: Wilson activity coefficient model for $T-x-y$ plots.

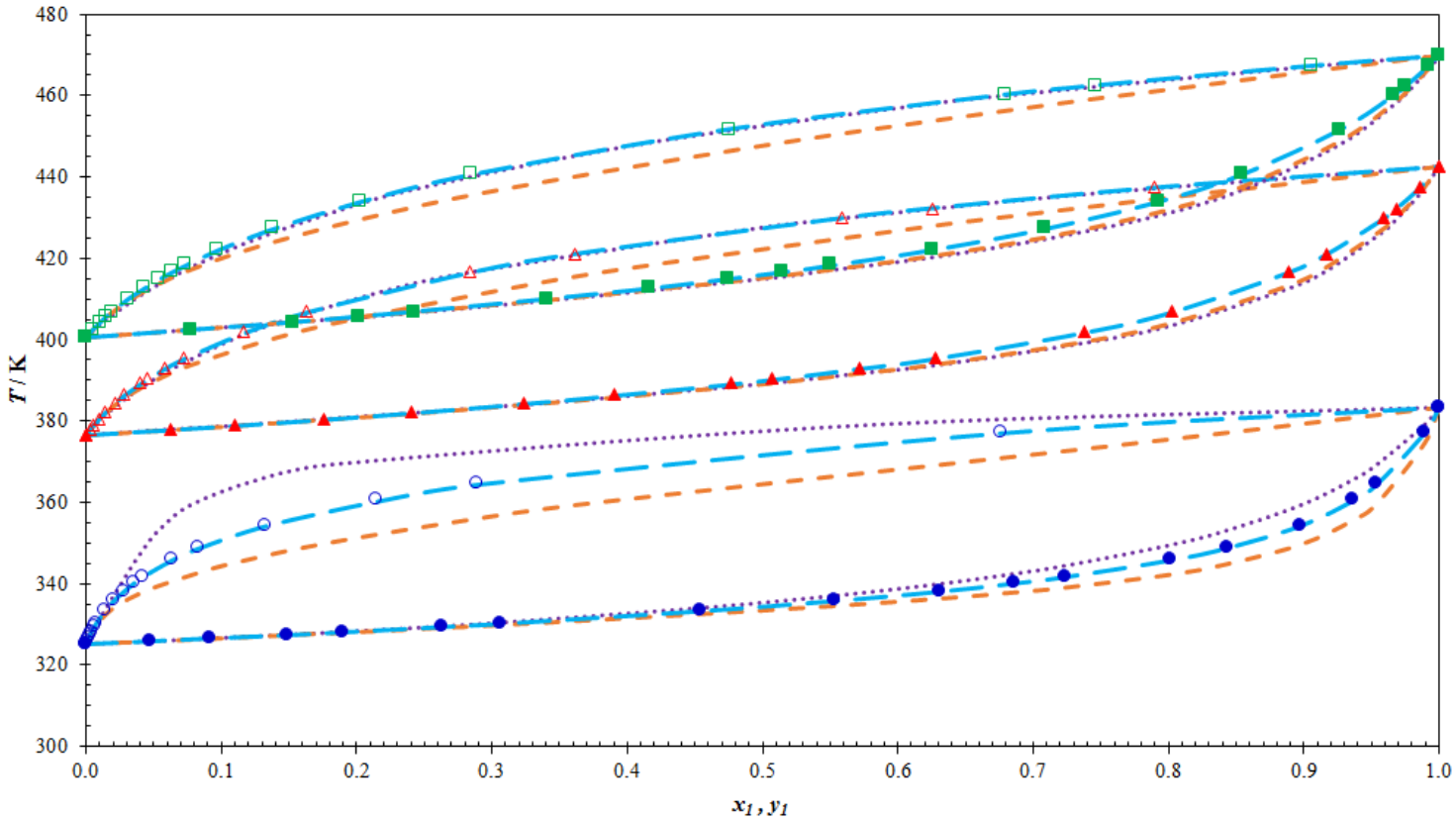

Figure 5.7 VLE phase diagrams for TBP (1) + n-dodecane (2). ●, ▲, ■: experimental data for $T-x$ plot at 0.13, 2.40 and 6.67 kPa, respectively; ○, Δ, □: experimental data for $T-y$ plot at 0.13, 2.40 and 6.67 kPa, respectively; ******: Raoult's law, ▬ ▬ ▬: NRTL, ▬ ▬: Wilson activity coefficient model for $T-x-y$ plots.

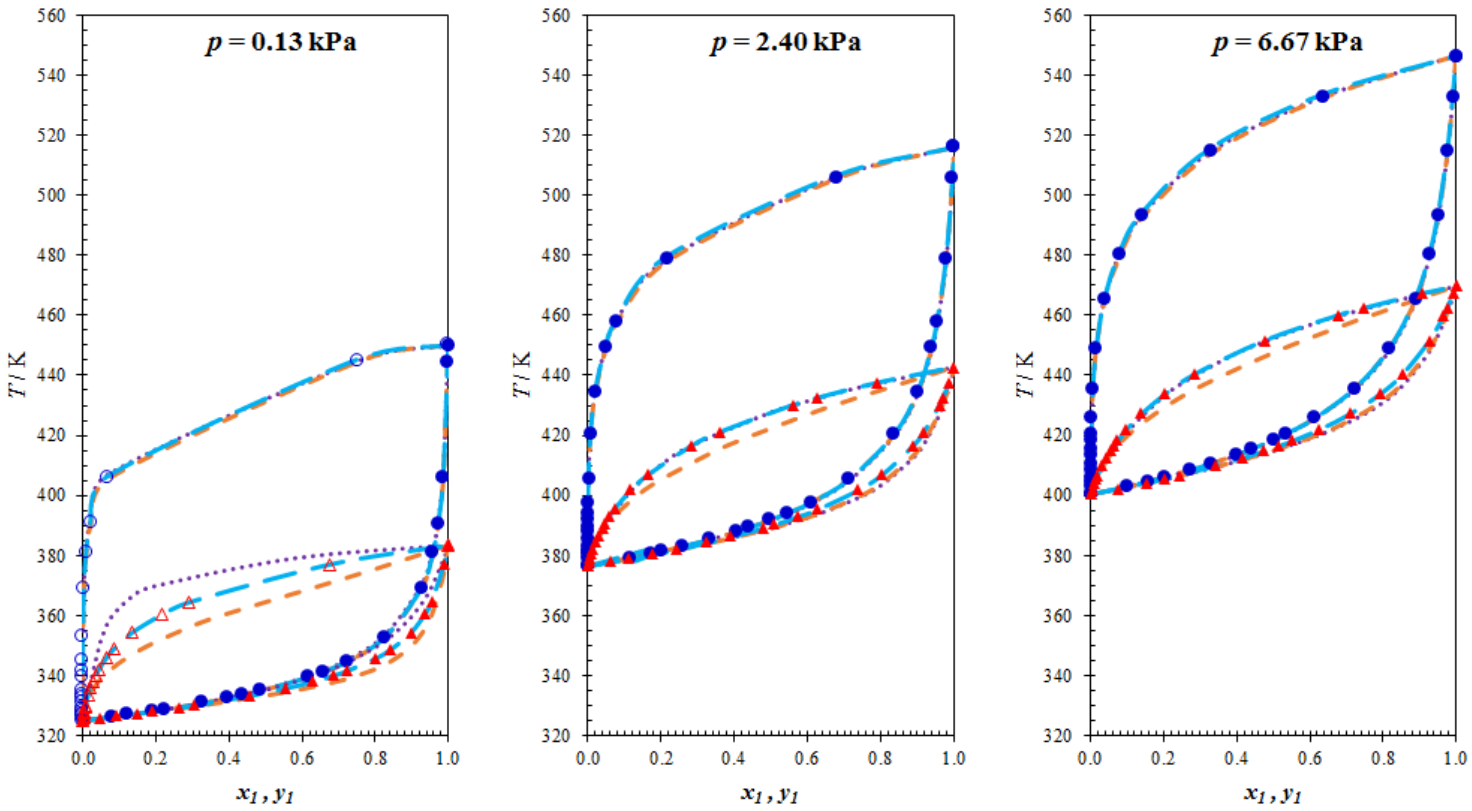

Figure 5.8 Comparison of VLE phase diagrams between D2EHPA (1) + n-dodecane (2) and TBP (1) + n-dodecane (2) at pressure of 0.13, 2.40 and 6.67 kPa. ●, ○: $T-x-y$ plots of D2EHPA (1) + n-dodecane (2); ▲, △: $T-x-y$ plots of TBP (1) + n-dodecane (2); ******: Raoult's law, ▬ ▬ ▬: NRTL, ▬▬▬: Wilson activity coefficient model for $T-x-y$ plots.

5.5.2 Thermodynamic consistency verification

All experimental data were verified using the homolographic method of Herington to see whether the data were consistent. Calculation results are shown in Figs. 5.9 and 5.10 together with Table 5.7.

Table 5.7 Thermodynamic consistency test of VLE data by Herington area test.

p (kPa)	T_{max} (K)	T_{min} (K)	S_+	S_-	D	J	$\lvert A^* \rvert$
			D2EHPA (1) + n-dodecane (2)				
0.13	325.2	450.0	0.01341	0.01169	6.8	57.6	0.00171
2.40	376.5	516.2	0.01093	0.00915	8.8	55.7	0.00177
6.67	400.4	546.3	0.01004	0.00826	9.7	54.7	0.00178
			TBP (1) + n-dodecane (2)				
0.13	325.2	383.4	0.09416	0.08593	4.6	26.8	0.00823
2.40	376.5	442.7	0.06815	0.06041	6.0	26.4	0.00774
6.67	400.4	469.9	0.06248	0.05502	6.3	26.0	0.00746

According to the Herington area test, when the value of $\lvert A^* \rvert < 3$, the isobaric VLE data are considered to be thermodynamically consistent i.e. the test is passed [31, 32]. Again, if $\lvert D - J \rvert < 10$, the test is passed. After calculation, the results in Table 5.7 of $\lvert A^* \rvert$ for the binary system of D2EHPA + n-dodecane and TBP + n-dodecane at pressures of 0.13, 0.67 and 6.67 kPa were < 3. Furthermore, all values of D were < J. This indicated that all the experimental data were thermodynamically consistent. Again, the very low values of $\lvert A^* \rvert$ indicated that the investigated binary mixtures were almost ideal although the values of $\lvert D - J \rvert$ were > 10. This was because of the large values of J or a large difference in the boiling points between the extractants (D2EHPA, TBP) and n-dodecane.

จุฬาลงกรณ์มหาวิทยาลัย
CHULALONGKORN UNIVERSITY

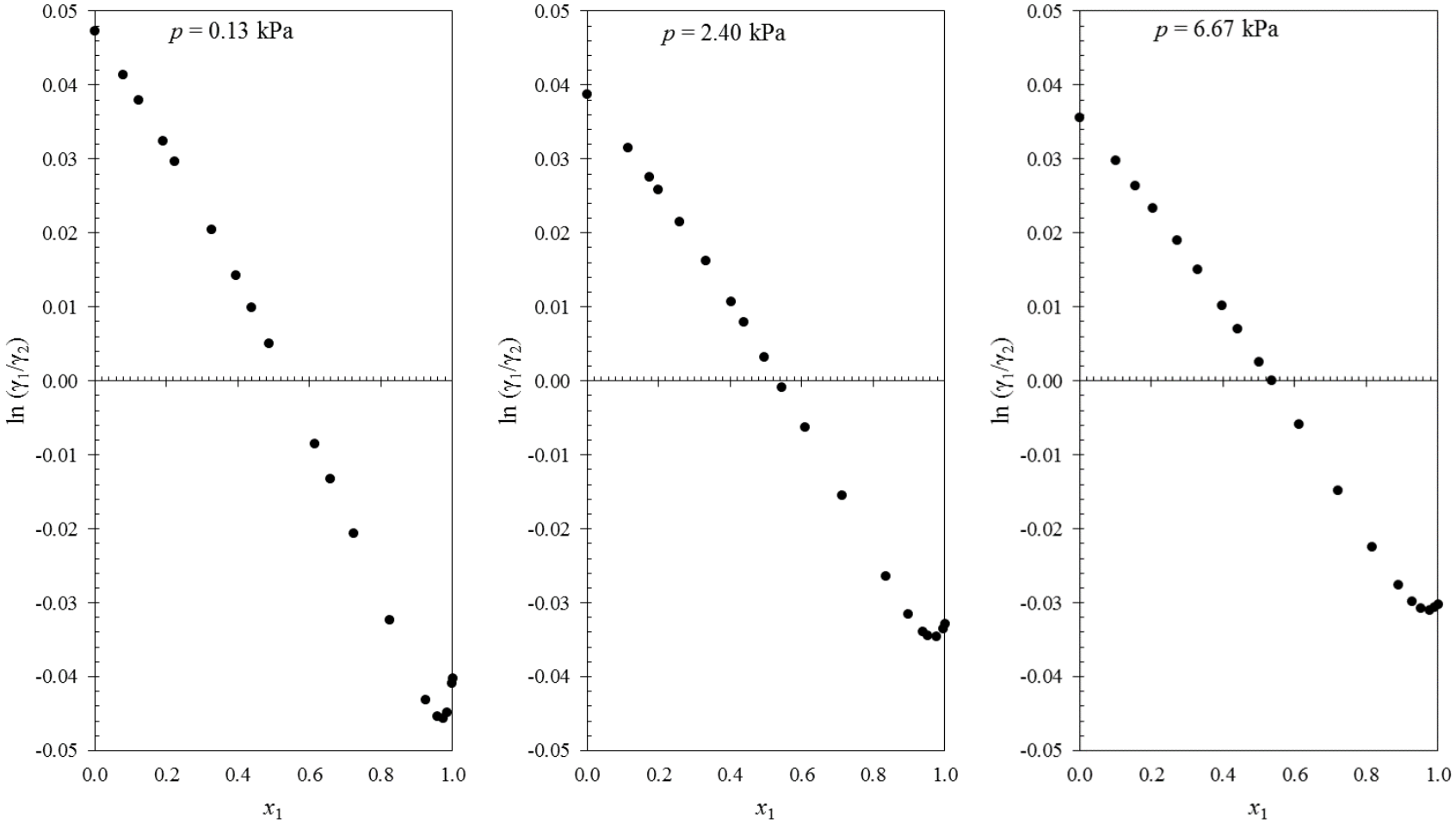

Figure 5.9 Diagrams of $\ln(\gamma_1/\gamma_2)$ to x_1 for the binary system of D2EHPA (1) + n-dodecane (2).

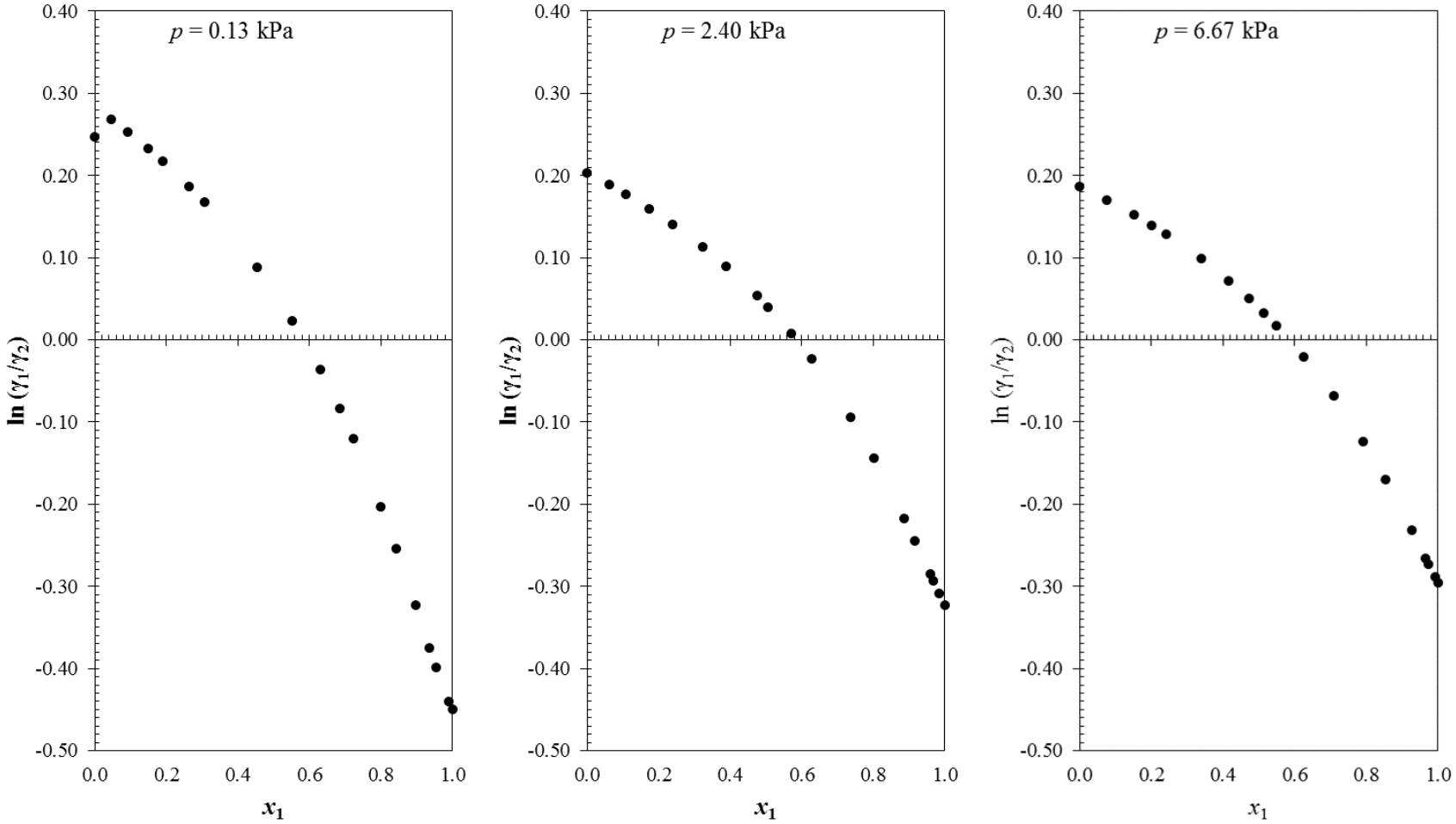

Figure 5.10 Diagrams of $\ln(\gamma_1/\gamma_2)$ to x_1 for the binary system of TBP (1) + n-dodecane (2).

As regards the Van Ness point test, Gmehling [33] and Onken suggested that isobaric VLE data are thermodynamically consistent when the average absolute deviation between calculated and measured vapor phase mole fraction (Δy) is < 0.01. According to the results in Table 5.7, all Δy values obtained by Raoult's law, NRTL and Wilson activity coefficient model for the binary systems of D2EHPA + n-dodecane and TBP + n-dodecane at pressures of 0.13, 2.40 and 6.67 kPa were found to be < 0.01 which indicated that the experimental data were thermodynamically consistent.

5.5.3 Data correlation

In order to improve results, the NRTL and Wilson activity coefficient models were used to calculate γ_i for each component. In the case of Raoult's law, γ_i is equal to 1. Then, the γ_i value was used to calculate vapor y_i under corresponding T and x_i. The correlation parameters of NRTL and Wilson models along with the root-mean-square deviation (RMSD) in the vapor- phase mole fraction composition, $\mathrm{RMSD}(y_1)$ and in temperature, $\mathrm{RMSD}(T)$ at three different pressures are listed in Table 5.8.

จุฬาลงกรณ์มหาวิทยาลัย
CHULALONGKORN UNIVERSITY

For the D2EHPA + n-dodecane system, it can be seen that the maximum values for $\mathrm{RMSD}(y_1)$ were 0.0008 according to Raoult's law, 0.0004 for the NRTL and 0.0006 for the Wilson models. For the TBP + n-dodecane system, the maximum $\mathrm{RMSD}(y_1)$ values of Raoult's law, NRTL and Wilson models were 0.0095, 0.0080 and 0.0003, respectively. Thus, differences between the experimental and calculated VLE data were found to be small. Results of the Raoult's law, NRTL and Wilson activity coefficient model are shown in Figs. 5.6 to 5.8.

At the lowest pressure of 0.13 kPa, the $\mathrm{RMSD}(y_1)$ values, by Raoult's law, of D2EHPA + n-dodecane showed a minimum of 0.0000. This indicated ideal behavior of VLE. In contrast, the mixture of TBP + n-dodecane affirmed negative deviations with 0.0095 of $\mathrm{RMSD}(y_1)$. Moreover, when pressure increased, both mixtures tended to deviate from ideality as a result of intramolecular interactions between different molecules.

จุฬาลงกรณ์มหาวิทยาลัย
CHULALONGKORN UNIVERSITY

Table 5.8 Parameters for the NRTL and Wilson models for D2EHPA (1) + n-dodecane (2) and TBP (1) + n-dodecane (2) at p = 0.13, 2.40 and 6.67 kPa.

		$g_{12}-g_{22}$ / J·mol^{-1}	$g_{21}-g_{11}$ / J·mol^{-1}	RMSD(y_1)	RMSD(T) / K
NRTL Model	p / kPa	D2EHPA (1) + n-dodecane (2)			
	0.13	961.03	-650.82	0.0003	0.05
	2.40	1015	-716.77	0.0004	0.05
	6.67	1035.9	-743.65	0.0004	0.05
		TBP (1) + n-dodecane (2)			
	0.13	3814.6	-949.37	0.0080	0.58
	2.40	3361.8	-1166.7	0.0057	0.37
	6.67	3427.1	-1267.2	0.0047	0.34
		$g_{12}-g_{11}$ / J·mol^{-1}	$g_{21}-g_{22}$ / J·mol^{-1}	RMSD(y_1)	RMSD(T) / K
Wilson Model	p / kPa	D2EHPA (1) + n-dodecane (2)			
	0.13	1429.9	-1204.2	0.0003	0.02
	2.40	1780.3	-1561.9	0.0005	0.12
	6.67	1969.5	-1754.1	0.0006	0.05
		TBP (1) + n-dodecane (2)			
	0.13	1657.4	132.2	0.0002	0.02
	2.40	2054.6	-591.2	0.0003	0.03
	6.67	2215.5	-769.9	0.0003	0.03
				RMSD(y_1)	RMSD(T) / K
Raoult's Law Model	p / kPa	D2EHPA (1) + n-dodecane (2)			
	0.13			0.0000	0.11
	2.40			0.0007	0.12
	6.67			0.0008	0.12
		TBP (1) + n-dodecane (2)			
				RMSD(y_1)	RMSD(T) / K
	0.13			0.0095	0.5953
	2.40			0.0078	0.4633
	6.67			0.0062	0.4221

5.6. Conclusions

In this study, the new experimental isobaric VLE data for the binary systems of D2EHPA + n-dodecane and TBP + n-dodecane were reported at pressures of 0.13, 2.40 and 6.67 kPa by a glass vapor-liquid equilibrium ebulliometer. The corresponding $T-x-y$ diagrams were plotted. VLE results showed that no azeotropic phenomenon existed. All the relative volatilities at the pressure points above were > 3 which meant that the low volatile organophosphoric extractants (D2EHPA and TBP) and n-dodecane diluent can be separated practically by vacuum distillation. Upon investigation, the VLE data passed the consistency of thermodynamics using the Herington area test and Van Ness point test. Raoult's law, NRTL and Wilson activity coefficient models were used to correlate the experimental data. Consequently, the corresponding binary interaction parameters of the model were obtained. Then, the calculated values were compared with the experimental data. The relative differences proved to be very small for all models. Thus, it can be seen that the experimental data were validated and proved to be reliable. The VLE data can provide a very important reference for further theoretical research and industrial applications.

จุฬาลงกรณ์มหาวิทยาลัย
CHULALONGKORN UNIVERSITY

5.7 Supplementary information

5.7.1 Saturated vapor pressure

(1) Antoine equation

In this study, the Antoine equation [1] is applied to predict the saturated vapor pressure for pure component of D2EHPA, TBP and n-dodecane. The typical form of the equation is:

$$\ln p_{\text{sat}} = A - \frac{B}{T + C} \tag{S5.1}$$

where p_{sat} is the saturated vapor pressure (Pa), T is temperature (K), while A, B and C are the regression constants.

5.7.2 Vapor liquid equilibrium

(1) Raoult's Law

The simple model for VLE represented by Raoult's law provides a description of ideal behavior of the mixture in vapor phase (as ideal gas) and liquid phase (as ideal solution). The mathematical expression which gives quantitative expression to Raoult's law is:

$$y_i p = x_i p_i^s \tag{S5.2}$$

where y_i and x_i are the mole fractions of the vapor and liquid phases, respectively. p is the system pressure, and p_i^s is the vapor pressure of pure component.

จุฬาลงกรณ์มหาวิทยาลัย
CHULALONGKORN UNIVERSITY

(2) Modified Raoult's Law

For non-ideal mixture, Raoult's Law equation is adapted for more realistic VLE results by incorporating two factors namely, the fugacity coefficient (φ_i) for gas non-ideality and the activity coefficient (γ_i) for non-ideality in liquid phase. When φ_i and γ_i is inserted, Raoult's law is as follows:

$$p y_i \varphi_i = p_i^s \varphi_i^s \gamma_i x_i \exp\left[V_i^l \left(\frac{p - p_i^s}{RT} \right) \right] \tag{S5.3}$$

where φ_i and φ_i^s are the fugacity coefficients of the mixture and pure component in the vapor phase. γ_i is the activity coefficient. V_i^l is the molar volume, and R is the universal gas constant.

In this study, the vapor phase can be considered as an ideal state at the low pressures of 0.13, 2.40 and 6.67 kPa. Thus, all of the terms of $\exp\left[V_i^l\left(\frac{p-p_i^s}{RT}\right)\right]$, φ_i, and φ_i^s are equal to 1 at ideal state. Therefore, Eq. (S5.3) can be reduced as in Eq. (S5.4):

$$\gamma_i = \frac{y_i p}{x_i p_i^s} \tag{S5.4}$$

The calculated γ_i values for VLE binary system using Eq. (S5.4) are listed in Tables 5.4 and 5.5.

5.7.3 Relative volatility

The relative volatility (α_{ij}) is a measure of the differences in volatilities of the components. For the three pressures studied, the relative volatility values are calculated via Eq. (S5.5) as follows:

$$\alpha_{ij} = \frac{(y_i / x_i)}{(y_j / x_j)} \tag{S5.5}$$

5.7.4 Activity coefficient and data correlation

In this study, all of the VLE data is correlated with Raoult's law, NRTL, and Wilson activity coefficient models.

CHULALONGKORN UNIVERSITY

(1) Raoult's Law model

$$\gamma_i = 1$$

(2) NRTL model [2]

The NRTL model is illustrated as follows in Eq. (S5.6):

$$\ln \gamma_i = x_j^2 \left[\frac{G_{ji}^2 \tau_{ji}}{\left(x_i + x_j G_{ji}\right)^2} + \frac{G_{ij}^2 \tau_{ij}}{\left(x_j + x_j G_{ij}\right)^2} \right] \tag{S5.6}$$

$$\tau_{ij} = \frac{g_{ij} - g_{jj}}{RT}, \qquad G_{ij} = \exp\left(-a_{ij}\tau_{ij}\right), \qquad a_{ij} = a_{ji}$$

where $g_{ij} - g_{jj}$ refers to the binary interaction energy parameter, and the randomness parameter (a_{ij}) is a constant equal to 0.3.

(3) Wilson activity coefficient model [3]

For the Wilson model, activity coefficients for binary system are defined as follows:

$$\ln \gamma_i = -\ln\left(x_i + A_{ij} x_j\right) + x_j \left[\frac{A_{ij}}{x_i + x_j A_{ij}} - \frac{A_{ji}}{x_j + x_i A_{ji}} \right] \tag{S5.7}$$

$$A_{ij} = \frac{V_j}{V_i} \exp\left(-\frac{g_{ij} - g_{ii}}{RT} \right)$$

$$V_i = \frac{RT_{c,i}}{p_{c,i}} z_{c,i}^{\tau_i}, \qquad \tau_i = 1 + \left(1 - T / T_{c,i}\right)^{2/7}$$

where $g_{ij} - g_{jj}$ is the binary interaction energy parameter. Meanwhile, the critical temperature ($T_{c,i}$), critical pressure ($p_{c,i}$) and compressibility factor ($z_{c,i}$) are shown in Table S5.1 below:

Table S5.1 Critical properties namely, T_c, P_c and , Z_c of D2EHPA, TBP and n-dodecane.

Component	T_c / K	p_c / Pa	z_c
D2EHPA [4]	864.8	3,109	0.2044
TBP [5]	817.0	4,376	0.2153
n-Dodecane [6]	658.2	1,810	0.2402

5.7.5 Thermodynamic consistency verification

The thermodynamic consistency test of the experimental VLE data is verified by the Herington area test and Van Ness point test.

(1) Herington area test [7]

Based on Gibbs-Duhem Theorem [8] as in Eqs. (S5.8) and (S5.9), the Herington consistency test is usually used to verify the experimental data which is described in accordance with Eqs. (S5.10) and (S5.11):

$$\sum_i x_i d\ln\gamma_i - \frac{V^E}{RT}dp + \frac{H^E}{RT^2}dT = 0 \tag{S5.8}$$

Over composition x_1 at constant p gives:

$$A^* = 100\left(\int_0^1 \ln\frac{\gamma_1}{\gamma_2}dx + \int_0^1 \varepsilon dx\right) \tag{S5.9}$$

where $\varepsilon = \left(\frac{H^E}{RT^2}\right)\left(\frac{\partial T}{\partial x_1}\right)_p$

According to Eq. (S5.8), an integration term containing ε for isobaric systems is estimated by an empirical equation by use of the total boiling range of the mixture. Empirical criteria require two values for the test namely, *D* and *J* as follows [9]:

$$D = 100 \times \left|\frac{S_+ - S_-}{S_+ + S_-}\right| \tag{S5.10}$$

where S_+ and S_- are obtained from $\ln(\gamma_1/\gamma_2) - x_1$ plot. S_+ is the area above x axis of the plot, and S_- is the area below the x axis.

$$J = 150 \times \frac{T_{\max} - T_{\min}}{T_{\min}} \tag{S5.11}$$

where $T_{\max}$ and $T_{\min}$ represent the maximum and minimum temperatures of the system, respectively.

(2) Van Ness point test [10]

The Van Ness point test is also used to verify the validity of the thermodynamic consistency of the experimental VLE data; the average deviation of the vapor mole fraction is defined as follows:

$$\Delta y = \frac{1}{n}\sum_{i=1}^{n}\left|y_i^{\exp} - y_i^{\text{cal}}\right| \tag{S5.12}$$

where n is the experimental point number, $y_i^{\exp}$ is the experimental mole fraction in the vapor phase, and y_i^{cal} is the mole fraction in the vapor phase calculated by Raoult's

law, NRTL and Wilson activity coefficient models. The values of $y_i^{\exp}$ and y_i^{cal} are listed in Tables 5.4 and 5.5.

In order to judge the consistency of the experimental values with the calculated values, the absolute deviation of vapor-phase mole fraction and the equilibrium temperature between the experimental with calculated values are listed in Tables 5.4 and 5.5 as in the manuscript. Both Δy and ΔT are calculated accordingly:

$$\Delta y = \left| y^{\exp} - y^{\text{cal}} \right| \tag{S5.13}$$

$$\Delta T = \left| T^{\exp} - T^{\text{cal}} \right| \tag{S5.14}$$

where $y^{\exp}$ and y^{cal} are the experimental and calculation mole fractions of D2EHPA (or TBP) in the vapor phase, respectively; $T^{\exp}$ and T^{cal} are the experimental calculation temperatures in the vapor phase, respectively. T^{cal} and y^{cal} are calculated by Raoult's law, NTRL and Wilson activity coefficient models; the values are listed in Tables 5.4 and 5.5.

In order to judge overall consistency, the root-mean-square deviation (RMSD) should be calculated. The RMSD is defined as follows:

$$\text{RMSD} = \sqrt{\frac{1}{n}\sum_{i=1}^{n}\left(U_i^{\exp} - U_i^{\text{cal}}\right)^2} \tag{S5.15}$$

where $U_i^{\exp}$ and U_i^{cal} are the experimental and calculated values, respectively. n is the number of experimental data points.

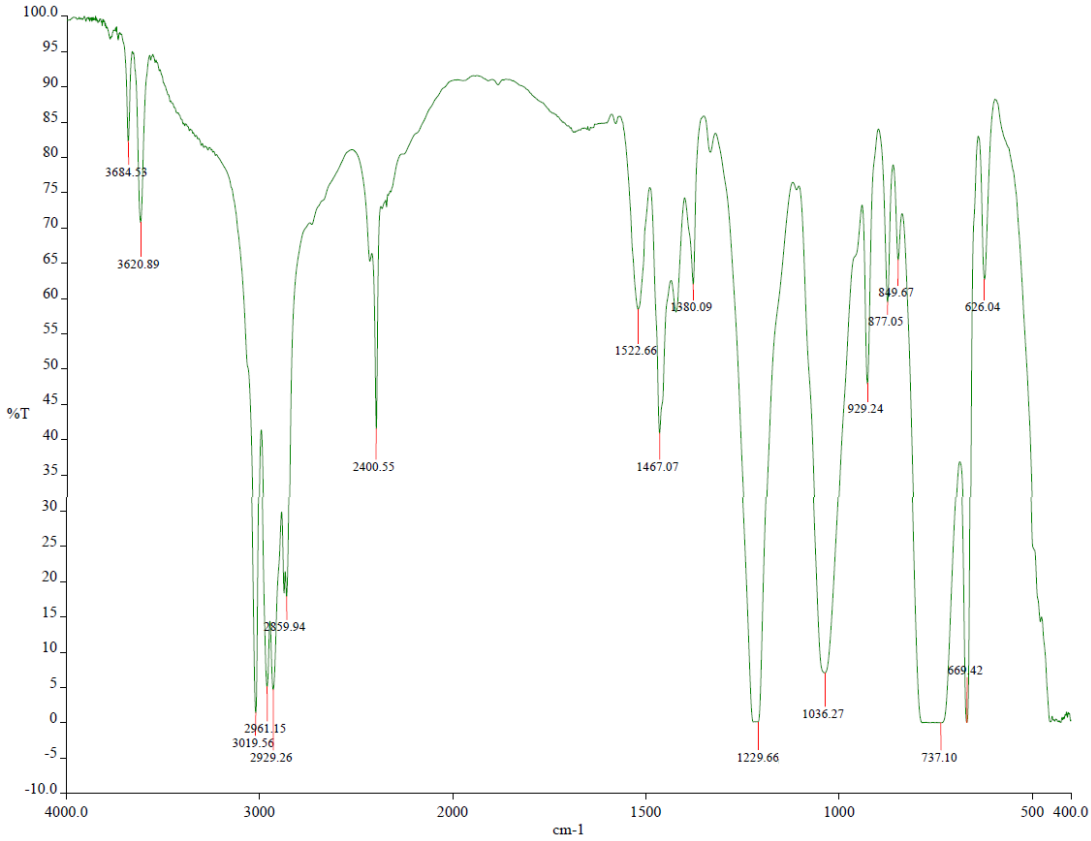

Figure S5.1 FT-IR spectrum of pure D2EHPA.

จุฬาลงกรณ์มหาวิทยาลัย
CHULALONGKORN UNIVERSITY

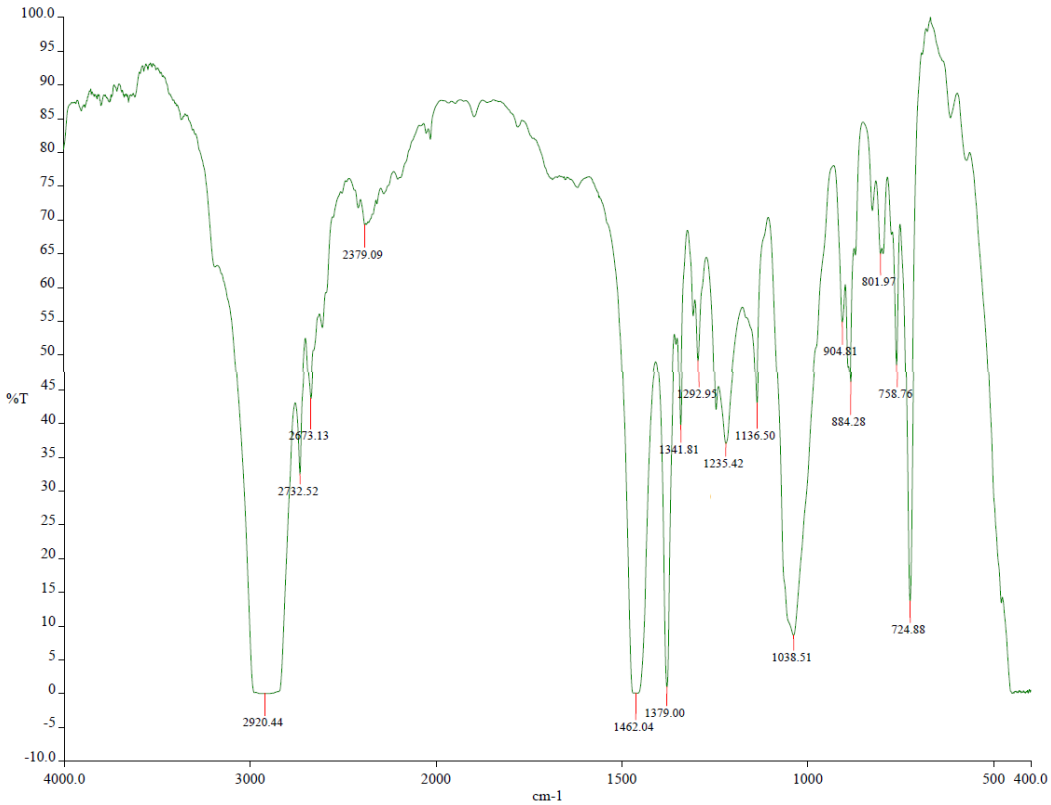

Figure S5.2 FT-IR spectrum of pure TBP.

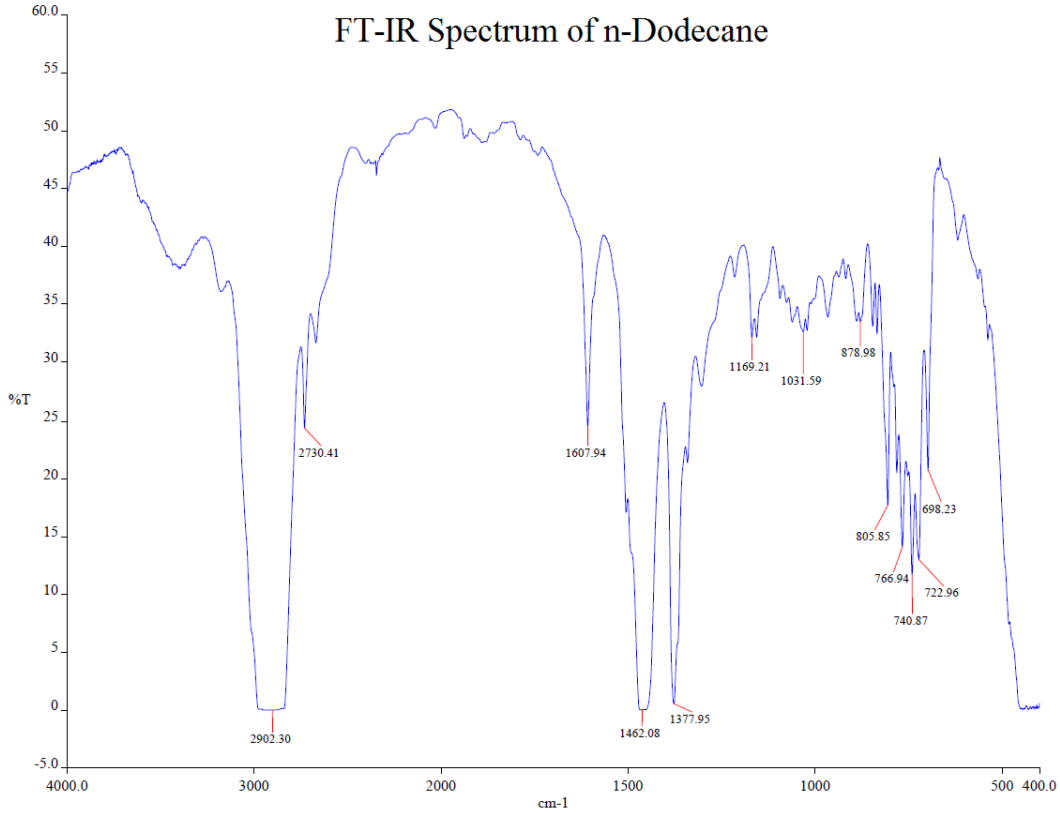

Figure S5.3 FT-IR spectrum of pure n-dodecane.

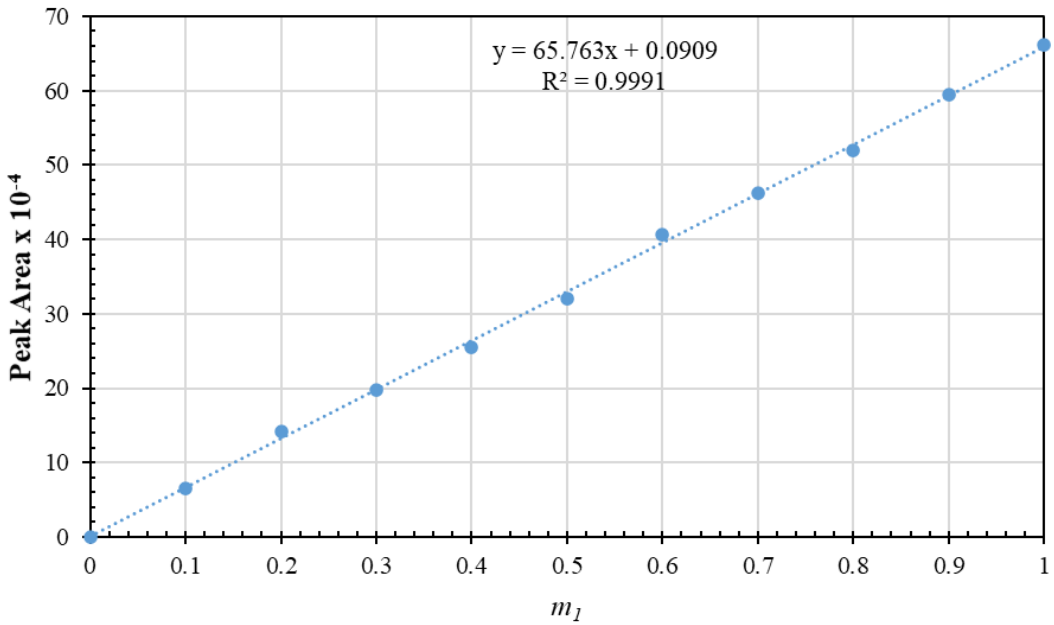

Figure S5.4 Calibration curve between mass fraction and peak area from FT-IR spectrum of D2EHPA (1) + n-Dodecane (2) binary mixtures.

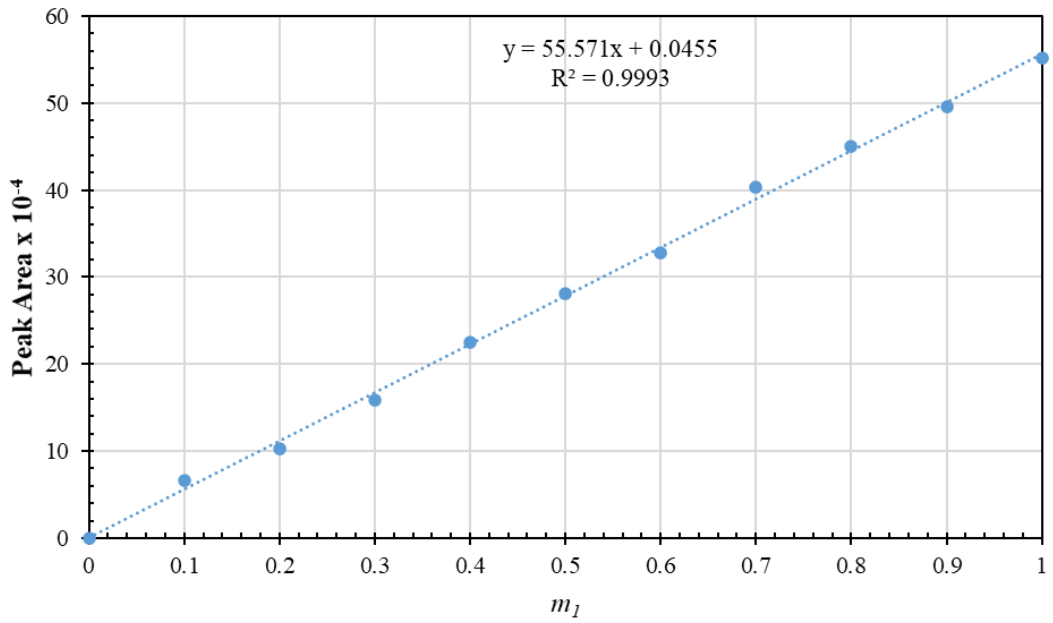

Figure S5.5 Calibration curve between mass fraction and peak area from FT-IR spectrum of TBP (1) + n-Dodecane (2) binary mixtures.

5.7.6 References for the supplementary information

[1] Antoine, C. (1888). "Vapor Pressure: a new relationship between pressure and temperature." *Comptes Rendus des Séances de l'Académie des Sciences*, 107, 681–684, 778–780, 836–837.

[2] Renon, H., and Prausnitz, J. M. (1968). "Local Compositions in Thermodynamic Excess Functions for Liquid Mixtures." *AIChE J.* , 14, 135−144.

[3] Wilson, G. M. (1964). "Vapor-Liquid Equilibrium. XI. A New Expression for the Excess Free Energy of Mixing." *J. Am. Chem. Soc.*, 86, 127−130.

[4] Kumar, S., Balasubramonian, S., Sivakumar, D., Mudali, U. K., and Natarajan, R. (2011). "PVT Properties of Di-(2-Ethyl Hexyl) Phosphoric Acid." *J. Radioanal. Nucl. Chem.*, 289, 883-884.

[5] Kumar, S., Mudali, U. K., and Natarajan, R. (2011). "PVT Properties of PUREX/UREX Solvent Tri-n-Butyl Phosphate." *J. Radioanal. Nucl. Chem.*, 289, 587–589.

[6] Rosenthal, D. J., and Teja, A. S. (1989). "The critical properties of n-alkanes using a low-residence time flow apparatus." *AIChE J.*, 35, 1829-1834.

[7] Herington, E. F. G. (1951). "Tests for the Consistency of Experimental Isobaric Vapor−Liquid Equilibrium Data." *J. Inst. Petrol.*, 37, 457−470.

[8] Smith, J. M., Ness, H. C. V., and Abbott, M. M. (2001). *Introduction to Chemical Engineering Thermodynamics*, McGraw-Hill, New York.

[9] Wisniak, J. (1993). "A new test for the thermodynamic consistency of vapor-liquid equilibrium." Ind. Eng. Chem. Res., 32, 1531-1533.

[10] Ness, H. C. V., Byer, S. M., and R. E, G. (1973). "Vapor−Liquid Equilibrium: Part I. An Appraisal of Data Reduction Methods." AIChE J., 19, 238−244.

5.8 Acknowledgements

This work was supported by the Research and Researcher for Industry (RRI) of Thailand Research Fund (TRF) [grant numbers PHD60I005]; Mektec Manufacturing corporation (Thailand) ltd.; the Mass Separation Laboratory, Department of Chemical Engineering, Chulalongkorn University as well as sincere thanks also go to Department of Mining and Petroleum Engineering, Chulalongkorn University.

5.9 References

[1] F. Xie, T.A. Zhang, D. Dreisinger, F. Doyle, A critical review on solvent extraction of rare earths from aqueous solutions, Miner.Eng. 56 (2014) 10–28.

[2] R. Sarkar, S. Ray, S. Basu, Synergism in solvent extraction and solvent extraction kinetics, J. Chem. Bio. Phy. Sci. Sec. A 4 (2014) 3156-3181.

[3] J. Deng, Y. Zhang, W. Jiang, Q. Mei, D. Liu, Harmless, industrial vacuum-distillation treatment of noble lead, Vacuum 149 (2018) 306-312.

[4] Y. Zhang, J. Deng, W. Jiang, Q. Mei, D. Liu, Application of vacuum distillation in refining crude lead, Vacuum 148 (2018) 140-148.

[5] C.B. Nan, H.W. Yang, B. Yang, D. Liu, H. Xiong, Experimental and modeling vapor-liquid equilibria: Separation of Bi from Sn by vacuum distillation, Vacuum 135 (2017) 109-114.

[6] P.V. Anand, R. Rajeev, P. Velavendan, N.K. Pandey, U.K. Mudali, Modeling and simulation of diluent recovery unit in PUREX solvent regeneration system, Prog. Nucl. Energ. 104 (2018) 359-367.

[7] N.J.M. Kuipers, A.E. Wentink, A.B.d. Haan, J. Scholtz, H. Mulder, Functionalized solvents for olefin isomer purification by reactive extractive distillation, Chem. Eng. Res. Des. 85 (2007) 88-99.

[8] S. Balasubramonian, R.K. Srivastav, S. Kumar, D. Sivakumar, M. Sampath, U.K. Mudali, R. Natarajan, , Flash point prediction for the binary mixture of phosphatic solvents and n-dodecane from UNIFAC group contribution model, J. Loss Prev. Process Ind. 33 (2015) 183-187.

จุฬาลงกรณ์มหาวิทยาลัย
Chulalongkorn University

[9] J.A. Partridge, R.C. Jensen, Purification of di-(2-ethylhexyl) phosphoric acid by precipitation of copper(II) di-(2-ethylhexyl) phosphate, J. Inorg. Nucl. Chem. 31 (1969) 2587-2589.

[10] A. Cheraghi, M.S. Ardakani, E.K. Alamdari, D.H. Fatmesari, D. Darvishi, S.K. Sadrnezhaad, Thermodynamics of vanadium (V) solvent extraction by mixture of D2EHPA and TBP, Int. J. Miner. Process. 138 (2015) 49-54.

[11] A.R. Gillens, B.A. Powell, Rapid quantification of TBP and TBP degradation product ratios by FTIR-ATR, J. Radioanal. Nucl. Chem. 296 (2013) 859–868

[12] B.N. Taylor, C.E. Kuyatt, NIST Technical Note 1297, in: N.I.o.S.a.T. (NIST) (Ed.) 1994, pp. 1-20.

[13] E.C. Voutsas, C. Pamouktsis, D. Argyris, G.D. Pappa, Measurements and thermodynamic modeling of the ethanol-water system with emphasis to the azeotropic region, Fluid Phase Equilib. 308 (2011) 135– 141.

[14] C.B. Williamham, W.J. Taylor, J.M. Pignocco, F.D. Rossini, Vapor Pressures and Boiling Points of Some Paraffin, Alkylcyclopentane, Alkylcyclohexane, and Alkylbenzene Hydrocarbons, J. Res. Natl. Bur. Stand. (U.S.) 35(3) (1945) 219-244.

[15] D.L. Camin, F.D. Rossini, Physical Properties of Fourteen API Research Hydrocarbons, C9 to C15, J. Phys. Chem. 59(11) (1955) 1173-1179.

[16] T. Wongsawa, N. Sunsandee, A.W. Lothongkum, U. Pancharoen, S. Phatanasri, The Role of Organic Diluents in the Aspects of Equilibrium, Kinetics and Thermodynamic Model for Silver Ion Extraction Using an Extractant D2EHPA, Fluid Phase Equilib. 388 (2015) 22-30.

[17] S. Kumar, S. Balasubramonian, D. Sivakumar, U.K. Mudali, R. Natarajan, PVT Properties of Di-(2-Ethyl Hexyl) Phosphoric Acid, J. Radioanal. Nucl. Chem. 289 (2011) 883-884.

[18] S. Kumar, U.K. Mudali, R. Natarajan, PVT Properties of PUREX/UREX Solvent Tri-n-Butyl Phosphate, J. Radioanal. Nucl. Chem. 289 (2011) 587–589.

จุฬาลงกรณ์มหาวิทยาลัย
CHULALONGKORN UNIVERSITY

[19] K. Panneerselvam, M.P. Antony, T.G. Srinivasan, P.R.V. Rao, Estimation of Normal Boiling points of Trialkyl Phosphates using Retention indices by Gas Chromatography, Thermochim. Acta 511 (2010) 107-111.

[20] R.S. Edmundson, Dictionary of Organophosphorus Compounds, Chapman and Hall Ltd., New York, London, 1988.

[21] G.H. Härtel, Low-volatility polar organic solvents for sulfur dioxide hydrogen sulfide and carbonyl sulfide, J. Chem. Eng. Data 30 (1985) 57-61.

[22] L.L. Burger, R.M. Wagner, Preparation and Properties of Some Organophosphorus Compounds, Ind. Eng. Chem. Chem. Eng. Data Ser. 3 (1958) 310-313.

[23] A.A. Foxton, G.H. Jeffery, A.I. Vogel, Physical properties and chemical constitution. XLIX. The refractivities, densities, and surface tensions of some organophosphorus compounds, J. Chem. Soc. (1966) 249-253.

[24] A.I. Vogel, D.M. Cowan, Physical Properties and Chemical Constitution VII. Alkyl Sulfides, Disulfides, Sulfites, Sulfates, and Orthophosphates, J. Chem. Soc. (1943) 16-24.

[25] W.G. Skene, M.E. Krzymien, Vapor Pressure of Tri-n-butyl Phosphate, J. Chem. Eng. Data 40 (1995) 394-397.

[26] D.L. Morgan, R. Kobayashi, Direct vapor pressure measurements of ten n-alkanes in the C10-C28 range, Fluid Phase Equilib. 97 (1994) 211-242.

[27] A. Dejoz, V. Gonzalez-Alfaro, P.J. Miguel, M.I. Vazquez, Isobaric Vapor-Liquid Equilibria for Binary Systems Composed of Octane, Decane, and Dodecane at 20 kPa, J. Chem. Eng. Data 41 (1996) 93-96.

[28] M. Casserino, D.R. Blevins, R.N. Sanders, An improved method for measuring vapor pressure by DSC with automated pressure control, Thermochim. Acta 284 (1996) 145-152.

[29] H.S. Myers, M.R. Fenske, Measurement and Correlation of Vapor Pressures Data for High Boiling Hydrocarbons, Ind. Eng. Chem. 47 (1955) 1652-1658.

จุฬาลงกรณ์มหาวิทยาลัย
Chulalongkorn University

[30] W. Srirachat, U. Pancharoen, S. Kheawhom, An investigation of saturated vapor pressure regarding low-volatility organophosphorus extractants Di-(2-ethylhexyl) phosphoric acid and tributyl phosphate: Correlation and thermodynamics study, Vacuum 156 (2018) 237-247.

[31] K. Kurihara, Y. Egawa, K. Ochi, K. Kojima, Evaluation of thermodynamic consistency of isobaric and isothermal binary vapor-liquid equilibrium data using PAI test, Fluid Phase Equilib. 219 (2004) 75-85.

[32] K. Kojima, H.M. Moon, K. Ochi, Thermodynamic Consistency Test of Vapor-Liquid Equilibrium Data, Fluid Phase Equilib. 56 (1990) 269-284.

[33] A. Fredenslund, J. Gmehling, P. Rasmussen, Vapor-liquid equilibria using UNIFAC, Elsevier, Amsterdam, 1977.

จุฬาลงกรณ์มหาวิทยาลัย
CHULALONGKORN UNIVERSITY

CHAPTER VI

CONCLUSION

6.1 Conclusion

Hollow fiber supported liquid membrane (HFSLM) is a cutting-edge system that has been well applied in the separation processes and can be regarded as a promising system for As Low As Reasonably Achievable (ALARA) mass separation.

In this work, it is noted that HFSLM can effectively extract and recover Ni^{2+} from the real rinse wastewater of the electroless nickel immersion gold (ENIG) plating process containing $[Au(CN)_2]^-$ and other ions. Both D2EHPA, an acidic type extractant, and TBP, a solvating type extractant are capable of extracting Ni^{2+} and $[Au(CN)_2]^-$. At equal concentration, D2EHPA attained a slightly higher extraction percentage and distribution ratio of Ni^{2+} ions than TBP. Thus, it is seen that selective extraction in terms of selectivity of Ni^{2+} relative to $[Au(CN)_2]^-$ is improved when D2EHPA is used. In addition, it is evident that using the mixture of D2EHPA/TBP extractants yielded the highest Ni^{2+} extraction efficiency followed by the single extractants i.e. D2EHPA and TBP, respectively. The synergistic coefficient of the D2EHPA/TBP extractants for Ni^{2+} extraction ($SC_{Ni} > 1$) indicates that synergism occured. Furthermore, the synergistic mixture D2EHPA/TBP can transport the Ni^{2+} ions much faster than a single extractant. Thus, as regards selective separation, the combination of D2EHPA/TBP extractants proved to be the most suitable ions carrier system via HFSLM as a result of their synergism to target Ni^{2+} as well as their antagonism to non-target $[Au(CN)_2]^-$ for improving extraction percentage of Ni^{2+} ($\%E_{Ni}$), distribution ratio (D_{Ni}) and selectivity

($S_{Ni/Au}$). The viability to separate Ni^{2+} is established by controlling the influence of operating conditions. Under optimum conditions, a complete separation of Ni^{2+} was achieved: 85.70% of extraction and 83.2% of stripping (recovery). The optimized conditions found proved to be the synergistic extractants: 0.25 mol/L D2EHPA mixed with 0.25 mol/L TBP, 0.50 mol/L HCl as a strippant and 200 mL/min of flow rate for both aqueous solutions.

The overall contents of this dissertation cover the following studies:

The superior extraction of Ni^{2+} over $[Au(CN)_2]^-$ from the rinse wastewater of the ENIG plating process was investigated via the HFSLM system. D2EHPA, and TBP were employed as extractants. Results show that the binary mixtures having acidic/neutral extractants of D2EHPA/TBP yielded the highest selectively extracting of Ni^{2+} from $[Au(CN)_2]^-$ at low concentrations. The HFSLM technique illustrates the selective extraction of Ni^{2+} over other conventional techniques. The successful separation of Ni^{2+} ions from the real rinse wastewater of the ENIG plating process via HFSLM proved its worth that it can be a most useful technique in the integrated operation of the ENIG plating process.

จุฬาลงกรณ์มหาวิทยาลัย
CHULALONGKORN UNIVERSITY

Various types of vegetable oil (palm, sunflower, soybean, coconut and rice bran) were investigated as eco-friendly benign diluents. Herein, all vegetable oil-based diluents loaded with organophosphorus extractants: D2EHPA and TBP demonstrate their effectiveness for the selective elimination of Ni^{2+}.

Besides, a mathematical model was developed on the basis of the conservation of mass. Axial convection, axial diffusion, radial diffusion as well as chemical reactions were investigated via mathematical modeling. The mathematical model was developed to predict the concentration of Ni^{2+} in both aqueous solutions. Results indicate that the

model proved to be an effective approach for predicting the transportation of Ni^{2+} across the HFSLM system. In the liquid membrane, only the diffusion in the radial direction took place. Thus, axial convection, axial diffusion, radial diffusion and the chemical reactions were involved in mass transfer across HFSLM and considered as an important concept for accurate prediction in the unsteady state model. This robust model with its high accuracy provides a greater understanding of the transport mechanisms across the HFSLM system. A design scale-up for industrial application could prove useful.

Furthermore, the p_{sat} for the low volatility organophosphorus extractants over the temperature range T = (450.5 – 546.2) K for D2EHPA and T = (383.8 – 469.9) K for TBP were determined by vacuum distillation method. Despite reaching high temperatures, the measured p_{sat} of these two extractants were relatively low, in the range of p_{sat} = (0.13 – 6.67) kPa. On investigation, it was observed that the p_{sat} values of D2EHPA were lower than that of TBP due to stronger intermolecular H-bonding. The correlation results of the experimental p_{sat} were found to be in good agreement with the estimated values as indicated by the low percentage of RAD for these models, namely Antoine (0.0089 – 0.0230) %, August (0.2191 – 0.2193) %, Riedel vapor pressure (0.0321 – 0.1305) % and Wagner equation (0.0076 – 0.0080) %. Then, the thermodynamic properties of $\Delta_{vap}H$ and $\Delta_{vap}S$ were calculated. Thus, it was observed that when temperature increased, $\Delta_{vap}H$ and $\Delta_{vap}S$ decreased. The calculated ΔS_{vap} also showed positive departures from Trouton's rule. Furthermore, the C_{σ}^{l} were determined within the experimental temperature ranges. On further investigation, the relevant data may provide some useful information for the design and development of vacuum distillation and evaporation processes for the recovery and recycling of organic waste.

Additionally, the new experimental isobaric VLE data for the binary systems of D2EHPA + n-dodecane and TBP + n-dodecane were reported at pressures of 0.13, 2.40 and 6.67 kPa by a glass vapor-liquid equilibrium ebulliometer. The corresponding T x

y diagrams were plotted. VLE results showed that no azeotropic phenomenon existed. All the relative volatilities at the pressure points were > 3, which meant that the low volatile organophosphoric extractants (D2EHPA and TBP) and n-dodecane diluent can be separated practically by vacuum distillation. Upon investigation, the VLE data passed the consistency of thermodynamics using the Herington area test and Van Ness point test. Raoult's law, NRTL and Wilson activity coefficient models were used to correlate the experimental data. Consequently, the corresponding binary interaction parameters of the model were obtained. Then, the calculated values were compared with the experimental data. The relative differences proved to be very small for all models. Thus, it can be seen that the experimental data were validated and proved to be reliable. The VLE data can provide a very important reference for further theoretical research and industrial applications.

6.2 Limitation

A major concern regarding HFSLM is the stability of the liquid membrane in terms of long time performance. This is mainly due to the loss of extractant (carrier) and/or diluent from the membrane support, which has an influence on both the flux and selectivity of the membrane. In consideration of this, further study on the stability of the liquid membrane should be considered for scaling up for industrial applications.

6.3 Recommendations for future research

The advantages of HFSLM over conventional methods viz. less chemical used, high selectivity as well as low operating cost. HFSLM can easily be scaled up by operating in parallel or in series mode in order to yield higher capacity. Regards, simultaneous extraction and stripping of target species contribute unit very compact

with less operating time and energy consumption. Following are recommendations for future research:

(1) Pretreatment of wastewater must be performed in order to prevent fouling in the system.

(2) A high concentration of acid and high temperature should be avoided since it can impair the polypropylene hollow fibers.

(3) Measurement of the solubility of extractant in aqueous solutions should be investigated.

จุฬาลงกรณ์มหาวิทยาลัย
CHULALONGKORN UNIVERSITY

APPENDICES

จุฬาลงกรณ์มหาวิทยาลัย
CHULALONGKORN UNIVERSITY

APPENDIX A

LIST OF PUBLICATION

[1] Wanchalerm Srirachat, Ura Pancharoen, Soorathep Kheawhom, An investigation of saturated vapor pressure regarding low-volatility organophosphorus extractants Di-(2-ethylhexyl) phosphoric acid and tributyl phosphate: Correlation and thermodynamics study, Vacuum 156 (2018) 237-247. DOI: https://doi.org/10.1016/j.vacuum.2018.07.036

[2] Wanchalerm Srirachat, Kreangkrai Maneeintr, Ura Pancharoen, Soorathep Kheawhom, Isobaric vapor-liquid equilibrium for binary system related to the organophosphoric extractant of D2EHPA + n-dodecane and TBP + n-dodecane at 0.13, 2.40 and 6.67 kPa, Vacuum 160 (2019) 60-69. DOI: https://doi.org/10.1016/j.vacuum.2018.11.011

[3] Wanchalerm Srirachat, Parnuwat Usapein, Ura Pancharoen, Soorathep Kheawhom, Selective separation of trace nickel(II) and gold(I) ions via hollow fiber supported liquid membrane enhanced by synergistic extractants D2EHPA/TBP, Arabian Journal of Chemistry 14 (2021) Article 103427. DOI: https://doi.org/10.1016/j.arabjc.2021.103427

[4] Wanchalerm Srirachat, Thidarat Wongsawa, NitiSunsandee, Ura Pancharoen, Soorathep Kheawhom, Phase equilibrium for ternary liquid systems of water + di-(2-ethylhexyl)phosphoric acid + organic diluents: Thermodynamic study,

Fluid Phase Equilibria 401 (2015) 34-47. DOI: https://doi.org/10.1016/j.fluid.2015.05.017

[5] Wanchalerm Srirachat, Thanaporn Wannachod, Ura Pancharoen, Soorathep Kheawhom, Effect of polarity and temperature on the binary interaction between D2EHPA extractant and organic solvents (kerosene, n-heptane, chlorobenzene and 1-octanol): Experimental and thermodynamics, Fluid Phase Equilibria 434 (2017) 117-129.

DOI: https://doi.org/10.1016/j.fluid.2016.11.029

[6] Srestha Chaturabul, Wanchalerm Srirachat, Thanaporn Wannachod, Prakorn Ramakul, Ura Pancharoen, SoorathepKheawhom, Separation of mercury(II) from petroleum produced water via hollow fiber supported liquid membrane and mass transfer modeling, Chemical Engineering Journal 265 (2015) 34-46.

DOI: https://doi.org/10.1016/j.cej.2014.12.034

จุฬาลงกรณ์มหาวิทยาลัย
CHULALONGKORN UNIVERSITY

REFERENCES

จุฬาลงกรณ์มหาวิทยาลัย
CHULALONGKORN UNIVERSITY

จุฬาลงกรณ์มหาวิทยาลัย
CHULALONGKORN UNIVERSITY

VITA

NAME

DATE OF BIRTH

PLACE OF BIRTH

INSTITUTIONS ATTENDED 2013-2016 M.Eng. (Chemical Engineering), Department of Chemical Engineering, Faculty of Engineering, Chulalongkorn University
2007-2011 B.Sc.(Chemistry), Department of Chemistry, Faculty of Science, Mahidol University

HOME ADDRESS 1182/23 soi Wachiratham Satit 57 Sukhumvit road Bangchak Phrakhanong Bangkok 10260

PUBLICATION

[1] Srestha Chaturabul, Wanchalerm Srirachat, Thanaporn Wannachod, Prakorn Ramakul, Ura Pancharoen, SoorathepKheawhom, Separation of mercury(II) from petroleum produced water via hollow fiber supported liquid membrane and mass transfer modeling, Chemical Engineering Journal 265 (2015) 34-46.
DOI: https://doi.org/10.1016/j.cej.2014.12.034

[2] Wanchalerm Srirachat, Thidarat Wongsawa, NitiSunsandee, Ura Pancharoen, Soorathep Kheawhom, Phase equilibrium for ternary liquid systems of water + di-(2-ethylhexyl)phosphoric acid + organic diluents: Thermodynamic study, Fluid Phase Equilibria 401 (2015) 34-47.
DOI: https://doi.org/10.1016/j.fluid.2015.05.017

[3] Wanchalerm Srirachat, Thanaporn Wannachod, Ura Pancharoen, Soorathep Kheawhom, Effect of polarity and temperature on the binary interaction between D2EHPA extractant and organic solvents (kerosene, n-heptane, chlorobenzene and 1-octanol): Experimental and thermodynamics, Fluid Phase Equilibria 434 (2017) 117-129.
DOI: https://doi.org/10.1016/j.fluid.2016.11.029

[4] Wanchalerm Srirachat, Ura Pancharoen, Soorathep Kheawhom, An investigation of saturated vapor pressure regarding low-volatility organophosphorus extractants Di-(2-ethylhexyl) phosphoric acid and tributyl phosphate: Correlation and thermodynamics study, Vacuum 156 (2018) 237-247.
DOI: https://doi.org/10.1016/j.vacuum.2018.07.036

[5] Wanchalerm Srirachat, Kreangkrai Maneeintr, Ura Pancharoen, Soorathep Kheawhom, Isobaric vapor-liquid equilibrium for binary system related to the organophosphoric extractant of D2EHPA + n-dodecane and TBP + n-dodecane at 0.13, 2.40 and 6.67 kPa, Vacuum 160 (2019) 60-69.
DOI: https://doi.org/10.1016/j.vacuum.2018.11.011

[6] Wanchalerm Srirachat, Parnuwat Usapein, Ura Pancharoen, Soorathep Kheawhom, Selective separation of trace nickel(II) and gold(I) ions via hollow fiber supported liquid membrane enhanced by synergistic extractants D2EHPA/TBP, Arabian Journal of Chemistry 14 (2021) Article 103427.
DOI: https://doi.org/10.1016/j.arabjc.2021.103427

[7] Wanchalerm Srirachat, Natthapol Traiwongsa, Kittamuk Purktimatanont, Soorathep Kheawhom, Ura Pancharoen, Journal of the Taiwan Institute of Chemical Engineers. In Press.

จุฬาลงกรณ์มหาวิทยาลัย
CHULALONGKORN UNIVERSITY